NASA Contractor Report 3867

Free Jet Feasibility Study of a Thermal Acoustic Shield Concept for AST/VCE Application— Dual Stream Nozzles

B. A. Janardan, J. F. Brausch,
and R. K. Majjigi

CONTRACT NAS3-22137
MARCH 1985

NASA

NASA Contractor Report 3867

Free Jet Feasibility Study of a Thermal Acoustic Shield Concept for AST/VCE Application— Dual Stream Nozzles

B. A. Janardan, J. F. Brausch,
and R. K. Majjigi
General Electric Company
Cincinnati, Ohio

Prepared for
Lewis Research Center
under Contract NAS3-22137

National Aeronautics
and Space Administration

**Scientific and Technical
Information Branch**

1985

TABLE OF CONTENTS

TABLE OF CONTENTS (Concluded)

1.0 INTRODUCTION

1.1 BACKGROUND

Recent investigations have studied various concepts aimed at reducing the noise of supersonic exhausts to environmentally acceptable levels. These include the variable cycle engine (VCE) concept that was demonstrated with a coannular nozzle on YJ101 test-bed engine (Reference 1) and a variety of mechanically suppressed configurations with (References 2 and 3) and without (References 4 and 5) treated ejectors. Typical exhaust configurations that are applicable to an advanced supersonic transport (AST) propulsion system are shown schematically in Figure 1. A preliminary system design study, conducted with a thermal acoustic shield (TAS) on a coannular configuration, has shown greater suppression with moderate penalties in weight and performance. A schematic of a full-scale design using TAS at takeoff is illustrated in Figure 2 (from Reference 6). In this design, the bypass flow is ducted from the outer fan passage through strut-duct extensions of the turbine frame onto the center plug nozzle. The high-temperature core gas flows through the high-radius-ratio outer nozzle. Additional acoustic suppression is obtained by opening the thermal shield nozzle, which provides a hot, low-velocity gas shield around the lower half of the nozzle. At other operating conditions the thermal shield nozzle is closed.

The thermal acoustic shield concept (also referred to as fluid-layer shield) has been demonstrated in scale-model experimental studies (References 4 and 7 through 11). In this concept the reflection/refraction properties of a high-temperature, low-velocity stream shielding the primary jet, either partially or fully, decrease acoustic transmission to the observer (Figure 3). High-frequency sound from sources near the nozzle exit is refracted by the high-temperature, partial shield (Figure 3a). Under certain conditions this results in a total reflection of the sound away from the observer. The degree of refraction decreases with distance for sources away from the nozzle exit because of weakening of the shield flow, and hence suppression is less effective for low-frequency sound from sources downstream of the nozzle exit. In addition, refractive bending of the low-frequency sound, unlike total reflection of high-frequency sound, can result in the redistribution of acoustic energy from one angle to another. In the case of a fully shielded configuration (Figure 3b), the overall effect of the shield flow is similar to that of the partially shielded nozzle except that the high-frequency sound is subjected to multiple internal reflections. This property of attenuating high-frequency sound indicates that thermal acoustic shields can be used beneficially in conjunction with the high-frequency-dominated, mechanically suppressed, coannular configurations to reduce jet noise even more (Figure 1b).

Measured acoustic data obtained in a simple thermal shield concept demonstration experiment (Reference 4) are presented in Figure 4. The setup consisted of an annular, segmented, shield jet concentrically surrounding a small, high-speed jet. The data indicate that shielding occurred at large directivity angles, and the effectiveness of the shield increased with the thickness.

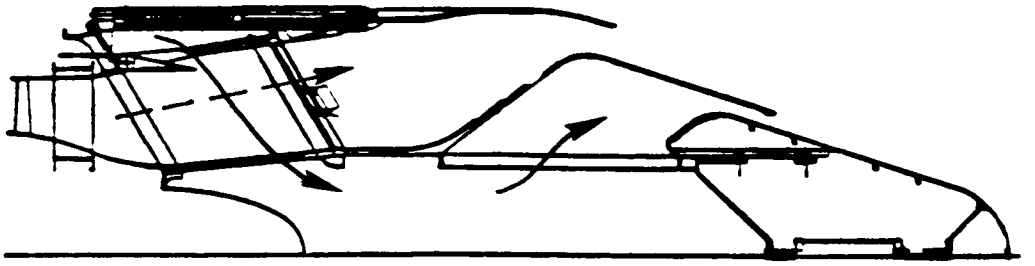

a) Unsuppressed Coannular Nozzle

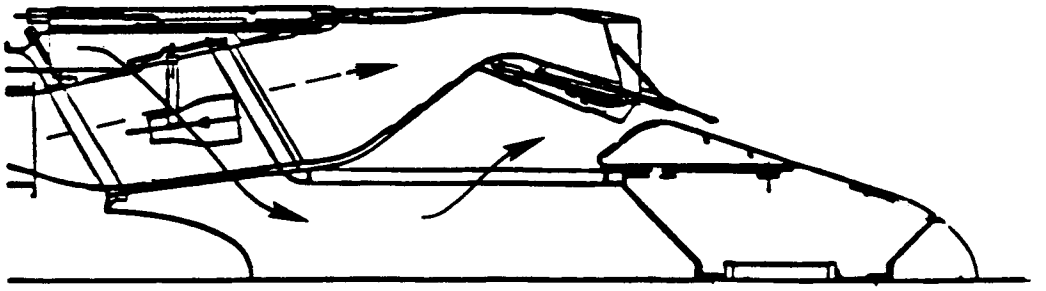

b) Outer Stream Suppressed Coannular Nozzle

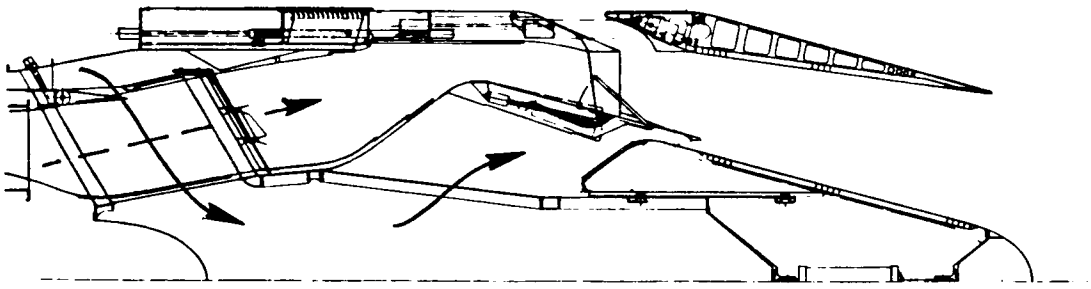

c) Outer Stream Suppressed Coannular Nozzle with Treated Ejector.

Figure 1. Schematics of Coannular Nozzle Configurations Applicable to Advanced Supersonic Transport Propulsion Systems.

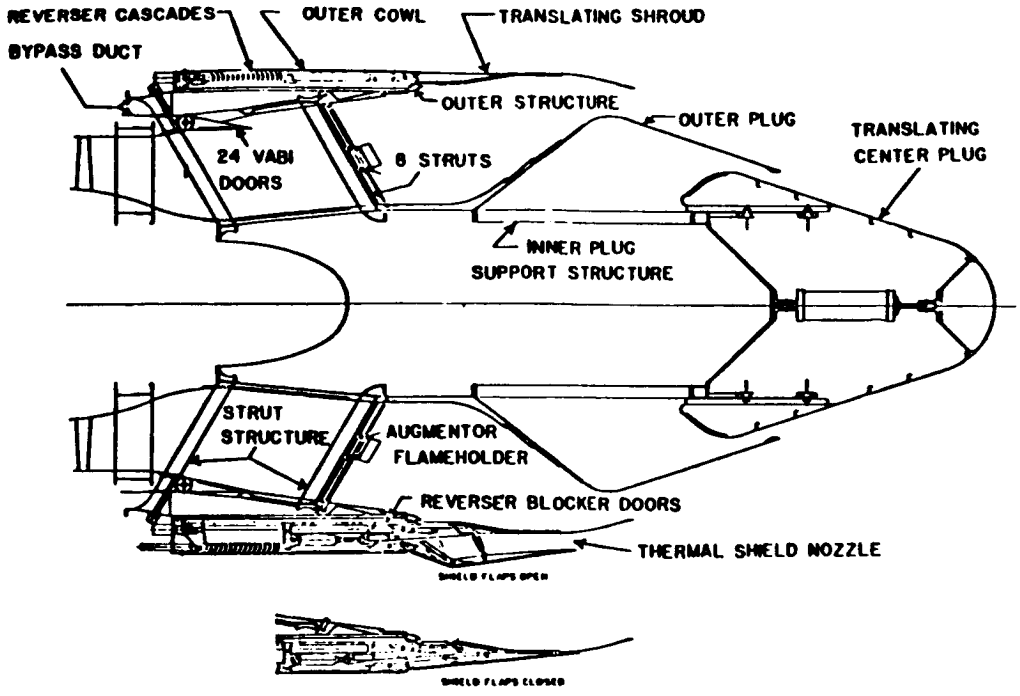

a) Schematic Arrangement

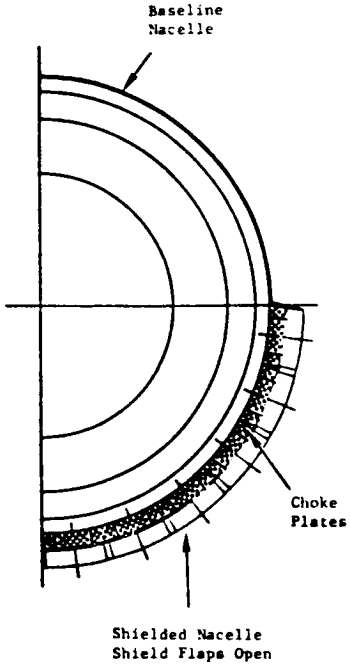

b) Aft View with Shield Flaps Open

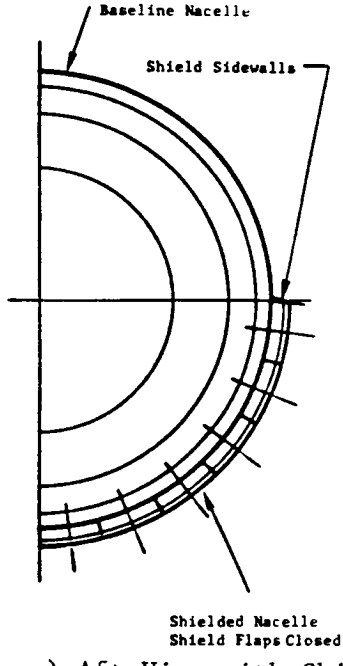

c) Aft View with Shield Flaps Closed

Figure 2. Full-Scale Design of a Coannular Nozzle with a Partial Thermal Acoustic Shield.

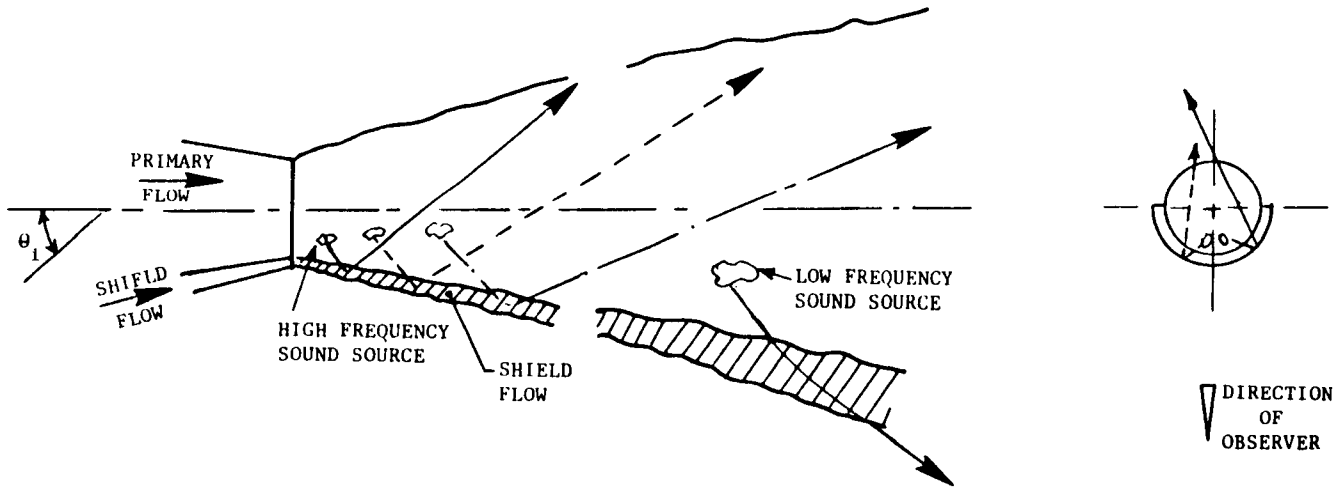

a) SEMI-ANNULAR SHIELD

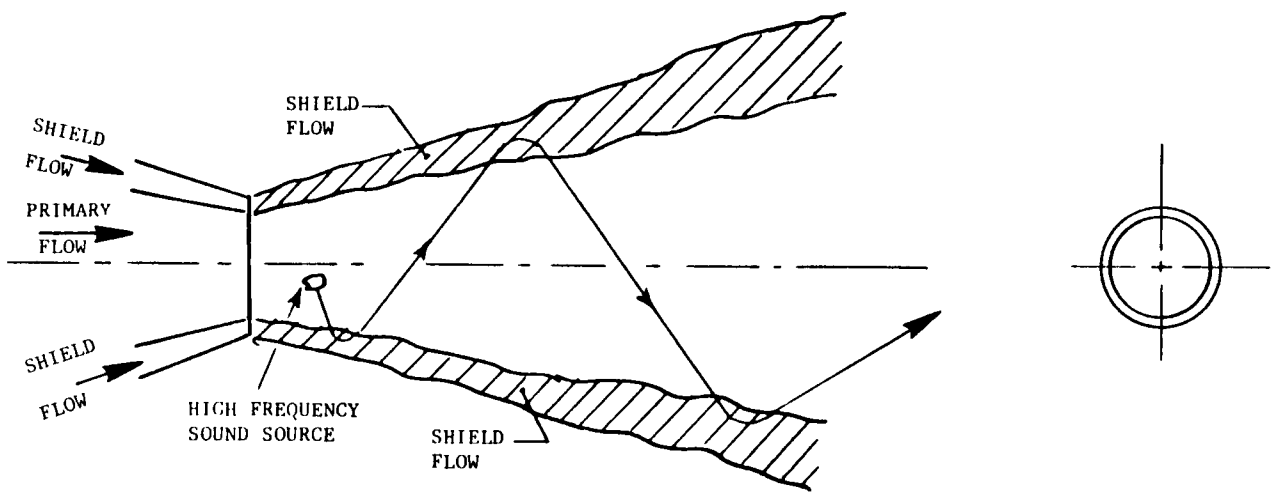

b) FULL-ANNULAR SHIELD

Figure 3. Schematic of Thermal Acoustic Shield Configurations.

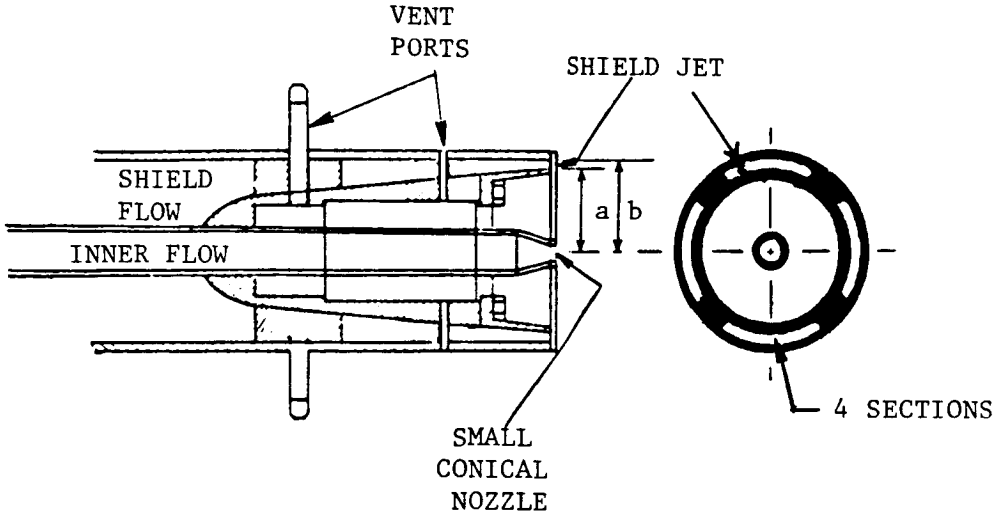

a) SCHEMATIC OF THE EXPERIMENTAL SET-UP

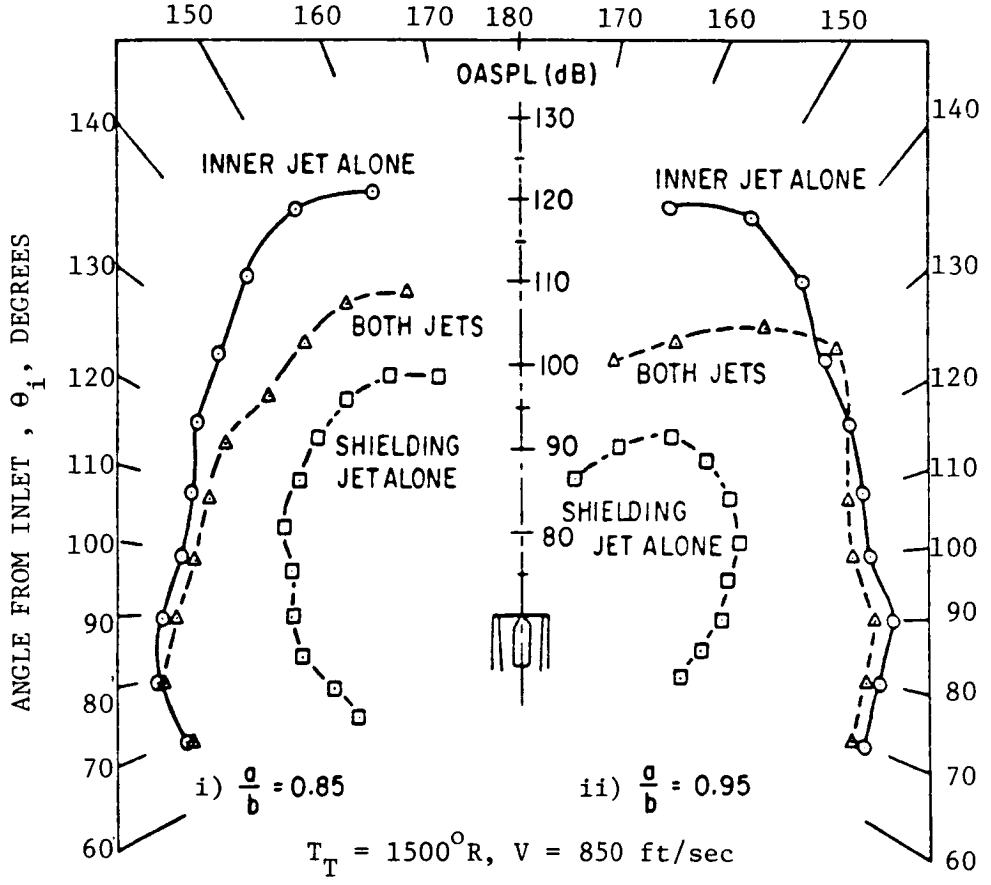

b) TYPICAL OASPL - DIRECTIVITY

Figure 4. Acoustic Data Measured with a Shield Around a High-Speed Jet.

Also, it is shown in Reference 4 that the acoustic shielding arrangement reduced the sound power radiated by the high-speed jet. In an exploratory scale-model study (typical of an engine nozzle setup) conducted to determine the benefit of a semiannular shield around a conical nozzle (Reference 9), it has been shown that the noise levels associated with a partly-shielded conical nozzle are lower than those of the conical nozzle at large directivity angles (Figure 5). This is indicated by representative data presented in Figure 5b. Additionally, as shown in Figure 5c, the sound pressure level (SPL) benefit from the shield was noted to increase with frequency. These data also indicate that there is an optimum shield-to-nozzle velocity ratio at which the high-frequency attenuation is a maximum. Similar benefits from thermal shields with high-radius-ratio, unsuppressed, annular plug nozzles operating at "intermediate" jet velocities were noted in Reference 10.

This program was initiated to develop a technology base for the thermal acoustic shield concept as a noise-reduction device. This was to be accomplished by using scale-model engine nozzles. The objectives were to:

- Determine the acoustic benefit of a thermal shield, for both unsuppressed and mechanically suppressed (multichute suppressor) annular and coannular plug nozzles, in static and free-jet environments.

- Evaluate the sensitivity of the acoustic benefit of the thermal shield to aerodynamic parameters such as nozzle velocity ratio, thermal shield velocity ratio, static temperature ratio, and geometric parameters such as shield thickness and full versus partial shield.

- Measure mean and turbulent velocities in selected plumes, using a laser velocimeter, to aid in understanding the effect of shield flow on the nozzle plume.

- Estimate the influences of the shield stream on the base pressure, and hence the thrust coefficient, of the mechanically suppressed configurations by measuring the base static pressures.

- Modify an existing unified aerodynamic/acoustic prediction technique (General Electric's M*G*B model of Reference 4) to account for the asymmetric flow field of the partial-shielded configurations and provide a framework for interpretation of the experimental data.

The data obtained during the first phase of this investigation with the annular unsuppressed and suppressed plug nozzles are presented and discussed in detail in Reference 12. A brief summary of the scope and the significant results obtained during the single-flow study are reviewed below. The scope of the investigation with the unsuppressed and suppressed coannular plug configuration is described in Subsection 1.3.

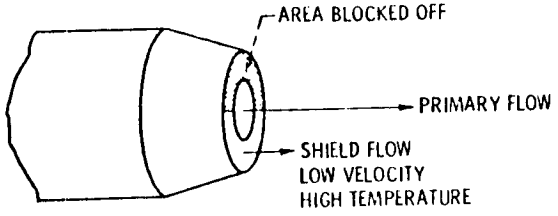

a) PERSPECTIVE VIEW OF NOZZLE

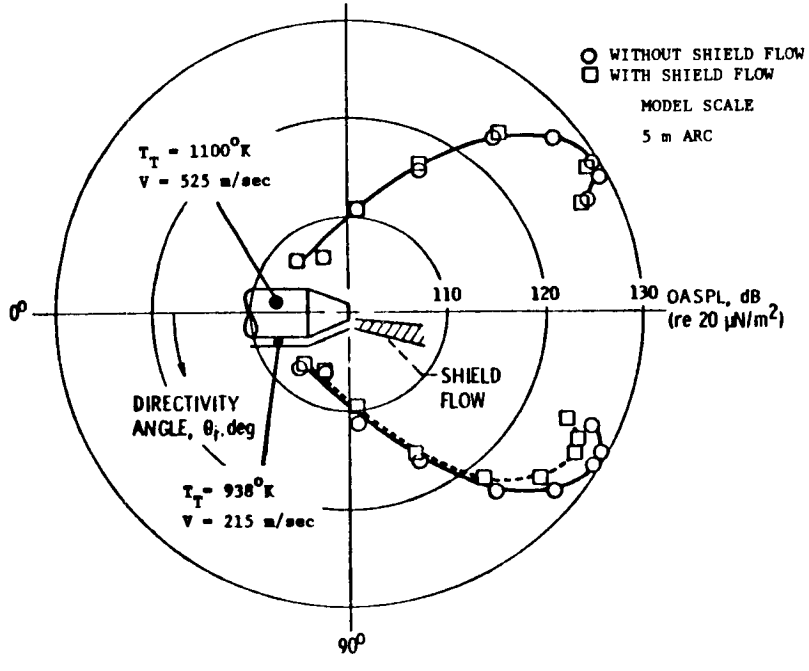

b) OASPL - DIRECTIVITY

CONICAL NOZZLE NOMINAL FLOW CONDITIONS

	VELOCITY RATIO, V^s/V^o	PRESSURE RATIO, P_r^o	TEMPERATURE, T_T^o, °K	VELOCITY, V^o, mps
O	0.33	2.15	1098	666
□	.38	1.74	1102	575
◇	.38	2.14	810	570
△	.42	1.56	1104	518
◁	.44	1.75	809	494
▷	.50	1.55	804	440
□	.63	2.18	306	349
◇	.73	1.80	291	301
△	.82	1.57	294	266

T_T^s = 942°K
V^s = 219 m/sec

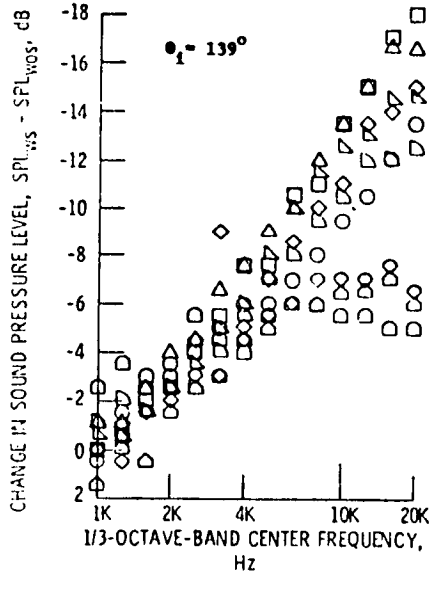

c) SPL BENEFIT AS A FUNCTION OF SHIELD-TO-JET VELOCITY RATIO

Figure 5. Effect of a Semiannular Thermal Acoustic Shield on Directivity and Spectra of a Conical Nozzle.

1.2 SINGLE-FLOW STUDY

A total of nine configurations (designated TAS-1 through TAS-9) employing single-flow, annular, primary nozzles were tested. They are listed below:

Unsuppressed Configurations

TAS-1: Baseline unsuppressed annular plug nozzle

TAS-2: Unsuppressed annular plug nozzle with 180° shield of 1.2 cm (0.48 in.) thickness

TAS-3: Unsuppressed annular plug nozzle with 180° shield of 2.5 cm (0.97 in.) thickness

TAS-4: Unsuppressed annular plug nozzle with 360° shield of 1.2 cm (0.48 in.) thickness

TAS-5: Convergent-divergent annular plug nozzle with 180° shield of 1.2 cm (0.48 in.) thickness

Mechanically Suppressed Configurations

TAS-6: Baseline 32-chute annular plug suppressor nozzle

TAS-7: 32-chute annular plug suppressor nozzle with 180° shield of 1.2 cm (0.48 in.) thickness

TAS-8: 32-chute annular plug suppressor nozzle with 180° shield of 2.5 cm (0.97in.) thickness

TAS-9: 32-chute annular plug suppressor nozzle with 360° shield of 1.2 cm (0.48 in.) thickness

Acoustic data were obtained for 314 acoustic test points. Mean and turbulent velocity data for 10 of the plumes associated with 4 of the configurations were measured using the laser velocimeter. The significant observations obtained from analyses of the acoustic data (Reference 12) are summarized briefly below.

a. For a given shield flow rate, a 180° partial thermal acoustic shield reduces primary nozzle jet noise more than a full 360° shield does.

b. Shield thickness has a significant bearing on the noise reduction potential of a thermal acoustic shield. A thicker shield, 2.5 cm (0.97 in.) was observed to be more effective in noise suppression than a thinner shield of 1.2 cm (0.48 in.).

c. The noise reduction potential of a thermal acoustic shield was observed to decrease with increasing primary jet velocity.

d. A thermal acoustic shield yields a larger perceived noise level (PNL) reduction for a mechanically suppressed plug nozzle than that obtained using an unsuppressed annular plug nozzle. The shielding effect of a thermal acoustic shield is the dominant effect for the unsuppressed annular plug nozzle, and shielding and source-modification effects are significant for mechanically suppressed nozzles.

e. The important noise-reduction mechanisms observed with the thermal acoustic shield are:

- Intermediate- and high-frequency noise reduction, at shallow aft angles to jet axis, due to the total reflection of sound waves from the primary jet by the shield flow.
- Intermediate- and high-frequency noise reduction, in the front quadrant and at $\theta_i = 90°$, due to source strength modification by the thermal acoustic shield flow.
- Low-frequency noise amplification, in the aft quadrant, due to elongation of jet plume by the thermal acoustic shield flow.

Observation (e) is made clear by the data presented in Figure 6 (from Reference 12) that show the influence of the 2.5-cm (0.97-in.) thick, 180° shield on the directivity of the various one-third-octave-band frequencies of unsuppressed annular plug and 32-chute suppressor nozzles at a typical Advanced Supersonic Transport/Variable Cycle Engine (AST/VCE) approach cycle condition. Significant aft quadrant suppression of the high-frequency noise is noted for both the unsuppressed and the 32-chute suppressor nozzles. For the 4 kHz band, the maximum suppression is approximately 20 dB at $\theta_i = 140°$ for both the unsuppressed and the 32-chute suppressor nozzles. For the unsuppressed nozzle, suppression increases with frequency at all aft-quadrant angles. However, such a trend is observed for the 32-chute suppressor nozzle only at aft-quadrant angles of $\theta_i = 140°$ and 150°. The rapid increase in suppression of high-frequency noise in the aft quadrant is attributed to the shielding effect. Based on the aerodynamic conditions of the shield and primary jets, the critical angle $(\theta_i)_{cr}$ for total reflection can be calculated by the following relationship (Reference 13):

$$\cos (\theta_i)_{cr} = \frac{1}{M_c + (a/a_{amb})} \tag{1}$$

where M_c is the noise source (eddy) convection Mach number, a is the local sonic speed in the flow through which the eddy is convecting, and a_{amb} is the ambient speed of sound.

Sym.	Frequency, Hz
○	250
□	500
◇	1000
△	2000
◺	4000

A_T = 1400 In.^{2}

Static

Approach Cycle

Conf.	Test Point	Core Jet V^o, fps	Core Jet T_T^o, °R	Core Jet P_r^o	Shield Jet V^s, fps	Shield Jet T_T^s, fps	Shield Jet P_r^s	Mixed Cond. V^{mix}, fps	Mixed Cond. T_T^{mix}, °R	Mixed Cond. P_r^{mix}
TAS-1	101	1340	1252	1.558	- - - -	NO SHIELD	- -	1340	1252	1.558
TAS-3	317	1341	1256	1.556	793	1246	1.162	1185	1253	1.407

Conf.	Test Point	Core Jet V^o, fps	Core Jet T_T^o, °R	Core Jet P_r^o	Shield Jet V^s, fps	Shield Jet T_T^s, fps	Shield Jet P_r^s	Mixed Cond. V^{mix}, fps	Mixed Cond. T_T^{mix}, °R	Mixed Cond. P_r^{mix}
TAS-6	601	1341	1267	1.550	- - - -	NO SHIELD	- -	1341	1267	1.550
TAS-8	817	1323	1240	1.546	801	1244	1.166	1176	1241	1.405

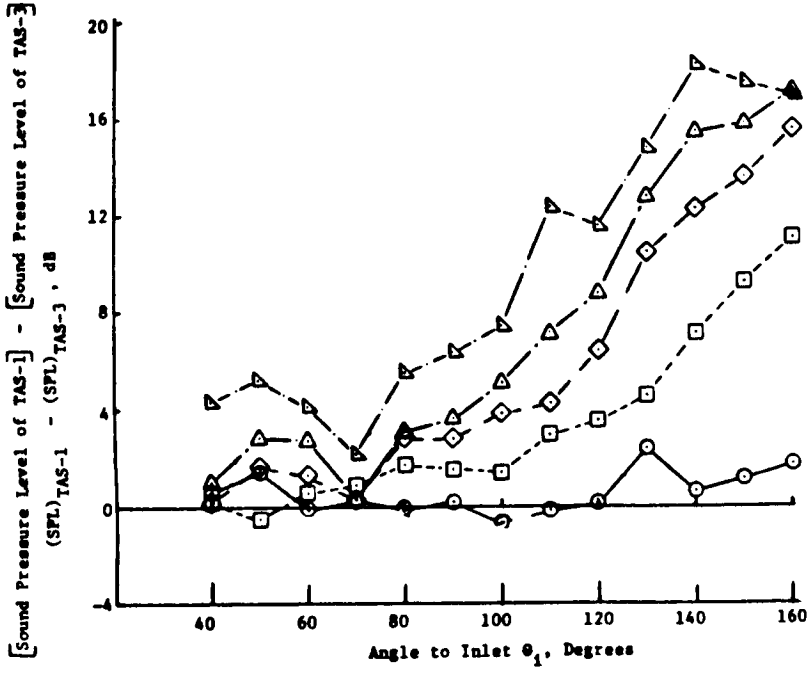

(a) Unsuppressed

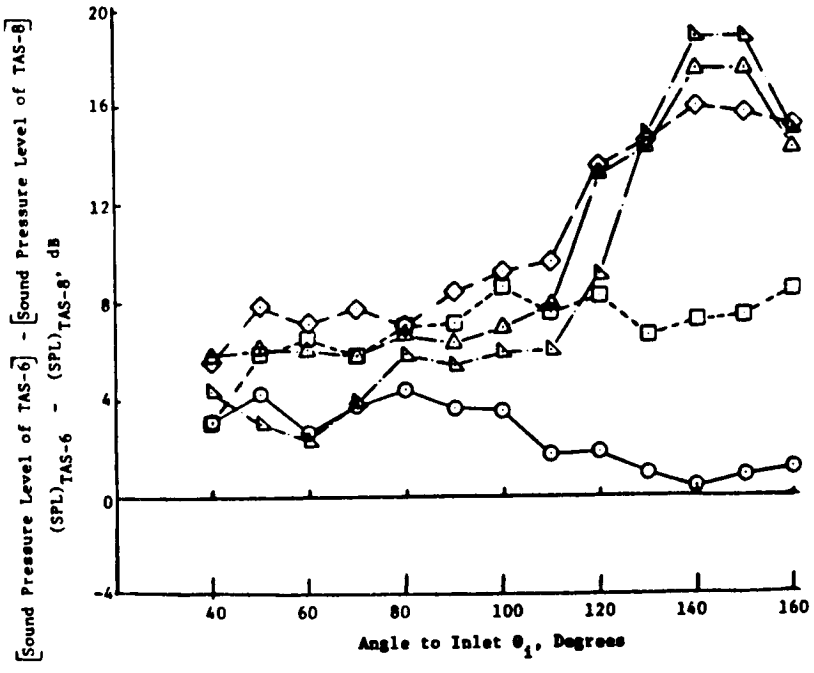

(b) Mechanically Suppressed

Figure 6. Influence of 180° Shield of 0.97 Inch Thickness on the Directivity of Various One-Third Octave Band Frequencies of Unsuppressed and Suppressed Annular Plug Nozzles at Approach Conditions.

The above relationship is based upon ray acoustics and assumes a plug flow model for the jets. The eddy convection Mach number, M_c, is calculated empirically using the correlations suggested in Reference 13 which follow:

$$M_c = \frac{1}{2}\left[0.55 + \frac{0.39}{V^s/V^o}\right]\frac{V^o}{a_{amb}} \qquad \text{(For unsuppressed nozzles)} \qquad (2)$$

$$M_c = \frac{1}{2}\left[0.4 + \frac{0.2}{V^s/V^o}\right]\frac{V^o}{a_{amb}} \qquad \text{(For mechanically suppressed nozzles)} \qquad (3)$$

Using the above equations, the critical angles for total reflection for the approach-power flow conditions for the unsuppressed and suppressed annular plug nozzles are calculated to be 117° and 122° respectively. The measured data confirm that, for $\theta_i > 120°$, the partial shield effectively suppresses the high-frequency waves that behave like acoustic rays. This implies that internal reflection is one of the dominant mechanisms at shallow angles to the jet axis. However, with nozzle jets having axially distributed sources, there is no abrupt onset of the noise cutoff mechanism for the high-frequency waves as implied by the acoustic ray concept of total internal reflection.

It can be seen from Figure 6 that for frequencies equal to or greater than 250 Hz, the noise in the front quadrant for both the unsuppressed and suppressed annular plug nozzles is reduced by the shield flow. This reduction in the front quadrant and at $\theta_i = 90°$ occurs because changes in the velocity and temperature gradients by the partial shield modify the sources. The partial shield reduces the velocity and temperature gradients of the core jet near the jet exit plane, thereby reducing the source strength of the eddies close to the exit plane. However, reducing the gradients of velocity by the shield results in lengthening of the jet in the axial direction, which in turn leads to more low-frequency jet noise.

The above analysis is repeated for a typical AST/VCE cutback cycle condition in Figure 7. The shield suppression characteristics in the aft quadrant for the unsuppressed annular plug nozzle for the cutback case (see Figure 7a) resemble those of the annular plug nozzle for the approach case, that is, as frequency increases so does the suppression; and the 4000 Hz frequency shows a peak suppression of about 22 dB at both $\theta_i = 150°$ and 160°. Compared to the approach case, the cutoff mechanism seems to set in rather abruptly. Also, noise reduction due to source modification is smaller in the front quadrant. Both of these observations indicate a reduced mixing of the shield and primary jets for the cutback case. In the case of the 32-chute suppressor at cutback (see Figure 7b), the 4000 Hz frequency yields about the same maximum value of suppression in the aft quadrant as in the approach case, namely, 19 dB. The 250 Hz and 500 Hz octave bands show amplification in the aft quadrant for the cutback case, unlike that at approach. The partial shield shows larger values

Sym.	Frequency, Hz
○	250
□	500
◇	1000
△	2000
◺	4000

A_T = 1400 In.^{2}

Static

Approach Cycle

Conf.	Test Point	Core Jet V°, fps	Core Jet T_T°, °R	Core Jet P_r°	Shield Jet V^{s}, fps	Shield Jet T_T^{s}, fps	Shield Jet P_r^{s}	Mixed Cond. V^{mix}, fps	Mixed Cond. T_T^{mix}, °R	Mixed Cond. P_r^{mix}
TAS-1	105	1851	1504	2.074	- - - -	NO SHIELD	- -	1851	1504	2.074
TAS-3	321	1852	1507	2.073	1112	1504	1.280	1649	1506	1.760

Conf.	Test Point	Core Jet V°, fps	Core Jet T_T°, °R	Core Jet P_r°	Shield Jet V^{s}, fps	Shield Jet T_T^{s}, fps	Shield Jet P_r^{s}	Mixed Cond. V^{mix}, fps	Mixed Cond. T_T^{mix}, °R	Mixed Cond. P_r^{mix}
TAS-6	605	1847	1508	2.061	- - - -	NO SHIELD	- -	1847	1508	2.061
TAS-8	821	1842	1491	2.072	1115	1495	1.284	1647	1492	1.768

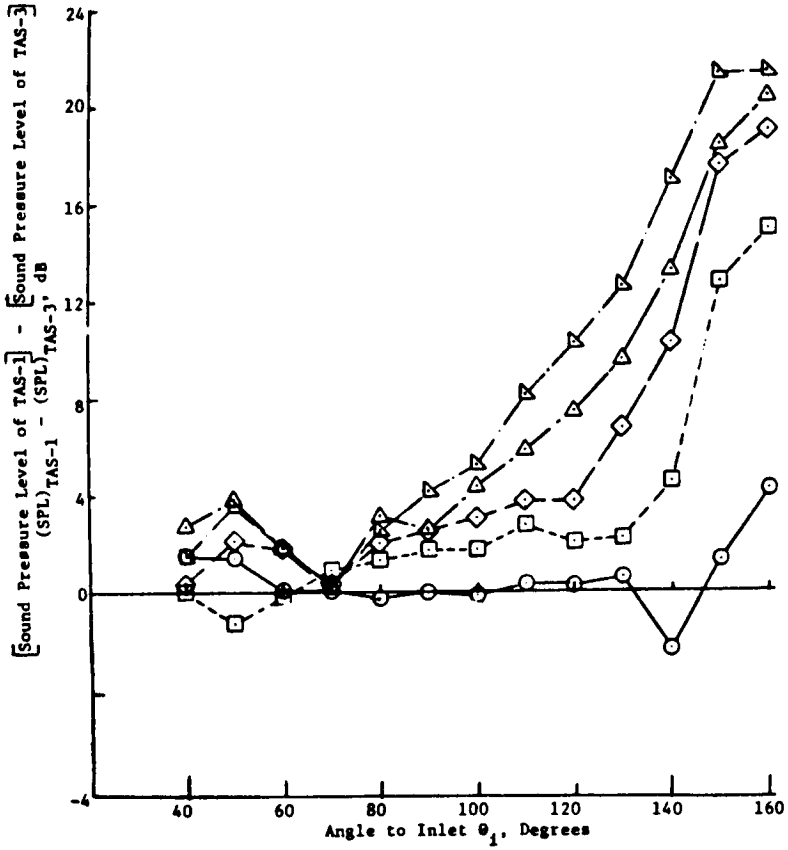

a) UNSUPPRESSED

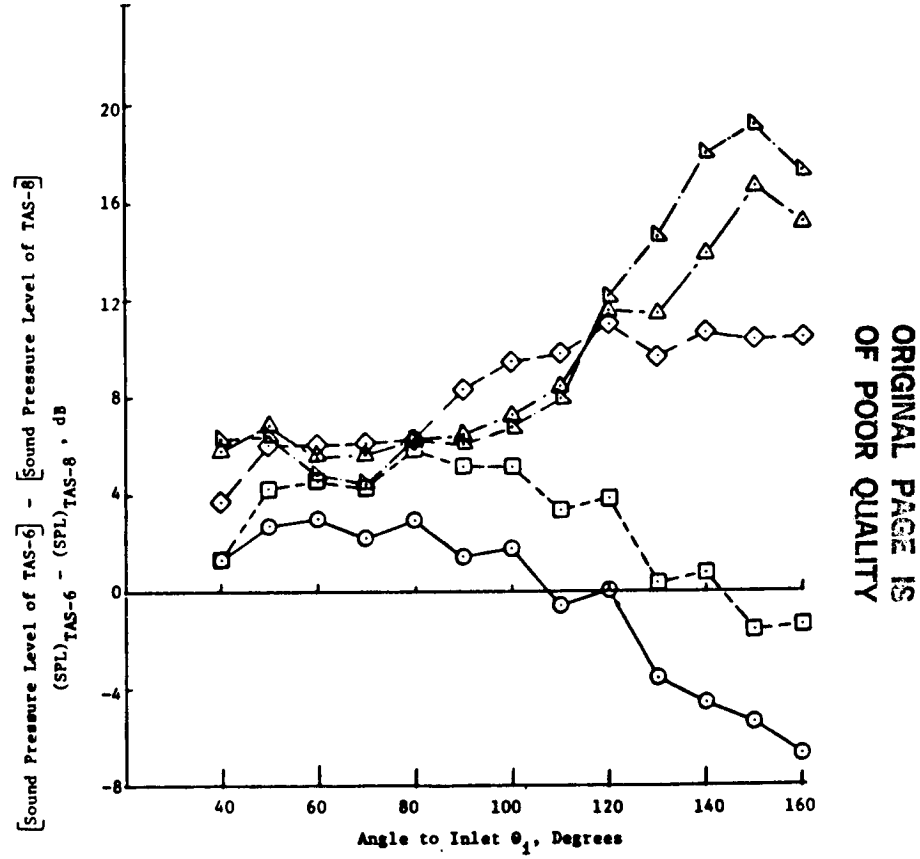

b) MECHANICALLY SUPPRESSED

Figure 7. Influence of 180° Shield of 2.5 cm (0.97 in) Thick on the Directivity of Various One-Third Octave Band Frequencies of Unsuppressed Annular Plug Nozzles at Cutback Condition.

of source reduction in the front quadrant for the suppressor nozzle. This is attributable to the differences in the mixing characteristics between the 32-chute suppressor and unsuppressed annular plug nozzles. For the 32-chute suppressor nozzle with the partial shield, only two of the higher frequencies examined (2000 Hz and 4000 Hz) show features of total reflection, whereas with the unsuppressed annular plug nozzle, all the frequencies considered except the lowest show features of total reflection in the aft quadrant. This suggests that source modification is more important for the 32 chute suppressor nozzle than for the unsuppressed annular plug nozzle with the partial thermal acoustic shield.

Figure 8 shows the influence of the partial TAS on the directivity of various one-third-octave-band frequencies, at a typical AST/VCE takeoff condition, for unsuppressed annular plug and 32 chute suppressor nozzles. The noise suppression features of the partial shield on the unsuppressed annular plug nozzle resemble those at the cutback condition. However, in the case of the 32-chute suppressor nozzle, only the 4000 Hz frequency shows features of total reflection, and source modification appears to be dominant at takeoff. There is considerable amplification of the 250 Hz and 500 Hz frequencies in the aft quadrant by the partial TAS for the 32-chute suppressor nozzle. Such amplifications at 250 and 500 Hz are not observed in the case of the unsuppressed annular plug nozzle. This is another indication of the different mixing features of the unsuppressed annular plug and the 32 chute suppressor nozzles with partial shields.

1.3 DUAL-FLOW STUDY

The dual-flow study was begun with objectives similar to those of the single-flow investigation. Detailed acoustics and diagnostic flow data were measured at typical VCE operating nozzle temperatures and pressure ratios in order to determine the effectiveness of thermal acoustic shields with coannular plug nozzles, and their possible application to advanced supersonic transports. A total of nine configurations (designated TAS-10 through TAS-12 and TAS-14 through TAS-19) employing dual-flow coannular primary nozzles were tested. The required shield jets were bled from the heated stream that supplied the flow to the outer annulus of the coannular nozzles and passed through different sets of choke plates to obtain selected shield-to-outer stream velocity ratios ($V_r^{s,o}$). The tested configurations are listed below.

Unsuppressed Configurations

TAS-10: Baseline unsuppressed Coannular Plug Nozzle

TAS-11: Unsuppressed Coannular Plug Nozzle with 180° Shield of 2.5 cm (0.97 inch) thickness and operated at $V_r^{s,o} = 0.64$*

* These ratios refer to typical takeoff conditions only.

Sym.	Frequency, Hz
○	250
□	500
◇	1000
△	2000
◺	4000

A_T = 1400 In.^{2}

Static

Approach Cycle

Conf.	Test Point	Core Jet V^o, fps	Core Jet T_T^o, °R,	Core Jet P_r^o	Shield Jet V^s, fps	Shield Jet T_T^s, fps	Shield Jet P_r^s	Mixed Cond. V^{mix}, fps	Mixed Cond. T_T^{mix}, °R	Mixed Cond. P_r^{mix}
TAS-1	109	2210	1631	2.693	- - - -	NO SHIELD	- -	2210	1631	2.693
TAS-3	325	2221	1644	2.700	1319	1642	1.379	1994	1643	2.178

Conf.	Test Point	Core Jet V^o, fps	Core Jet T_T^o, °R,	Core Jet P_r^o	Shield Jet V^s, fps	Shield Jet T_T^s, fps	Shield Jet P_r^s	Mixed Cond. V^{mix}, fps	Mixed Cond. T_T^{mix}, °R	Mixed Cond. P_r^{mix}
TAS-6	609	2234	1662	2.701	- - - -	NO SHIELD	- -	2234	1662	2.701
TAS-8	825	2211	1631	2.695	1323	1619	1.388	1990	1628	2.188

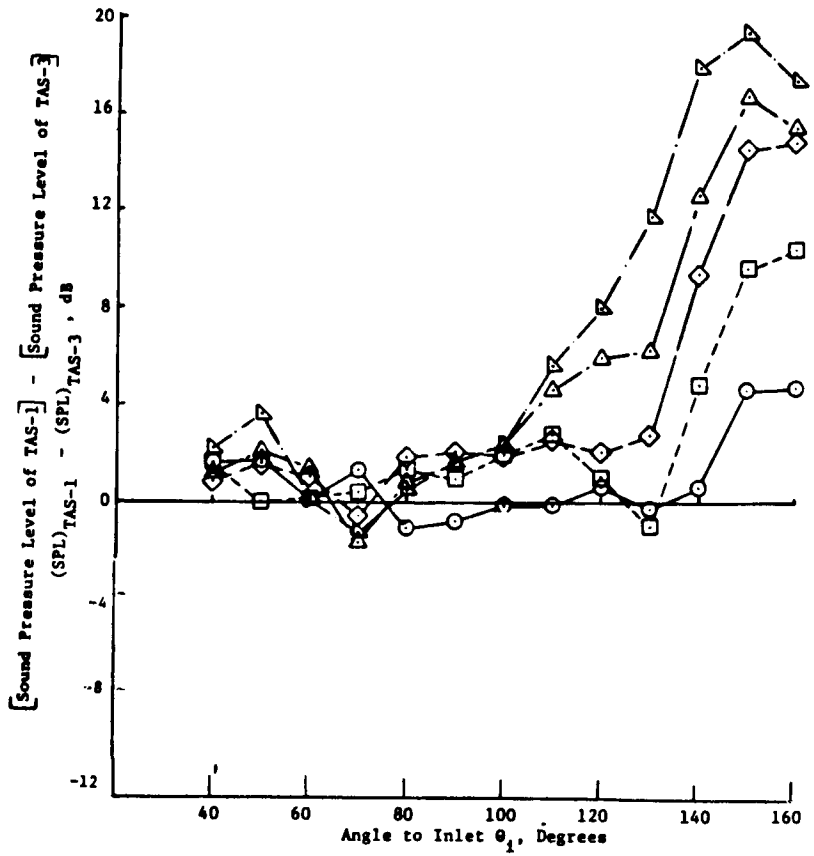

a) UNSUPPRESSED

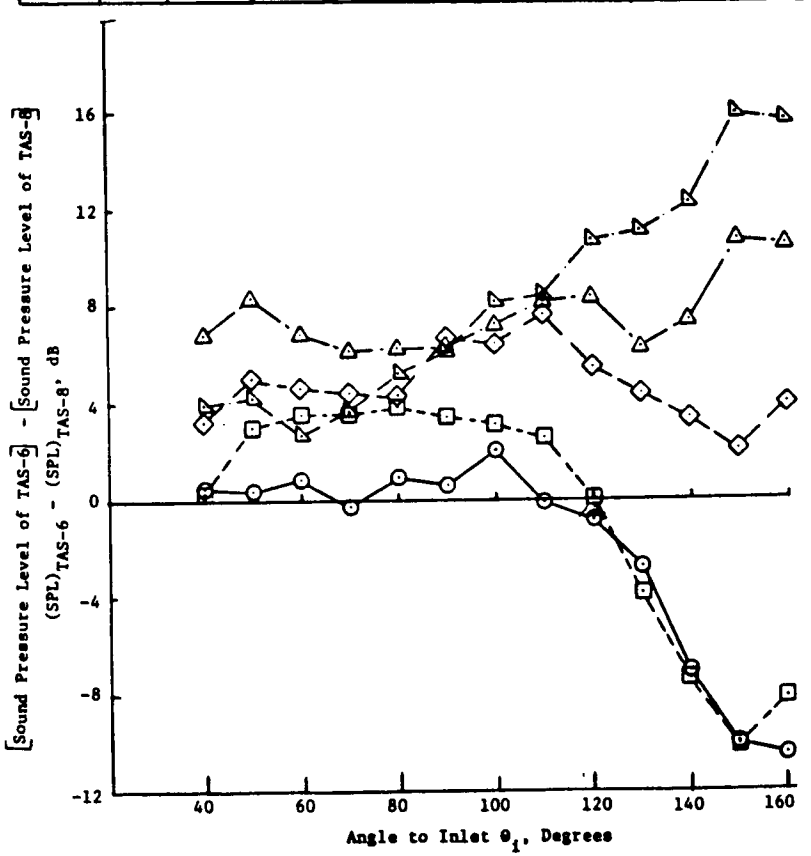

b) MECHANICALLY SUPPRESSED

Figure 8. Influence of 180° Shield of 2.5 cm (0.97 in) Thick on the Directivity of Various One-Third Octave Band Frequencies and Suppressed Annular Plug Nozzle at Takeoff Condition.

TAS-12: Unsuppressed Coannular Plug Nozzle with 180° Shield of 2.5 cm (0.97 inch) thickness and operated at $V_r^{s,o}$ = 0.83*

TAS-14: Unsuppressed Coannular Plug Nozzle with 360° Shield of 1.2 cm (0.5 inch) thickness and operated at $V_r^{s,o}$ = 0.83*

Mechanically Suppressed Configurations

TAS-15: Baseline Coannular Plug Nozzle with 20-Chute Outer Stream Suppressor

TAS-16: Coannular Plug Nozzle with 20-Chute Outer-Stream Suppressor and with 180° Shield of 2.5 cm (0.97 inch) thickness and operated at $V_r^{s,o}$ = 0.64*

TAS-17: Coannular Plug Nozzle with 20-Chute Outer Stream Suppressor and with 180° Shield of 2.5 cm (0.97 inch) thickness and operated at $V_r^{s,o}$ = 0.83*

TAS-18: Coannular Plug Nozzle with 20-Chute Outer-Stream Suppressor and with 180° Shield of 2.5 cm (0.97 inch) thickness and operated at $V_r^{s,o}$ = 0.48*

TAS-19: Coannular Plug Nozzle with 20-Chute Outer-Stream Suppressor and with 360° Shield of 1.3 cm (0.50 inch) thickness and operated at $V_r^{s,o}$ = 0.83*

A total of 136 acoustic test points were conducted with these configurations. During acoustic tests with configurations TAS-15 through TAS-18, static pressure data in the chute base region were measured in order to estimate the effect of shield stream on the suppressor base drag. Mean and turbulent velocity measurements were conducted on four different plumes using a laser velocimeter. Detailed descriptions of the model nozzle configurations, along with a brief description of the facility, are given in Section 2.0 of this report. The aerodynamic flow conditions of the acoustic and laser velocimeter test points are tabulated in Section 3.0.

Measured acoustic and diagnostic data are presented and discussed in Section 4.0. The objective is to demonstrate the benefit of thermal acoustic shields. Section 4.0 is divided into two major subsections that discuss the influence of the various thermal acoustic shields on the baseline unsuppressed, high-radius-ratio, coannular plug nozzle (TAS-10) and the baseline suppressed, coannular plug nozzle (TAS-15). Under each of the subsections, the acoustic characteristics of the baseline nozzle are presented and the effects of the partial shield (orientation and shield-to-outer stream velocity) and full shield are discussed. The relevant mean and turbulent velocity profiles measured with the partial shield are also presented. In addition, the subsection

* These ratios refer to typical takeoff conditions only.

on the suppressor nozzle characteristics contains base pressure data that describe the effect of the shield flow on the suppressor base drag.

The measured velocity data obtained using the unsuppressed coannular plug nozzle with the partial shield are compared with the corresponding predictions of a modified M*G*B model in Section 5.0. Details of the modifications to the model are described, and typical measured and predicted acoustic data comparisons that indicate similar trends in the acoustic suppression in the aft quadrant are presented.

2.0 TEST FACILITY AND SCALE-MODEL CONFIGURATIONS

All of the acoustic and diagnostic tests of this program were conducted in General Electric's Anechoic Free-Jet Facility at Evendale, Ohio. Brief descriptions of the facility, data acquisition and reduction procedures, and scale model test nozzles are presented in this section. Detailed descriptions of the facility and acoustic data acquisition, reduction, and flight transformation procedures are supplied in References 14 through 16.

2.1 ANECHOIC FREE-JET FACILITY

The facility, shown schematically in Figure 9, is a cylindrical chamber 13.1 meters (43 feet) in diameter and 21.95 meters (72 feet) high. The inner surfaces of the chamber are lined with anechoic wedges made of fiberglass wool to yield an absorption coefficient of 0.99 at frequencies above 220 Hz. Descriptions and results of the tests conducted to determine the acoustic characteristics of the anechoic chamber (such as inverse square law tests) and the mean velocity and turbulence intensity distributions in the free jet are presented in Reference 15.

The streams of heated air needed for a dual-flow arrangement are produced by two separate burners and flow through silencers and plenum chambers before entering the test nozzle. The tertiary air comes from a 250,000-scfm (50 inches water column static pressure) fan driven by a 3500-hp electric motor. The air from the tertiary fan is routed through a silencer plenum chamber and then discharged through the 1.2-m (4-foot) exhaust to simulate a free jet up to a Mach number of 0.41. Free-jet Mach number is varied by controlling the tertiary airflow rate with adjustable fan inlet vanes. The combined airflow is finally exhausted through a "T" stack situated directly over the nozzles in the ceiling of the chamber.

2.1.1 Aerodynamic Data Acquisition and Reduction

The facility operating parameters are monitored during testing at the control console to ensure that prescribed facility limits are not exceeded and to set the test-point conditions. The pressures associated with the two heated streams are measured with rakes located upstream of nozzle exits and are used for setting the desired nozzle pressure ratios. These parameters are also routed through the Dymec scanning system and recorded along with nozzle performance data by the aerodynamic data handling (ADH) system. Facility temperatures are monitored at the control console using a Doric multichannel temperature indicator. The unit has a 24 channel capability and is designed for use with Type K thermocouples (chromel-alumel). It is used for safety monitoring and setting test-point temperatures for the dual-flow system. A system schematic is shown in Figure 10.

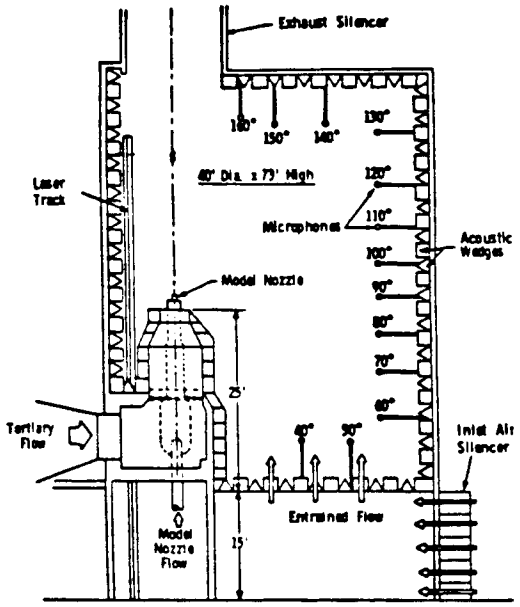

Angle (Degrees)	Radial Distance r	Radial Distance r/t
40	7.92	26.0
50	9.48	31.1
60	9.50	31.18
70	8.76	28.73
80	8.36	27.42
90	8.23	27.00
100	8.36	27.42
110	8.76	28.73
120	9.5	31.18
130	10.74	35.25
140	9.17	30.17
150	8.23	27.0
160	7.92	26.0

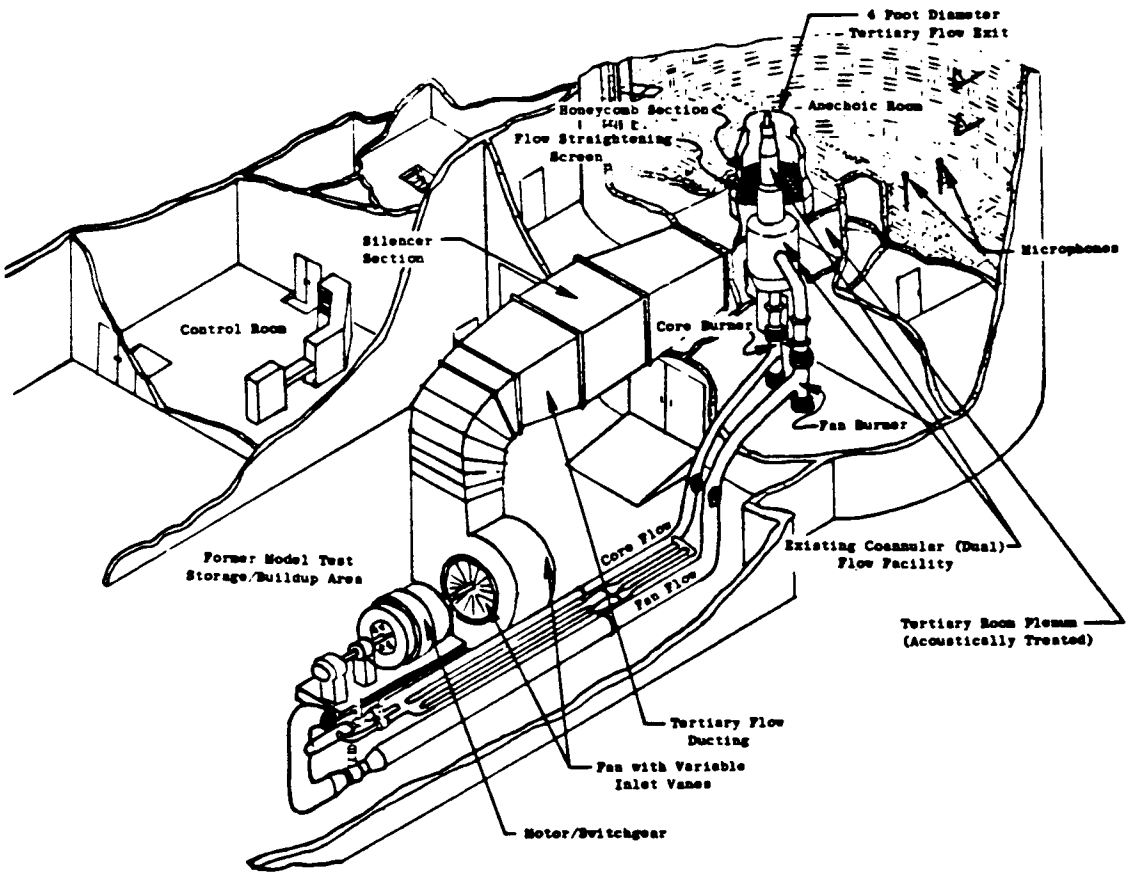

Figure 9. Anechoic Free-Jet/Jet Noise Facility Schematic.

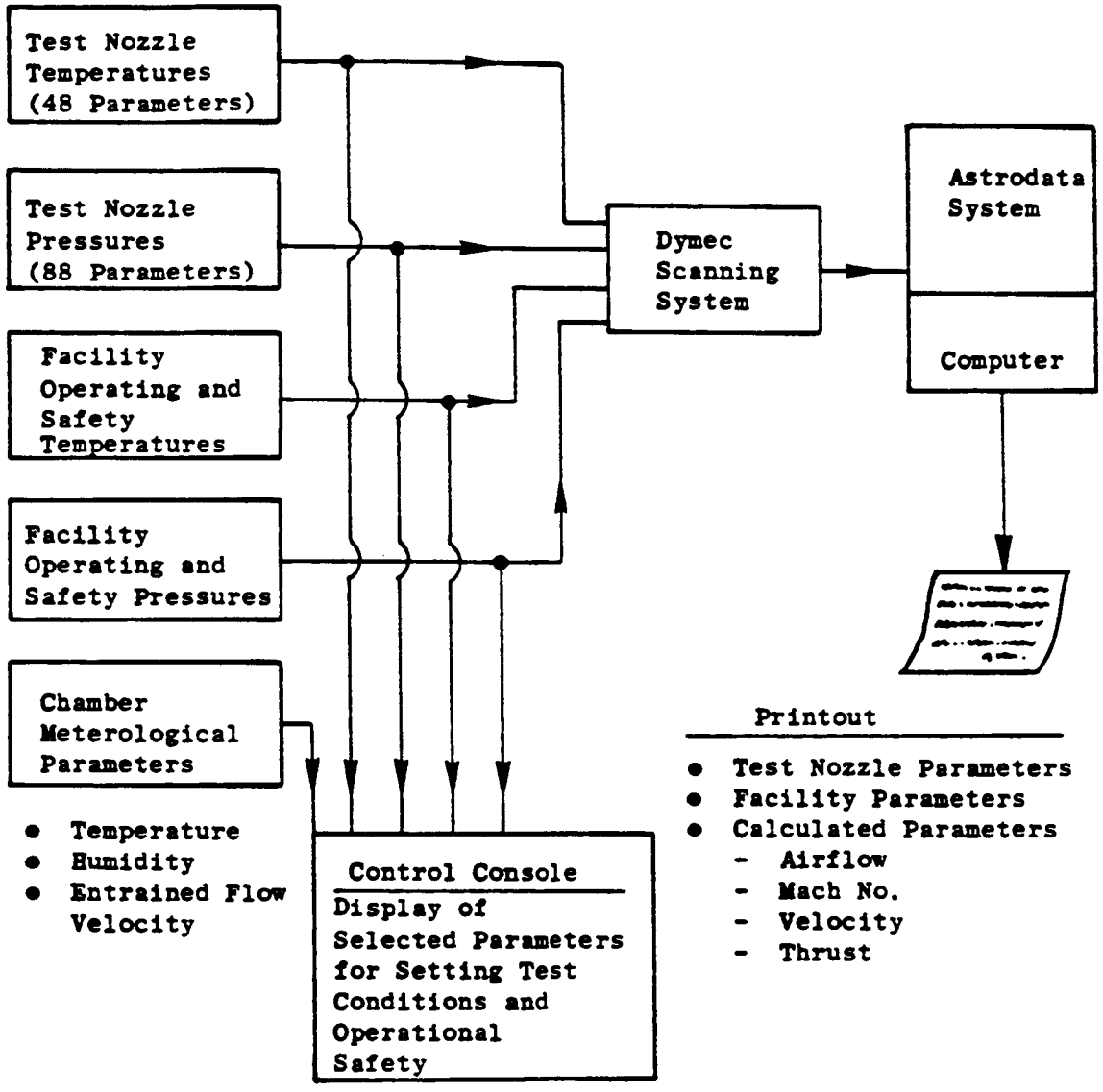

Figure 10. General Electric Anechoic Chamber Aerodynamic Data Processing System.

Special multielement rakes have been installed to measure aerodynamic flow parameters of the dual flow streams. They employ four individual rakes, two in each stream, each having three pressure and three temperature elements positioned at the centers of six equal area annular segments of the flow stream. These rakes use shielded Type K chromel-alumel thermocouples which have a recovery factor very close to unity. Pressure measurement accuracy is limited by the accuracy of the transducer used for the measurement. The scanivalve transducers that are used are rated 0.1% of full-scale range.

Aerodynamic flow parameters are calculated from the acquired temperature and pressure information. The input information for nozzle performance consists of ambient pressure (P_{amb}), nozzle discharge total temperature (T_T), and nozzle total pressure (P_T). For the case of tertiary flow, similar parameters are measured. Output of the processing program consists of tabulations of the individual input parameters with their identification, averages of similar parameters (for example, P_T rake average), and calculated parameters such as flow rates, Mach number, ideal velocity, and ideal thrust.

2.1.2 Acoustic Data Acquisition and Reduction

A flow chart of the acoustic data acquisition and reduction system is shown in Figure 11. This system has been optimized to obtain the acoustic data up to the 80 kHz 1/3-octave-band center frequency. B&K 4135, 0.64-cm condenser microphones with the microphone grid caps removed to obtain the best frequency response are used to gather 80 kHz data. The cathode followers used in the chamber are transistorized B&K 2619 with B&K 2801 power supply systems operated in the direct mode. The output of the microphone system is connected to a line driver that adds 10 dB of amplification to the signal as well as adding "preemphasis" to the high frequency portion of the spectrum. The net effect of this amplifier is a 10 dB gain at all frequencies, plus an additional 3 db at 40 kHz and 6 dB at 80 kHz from preemphasis. This increases the ability to measure low amplitude, high frequency data. In order to remove low frequency noise, high pass filters, with attenuations of approximately 26 dB at 12.5 Hz decreasing to 0 dB at 200 Hz, are installed in the system.

The tape recorder amplifiers have a variable gain from -10 dB to +60 dB in 10 dB steps and are able to trim gain in order to normalize incoming signals. High-pass filters incorporated into the acoustic data acquisition systems enhance high frequency data previously lost in the tape recorder electronic noise floor for microphones from 110° to 160°. The microphone signal below the 20-Hz 1/3-octave band is filtered out, and the gain is increased to boost the "signal-to-noise" ratio of the remaining high frequency signal. For microphones from 110° to 160°, both the filtered and unfiltered signals are recorded on tape. The sound pressure levels for frequencies below 20 kHz are calculated using the unfiltered signal; above 20 kHz the filtered signal is used. The final jet noise spectrum at a given angle is obtained by computationally merging these two spectra.

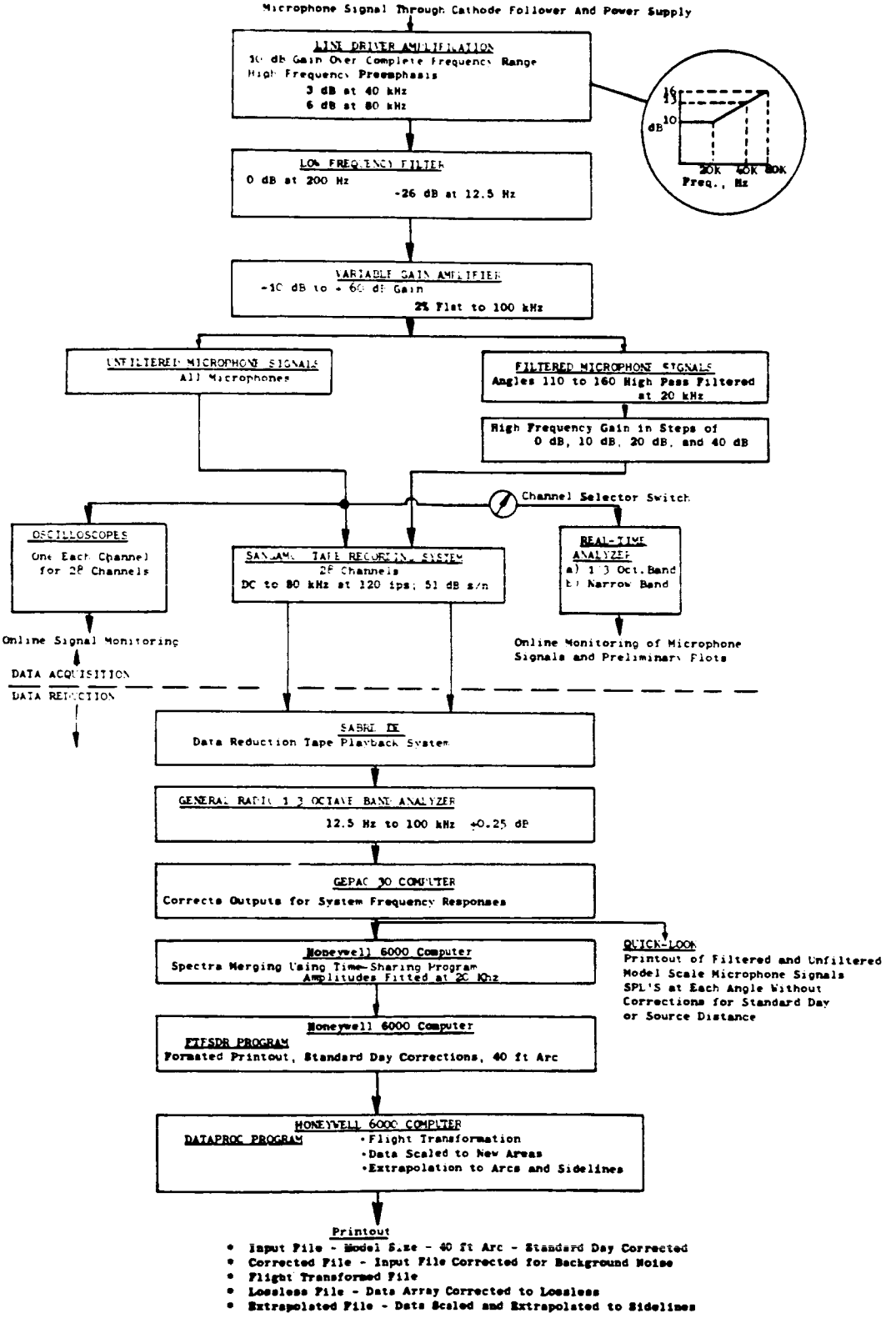

Figure 11. Acoustic Data Acquisition and Reduction System.

The main system for recording acoustic data is a Sangamo/Sabre IV 28-track FM recorder. The system is set up for wide band Group I (intermediate band double extended) at 120-ips tape speed. Operating at 120-ips tape speed extends the dynamic range to that needed to get the high frequency/low amplitude portion of the acoustic signal. The tape recorder is set up for ±40% carrier deviation with a recording level of 8 volts peak-to-peak. During recording, the signal gain is adjusted to maximum without exceeding the 8 volt peak-to-peak level.

Individual monitor scopes are used to observe signal characteristics during operation. On-line data is monitored through a Rockland narrow band analyzer and a spectral Dynamics SD345 analyzer with outputs presented on display scopes and hard copy equipment.

Standard data reduction is conducted in the General Electric AEBG Instrumentation Data Room (IDR). The analog data tapes are played back on a CDC-3700B tape deck with electronics that can reproduce signal characteristics within the specifications indicated for wide band Groups I and II. An automatic shuttling control is incorporated into the system. In normal operation, a tone is inserted on the recorder at the time slot designated for data analysis. Tape control automatically shuttles the tape, sending an integration start signal to the analyzer at the tone as the tape moves forward. The motion continues until an "integration complete" is received from the analyzer, at which time the tape direction is reversed. The tape restarts at the tone, advancing forward to the next channel to be analyzed, until all the channels have been processed. A time code generator is also used to signal the tap position of the readings as directed by the computer program control. After each total reading is completed, the number of the tape channel at each point is advanced to the next reading.

All 1/3-octave analyses are performed on a General Radio 1921 1/3-octave analyzer. Normal integration time is set for 16 seconds to ensure good interaction for the low frequency content. The analyzer has 1/3-octave filter sets from 12.5 Hz to 100 kHz and has a rated accuracy of ±1/4 dB in each band. Each data channel passes through an interface to the INTERDATA computer. Here the data are corrected for the frequency response of the microphones and are also corrected to standard day (15° C or 59° F, 70% RH) atmospheric attenuation conditions using the Shields and Bass model (Reference 17). They are then processed to calculate the perceived noise level and OASPL from the spectra. For calculation of the acoustic power, scaling to other nozzle sizes, or extrapolation to different far-field distances, the data are sent to the Honeywell 6000 computer for processing. The SPL's are transmitted through a direct time-sharing link to the 6000 computer through a 1200 baud modem. In the 6000 computer, the data are processed through the Flight-Transformed Full-Scale Data Reduction (FTFSDR) program where the appropriate calculations are made. The data are printed out on a high-speed remote terminal.

The detailed data processing flow chart is shown in Figure 12. The as-measured data are first extrapolated from the measured distance to a common

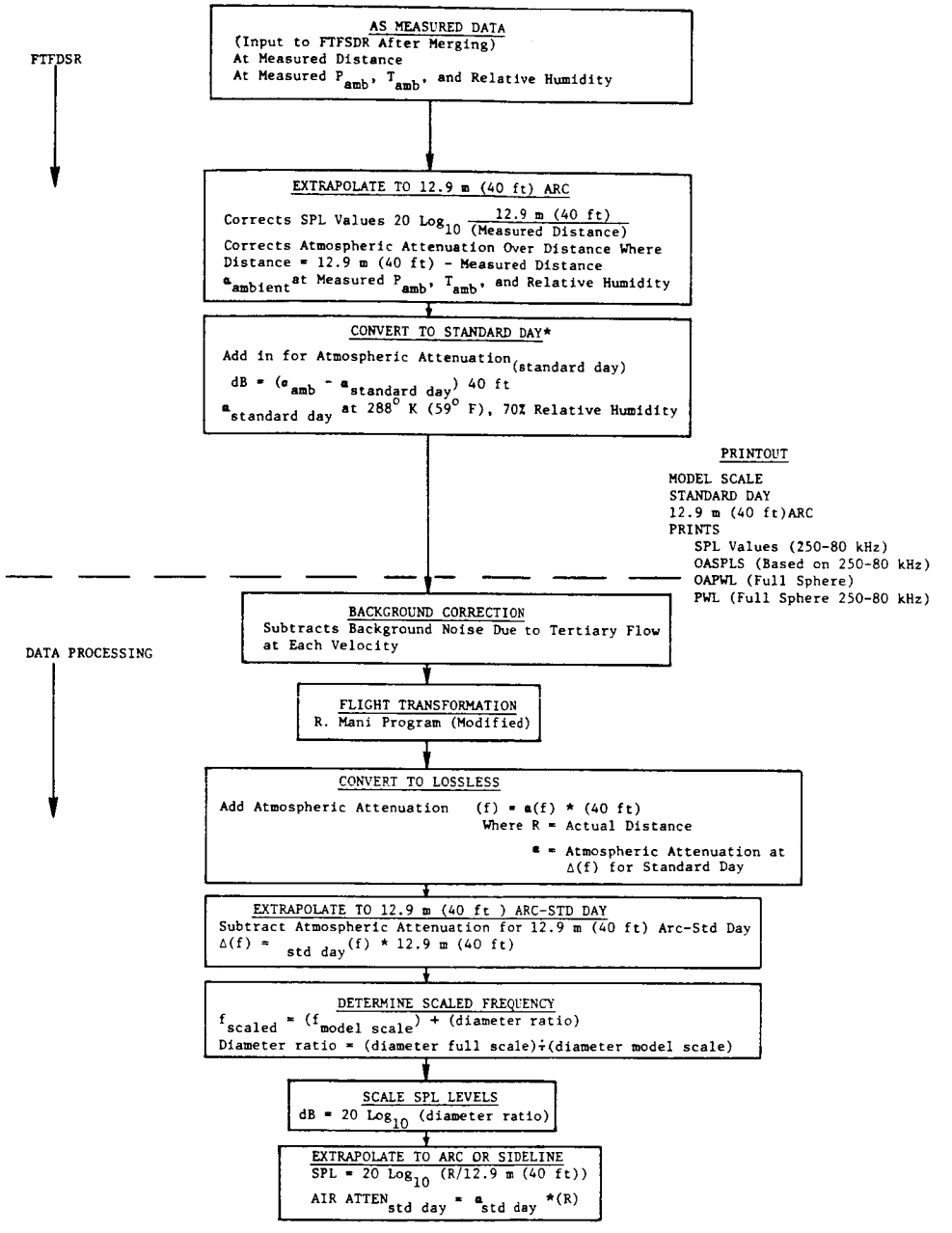

Figure 12. Acoustic Data Flow Chart.

12.3 meter (40 foot) arc. This is accomplished by subtracting both the distance correction [that is, 20 log (40 foot distance/measured distance)] and the atmospheric attenuation correction over the Δ distance (that is, where Δ distance = 40 feet - measured distance). The Shields and Bass Pure Tone Method (Reference 17) is used for all atmospheric attenuation corrections. The data are then converted to standard day at the 12.3 meter (40-foot) arc location by adding in the standard day correction. The data are tabulated for SPL, OASPL, and PWL (for full sphere and based on the lossless data). For this program, scale model data below the chamber cutoff frequency of 220 Hz are ignored. Next, the scale model data are corrected for background noise using the background noise spectra obtained from the tertiary jet at the chosen simulated flight velocity. The corrected scale model data are next processed through the flight transformation procedure to obtain data representative of the noise produced in actual flight.

2.2 LASER VELOCIMETER SYSTEM

The concept of using a Laser Velocimeter to get the mean and turbulent velocity profiles may be described as follows. Two beams of monochromatic light intersect at a point in space and set up a fringe pattern of known spacing. The flow is seeded with small particles which pass through the measuring volume. The light scattered from the particles is collected, and the laser signal processor measures the time it takes for the particles to pass through each fringe. Knowing the distance and time for each validated particle enables the construction of the histogram. Then by statistical techniques the mean value (which corresponds to the mean velocity) and the standard deviation (which corresponds to the turbulent velocity) are constructed.

2.2.1 General Arrangement

The laser velocimeter (LV) used during this program is a system developed under a USAF/DOT-sponsored program and reported in detail in Reference 18. The basic optics system is a differential Doppler, backscatter, single-package arrangement of proven ruggedness. Figure 13 shows a photograph of the LV system in the General Electric Anechoic Test Facility. The dimensions of the control volume are 0.636 cm (0.25 inch) for the major axis and 0.518 cm (0.020 inch) for the minor axes. The range of the LV control volume from the laser hardware is 2.16 m (85.0 inches). The three steering mirrors and the beam splitter are mounted on adjustable supports made of the same aluminum alloy to eliminate temperature-alignment problems. The LV is mounted on a platform that is capable of remote actuation in the vertical and horizontal planes.

The flow is seeded with titanium dioxide powder of nominal 1-micron diameter in the supply air to the burner and at the region of the nozzle to seed the entrained air. The powder-feeder equipment used is as described in Reference 18, except that the fluidized bed column supply air is heated to about 394.1 K (250° F) to prevent powder aggregation by moisture absorption.

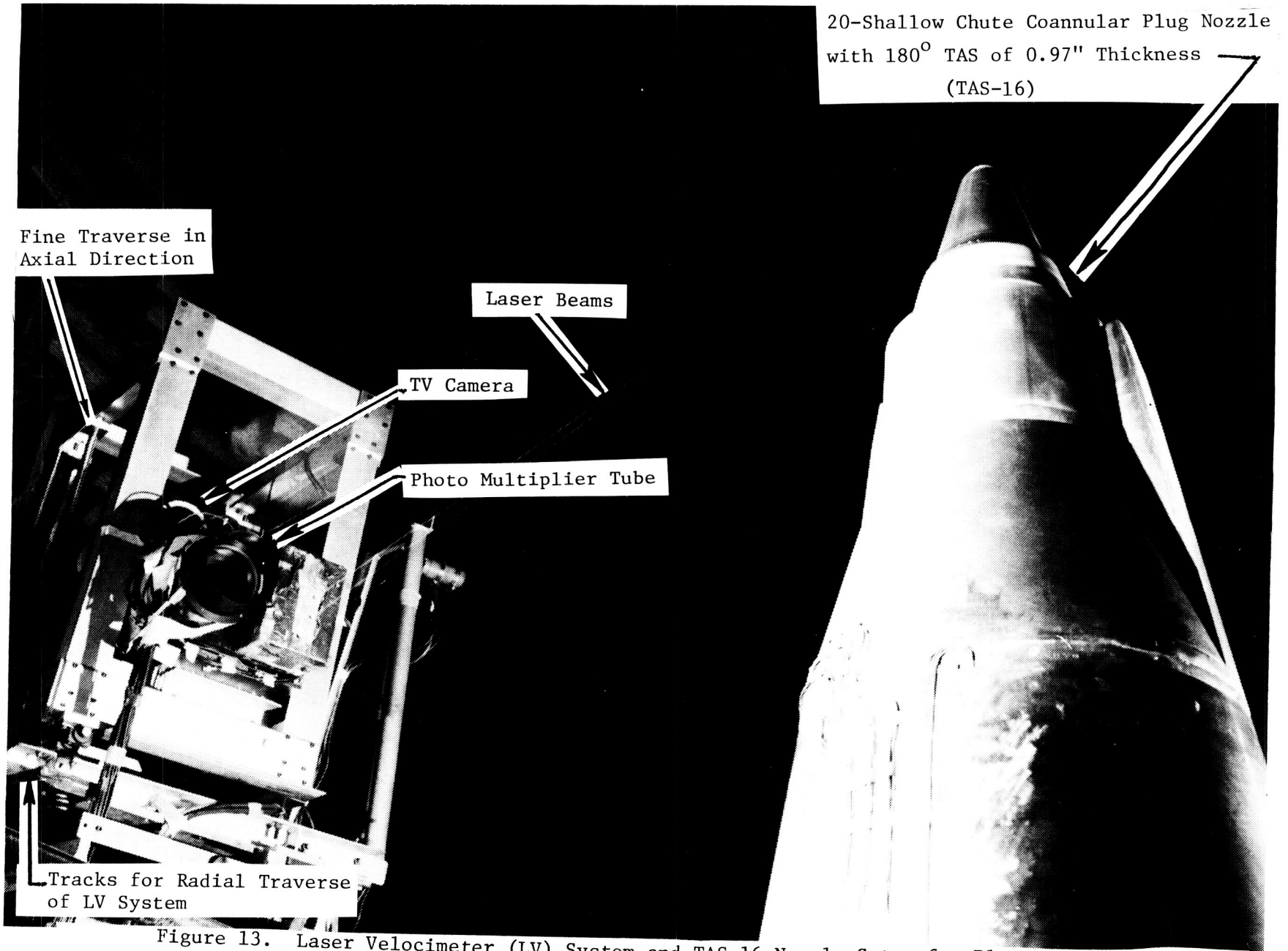

Figure 13. Laser Velocimeter (LV) System and TAS-16 Nozzle Setup for Plume Survey in Anechoic Jet Noise Facility.

2.2.2 Signal Processing and Data Reduction

The LV signal processor used is a direct-counter (time-domain) type similar to that reported in References 18 and 19, but with improvements that lower the rate of false validations and sharpen linearity and resolution. Turbulent-velocity probability distributions (histograms) are recorded by an NS633 pulse-height, 256-channel analyzer. All the data acquired from the laser unit are transmitted to a minicomputer system which stores the data on diskettes and performs all the necessary data reduction functions.

A histogram is an estimate of the first-order probability density of the amplitude of a given sample. To obtain a velocity histogram, the time-dependent LV velocity, V(t), is accumulated and divided into classes bounded by values of velocity increments V_i. For each independent sample of velocity, a class interval is formed such that $V_i \leq V(t) \leq V_{i+1}$. During a measurement period, K_i number of velocity samples are accumulated in each sample class V_i. From the total sample of measured velocity points, the histogram is constructed. The mean and turbulent velocities are derived from the histogram as follows:

Mean Velocity

The mean velocity of the jet, $\bar{V}$, obtained from the discrete velocity sample is calculated by:

$$\bar{V} = \sum_{\substack{\text{All Class} \\ \text{Intervals}}} \left(\frac{V_{i+1} + V_i}{2} \right) \frac{k_i}{N} \qquad (4)$$

where

$\frac{V_{i+1} + V_1}{2}$ is the value of the sampled axial velocity component at center of the class interval

k_i is the number of velocity samples in the class interval

N is the total number of velocity samples ($= \Sigma k_i$) in the histogram

Turbulent Velocity

To obtain the turbulent velocity, V', from the sampled data contained in the histogram, the standard square root of the statistical variance is performed. This is calculated using the following equation:

$$V' = \sum_{\substack{\text{All Class} \\ \text{Velocities}}} \left[\left(\frac{\frac{V_{i+1} + V_i}{2} - \bar{V}}{N} \right)^2 k_i \right]^{1/2} \qquad (5)$$

In addition to the above described stationary mode of LV operation for the determination of mean and turbulent velocities at discrete points, the LV can be operated in a traversing mode to obtain continuous profiles of mean velocities. These traverses are possible along any of the three LV axes. During these traverses, the data describing the velocity levels and the location of the measurement volume are recorded continuously on an X-Y plotter. The traversing speeds are adjusted and traverses are repeated to well define mean velocity profiles. While exact sampling rates during these traverses are not recorded in any way, it is felt that an estimated rate of approximately 100 samples per centimeter (250 samples per inch) of traverse is needed for a well-defined, smooth profile.

The LV software has been modified recently to allow mean velocity data to be obtained during any of the traverses from minihistograms in the form of plots of mean velocity data points as a function of traverse location. During the current program, the mean velocity data measured with the minihistograms have been obtained from the acceptable data samples set to 20. This number of acceptable samples yields an estimated 5% error in the LV mean velocity measurements with a statistical 95% confidence level for a given turbulent velocity ratio ($V'/\bar{V}$) of 10%.

Mean velocity traces obtained during typical axial and radial traverses are provided in Figure 14. In addition to the traverse mode of LV operation, point histograms were taken at given locations along most of the traverses in order to acquire both turbulent and mean velocity data. In this stationary mode of LV operation, the number of acceptable samples is set to 1,000. This number of data samples yields an estimated 5% error in the turbulent velocity and less than 1% error in the measured mean velocity. The mean velocities so measured at fixed locations along the traverses of Figure 14 are presented also in this figure. An examination of the data indicates that the mean velocities measured with minihistograms and point histograms are in good agreement and the mean velocity profiles obtained from minihistograms are adequate.

2.3 SCALE-MODEL NOZZLES

The principal objective of this study was to develop a technology base for a thermal acoustic shield (TAS) concept for Advanced Supersonic Technology/Variable Cycle Engine (AST/VCE) application by experimentally evaluating the influence of selected geometric and aerodynamic flow variables and of simulated flight on the acoustic behavior of unsuppressed and mechanically suppressed coannular plug nozzles with thermal acoustic shield. Earlier

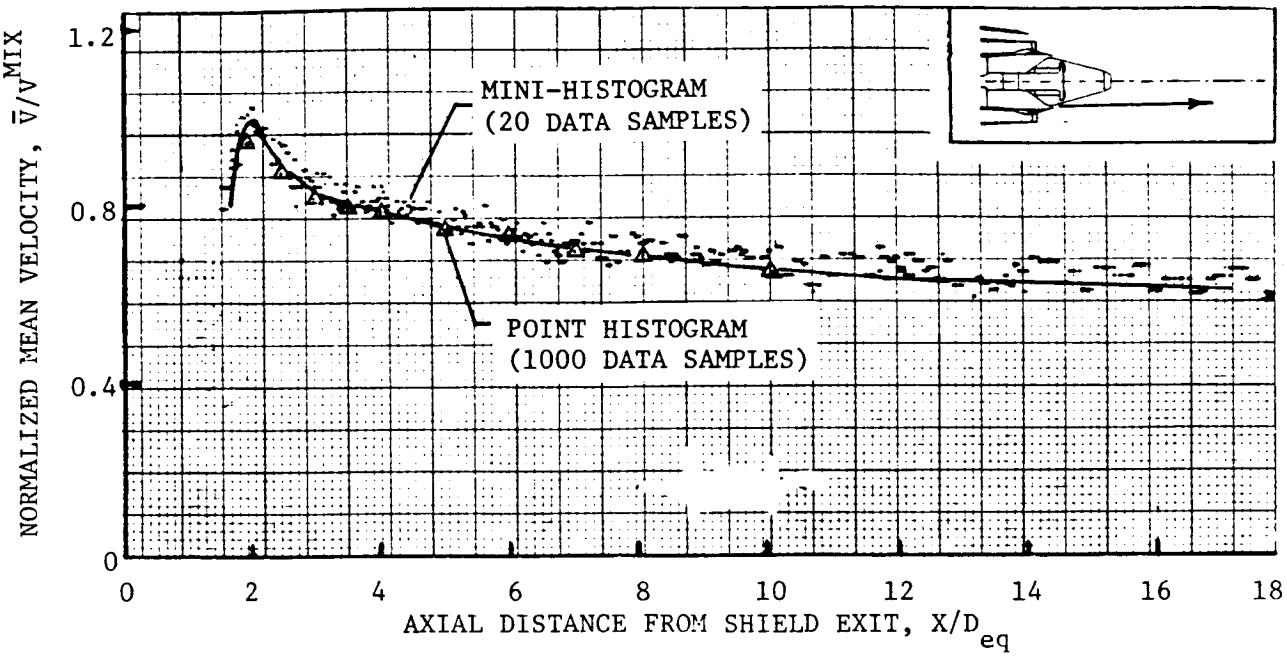

a) Typical Axial Velocity Profile.

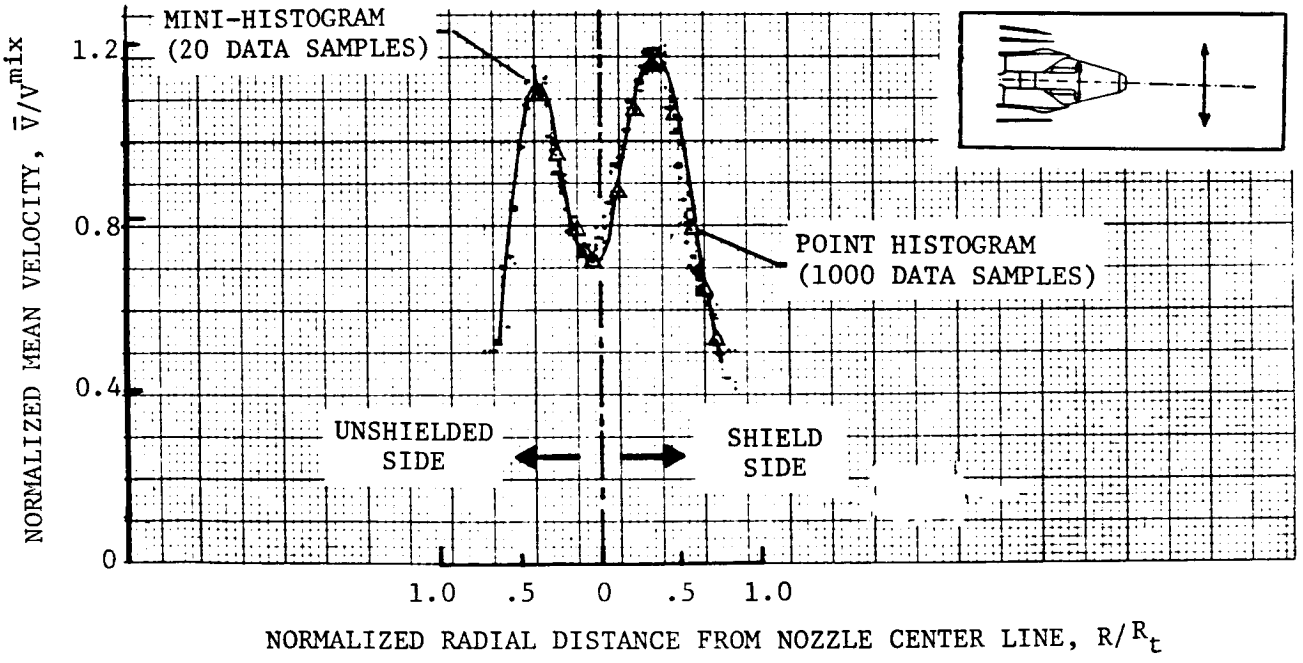

b) Typical Radial Velocity Profile.

Figure 14. Comparison of Velocity Data Obtained with Minihistograms and Point Histograms During Typical Axial and Radial Traverses.

investigation (Reference 12) within this contract looked into application of thermal acoustic shields to unsuppressed and mechanically suppressed annular plug nozzles.

Nine configurations were designed and fabricated to meet the objectives of this dual-flow thermal acoustic shield phase of this program. Four of these configurations have an unsuppressed coannular plug nozzle and the remaining five have a coannular plug nozzle with a 20-chute outer-stream suppressor. The nine configurations are described below:

Unsuppressed Coannular Configurations

TAS-10: Baseline Unsuppressed Coannular Plug Nozzle, Figure 15.

TAS-11: Unsuppressed Coannular Plug Nozzle with 180° Shield of 2.46 cm (0.97 inch) thickness and operated at $V_I^{s,o}$ = 0.64, Figures 16, 17, and 18.

TAS-12: Unsuppressed Coannular Plug Nozzle with 180° Shield of 2.46 cm (0.97) inch thickness and operated at $V_I^{s,o}$ = 0.83, Figures 16, 17, and 18.

TAS-14: Unsuppressed Coannular Plug Nozzle with 360° Shield of 1.27 cm (0.50 inch) thickness and operated at $V_I^{o,s}$ = 0.83, Figure 19.

Mechanically Suppressed Coannular Configurations

TAS-15: Baseline Coannular Plug Nozzle with 20-Chute Outer-Stream Suppressor, Figures 20 and 21.

TAS-16: Coannular Plug Nozzle with 20-Chute Outer-Stream Suppressor and with 180° Shield of 2.5 cm (0.97 inch) thickness and operated at $V_I^{s,o}$ = 0.64, Figure 22.

TAS-17: Coannular Plug Nozzle with 20-Chute Outer-Stream Suppressor and with 180° Shield of 2.5 cm (0.97 inch) thickness and operated at $V_I^{s,o}$ = 0.83, Figure 22

TAS-18: Coannular Plug Nozzle with 20-Chute Outer-Stream Suppressor and with 180° Shield of 2.5 cm (0.97 inch) thickness and operated at $V_I^{s,o}$ = 0.48, Figure 22.

TAS-19: Coannular Plug Nozzle with 20-Chute Outer-Stream Suppressor and with 360° Shield of 1.3 cm (0.50 inch) thickness and operated at $V_I^{s,o}$ = 0.83, Figure 23.

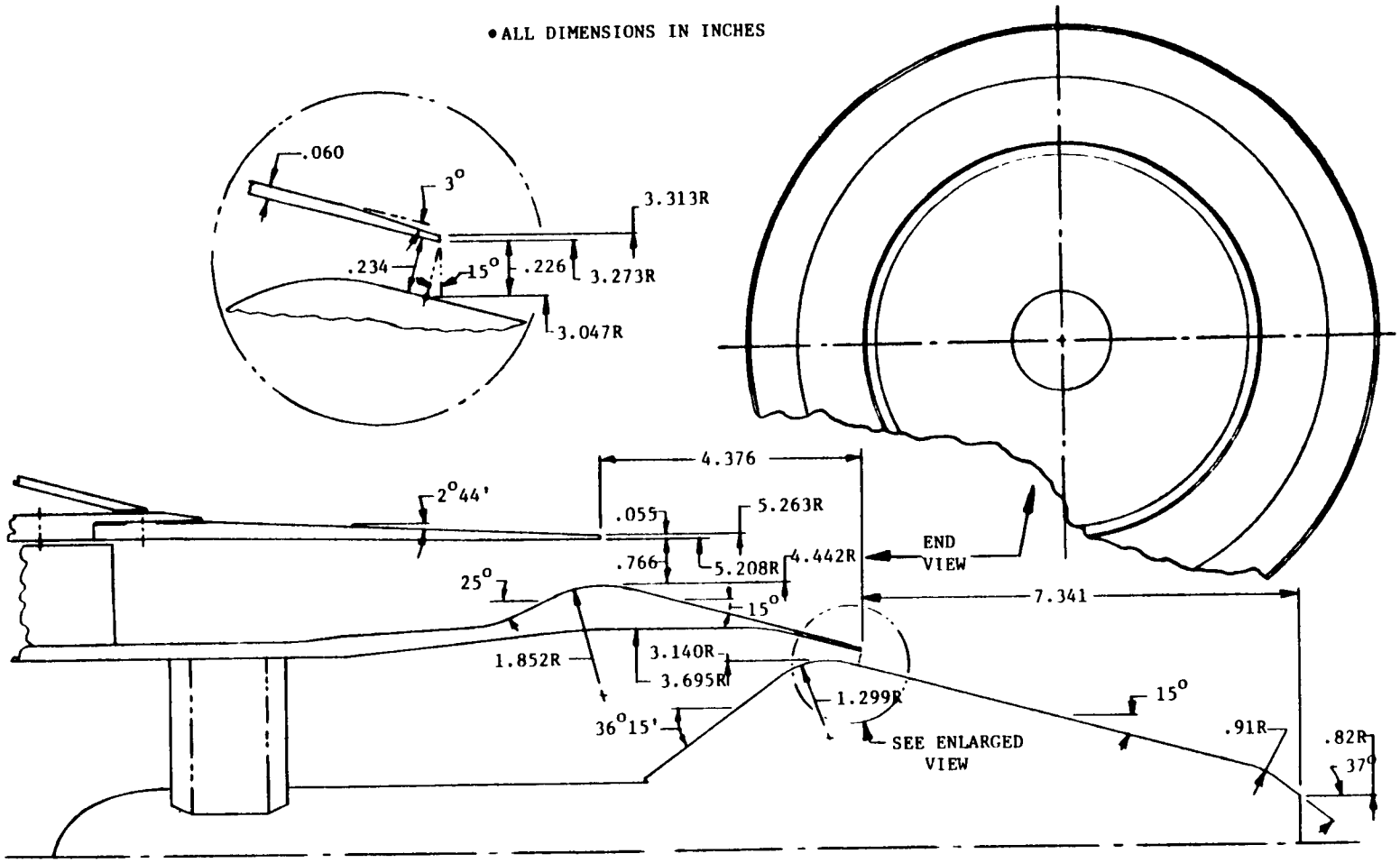

Figure 15. Schematic of Baseline Unsuppressed Coannular Plug Nozzle, Configuration TAS-10.

- All dimensions in inches
- Otherwise same as in Figure 15

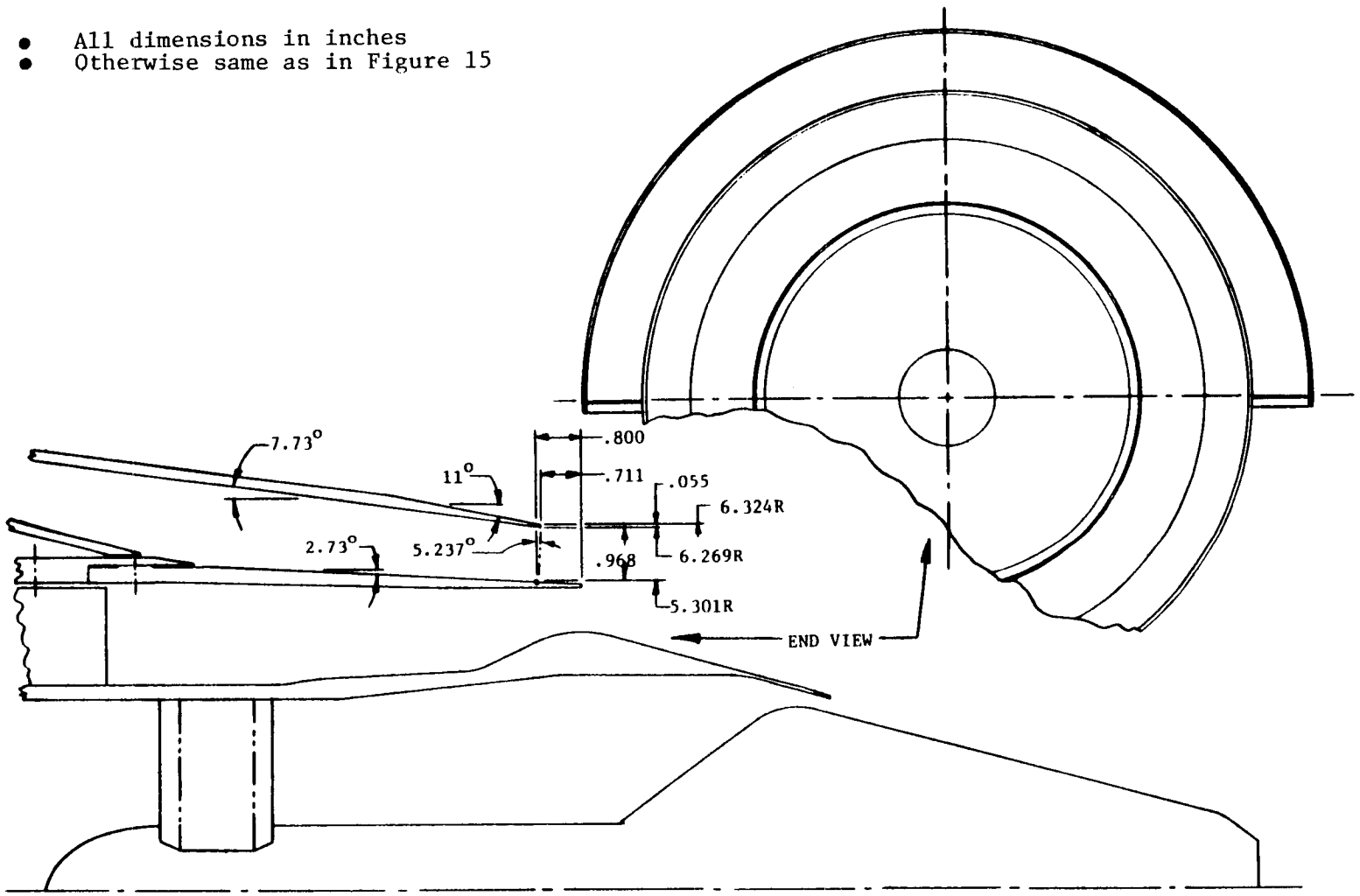

Figure 16. Schematic of Unsuppressed Coannular Plug Nozzle with 180° Shield, Configurations TAS-11 and TAS-12.

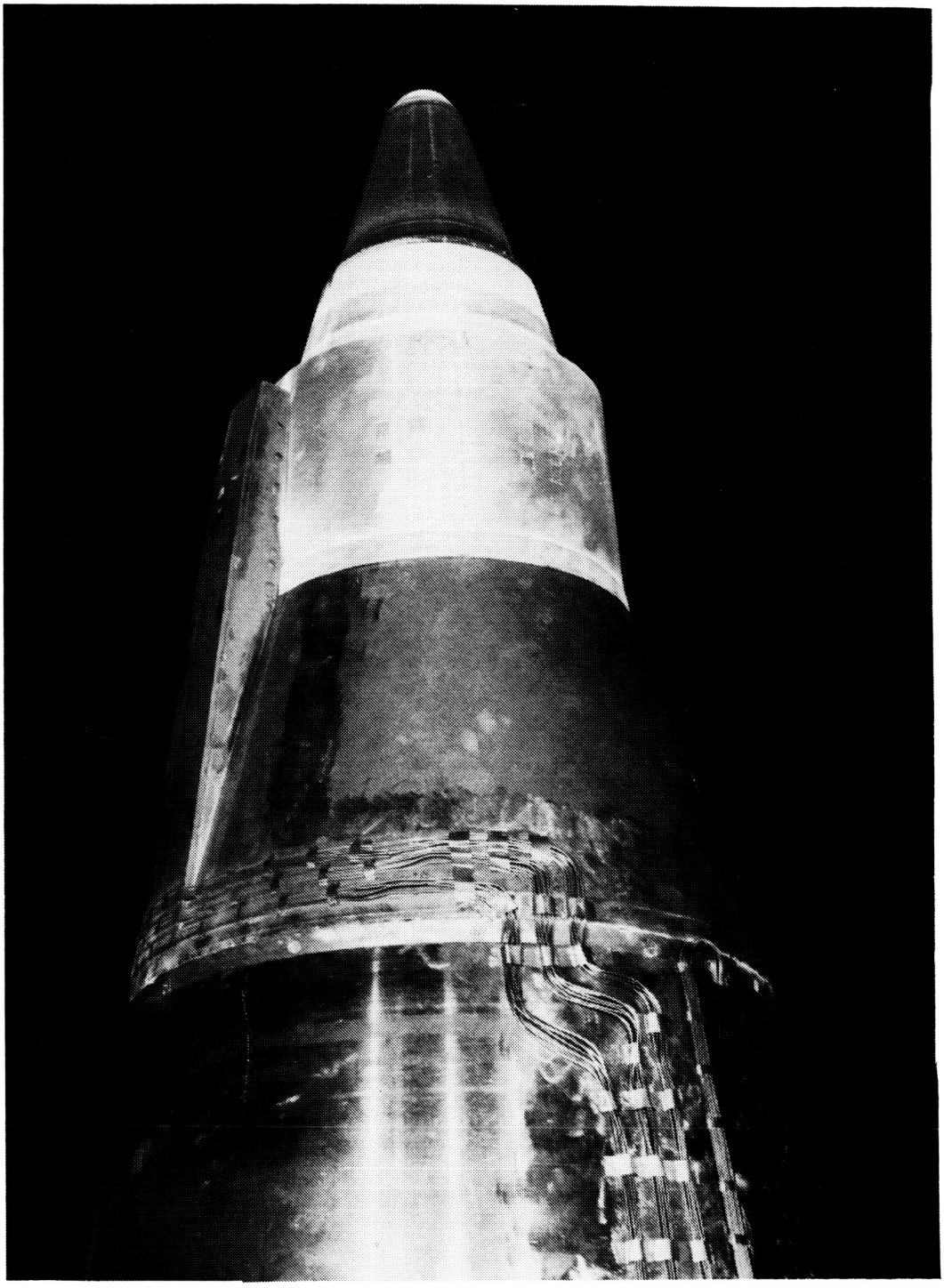

Figure 17. Unsuppressed Coannular Plug Nozzle with 180° Shield in Anechoic Test Facility, Configuration TAS-11 and TAS-12.

ORIGINAL PAGE IS
OF POOR QUALITY

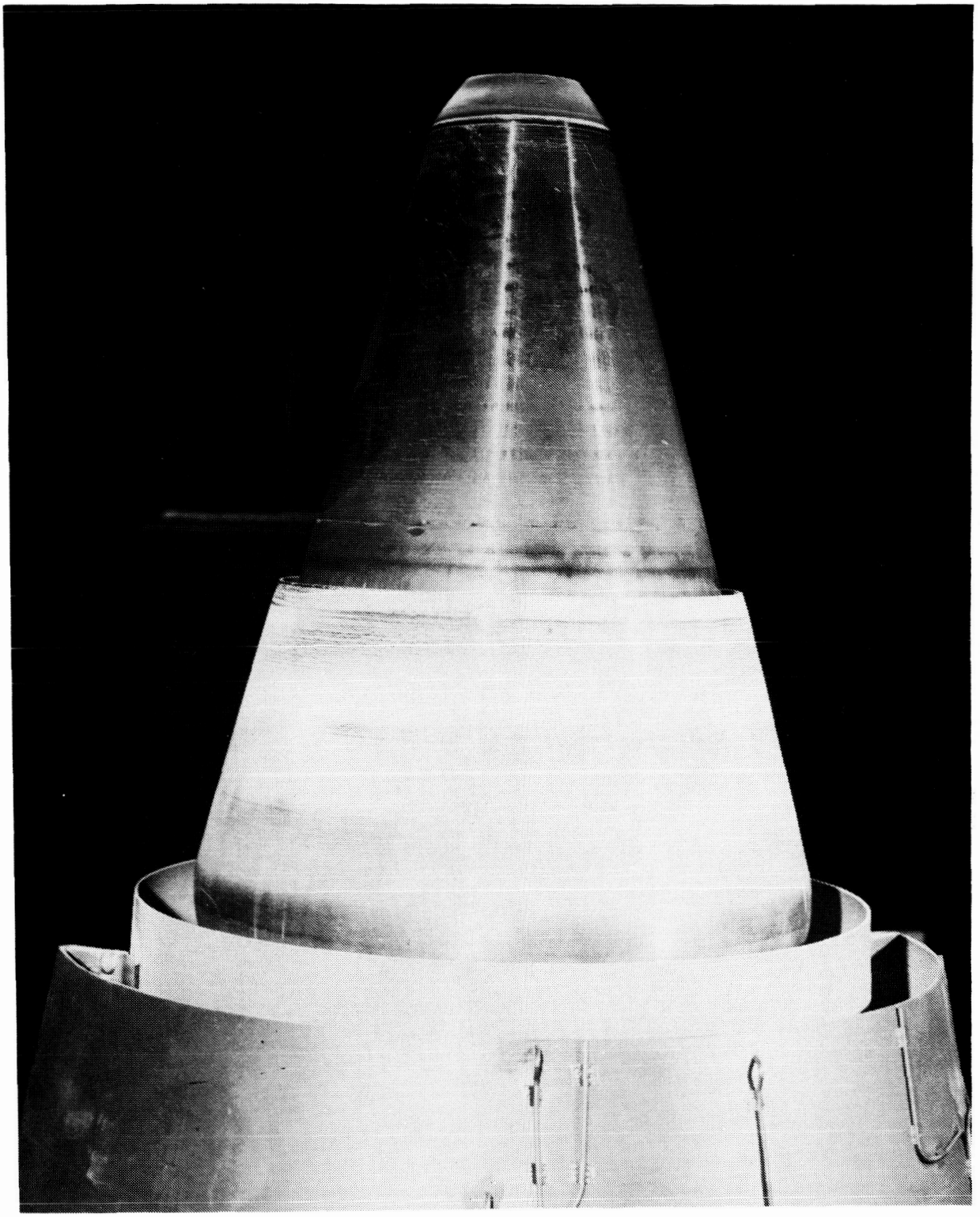

Figure 18. Unsuppressed Coannular Plug Nozzle with 180° Shield in Anechoic Test Facility, Configurations TAS-11 and TAS-12 (Detail).

- All dimensions in inches
- Otherwise same as in Figure 15

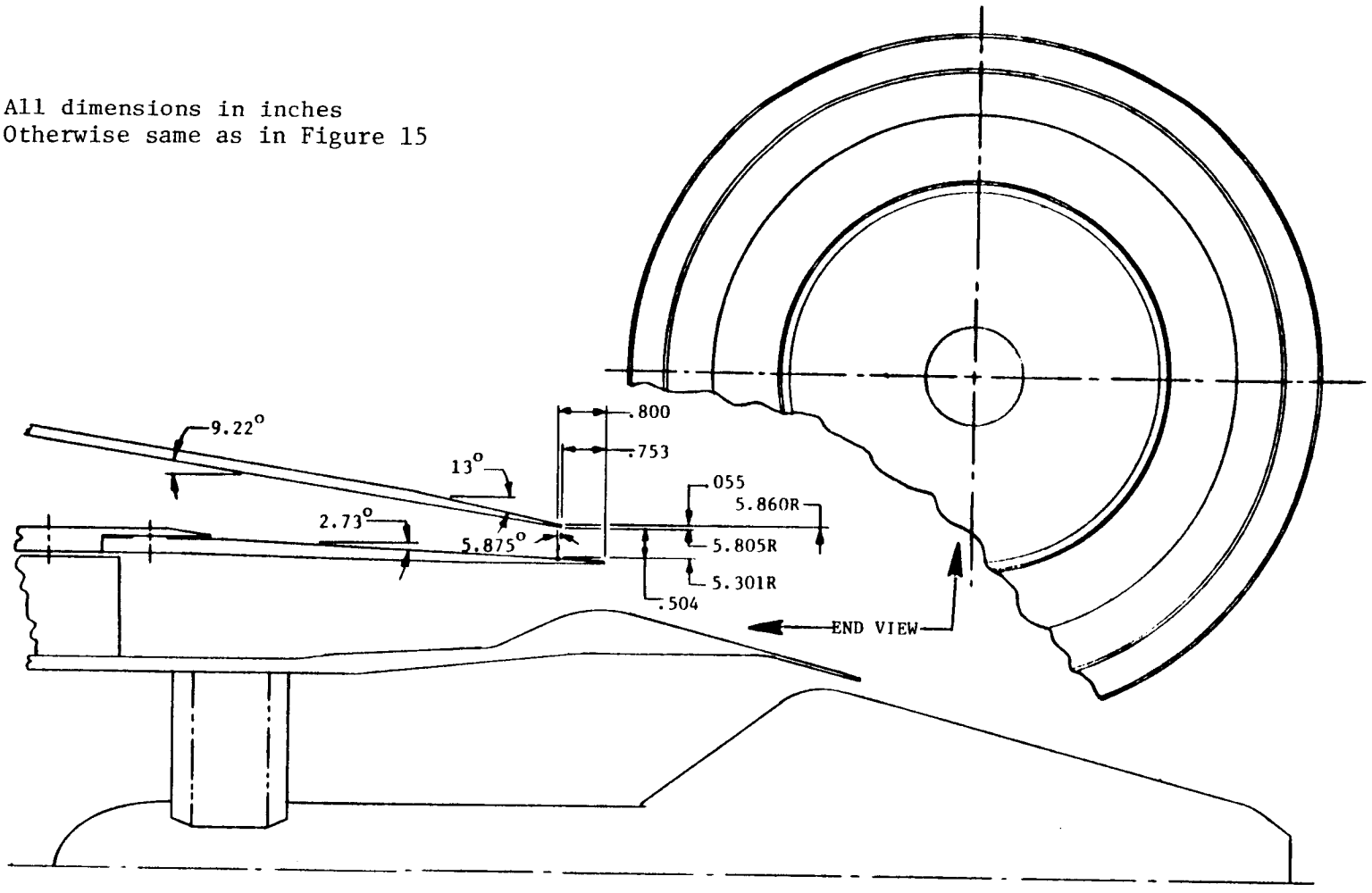

Figure 19. Schematic of Unsuppressed Coannular Plug Nozzle with 360° Shield, Configuration TAS-14.

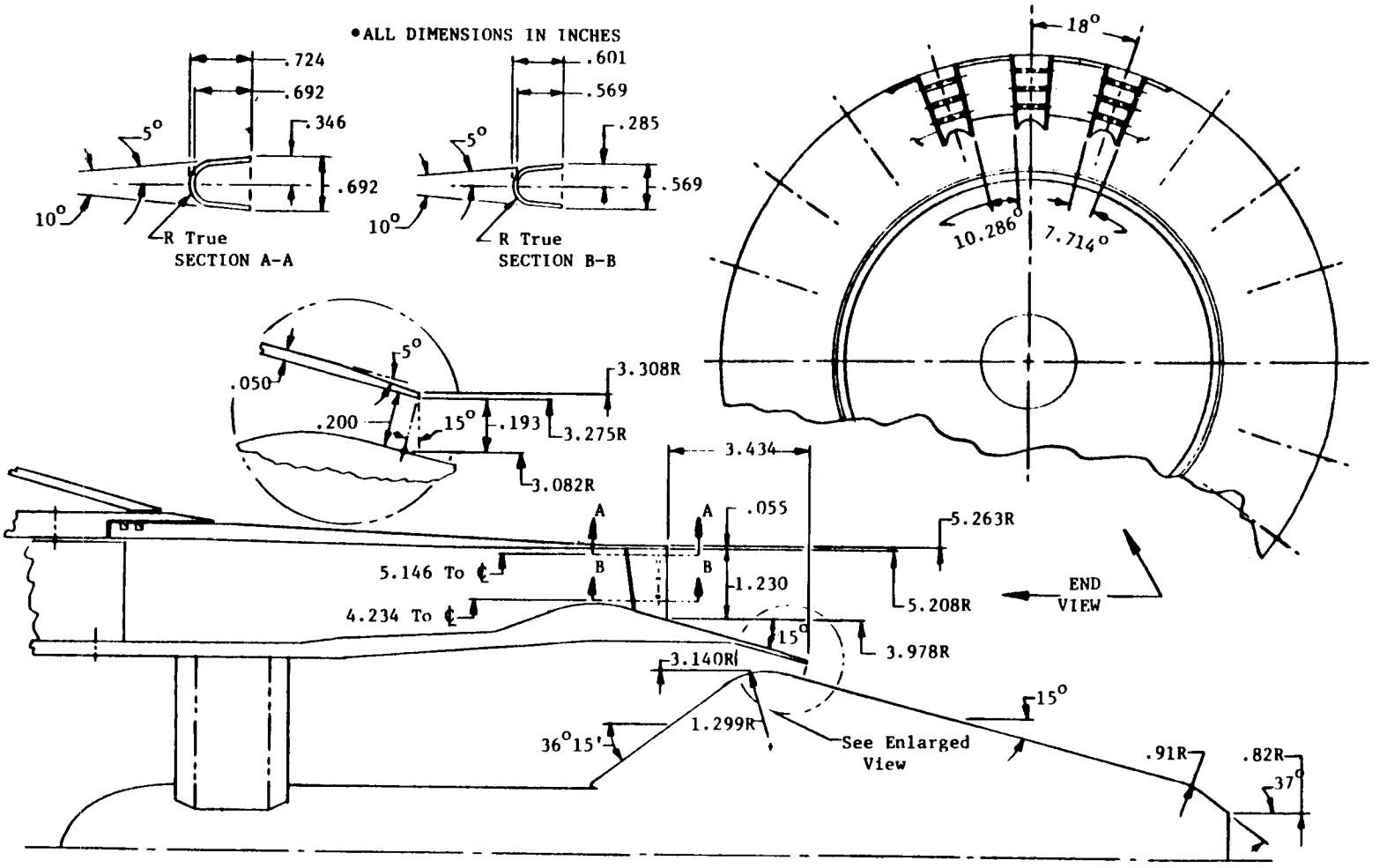

Figure 20. Schematic of Coannular Plug Nozzle with 20-Chute Outer-Stream Suppressor, Configuration TAS-15.

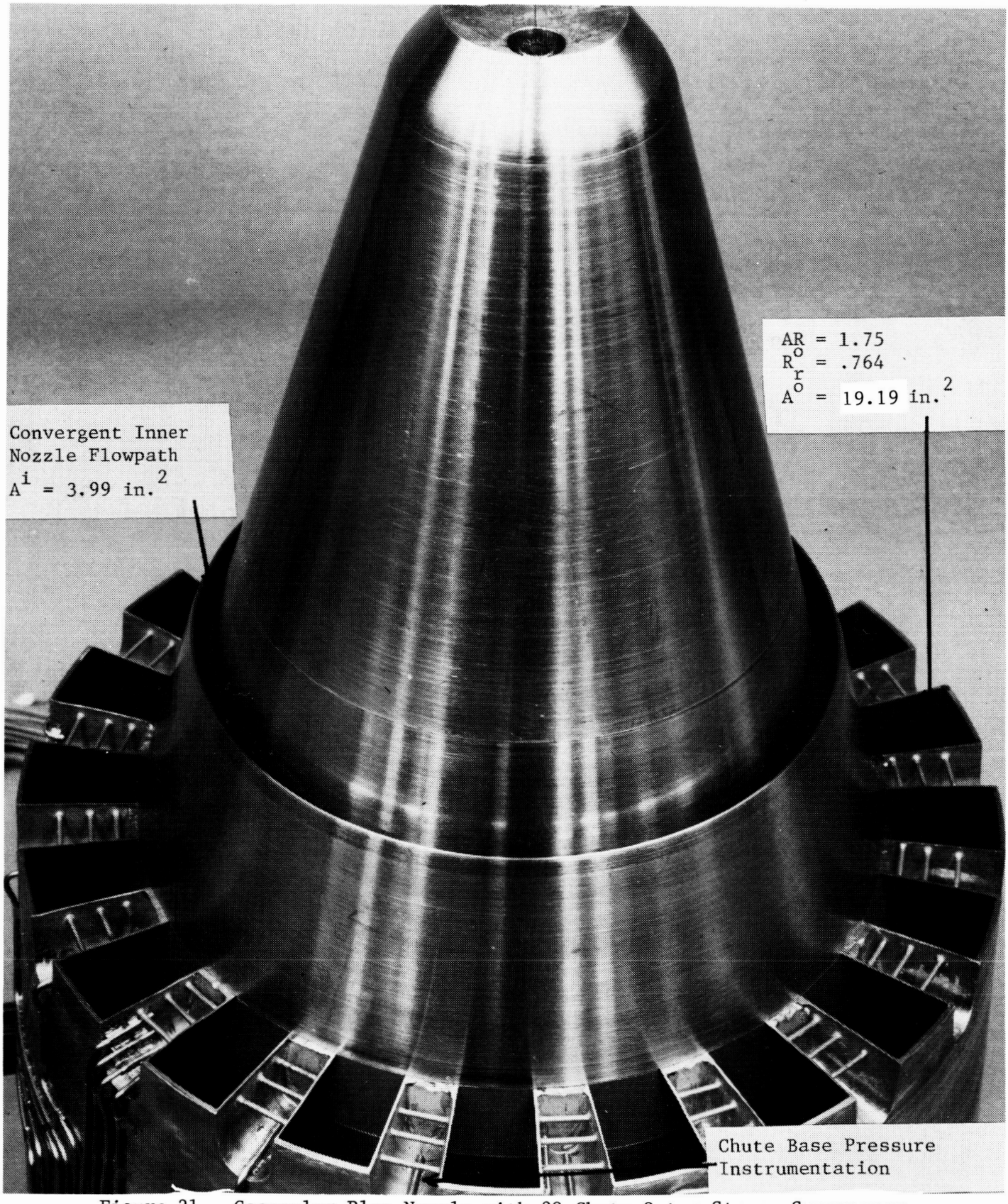

Figure 21. Coannular Plug Nozzle with 20-Chute Outer-Stream Suppressor, Configuration TAS-15.

- All dimensions in inches
- Otherwise same as in Figure 20

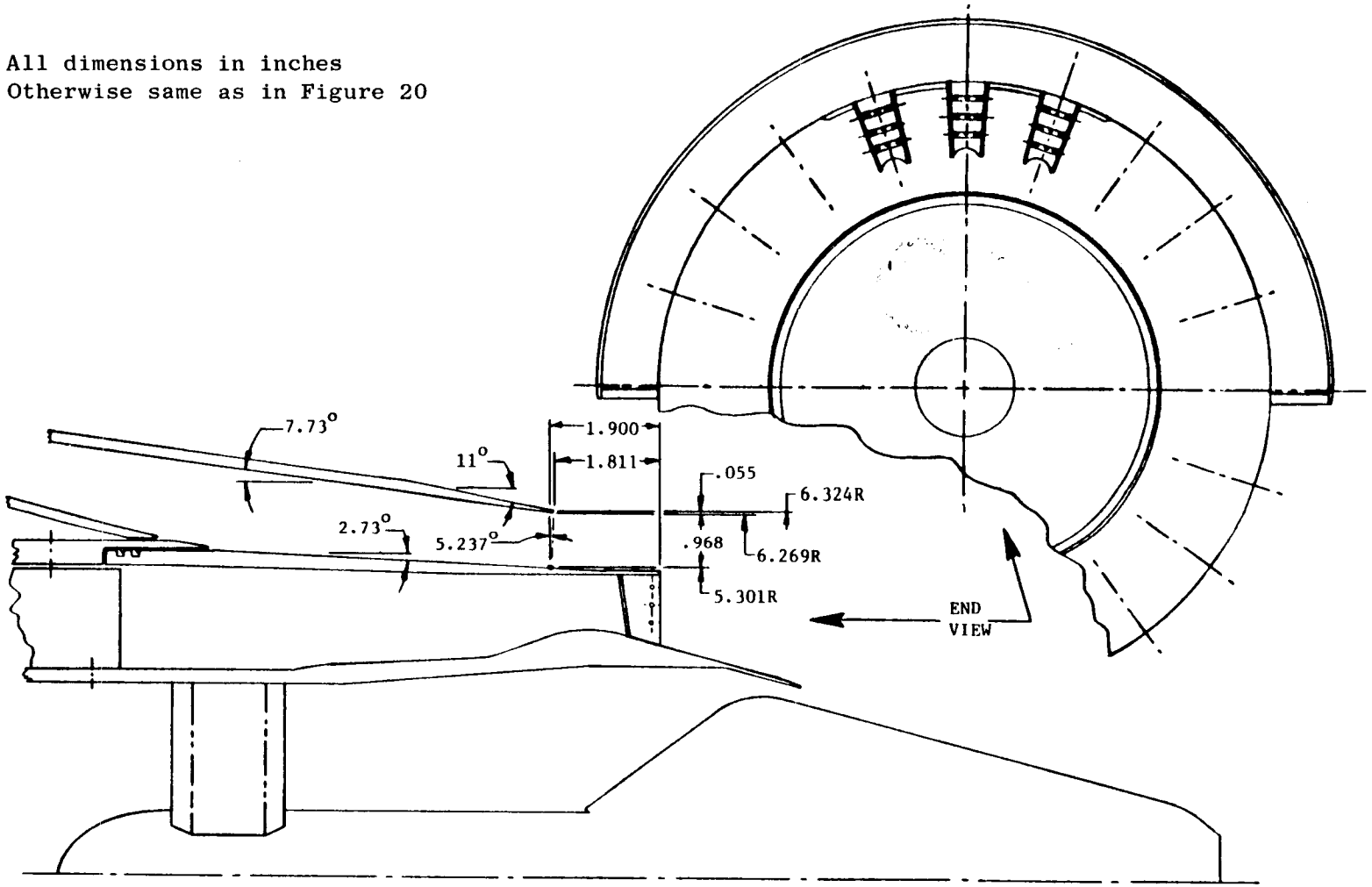

Figure 22. Schematic of Coannular Plug Nozzle with 20-Chute Outer-Stream Suppressor and 180° Shield, Configurations TAS-16, TAS-17, and TAS-18.

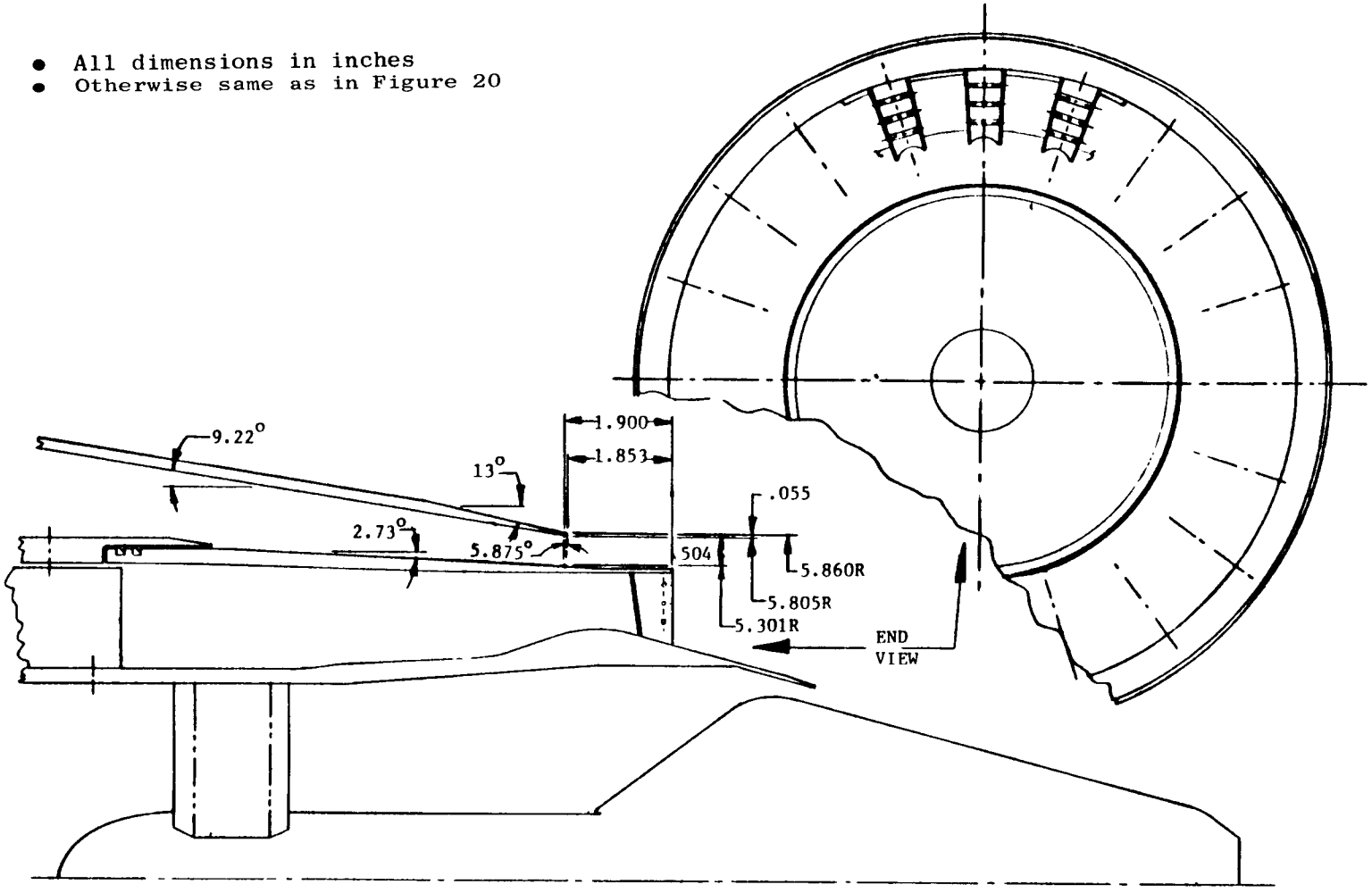

Figure 23. Schematic of Coannular Plug Nozzle with 20-Chute Outer-Stream Suppressor and 360° Shield, Configuration TAS-19.

The nine configurations are grouped as baseline (TAS-10 and -15) and thermal acoustic shielded (TAS-11, -12, -14, -16, -17, -18 and -19). The test configuration design details are discussed in Sections 2.3-1 and 2.3-2 for these two groups, respectively. Details including design methodology, supply system, individual part drawings and photos, and application of instrumentation are provided in Reference 20.

Tables I and II present a summary of the significant geometric parameters of the baseline coannular configurations and of the various shield nozzles, respectively.

2.3.1 Baseline Coannular Configurations

TAS-10 is the baseline unsuppressed and TAS 15 is the baseline suppressed configuration without TAS. Significant geometric details of the outer and inner nozzles of these two baseline configurations are given below:

Unsuppressed Coannular Plug Nozzle: TAS-10

The baseline unsuppressed coannular plug configuration (see Figure 15 and Table I) has geometric flow areas of A^o = 23.22 in^2, A^i = 4.64 in^2, and A^T = 27.86 in^2 for a total area equivalent diameter, D_{eq}, of 5.957 in., and a system area ratio, $A_T^i,^o$, of 0.20. The nozzle has convergent flowpath terminations on the inner and outer nozzles. The choices of radius ratios, plug angle, and so forth, are based on previous experiences (References 1 and 21) which have shown this configuration to be more practical and noise effective than a convergent circular nozzle. Most of the aerodynamic flowlines are identical to those of the baseline coannular nozzle system tested on the YJ101 engine (Reference 1). To ensure interchangeability of the shield hardware, the outer-flowpath physical dimensions of TAS-10 were set equal to those of the existing 20-chute suppressor nozzle.

Coannular Plug Nozzle with 20-Chute Outer-Stream Suppressor: TAS-15

The 20-chute coannular suppressor (see Figures 20, 21, and Table I) was fabricated and tested under Contract NAS3-21608 (Reference 22). It was subsequently tested as a single flow turbojet suppressor within Contract NAS3-22514 (Reference 23) and as a dual flow system under Contract NAS3-23166 (Reference 24). This nozzle is a scale model of the test-bed engine suppressor built for the YJ101 Engine (Reference 25).

The outer nozzle uses 20 chutes of radial exit-plane planform and has a suppressor area ratio, $A_{Annulus}/A_{Flow}$, of 1.75. Geometric flow areas of A^o = 128.36 cm^2 (19.90 in^2) and A^1 = 25.74 cm^2 (3.99 in^2) result in a total flow area of 154.09 cm^2 (23.89 in^2) and a total area equivalent diameter of 14.02 cm (5.52 in), and a shield system area ratio of 0.20. Additional details and manufacturing drawings of the suppressor nozzle are provided in Appendix II of Reference 26.

Table I. Geometric Parameters of the Outer and Inner Nozzles of Baseline Configurations.

	Baseline Configuration	
	Unsuppressed	Suppressed
Outer Nozzle:		
Unsuppressed/20-Chute	Unsuppressed	20-Chute
Throat Height, h^o, cm (in)	1.97 (0.766)	3.12 (1.230)
Throat Area, A^o, cm^2 (in^2)	149.82 (23.222)	128.36 (19.90)
Hub Radius at Throat, R_h^o, cm (in)	11.28 (4.442)	10.10 (3.978)
Tip Radius at Throat, R_t^o, cm (in)	13.22 (5.208)	13.22 (5.208)
Throat Radius Ratio, R_r^o	0.853	0.764
Termination Shape	Convg.	Convg.
Exit Plane Discharge Angle Relative to Axis θ_{th}^o, deg.	0	0
Number of Suppressor Elements	-	20
Supr. Elemental Planform Shape	-	Radial
Suppressor Area Ratio, AR	-	1.75
Angle Subtended by Each Chute, θ^{chute}, deg.	-	7.714
Angle Subtended by Each Flow Element θ^{flow}, deg.	-	10.286
Chute Depth-to-Width Ratio	-	1.0
Chute Entrance Design Mach Number	-	0.7
Inner Nozzle:		
Throat Height, h^i, cm (in)	0.59 (0.234)	0.51 (0.200)
Throat Area, A^i, cm^2 (in^2)	29.95 (4.644)	25.74 (3.99)
Hub Radius at Throat, R_h^i, cm (in)	7.74 (3.047)	7.83 (3.082)
Tip Radius at Throat, R_t^i, cm (in)	8.31 (3.273)	8.32 (3.275)
Throat Radius Ratio, R_r^i	0.931	0.941
Termination Shape	Convg.	Convg.
Exit Plane, Discharge Angle Relative to Axis, θ_{th}^i, deg.	15	15
Unshielded Configuration Designation	TAS-10	TAS-15

Table II. Geometric Parameters of the Shielded Nozzles.

Parameter	Configuration			
	Unsuppressed		Suppressed	
	Partial Shield	Full Shield	Partial Shield	Full Shield
Shield Nozzle:				
Shield Arc, deg.	180	360	180	360
Shield Height, h^s, cm (in)	2.46 (0.968)	1.28 (0.504)	2.46 (0.968)	1.28 (0.504)
Hub Radius at Throat, R^s_h, cm (in)	13.46 (5.301)	13.46 (5.301)	13.46 (5.301)	13.46 (5.301)
Tip Radius at Throat, R^s_t, cm (in)	15.92 (6.269)	14.74 (5.805)	15.92 (6.269)	14.74 (5.805)
Radius Ratio at Throat, R^s_r	0.846	0.913	0.846	0.913
Throat Area, A^s, cm^2 (in^2)	113.80 (17.664)	115.80 (17.664)	113.80 (17.664)	113.80 (17.664)
Shield Hub Flowpath Angle at Throat, θ^s_h, deg.	2.73	2.73	2.73	2.73
Shield Tip Flowpath Angle at Throat, θ^s_t, deg.	7.73	9.22	7.73	9.22
Axial Distance, Shield to Primary Nozzle Exit Plane, l^s, cm (in)	1.81 (0.711)	1.91 (0.753)	4.60 (1.811)	4.71 (1.853)
Exit Plane Discharge Angle Relative to Axis, θ^s_{th}, deg.	5.237	5.875	5.237	5.875
Shielded Configuration Designation	TAS-11 TAS-12	TAS-14	TAS-16 TAS-17 TAS-18	TAS-19

2.3.2 Thermal Acoustic Shield Nozzle Configurations

A 180°-shield nozzle and a 360°-shield nozzle were designed and fabricated. Each was designed to be interchangeable with the baseline unsuppressed (TAS-10) and the baseline suppressed (TAS-15) coannular nozzles, to yield shielded Configurations TAS-11, -12, and -14 through -19. As both the shield and outer streams are supplied from the same heated air source, shield-to-outer stream velocity ratio, $V_r^{s,o}$, was varied through physical changes in the flow condition of choke plate hardware.

The 180° and 360° shields are designed for the same exit areas and have shield exit plane thicknesses of 2.46 cm (0.97 in.) and 1.28 cm (0.50 in.), respectively. These are in reasonable agreement with the shield thicknesses of 0.97 in. and 0.48 in. that were employed earlier with the annular baseline nozzles of this program (Reference 14). Photos of the 180° shield as applied to the unsuppressed coannular nozzle are presented in Figures 17 and 18.

The set-back distances of the 180° and 360° shield exit planes, relative to the outer stream of the baseline unsuppressed coannular nozzle were 1.80 cm (0.71 in.) and 1.90 cm (0.75 in.) respectively. These were similar to those of the annular unsuppressed configurations. The design parameter held constant when applying the 180° and 360° shield nozzles to the 20-chute suppressor, as compared to the Single Flow 32-chute suppressor, was the distance from the shield nozzle throat plane to the leading edge of the chute cross section at the tip (approximately 3.05 cm, 1.2 inches, in both designs).

Unsuppressed Coannular Plug Nozzle With Thermal Acoustic Shields: TAS-11, -12, and -14

Based on the results of the single flow thermal acoustic shield study (Reference 14), the following cycle condition was selected as a "derated" takeoff point for the coannular configurations:

$P_r^o = 3.025$	$P_r^i = 2.056$	$V_r^{i,o} = 0.60$
T_T^o, ° R = 1630	T_T^i, ° R = 870	
V^o, m/s (ft/s) = 715 (2325)	V^i, m/s (ft/s) = 429 (1395)	
W^o, pps = 13.4	W^i, pps = 2.5	

As the flows to the outer nozzle of the coannular and to the shield nozzle are supplied from a common source, each shield test configuration required definition of a "design-point" shield-to-outer-stream velocity ratio, $V_r^{s,o}$, so as to select the proper choke plate system in the shield flow. These "design-point" values of $V_r^{s,o}$ were selected as 0.64 and 0.83 for the shielded unsuppessed coannular configurations. Selection of the proper choke plates then resulted in the following shield flow parameters at the selected "derated" takeoff condition:

- TAS-11, Unsuppressed Coannular Plug Nozzle with 180° shield, $V_r^{s,o}$ = 0.64 (Figures 16, 17, and 18).

P_r^s = 1.50	W^s,pps = 4.8
T_T^s, ° R = 1630	$V_r^{s,o}$ ≈ 0.64
V^s, m/s (fps) = 446.5 (1465)	$W_r^{s,o}$ ≈ 0.35

- TAS-12, Unsuppressed Coannular Plug Nozzle with 180° shield, $V_r^{s,o}$ = 0.83 (Figures 16, 17, and 18).

P_r^s = 2.04	W^s,pps = 6.7
T_T^s, ° R = 1630	$V_r^{s,o}$ ≈ 0.83
V^s, m/s (fps) = 582.5 (1910)	$W_r^{s,o}$ ≈ 0.50

- TAS-14, Unsuppressed Coannular Plug Nozzle with 360° shield, $V_r^{s,o}$ = 0.83 (Figure 19).

P_r^s = 2.04	W^s,pps = 6.7
T_T^s, ° R = 1630	$V_r^{s,o}$ ≈ 0.83
V^s, m/s (fps) = 582.5 (1910)	$W_r^{s,o}$ ≈ 0.50

Coannular Plug Nozzle With 20-Chute Outer Stream Suppressor with Thermal Acoustic Shields: TAS-16, -17, -18, and -19

Application of the 180° and 360° shields to the baseline coannular plug nozzle with 20-chute outer-stream suppressor along with the selected choke plate geometry resulted in the following shield flow parameters at the selected "derated" takeoff condition:

- TAS-16, Coannular Plug Nozzle with 20-Chute Outer-Stream Suppressor with 180° Shield, $V_r^{s,o}$ = 0.64 (Figure 22).

P_r^s = 1.50	W^s,pps = 4.8
T_T^s, ° R = 1630	$V_r^{s,o}$ ≈ 0.64
V^s, m/s (fps) = 446.5 (1465)	$W_r^{s,o}$ ≈ 0.35

- TAS-17, Coannular Plug Nozzle with 20-Chute Outer-Stream Suppressor with 180° Shield, $V_r^{s,o}$ = 0.83 (Figure 22).

P_r^s = 2.04	W^s,pps = 6.7
T_T^s, ° R = 1630	$V_r^{s,o}$ ≈ 0.83
V^s, m/s (fps) = 582.5 (1910)	$W_r^{s,o}$ ≈ 0.50

- TAS-18, Coannular Plug Nozzle with 20-Chute Outer-Stream Suppressor with 180° Shield, $V_r^{s,o}$ = 0.48 (Figure 22).

P^s_r = 1.235	W^s,pps = 3.3
T^s_T, ° R = 1630	$V^{s,o}_r$ ≈ 0.48
V^s, m/s (fps) = 326.3 (1070)	$W^{s,o}_r$ ≈ 0.25

- TAS-19, Coannular Plug Nozzle with 20-Chute Outer-Stream Suppressor with 360° Shield, $V^{s,o}_r$ = 0.83 (Figure 23).

P^s_r = 2.045	W^s,pps = 6.7
T^s_T, ° R = 1630	$V^{s,o}_r$ ≈ 0.83
V^s, m/s (fps) = 582.5 (1910)	$W^{s,o}_r$ ≈ 0.50

In designing the flow conditioning choke plate hardware, sufficient mechanical flexibility had been allowed so as to tune in the physical hardware during calibration and obtain the desired design values for $V^{s,o}_r$. Off-design-point operation was accomplished by setting the desired inner and outer stream flow conditions with no change in the selected choke plate geometry. The resultant shield exit cycle conditions of these off-design points were determined through shield instrumentation during the detailed calibration. Calibration details and results are summarized in Reference 27.

3.0 ACOUSTIC AND DIAGNOSTIC TEST MATRICES

A total of 136 acoustic test points were conducted with the coannular configurations described in Section 2.3. The distribution of the test points over unsuppressed and suppressed coannular test configurations is summarized in Table III. The majority of the test points simulate an operating line of AST/VCE engines, taking into consideration the facility total temperature limits (a maximum of 1730° R). Mean and turbulent velocity measurements were conducted on four different plumes of nozzle configurations using the LV.

3.1 ACOUSTIC TESTS

Figure 24 specifies the variables that summarize the aerodynamic conditions of the acoustic test points. In addition to the inner, outer, and shield jet parameters, the tabulated data contain the mixed conditions that are calculated on a mass-averaged basis for velocity and total temperature. The mass-averaged velocity (V^{mix}) and the mass-averaged total temperature (T_T^{mix}) are calculated using the following expressions:

$$V^{mix} = \frac{W^o V^o + W^i V^i + W^s V^s}{W^o + W^i + W^s} \tag{6}$$

and

$$T_T^{mix} = \frac{W^o T_T^o + W^i T_T^i + W^s T_T^s}{W^o + W^i + W^s} \tag{7}$$

The mass averaged velocity V^{mix} can be referred to also as specific thrust since it is defined as total-thrust/total-weight-flow. T_T^{mix} also can be referred to as stagnation specific enthalpy since it is defined as total-stagnation-enthalpy/total-weight-flow. From the known V^{mix} and T_T^{mix} other mixed flow parameters have been calculated by using standard isentropic relations. The mixed stream data are employed to calculate the mixed jet velocity parameter (LVM) and mixed shock strength parameter (LBM). They are defined as follows:

$$LVM = 10 \log \left(V^{mix}/a_{amb}\right) \tag{8}$$

$$LBM = 10 \log \beta^{eff} \tag{9}$$

where

$$\beta^{eff} = \left[\left(M^{eff}\right)^2 - 1\right]^{1/2} \tag{10}$$

Table III. Summary of Acoustic Tests.

Baseline Nozzle	Shield		Test Points		$V_r^{s,o}$= V^s/V^o	Configuration
	Type	Orientation	Static	Flight		
Unsuppressed Coannular Plug Nozzle	No Shield	---	14	7	0.0	TAS-10
	180° Partial Shield	Sideline	5	5	0.64	TAS-11
		Community	5	5		
		Sideline	6	7	0.83	TAS-12
	360° Full Shield	Axi-Symmetric	7	6	0.83	TAS-14
Mechanically Suppressed Coannular Plug Nozzle with 20-Shallow-Chute Suppressor in Outer Stream	No Shield	---	6	6	0.0	TAS-15
	180° Partial Shield	Sideline	5	5	0.64	TAS-16
		Community	7	5		
		Community	7	6	0.83	TAS-17
		Community	5	5	0.48	TAS-18
	360° Full Shield	Axi-Symmetric	6	6	0.83	TAS-19
		Total	73	63		
			136			

Note: The shield to outer stream velocity ratios of this table correspond to a typical takeoff condition of $P_r^o \sim 3.025$, $T_T^o \sim 1640°$ R and $P_r^i \sim 2.28$, $T_T^i \sim 880°$ R.

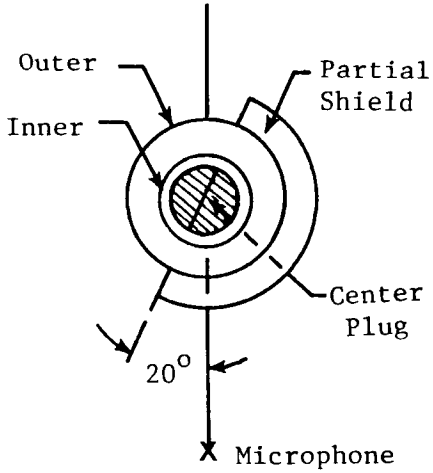

Sideline Orientation

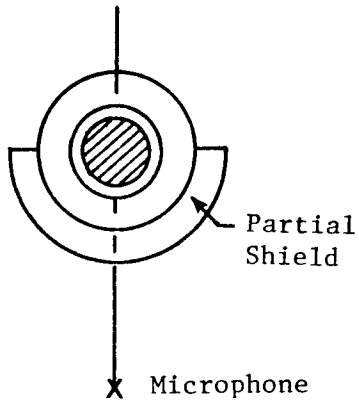

Community Orientation

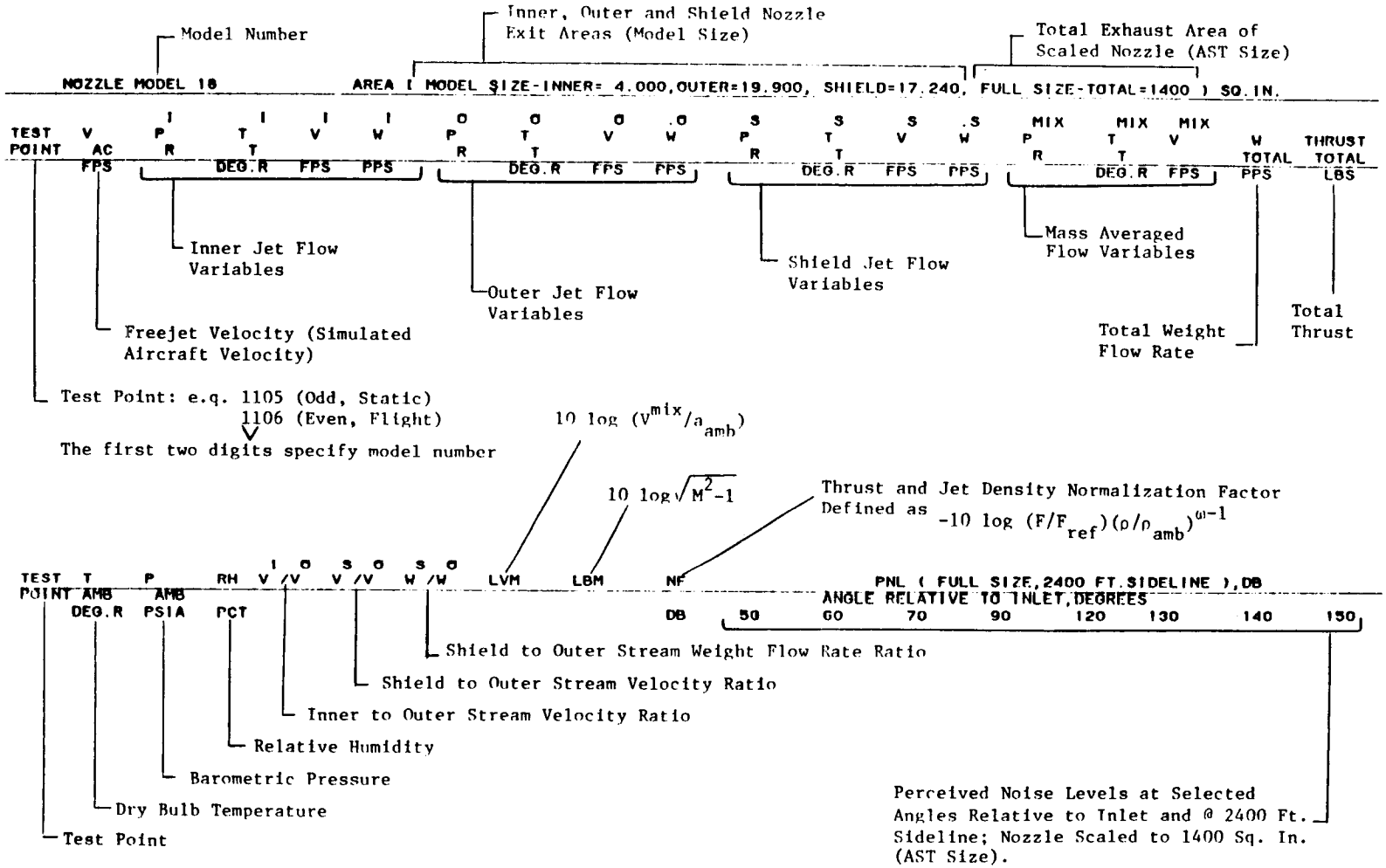

Figure 24. Description of Aerodynamic Data Sheet (English Units).

$$M^{eff} = \left\{ \frac{2}{\gamma - 1} \left[\left(P_r^{eff} \right)^{\frac{\gamma - 1}{\gamma}} - 1 \right] \right\}^{1/2} \tag{11}$$

and

$$P_r^{eff} = \frac{P_r^{o} A^{o} + P_r^{i} A^{i} + P_r^{s} A^{s}}{A^{o} + A^{i} + A^{s}} \tag{12}$$

In the above expressions, P_r is the pressure ratio and A is the flow area of the nozzle. The superscripts o, i, and s refer to outer, inner, and shield streams, respectively, and the value of $\gamma = 1.4$.

The ambient pressure and temperature, along with the relative humidity in the GE Anechoic Facility at the time of the test, and acoustic data extrapolated to a 731.5m (2400-ft) sideline and scaled to an AST product size of 0.902 m^2 (1400 $in.^2$) also are presented in the tables. The selected acoustic data correspond to microphone locations of θ_i = 50°, 60°, 70°, 90°, 120°, 130°, 140° and 150°.

The normalization factor (NF) found in these tables is employed to normalize the measured perceived noise level (PNL) to a reference thrust (F_{ref} = 5130 lb) and jet density as follows:

PNLN = Normalized PNL = PNL + NF

where

$$NF = -10 \log (F/F_{ref}) (\rho^{mix}/\rho_{amb})^{\omega - 1} \tag{13}$$

The aerodynamic flow conditions and selected PNL acoustic data of the test nozzles TAS-10 through TAS-19 are prescribed in Tables IV through XII, respectively.

3.1.1 Test Matrices of Unsuppressed Coannular Plug Nozzles

A total of 67 acoustic test points were completed on the unsuppressed coannular plug nozzle with and without thermal acoustic shields. The test configurations consisted of:

a. The baseline coannular nozzle (TAS-10)

b. The baseline TAS-10 with the 0.97-in.-thick 180° shield and the choke plates selected to give V^s/V^o of 0.64 and 0.83 (TAS-11 and 0.83 (TAS-11 and TAS-12) at a typical takeoff condition

c. The baseline TAS-10 with the 0.5-in.-thick 360° shield (TAS-14) with the choke plates identical to those of TAS-12 to give $V^s/V^o \approx 0.83$.

Table IV. Test Matrix for Baseline Coannular Plug Nozzle, TAS-10 (English Units).

NOZZLE MODEL 10 , AREA (MODEL SIZE-INNER= 4.640,OUTER=23.400, SHIELD= 0.000, FULL SIZE-TOTAL=1399) SQ.IN.

TEST POINT	V AC FPS	I P R	I T T DEG.R	I V FPS	I W PPS	O P R	O T T DEG.R	O V FPS	O W PPS	S P R	S T T DEG.R	S V FPS	S W PPS	MIX P R	-MIX T T DEG.R	MIX V FPS	W TOTAL PPS	THRUST TOTAL LBS
1001	0	1.576	814	1092	97.5	1.940	1236	1604	489.3	1.000	519	0	0.	1.873	1166	1519	586.8	27703
1002	400	1.574	874	1130	93.9	1.948	1256	1622	483.4	1.000	519	0	0.	1.880	1194	1542	577.4	27664
1003	0	1.569	817	1089	96.8	2.060	1380	1765	488.4	1.000	519	0	0.	1.967	1287	1653	585.2	30063
1004	400	1.581	892	1147	93.5	2.093	1349	1762	499.6	1.000	519	0	0.	2.000	1277	1665	593.1	30686
1005	0	1.747	808	1197	110.8	2.330	1474	1958	535.3	1.000	519	0	0.	2.213	1360	1828	646.1	36700
1006	400	1.761	856	1239	108.6	2.403	1531	2028	536.8	1.000	519	0	0.	2.276	1417	1895	645.4	38025
1007	0	1.862	875	1308	113.9	2.631	1553	2133	589.4	1.000	519	0	0.	2.482	1444	2000	703.4	43718
1008	400	1.878	900	1335	113.3	2.704	1567	2170	597.1	1.000	519	0	0.	2.545	1461	2036	710.4	44966
1009	0	2.043	893	1408	122.1	2.986	1629	2305	659.5	1.000	519	0	0.	2.805	1514	2165	781.6	52597
1010	400	2.087	911	1440	121.1	3.048	1653	2341	655.2	1.000	519	0	0.	2.864	1537	2201	776.3	53096
1011	0	2.316	929	1543	133.9	3.594	1668	2493	774.4	1.000	519	0	0.	3.356	1559	2353	908.3	66430
1012	400	2.336	916	1539	135.2	3.619	1676	2505	772.9	1.000	519	0	0.	3.377	1563	2361	908.2	66640
1013	0	1.752	842	1223	108.9	2.692	1552	2154	601.9	1.000	519	0	0.	2.514	1443	2012	710.7	44441
1015	0	1.750	841	1221	108.8	3.024	1626	2314	659.4	1.000	519	0	0.	2.787	1515	2160	768.2	51567
1017	0	1.742	875	1241	106.1	3.598	1670	2495	774.3	1.000	519	0	0.	3.274	1574	2344	880.5	64153
1019	0	1.899	886	1335	113.0	3.021	1663	2341	654.7	1.000	519	0	0.	2.812	1549	2193	767.7	52317
1021	0	2.279	897	1503	134.7	3.010	1620	2306	660.2	1.000	519	0	0.	2.859	1497	2170	794.9	53601
1022	400	2.297	867	1484	136.7	3.039	1666	2348	650.8	1.000	519	0	0.	2.879	1527	2198	787.5	53804
1023	0	2.611	898	1608	153.4	3.023	1628	2316	658.5	1.000	519	0	0.	2.918	1490	2182	811.9	55066
1025	0	2.815	919	1681	163.8	3.020	1630	2316	658.5	1.000	519	0	0.	2.948	1488	2190	822.4	55964
1027	0	3.011	912	1720	176.0	3.013	1628	2313	657.6	1.000	519	0	0.	2.971	1477	2188	833.5	56681

TEST POINT	T AMB DEG.R	P AMB PSIA	RH PCT	I V /V	O V /V	S V /V	O W /W	S W /W	LVM	LBM	NF DB	PNL (FULL SIZE,2400 FT.SIDELINE),DB ANGLE RELATIVE TO INLET,DEGREES 50	60	70	90	120	130	140	150
1001	511	14.368	41.	0.68	0.		0.		1.37	-10.00	-4.6	82.2	84.6	84.6	91.4	94.9	95.1	94.5	91.4
1002	510	14.257	64.	0.70	0.		0.		1.44	-10.00	-4.4	84.0	85.7	84.2	88.7	90.4	89.1	86.7	80.8
1003	513	14.306	39.	0.62	0.		0.		1.73	-5.58	-4.5	84.0	86.4	86.7	93.2	96.7	97.4	96.7	94.4
1004	509	14.229	69.	0.65	0.		0.		1.77	-4.95	-4.6	86.4	88.3	87.3	91.4	92.9	92.4	89.7	83.8
1005	513	14.340	39.	0.61	0.		0.		2.16	-2.68	-5.2	88.2	91.1	91.2	97.3	100.2	100.9	100.6	99.5
1006	509	14.222	71.	0.61	0.		0.		2.34	-2.34	-5.2	92.9	95.1	94.0	97.4	98.5	98.0	96.2	91.0
1007	513	14.364	41.	0.61	0.		0.		2.55	-1.51	-5.8	91.7	94.2	94.6	100.2	103.3	104.5	105.9	104.4
1008	510	14.221	70.	0.62	0.		0.		2.65	-1.32	-5.9	96.5	98.1	97.0	101.0	102.7	102.3	100.9	95.7
1009	512	14.504	42.	0.61	0.		0.		2.90	-0.68	-6.6	98.4	100.2	100.2	104.5	107.0	109.7	113.6	110.4
1010	509	14.219	74.	0.62	0.		0.		2.99	-0.57	-6.6	98.8	100.6	100.0	103.4	105.3	105.1	105.0	99.8
1011	511	14.312	58.	0.62	0.		0.		3.27	0.17	-7.7	99.1	101.1	101.8	107.5	109.4	112.1	115.0	108.4
1012	509	14.221	74.	0.61	0.		0.		3.29	0.20	-7.7	103.7	105.4	104.4	107.9	108.6	109.5	109.5	103.2
1013	511	14.322	58.	0.57	0.		0.		2.59	-1.41	-5.9	92.0	94.6	95.2	100.4	103.7	105.0	106.0	103.8
1015	513	14.306	43.	0.53	0.		0.		2.89	-0.72	-6.5	94.3	96.8	97.7	102.9	105.9	107.6	109.0	106.0
1017	512	14.302	51.	0.50	0.		0.		3.25	0.06	-7.5	97.5	100.2	100.8	106.6	109.2	112.2	114.2	108.8
1019	512	14.385	40.	0.57	0.		0.		2.96	-0.67	-6.5	94.9	97.2	98.0	103.3	106.1	108.0	110.1	106.3
1021	513	14.360	41.	0.65	0.		0.		2.91	-0.57	-6.7	96.8	98.8	98.6	104.3	106.4	108.1	110.8	108.0
1022	509	14.227	74.	0.63	0.		0.		2.98	-0.52	-6.7	99.7	101.1	100.2	103.6	105.8	105.8	104.9	100.2
1023	513	14.297	41.	0.69	0.		0.		2.93	-0.45	-6.9	95.2	97.9	98.5	103.9	106.8	108.7	110.8	107.3
1025	513	14.320	41.	0.73	0.		0.		2.95	-0.39	-7.0	96.0	98.5	98.7	104.0	106.6	108.9	112.8	107.3
1027	513	14.326	40.	0.74	0.		0.		2.94	-0.35	-7.1	97.7	100.0	99.8	105.0	106.6	108.5	112.1	107.2

Table V. Test Matrix for Unsuppressed Coannular Plug Nozzle with 180° TAS at $V_r^{s,o}$ = 0.64, Sideline and Community Orientations, TAS-11 (English Units).

NOZZLE MODEL 11 , AREA (MODEL SIZE-INNER= 4.640,OUTER=23.400, SHIELD=17.240, FULL SIZE-TOTAL=1400) SQ.IN.

TEST POINT	V AC FPS	I P R	I T T DEG.R	I V FPS	I W PPS	O P R	O T T DEG.R	O V FPS	O W PPS	S P R	S T T DEG.R	S V FPS	S W PPS	MIX P R	MIX T T DEG.R	MIX V FPS	W TOTAL PPS	THRUST TOTAL LBS	
1103	0	1.566	824	1091	59.5	2.111	1397	1802	308.1	1.235	1380	987	110.9	1.735	1322	1525	478.5	22676	Sideline Orientation
1104	400	1.571	825	1096	59.7	2.092	1390	1788	306.8	1.241	1356	989	113.3	1.727	1312	1513	479.9	22567	
1105	0	1.746	831	1212	67.6	2.389	1488	1993	339.7	1.307	1468	1142	122.4	1.920	1399	1697	529.7	27932	
1106	400	1.753	837	1221	67.7	2.377	1478	1981	338.2	1.317	1445	1148	125.3	1.917	1388	1688	531.1	27856	
1107	0	1.873	879	1317	70.8	2.685	1554	2154	373.6	1.393	1534	1294	134.7	2.117	1467	1851	579.2	33326	
1108	400	1.875	856	1300	71.9	2.693	1506	2122	379.4	1.410	1471	1288	140.5	2.125	1418	1824	591.8	33550	
1109	0	2.272	910	1512	82.7	3.025	1657	2338	407.0	1.499	1640	1472	146.1	2.371	1556	2031	635.7	40137	
1110	400	2.286	942	1543	81.5	3.043	1653	2340	408.7	1.523	1616	1488	150.4	2.391	1554	2038	640.6	40580	
1111	0	2.317	906	1524	84.5	3.604	1631	2466	489.5	1.709	1613	1665	173.8	2.763	1545	2174	747.8	50517	
1112	400	2.327	893	1517	85.4	3.609	1639	2474	488.0	1.731	1602	1678	177.0	2.772	1546	2177	750.3	50773	
1133	0	1.579	821	1099	60.3	2.081	1383	1778	305.4	1.223	1370	960	108.4	1.718	1309	1504	474.0	22164	Community Orientation
1134	400	1.573	834	1103	59.5	2.092	1382	1783	306.1	1.238	1350	980	112.7	1.726	1307	1509	478.3	22436	
1135	0	1.747	825	1208	67.9	2.385	1501	2000	336.3	1.299	1485	1136	120.2	1.915	1410	1700	524.4	27699	
1136	400	1.756	820	1210	68.5	2.388	1483	1989	336.8	1.317	1446	1150	125.3	1.921	1389	1690	530.6	27875	
1137	0	1.869	865	1304	71.2	2.677	1543	2143	372.5	1.383	1529	1278	133.4	2.108	1456	1840	577.1	32995	
1138	400	1.875	888	1324	70.5	2.696	1575	2172	369.7	1.408	1538	1315	137.0	2.125	1482	1865	577.2	33460	
*1139	0	2.283	905	1512	83.0	3.009	1632	2314	406.3	1.487	1617	1447	145.3	2.359	1533	2011	634.5	39659	
*1140	400	2.275	943	1540	80.8	3.020	1642	2325	405.7	1.514	1607	1473	149.6	2.374	1545	2025	636.1	40035	
1141	0	2.319	886	1508	85.2	3.619	1613	2456	492.7	1.707	1595	1654	174.6	2.768	1527	2162	752.5	50571	
1142	400	2.327	889	1513	85.1	3.624	1617	2459	491.0	1.734	1585	1671	178.3	2.780	1527	2166	754.4	50792	

* Indicates Additional LV Plume Measurements; Refer to Table XIII.

TEST POINT	T AMB DEG.R	P AMB PSIA	RH PCT	T O V /V	S O V /V	S O W /W	LVM	LBM	NF DB	PNL (FULL SIZE, 2400 FT SIDELINE), DB ANGLE RELATIVE TO INLET, DEGREES 50	60	70	90	120	130	140	150	
1103	488	14.310	66.	0.61	0.55	0.36	1.48	-10.00	-3.4	83.9	85.6	85.6	92.4	96.7	97.9	96.2	92.9	Sideline
1104	489	14.346	66.	0.61	0.55	0.37	1.45	-10.00	-3.3	84.7	85.5	84.7	89.4	90.6	90.8	88.4	83.4	
1105	488	14.400	61.	0.61	0.57	0.36	1.95	-8.94	-3.9	88.5	90.1	90.7	96.3	100.1	101.9	101.2	99.0	
1106	490	14.357	49.	0.62	0.58	0.37	1.92	-9.16	-3.9	89.9	91.8	90.5	94.3	94.8	95.8	93.9	89.6	
1107	488	14.408	63.	0.61	0.60	0.36	2.33	-3.62	-4.5	92.0	93.5	93.5	99.7	103.0	104.6	105.3	102.0	
1108	491	14.344	59.	0.61	0.61	0.37	2.25	-3.52	-4.7	93.3	95.1	94.0	98.0	98.4	99.3	98.1	93.6	
1109	488	14.395	70.	0.65	0.63	0.36	2.73	-2.01	-5.2	94.8	96.3	96.6	103.0	107.1	109.6	109.3	103.3	
1110	489	14.347	64.	0.66	0.64	0.37	2.74	-1.93	-5.2	97.4	98.4	97.1	101.3	102.3	104.7	104.6	98.7	
1111	489	14.390	64.	0.62	0.68	0.36	3.02	-0.85	-6.4	99.6	101.0	101.3	106.7	108.7	112.9	112.9	105.7	
1112	490	14.368	55.	0.61	0.68	0.36	3.02	-0.82	-6.4	102.9	103.7	102.8	106.7	106.6	108.5	108.4	102.9	
1133	496	14.316	85.	0.62	0.54	0.35	1.39	-10.00	-3.3	82.9	84.9	84.5	91.3	94.8	94.9	93.7	91.9	Community
1134	496	14.272	83.	0.62	0.55	0.37	1.40	-10.00	-3.4	84.3	85.4	84.0	88.6	88.8	89.7	88.6	82.5	
1135	496	14.348	82.	0.60	0.57	0.36	1.92	-9.64	-3.9	86.9	89.2	89.2	95.2	98.0	99.8	99.7	96.5	
1136	496	14.254	82.	0.61	0.58	0.37	1.90	-8.43	-3.9	89.3	91.2	90.0	93.5	93.3	94.8	93.8	89.2	
1137	496	14.353	81.	0.61	0.60	0.36	2.26	-3.70	-4.5	90.9	93.0	92.8	98.9	101.7	102.8	103.0	100.3	
1138	496	14.297	81.	0.61	0.61	0.37	2.32	-3.51	-4.5	93.0	94.6	93.2	97.6	97.8	99.9	98.8	93.9	
1139	496	14.330	82.	0.65	0.63	0.36	2.65	-2.07	-5.2	93.9	96.0	95.7	101.9	105.1	107.8	107.8	102.1	
1140	496	14.302	81.	0.66	0.63	0.37	2.68	-2.00	-5.2	96.6	98.2	97.0	100.5	101.0	104.5	104.1	97.8	
1141	496	14.342	84.	0.61	0.67	0.35	2.97	-0.83	-6.4	99.1	101.0	100.5	106.3	107.3	110.3	110.0	103.7	
1142	496	14.289	83.	0.62	0.68	0.36	2.98	-0.80	-6.4	102.5	103.9	102.6	106.0	105.5	107.8	108.0	101.8	

Table VI. Test Matrix for Unsuppressed Coannular Plug Nozzle with 180° TAS at $V_r^{s,o}$ = 0.83, Sideline Orientation, TAS-12 (English Units).

NOZZLE MODEL 12 , AREA (MODEL SIZE-INNER= 4.640,OUTER=23.400, SHIELD=17.240, FULL SIZE-TOTAL=1400) SQ.IN.

TEST POINT	V AC	I P R	I T T	I V	I W	O P R	O T T	O V	O W	S P R	S T T	S V	S W	MIX P R	MIX T T	MIX V	W TOTAL	THRUST TOTAL
	FPS		DEG.R	FPS	PPS		DEG.R	FPS	PPS		DEG.R	FPS	PPS		DEG.R	FPS	PPS	LBS
1203	0	1.568	842	1105	59.0	2.084	1404	1793	307.8	1.480	1390	1333	156.1	1.797	1336	1578	522.8	25644
1204	400	1.579	836	1109	59.7	2.108	1395	1799	311.3	1.509	1360	1349	162.3	1.821	1322	1585	533.3	26271
1205	0	1.756	824	1213	68.3	2.389	1497	1999	339.6	1.640	1466	1540	172.9	2.029	1415	1770	580.7	31947
1206	400	1.747	829	1212	67.7	2.395	1487	1995	341.9	1.673	1458	1553	176.9	2.044	1403	1771	588.5	32388
1207	0	1.867	896	1326	69.9	2.693	1563	2163	376.4	1.831	1553	1729	191.0	2.272	1487	1940	637.3	38438
1208	400	1.881	880	1321	71.1	2.682	1560	2157	373.9	1.864	1530	1738	193.0	2.281	1476	1937	638.0	38413
1209	0	2.279	908	1513	83.7	3.033	1657	2340	411.3	2.058	1642	1927	206.0	2.575	1563	2120	701.0	46182
1210	400	2.286	930	1534	82.8	3.033	1649	2334	411.3	2.081	1620	1927	209.4	2.586	1556	2119	703.5	46326
1211	0	2.324	901	1523	85.5	3.613	1539	2395	508.8	2.444	1531	2045	253.5	3.036	1472	2202	847.8	58033
1212	400	2.325	912	1532	85.0	3.607	1550	2403	505.7	2.473	1531	2057	256.5	3.043	1480	2211	847.2	58217
1220	400	3.031	827	1642	116.4	3.048	1668	2353	411.0	2.000	1637	1942	209.1	2.657	1536	2124	736.5	48619
1221	0	3.021	1144	1931	98.6	3.033	1653	2337	411.7	2.059	1638	1925	206.3	2.662	1578	2162	716.6	48165
1222	400	3.030	1137	1927	99.0	3.053	1656	2345	412.6	2.095	1626	1938	210.2	2.686	1576	2169	721.8	48668

TEST POINT	T AMB	P AMB	RH	I O V /V	S O V /V	S O W /W	LVM	LBM	NF	PNL (FULL SIZE,2400 FT.SIDELINE),DB ANGLE RELATIVE TO INLET,DEGREES						
	DEG.R	PSIA	PCT						DB	50	60	70	90	120	130	140	150
1203	503	14.522	46.	0.62	0.74	0.51	1.57	-10.00	-3.6	83.5	86.0	84.1	92.9	96.3	98.0	97.6	94.2
1204	502	14.468	48.	0.62	0.75	0.52	1.59	-10.00	-3.8	86.0	86.8	85.3	89.8	91.4	92.2	90.5	84.8
1205	504	14.441	45.	0.61	0.77	0.51	2.06	-4.45	-4.4	87.7	90.2	88.5	96.3	99.6	102.4	102.6	99.7
1206	502	14.451	42.	0.61	0.78	0.52	2.07	-4.24	-4.5	90.0	92.1	90.7	94.7	95.7	96.8	95.5	90.1
1207	503	14.512	47.	0.61	0.80	0.51	2.47	-2.42	-5.1	91.7	93.8	92.2	100.1	104.0	106.6	107.1	103.2
1208	502	14.463	47.	0.61	0.81	0.52	2.46	-2.38	-5.1	93.3	95.0	94.0	98.4	99.0	101.1	99.8	95.2
1209	503	14.508	45.	0.65	0.82	0.50	2.85	-1.27	-5.8	96.4	98.5	97.7	103.7	106.5	110.4	110.7	105.3
1210	502	14.474	49.	0.66	0.83	0.51	2.85	-1.24	-5.8	99.0	100.0	98.3	102.0	103.2	105.5	105.3	99.8
1211	503	14.470	46.	0.64	0.85	0.50	3.02	-0.31	-7.3	98.4	100.0	100.2	105.9	108.3	112.5	113.3	107.7
1212	501	14.468	47.	0.64	0.86	0.51	3.04	-0.30	-7.3	101.7	103.4	101.8	105.5	105.5	107.5	109.0	102.5
1220	503	14.475	64.	0.70	0.83	0.51	2.86	-1.01	-6.1	102.4	104.0	101.8	104.5	104.3	106.0	106.0	100.5
1221	502	14.499	46.	0.83	0.82	0.50	2.94	-1.06	-6.0	99.2	101.2	100.9	105.7	107.5	111.8	112.2	105.8
1222	504	14.458	44.	0.82	0.83	0.51	2.95	-1.00	-6.1	102.4	103.6	101.8	104.9	104.8	106.5	107.8	100.8

Table VII. Test Matrix for Unsuppressed Coannular Plug Nozzle with 360° TAS at $V_r^{s,o}$ = 0.83, TAS-14 (English Units).

NOZZLE MODEL 14 , AREA (MODEL SIZE-INNER= 4.640,OUTER=23.400, SHIELD=17.770, FULL SIZE-TOTAL=1399) SQ.IN.

TEST POINT	V AC	I P R	I T T	I V	I W	O P R	O T T	O V	O W	S P R	S T T	S V	S W	MIX P R	MIX T T	MIX V	W TOTAL	THRUST TOTAL
	FPS		DEG.R	FPS	PPS		DEG.R	FPS	PPS		DEG.R	FPS	PPS		DEG.R	FPS	PPS	LBS
1403	0	1.610	858	1145	59.7	2.054	1413	1783	296.9	1.500	1406	1362	161.2	1.789	1347	1578	517.8	25403
1404	400	1.604	823	1118	60.7	2.056	1432	1796	295.2	1.522	1390	1377	165.5	1.796	1348	1584	521.4	25665
1405	0	1.747	847	1225	66.2	2.310	1505	1970	323.3	1.651	1491	1551	177.3	1.987	1424	1752	566.8	30864
1406	400	1.752	843	1224	66.6	2.326	1507	1978	325.0	1.685	1466	1567	183.2	2.008	1417	1760	574.8	31436
1407	0	1.879	893	1330	69.7	2.614	1581	2146	356.9	1.848	1563	1746	195.9	2.232	1498	1929	622.5	37317
1408	400	1.889	890	1333	70.2	2.629	1558	2136	359.7	1.886	1521	1748	198.0	2.258	1472	1924	627.9	37544
1409	0	2.279	884	1493	83.3	2.940	1657	2312	391.3	2.074	1637	1933	210.5	2.525	1557	2096	685.1	44629
1410	400	2.293	952	1554	80.8	2.956	1660	2319	393.4	2.120	1623	1950	216.3	2.556	1565	2114	690.5	45366
1411	0	2.330	934	1552	82.8	3.494	1531	2363	485.2	2.478	1512	2046	262.5	2.981	1466	2182	830.5	56323
1412	400	2.318	944	1556	82.0	3.500	1530	2363	486.7	2.517	1500	2053	268.0	2.998	1463	2185	836.7	56815
1415	0	1.748	856	1232	65.9	2.919	1654	2303	389.2	2.071	1634	1929	210.5	2.462	1569	2079	665.6	43008
1421	0	3.034	1168	1955	96.2	2.968	1662	2323	394.2	2.085	1639	1941	211.5	2.631	1587	2157	701.9	47068
1422	400	3.074	1168	1965	97.3	2.957	1653	2314	393.3	2.120	1617	1947	216.2	2.644	1576	2154	706.8	47314

TEST POINT	T AMB	P AMB	RH	I O V /V	S O V /V	S O W /W	LVM	LBM	NF	PNL (FULL SIZE,2400 FT.SIDELINE),DB ANGLE RELATIVE TO INLET,DEGREES						
	DEG.R	PSIA	PCT						DB	50	60	70	90	120	130	140	150
1403	513	14.426	75.	0.64	0.76	0.54	1.53	-10.00	-3.6	83.6	85.7	84.9	92.2	96.1	97.8	97.4	94.8
1404	513	14.432	61.	0.62	0.77	0.56	1.54	-10.00	-3.6	84.4	85.8	84.2	88.6	88.8	92.3	90.3	86.3
1405	513	14.429	75.	0.62	0.79	0.55	1.98	-5.17	-4.1	87.3	89.5	88.7	95.3	100.1	101.3	101.3	99.3
1406	514	14.412	60.	0.62	0.79	0.56	1.99	-4.76	-4.3	89.0	90.1	88.5	93.0	93.1	96.9	95.7	91.9
1407	513	14.432	74.	0.62	0.81	0.55	2.40	-2.63	-4.9	91.3	93.2	92.4	98.9	103.4	105.3	106.1	102.7
1408	512	14.350	64.	0.62	0.82	0.55	2.39	-2.50	-5.0	91.6	93.3	92.1	96.7	97.5	100.7	100.0	95.9
1409	514	14.411	67.	0.65	0.84	0.54	2.75	-1.40	-5.6	96.2	98.2	97.2	102.9	106.2	108.3	110.8	105.6
1410	512	14.417	68.	0.67	0.84	0.55	2.80	-1.32	-5.7	98.3	99.9	97.8	101.4	103.0	105.3	105.6	101.5
1411	513	14.408	68.	0.66	0.87	0.54	2.93	-0.40	-7.2	95.9	97.9	97.3	103.4	108.1	111.1	112.5	106.8
1412	512	14.418	68.	0.66	0.87	0.55	2.94	-0.37	-7.2	98.6	100.2	98.6	103.2	105.5	107.9	108.8	104.7
1415	513	14.422	71.	0.53	0.84	0.54	2.72	-1.62	-5.4	93.3	95.3	94.6	101.5	106.0	108.5	110.1	106.0
1421	512	14.408	70.	0.84	0.84	0.54	2.89	-1.14	-5.9	99.7	101.6	101.1	105.7	107.8	110.6	112.4	106.0
1422	513	14.382	66.	0.85	0.84	0.55	2.88	-1.10	-5.9	104.0	104.9	102.3	104.8	105.4	106.5	108.5	103.4

Table VIII. Test Matrix for Suppressed Baseline Coannular Plug Nozzle, TAS-15 (English Units).

NOZZLE MODEL 15 , AREA (MODEL SIZE-INNER= 4.000,OUTER=19.900, SHIELD= 0.001, FULL SIZE-TOTAL=1400) SQ.IN.

TEST POINT	V AC FPS	I P R	I T T DEG.R	I V FPS	I W PPS	O P R	O T T DEG.R	O V FPS	O W PPS	S P R	S T T DEG.R	S V FPS	S W PPS	MIX P R	MIX T T DEG.R	MIX V FPS	W TOTAL PPS	THRUST TOTAL LBS
1501	0	1.578	827	1102	98.0	1.926	1203	1574	494.8	1.000	519	0	0.	1.863	1141	1496	592.8	27568
1502	400	1.600	823	1114	100.0	1.978	1223	1617	496.1	1.000	519	0	0.	1.908	1156	1532	596.1	28392
1503	0	1.571	820	1093	97.8	2.116	1310	1747	520.1	1.000	519	0	0.	2.016	1233	1643	617.9	31559
1504	400	1.604	817	1114	100.6	2.122	1397	1808	495.9	1.000	519	0	0.	2.021	1300	1691	596.5	31351
1505	0	1.889	817	1277	121.0	2.330	1468	1954	540.1	1.000	519	0	0.	2.235	1349	1830	661.1	37601
1506	400	1.786	819	1225	114.0	2.428	1491	2012	548.1	1.000	519	0	0.	2.298	1376	1876	662.1	38611
1507	0	1.745	874	1243	107.6	2.688	1560	2159	603.8	1.000	519	0	0.	2.512	1456	2020	711.5	44671
1508	400	1.907	884	1338	113.5	2.747	1561	2180	606.2	1.000	519	0	0.	2.587	1454	2047	719.8	45790
1509	0	2.328	899	1522	139.9	3.029	1642	2328	662.8	1.000	519	0	0.	2.880	1512	2187	802.6	54564
1510	400	2.318	908	1527	136.1	3.087	1641	2344	663.7	1.000	519	0	0.	2.928	1516	2205	799.8	54803
1511	0	2.326	898	1520	139.7	3.599	1671	2496	780.4	1.000	519	0	0.	3.354	1554	2348	920.2	67158
1512	400	2.371	903	1540	139.8	3.654	1672	2509	779.5	1.000	519	0	0.	3.407	1555	2362	919.3	67485

TEST POINT	T AMB DEG.R	P AMB PSIA	RH PCT	I O V /V	S O V /V	S O W /W	LVM	LBM	NF DB	PNL (FULL SIZE,2400 FT.SIDELINE),DB ANGLE RELATIVE TO INLET,DEGREES 50	60	70	90	120	130	140	150
1501	505	14.464	59.	0.70	0.	0.	1.33	-10.00	-4.7	84.0	86.9	88.0	94.3	95.6	94.2	92.0	88.3
1502	513	14.238	48.	0.69	0.	0.	1.40	-8.51	-4.7	89.5	91.7	90.9	95.2	95.3	91.7	87.2	82.1
1503	506	14.465	58.	0.63	0.	0.	1.73	-4.67	-4.9	86.2	89.1	90.0	96.4	97.4	96.2	94.9	91.8
1504	513	14.226	47.	0.62	0.	0.	1.82	-4.51	-4.6	91.4	93.5	93.2	97.5	98.3	95.0	91.0	85.6
1505	507	14.471	55.	0.65	0.	0.	2.19	-2.55	-5.4	91.1	94.1	95.4	100.1	100.0	99.0	98.2	93.7
1506	513	14.206	49.	0.61	0.	0.	2.27	-2.22	-5.4	96.1	97.5	97.6	100.8	101.2	98.6	94.8	89.5
1507	507	14.460	55.	0.58	0.	0.	2.62	-1.43	-5.9	93.8	97.6	98.4	103.0	103.4	101.2	100.1	96.5
1508	511	14.209	50.	0.61	0.	0.	2.66	-1.20	-6.1	98.8	101.5	101.6	104.0	103.9	101.5	98.4	92.7
1509	509	14.459	54.	0.65	0.	0.	2.96	-0.52	-6.8	95.6	99.5	100.6	105.4	104.8	103.6	102.3	99.1
1510	511	14.200	51.	0.65	0.	0.	2.98	-0.44	-6.8	100.8	103.7	103.3	106.3	105.9	103.9	100.7	95.1
1511	510	14.449	51.	0.61	0.	0.	3.27	0.18	-7.7	97.6	101.0	101.9	107.3	106.7	105.9	105.3	103.6
1512	511	14.217	49.	0.61	0.	0.	3.29	0.24	-7.8	102.7	105.3	104.3	107.9	107.9	105.8	102.2	97.3

Table IX. Test Matrix for Suppressed Coannular Plug Nozzle with 180° TAS at $V_r^{s,o}$ = 0.64, Sideline and Community, Orientation, TAS-16 (English Units).

NOZZLE MODEL 16 , AREA (MODEL SIZE-INNER= 4.000,OUTER=19.900, SHIELD=17.240, FULL SIZE-TOTAL=1400) SQ.IN.

TEST POINT	V AC FPS	I P R	I T T DEG.R	I V FPS	I W PPS	O P R	O T T DEG.R	O V FPS	O W PPS	S P R	S T T DEG.R	S V FPS	S W PPS	MIX P R	MIX T T DEG.R	MIX V FPS	W TOTAL PPS	THRUST TOTAL LBS
1603	0	1.565	821	1088	56.5	2.090	1387	1785	290.9	1.242	1373	996	124.1	1.699	1315	1494	471.5	21898
1604	400	1.581	831	1107	56.9	2.110	1403	1806	290.0	1.258	1369	1024	128.3	1.714	1325	1511	475.2	22316
1605	0	1.749	832	1215	64.2	2.376	1488	1988	318.9	1.317	1472	1159	136.5	1.882	1403	1675	519.7	27053
1606	400	1.766	839	1229	64.6	2.401	1521	2021	316.5	1.336	1479	1190	140.0	1.900	1425	1699	521.1	27525
1607	0	1.872	869	1309	67.5	2.685	1547	2148	353.1	1.407	1528	1310	151.2	2.079	1462	1828	571.8	32481
1608	400	2.096	885	1424	66.4	2.993	1556	2253	352.4	1.475	1518	1389	163.4	2.246	1469	1916	582.2	34673
1609	0	2.276	904	1509	79.4	2.970	1637	2307	378.9	1.500	1618	1463	162.0	2.293	1538	1984	620.3	38253
1610	400	2.296	893	1506	80.0	3.055	1649	2340	385.9	1.546	1608	1509	169.4	2.351	1543	2014	635.3	39763
1611	0	2.328	891	1515	81.7	3.615	1665	2495	457.3	1.734	1646	1703	192.4	2.713	1574	2177	731.4	49497
1612	400	2.343	901	1529	81.3	3.623	1670	2501	455.0	1.764	1632	1720	197.0	2.729	1574	2183	733.3	49757
1633	0	1.580	785	1075	58.5	2.097	1389	1790	286.9	1.243	1374	969	124.3	1.700	1310	1492	469.6	21774
1634	400	1.587	832	1112	57.2	2.125	1385	1802	290.1	1.269	1351	1035	131.8	1.722	1310	1509	479.1	22462
1635	0	1.755	841	1225	64.1	2.376	1495	1992	314.0	1.322	1476	1168	137.3	1.881	1409	1677	515.4	26868
1636	400	1.764	842	1230	64.5	2.405	1514	2017	314.2	1.346	1473	1203	142.5	1.902	1419	1697	521.2	27495
1637	0	1.877	889	1326	66.9	2.703	1567	2169	348.8	1.416	1543	1328	152.0	2.086	1481	1844	567.8	32547
1638	400	1.898	915	1356	64.6	2.721	1578	2183	347.3	1.445	1538	1362	157.3	2.108	1492	1862	569.3	32953
*1639	0	2.286	901	1510	79.0	3.042	1651	2338	382.3	1.527	1628	1497	165.6	2.335	1550	2012	626.8	39193
*1640	400	2.310	899	1516	79.3	3.071	1672	2362	380.7	1.563	1629	1537	170.8	2.362	1563	2032	630.8	39848
1641	0	2.334	918	1540	79.7	3.615	1687	2512	448.5	1.740	1663	1717	192.1	2.713	1596	2193	720.3	49092
1642	400	2.347	931	1555	79.2	3.645	1688	2520	449.6	1.785	1646	1744	198.5	2.745	1594	2203	727.3	49799
1645	0	3.032	1118	1911	93.9	3.038	1669	2350	379.1	1.520	1645	1498	163.6	2.412	1582	2066	636.5	40883
1651	0	1.707	882	1225	60.7	3.041	1652	2339	382.0	1.526	1630	1497	165.3	2.281	1569	1999	607.9	37769

Community Sideline
Orientation Orientation

* Indicates LV Plume Measurements; Refer to Table XIII.

TEST POINT	T AMB DEG.R	P AMB PSIA	RH PCT	I O V /V	S O V /V	S O W /W	LVM	LBM	NF DB	PNL (FULL SIZE, 2400 FT. SIDELINE), DB ANGLE RELATIVE TO INLET, DEGREES 50	60	70	90	120	130	140	150
1603	518	14.525	48.	0.61	0.56	0.43	1.27	-10.00	-3.2	83.5	85.0	86.3	93.5	93.2	93.4	90.9	87.7
1604	524	14.421	46.	0.61	0.57	0.44	1.29	-10.00	-3.2	87.7	88.2	88.0	93.2	90.6	88.7	84.2	79.7
1605	519	14.523	48.	0.61	0.58	0.43	1.76	-10.00	-3.8	87.6	89.4	90.7	96.5	96.3	96.9	94.3	90.9
1606	523	14.421	46.	0.61	0.59	0.44	1.80	-10.00	-3.8	91.8	91.8	91.2	96.5	94.0	93.1	88.3	84.5
1607	520	14.511	48.	0.61	0.61	0.43	2.13	-4.04	-4.4	90.9	92.4	93.9	99.1	98.5	99.1	97.8	95.2
1608	523	13.021	48.	0.63	0.62	0.46	2.33	-2.48	-4.6	94.4	95.0	94.8	99.4	96.1	95.2	91.2	87.3
1609	521	14.492	48.	0.65	0.63	0.43	2.49	-2.39	-5.0	92.8	94.4	95.7	100.9	101.4	102.4	102.1	99.1
1610	523	14.397	48.	0.64	0.64	0.44	2.54	-2.09	-5.1	95.6	96.6	97.0	101.2	99.1	98.4	95.7	91.0
1611	522	14.480	48.	0.61	0.68	0.42	2.89	-0.96	-6.2	94.7	96.6	98.0	103.9	105.3	106.9	106.9	103.9
1612	524	14.394	48.	0.61	0.69	0.43	2.89	-0.92	-6.2	98.0	99.1	99.5	103.7	102.9	102.7	100.9	97.2
1633	514	14.284	44.	0.60	0.56	0.43	1.27	-10.00	-3.2	82.8	85.6	85.7	93.2	92.1	90.6	88.8	84.9
1634	517	14.240	38.	0.62	0.57	0.45	1.31	-10.00	-3.3	86.9	89.0	87.8	93.0	88.7	84.4	83.2	76.8
1635	515	14.331	42.	0.61	0.59	0.44	1.78	-10.00	-3.7	87.5	90.5	90.4	96.6	96.1	95.6	93.0	90.4
1636	519	14.262	37.	0.61	0.60	0.45	1.82	-10.00	-3.7	90.9	92.6	91.0	96.4	92.9	87.9	87.8	81.3
1637	516	14.334	40.	0.61	0.61	0.44	2.19	-3.89	-4.4	89.4	92.8	93.3	99.5	98.6	99.2	97.1	94.9
1638	517	14.232	37.	0.62	0.62	0.45	2.23	-3.65	-4.4	93.8	96.4	94.7	99.3	95.7	91.9	91.5	85.9
1639	516	14.335	39.	0.65	0.64	0.43	2.57	-2.16	-5.0	91.4	94.7	95.2	101.2	100.7	101.8	102.1	99.7
1640	516	14.234	39.	0.64	0.65	0.45	2.61	-2.02	-5.1	96.3	98.3	96.9	101.1	98.3	98.2	95.5	90.1
1641	517	14.300	37.	0.61	0.68	0.43	2.93	-0.96	-6.0	93.6	96.8	97.3	104.1	104.1	106.2	106.5	102.8
1642	517	14.217	38.	0.62	0.69	0.44	2.95	-0.88	-6.1	98.6	100.7	98.6	103.3	101.6	102.3	101.4	96.8
1645	517	14.317	38.	0.61	0.64	0.43	2.68	-1.87	-5.2	91.6	94.9	95.1	101.5	102.0	102.6	103.0	100.7
1651	517	14.336	38.	0.52	0.64	0.43	2.54	-2.44	-4.8	91.1	94.5	95.0	100.4	100.4	101.5	101.1	98.8

Table X. Test Matrix for Suppressed Coannular Plug Nozzle with 180° TAS at $V_r^{s,o}$ = 0.83, Community Orientation, TAS-17 (English Units).

NOZZLE MODEL 17 , AREA (MODEL SIZE-INNER= 4.000,OUTER=19.900, SHIELD=17.240, FULL SIZE-TOTAL=1400) SQ.IN.

TEST POINT	V AC	I P R	I T T	I V	I W	O P R	O T T	O V	.O W	S P R	S T T	S V	.S W	MIX P R	MIX T T	MIX V	. W TOTAL	THRUST TOTAL
	FPS		DEG.R	FPS	PPS		DEG.R	FPS	PPS		DEG.R	FPS	PPS		DEG.R	FPS	PPS	LBS
1703	0	1.572	852	1114	55.8	2.100	1431	1819	283.1	1.492	1417	1359	172.0	1.788	1363	1587	510.9	25206
1704	400	1.587	833	1113	57.1	2.075	1385	1776	283.4	1.516	1356	1355	180.1	1.786	1314	1557	520.7	25201
1705	0	1.746	850	1226	63.4	2.385	1533	2027	311.7	1.656	1515	1568	190.6	2.011	1451	1782	565.7	31339
1706	400	1.761	839	1227	64.4	2.385	1484	1988	314.4	1.693	1451	1565	200.0	2.022	1401	1757	578.9	31618
1707	0	1.878	897	1333	66.7	2.686	1590	2179	343.0	1.834	1571	1740	209.4	2.239	1509	1939	619.1	37316
1708	400	1.879	879	1320	67.4	2.704	1566	2169	346.9	1.888	1532	1755	211.9	2.274	1481	1938	626.2	37710
1709	0	2.286	900	1509	78.8	3.060	1671	2358	380.8	2.072	1649	1939	224.3	2.562	1575	2123	683.9	45126
1710	400	2.297	913	1523	78.2	3.059	1655	2346	380.9	2.131	1618	1954	232.0	2.587	1559	2121	691.1	45556
1711	0	2.329	908	1530	79.8	3.593	1654	2482	449.4	2.441	1636	2114	265.4	2.983	1573	2264	794.6	55900
1712	400	2.337	919	1542	79.6	3.667	1676	2515	455.5	2.538	1646	2162	275.0	3.060	1592	2300	810.1	57905
1715	0	1.758	899	1268	62.2	3.041	1666	2349	379.0	2.065	1645	1932	223.9	2.502	1587	2108	665.1	43570
1721	0	3.021	1158	1944	91.6	3.057	1650	2342	382.9	2.071	1632	1928	225.5	2.643	1580	2157	700.1	46930
1722	400	3.046	1135	1929	93.0	3.054	1653	2343	380.6	2.116	1620	1947	230.3	2.660	1574	2159	704.0	47231

TEST POINT	T AMB	P AMB	RH	I O V /V	S O V /V	S O W /W	LVM	LBM	NF	PNL (FULL SIZE,2400 FT SIDELINE),DB ANGLE RELATIVE TO INLET,DEGREES						
	DEG.R	PSIA	PCT						DB	50	60	70	90	120	130	140	150
1703	520	14.299	21.	0.61	0.75	0.61	1.52	-10.00	-3.5	83.8	86.9	88.4	95.4	92.3	92.0	91.5	87.1
1704	510	14.245	29.	0.63	0.76	0.64	1.48	-10.00	-3.7	88.9	91.0	90.6	95.3	90.1	87.9	84.5	77.6
1705	520	14.300	21.	0.61	0.77	0.61	2.02	-4.71	-4.1	87.8	91.0	91.8	97.8	97.4	96.5	95.9	92.7
1706	512	14.242	24.	0.62	0.79	0.64	2.00	-4.52	-4.3	92.4	93.8	93.8	98.4	93.3	92.5	89.8	83.0
1707	520	14.294	19.	0.61	0.80	0.61	2.39	-2.59	-4.8	89.7	93.1	94.4	100.3	100.7	99.8	100.1	97.5
1708	514	14.249	27.	0.61	0.81	0.61	2.41	-2.41	-5.0	94.9	96.6	96.3	100.5	96.8	96.1	93.7	87.3
1709	520	14.288	22.	0.64	0.82	0.59	2.78	-1.31	-5.7	92.3	95.9	96.2	102.4	103.8	103.5	104.4	101.5
1710	516	14.221	26.	0.65	0.83	0.61	2.80	-1.23	-5.8	96.3	98.6	97.9	102.2	100.3	99.9	98.4	93.4
1711	518	14.269	25.	0.62	0.85	0.59	3.07	-0.39	-6.8	95.3	98.4	98.9	104.5	107.0	108.4	109.6	104.8
1712	518	14.266	20.	0.61	0.86	0.60	3.14	-0.26	-6.9	100.0	101.9	100.8	103.9	105.7	105.1	105.8	99.7
1715	520	14.289	25.	0.54	0.82	0.59	2.75	-1.50	-5.4	91.7	95.7	96.9	102.0	103.8	103.3	104.6	101.6
1721	519	14.286	24.	0.83	0.82	0.59	2.86	-1.11	-5.9	92.3	95.6	97.1	102.9	104.2	104.8	106.8	102.9
1722	516	14.228	25.	0.82	0.83	0.61	2.87	-1.06	-5.9	96.9	99.3	97.9	102.0	100.2	100.3	99.8	94.7

Table XI. Test Matrix for Suppressed Coannular Plug Nozzle with 180° TAS at $V_r^{s,o}$ = 0.48, Community Orientation, TAS-18 (English Units).

NOZZLE MODEL 18 , AREA (MODEL SIZE-INNER= 4.000,OUTER=19.900, SHIELD=17.240, FULL SIZE-TOTAL=1400) SQ.IN.

TEST POINT	V AC FPS	I P R	I T T DEG.R	I V FPS	I W PPS	O P R	O T T DEG.R	O V FPS	O W PPS	S P R	S T T DEG.R	S V FPS	S W PPS	MIX P R	MIX T T DEG.R	MIX V FPS	W TOTAL PPS	THRUST TOTAL LBS
1803	0	1.544	837	1084	55.0	2.056	1359	1749	289.6	1.096	1343	645	79.4	1.670	1288	1456	424.0	19186
1804	400	1.583	844	1117	56.6	2.105	1392	1796	286.8	1.123	1339	724	90.0	1.691	1310	1485	433.4	20000
1805	0	1.747	818	1204	64.7	2.361	1493	1985	313.1	1.142	1477	815	92.2	1.846	1397	1648	470.0	24067
1806	400	1.768	856	1244	64.1	2.404	1507	2012	314.7	1.164	1447	860	99.9	1.869	1408	1669	478.7	24832
1807	0	1.906	891	1343	65.2	2.719	1565	2173	345.9	1.185	1545	938	102.4	2.052	1475	1821	513.5	29066
1808	400	1.886	906	1344	66.7	2.717	1585	2187	346.3	1.212	1523	991	110.4	2.051	1485	1827	523.3	29716
1809	0	2.272	879	1466	79.6	3.021	1659	2338	379.2	1.256	1635	1115	116.7	2.256	1546	1972	575.6	35275
1810	400	2.300	861	1480	80.9	3.055	1682	2365	377.9	1.272	1616	1138	120.9	2.274	1554	1985	579.6	35763
1811	0	2.321	907	1527	79.9	3.588	1644	2473	452.3	1.375	1619	1304	141.1	2.586	1551	2116	673.3	44272
1812	400	2.336	912	1535	79.8	3.621	1647	2482	453.5	1.385	1594	1308	144.0	2.605	1549	2121	677.3	44650

TEST POINT	T AMB DEG.R	P AMB PSIA	RH PCT	I O V /V	S O V /V	S O W /W	LVM	LBM	NF	PNL (FULL SIZE,2400 FT SIDELINE),DB ANGLE RELATIVE TO INLET,DEGREES						
									DB	50	60	70	90	120	130	140	150
1803	525	14.545	68.	0.62	0.37	0.27	1.12	-10.00	-3.1	81.5	84.2	84.6	91.8	91.7	90.4	89.0	83.7
1804	523	14.251	74.	0.62	0.40	0.31	1.22	-10.00	-3.1	87.2	88.7	87.8	92.6	88.9	86.1	83.9	78.4
1805	523	14.374	73.	0.61	0.41	0.29	1.67	-10.00	-3.7	86.7	89.4	90.0	95.7	95.2	94.2	93.2	89.3
1806	520	14.260	81.	0.62	0.43	0.32	1.74	-10.00	-3.6	90.6	92.8	91.5	96.3	93.0	90.4	88.4	82.0
1807	521	14.120	77.	0.62	0.43	0.30	2.11	-5.17	-4.2	89.9	93.3	93.9	99.4	97.9	97.3	96.7	93.7
1808	519	14.242	85.	0.61	0.45	0.32	2.14	-5.00	-4.2	94.0	96.2	95.6	99.9	95.9	93.6	91.8	85.2
1809	521	14.358	80.	0.64	0.48	0.31	2.46	-2.84	-4.8	92.3	95.4	95.9	101.6	101.8	101.7	101.4	99.3
1810	519	14.247	86.	0.63	0.48	0.32	2.49	-2.68	-4.8	96.6	98.9	98.0	101.9	98.9	97.0	95.6	89.1
1811	520	14.332	80.	0.62	0.53	0.31	2.77	-1.40	-5.8	94.3	97.1	97.6	104.1	104.3	105.2	106.2	102.7
1812	520	14.251	81.	0.62	0.53	0.32	2.78	-1.34	-5.9	98.3	100.2	99.2	103.6	101.5	100.2	99.6	93.6

Table XII. Test Matrix for Suppressed Coannular Plug Nozzle with 360° TAS at $V_r^{s,o}$ = 0.83, TAS-19 (English Units).

NOZZLE MODEL 19 , AREA (MODEL SIZE-INNER= 4.000,OUTER=19.900, SHIELD=17.770, FULL SIZE-TOTAL=1399) SQ.IN.

TEST POINT	V AC FPS	I P R	I T DEG.R	I V FPS	I W PPS	O P R	O T DEG.R	O V FPS	O W PPS	S P R	S T DEG.R	S V FPS	S W PPS	MIX P R	MIX T DEG.R	MIX V FPS	W TOTAL PPS	THRUST TOTAL LBS
1903	0	1.578	817	1095	56.5	2.101	1379	1785	285.7	1.532	1369	1377	185.1	1.802	1315	1568	527.4	25703
1904	400	1.573	832	1102	55.8	2.110	1390	1798	284.8	1.561	1360	1400	190.4	1.817	1321	1582	531.0	26109
1905	0	1.751	830	1214	63.6	2.381	1477	1982	312.4	1.700	1465	1579	203.6	2.019	1402	1756	579.6	31639
1906	400	1.751	819	1206	64.0	2.376	1488	1988	309.4	1.727	1458	1596	207.7	2.027	1404	1762	581.0	31818
1907	0	1.871	871	1310	66.6	2.691	1563	2162	343.0	1.904	1546	1774	217.5	2.269	1483	1937	627.1	37746
1908	400	1.877	881	1320	66.4	2.701	1556	2161	344.2	1.945	1524	1788	223.2	2.292	1474	1941	633.8	38241
1909	0	2.278	905	1510	77.6	3.032	1649	2334	376.4	2.144	1631	1968	238.6	2.571	1559	2116	692.8	45543
1910	400	2.283	895	1503	77.9	3.042	1647	2335	376.3	2.189	1615	1983	243.8	2.595	1552	2119	698.0	45981
1911	0	2.324	896	1518	79.4	3.614	1658	2490	447.1	2.565	1643	2170	284.2	3.035	1578	2283	810.7	57515
1912	400	2.322	906	1526	78.7	3.613	1639	2475	448.6	2.607	1609	2164	291.2	3.054	1558	2273	818.5	57820
1921	0	3.018	1128	1916	91.8	3.045	1663	2348	375.9	2.155	1641	1981	238.7	2.662	1586	2168	706.4	47595
1922	400	3.033	1143	1933	91.3	3.043	1656	2342	375.1	2.188	1624	1987	242.7	2.677	1579	2168	709.1	47782

TEST POINT	T AMB DEG.R	P AMB PSIA	RH PCT	I O V /V	S O V /V	S O W /W	LVM	LBM	NF DB	PNL (FULL SIZE,2400 FT.SIDELINE),DB ANGLE RELATIVE TO INLET,DEGREES 50	60	70	90	120	130	140	150
1903	493	14.333	49.	0.61	0.77	0.65	1.58	-10.00	-3.7	84.8	87.5	88.5	95.4	94.2	94.4	93.3	89.1
1904	496	14.282	42.	0.61	0.78	0.67	1.61	-10.00	-3.8	89.7	91.7	91.1	96.1	90.9	89.6	86.5	80.2
1905	494	14.326	43.	0.61	0.80	0.65	2.07	-4.58	-4.3	87.4	90.5	91.9	98.0	96.6	98.0	97.9	95.1
1906	495	14.269	43.	0.61	0.80	0.67	2.08	-4.45	-4.3	91.7	94.5	94.1	98.6	94.0	92.7	90.5	84.5
1907	495	14.324	44.	0.61	0.82	0.63	2.49	-2.44	-5.0	89.8	92.5	93.7	99.9	99.2	101.5	101.8	99.4
1908	495	14.283	45.	0.61	0.83	0.65	2.50	-2.32	-5.1	93.0	95.8	95.4	99.8	97.0	95.1	94.7	90.3
1909	496	14.339	39.	0.65	0.84	0.63	2.87	-1.28	-5.8	91.7	94.0	95.1	101.1	103.3	105.3	107.8	103.6
1910	495	14.277	43.	0.64	0.85	0.65	2.88	-1.21	-5.8	95.3	97.3	96.6	100.8	100.4	99.5	100.0	95.9
1911	496	14.311	41.	0.61	0.87	0.64	3.20	-0.30	-6.9	94.3	96.5	97.4	104.1	106.5	109.8	111.8	104.7
1912	495	14.275	42.	0.62	0.87	0.65	3.18	-0.27	-7.0	97.5	99.7	99.1	103.2	104.2	104.9	104.3	99.7
1921	495	14.318	46.	0.82	0.84	0.63	2.98	-1.06	-5.9	92.7	95.0	96.0	102.3	104.2	107.2	110.6	104.4
1922	496	14.262	39.	0.83	0.85	0.65	2.98	-1.02	-6.0	96.2	97.8	97.2	101.4	100.6	101.4	102.0	97.4

Figures 25 and 26 describe the scope of acoustic tests on an engine operating line in terms of shield to outer stream velocity ratios as a function of mass averaged velocity, V_{mix}, and outer stream pressure ratio, p_r^o.

Test Matrix for Baseline Unsuppressed Coannular Plug Nozzle (TAS-10)

Table IV summarizes the test matrix for the baseline unsuppressed coannular plug nozzle. The distribution of the test points is as follows:

a. Test Points 1001, 1003, 1005, 1007, 1009, 1011, 1021, and 1002, 1004, 1006, 1008, 1010, 1012, and 1022 simulate typical engine operating conditions under static and simulated flight, respectively. The aerodynamic conditions of these test points have been selected to yield an inner to outer stream velocity ratio that is in the neighborhood of 0.6.

b. Test Points 1015, 1019, 1009, 1021, 1023, 1025, and 1027 yield variation in P_r^i (1.75, 1.90, 2.04, 2.28, 2.61, 2.82, and 3.01, respectively) for a fixed P_r^o of 3.02. The objective of these tests is to determine whether front quadrant noise can be reduced for a given supersonic outer stream by tuning the inner stream such that expansion waves of one stream cancel the compression waves of the other.

c. Test Points 1013, 1015, and 1017, having subsonic inner streams are to be compared with 1007, 1021, and 1011 that have supersonic inner streams to determine the benefit, if any, of subsonic inner streams on front quadrant shock noise.

Test Matrices for Unsuppressed Coannular Plug Nozzle With 180° Shield (TAS-11 and -12)

As described in Table III, the unsuppressed coannular plug nozzle with the 180° partial thermal acoustic shield was tested at shield to outer stream velocity ratio, $V_r^{s,o}$, of 0.64* (TAS-11) and 0.83* (TAS-12) to investigate the sensitivity of $V_r^{s,o}$ on the acoustic benefit of a thermal acoustic shield. Tables V and VI summarize the test matrices for TAS-11 and TAS-12, respectively. The distribution of test points is as follows:

a. Test Points 1103 through 1112 and 1113 through 1142 of TAS-11 simulate typical engine operating conditions with the shield in sideline and community orientations, respectively.

*These ratios refer to a typical AST/VCE takeoff condition only.

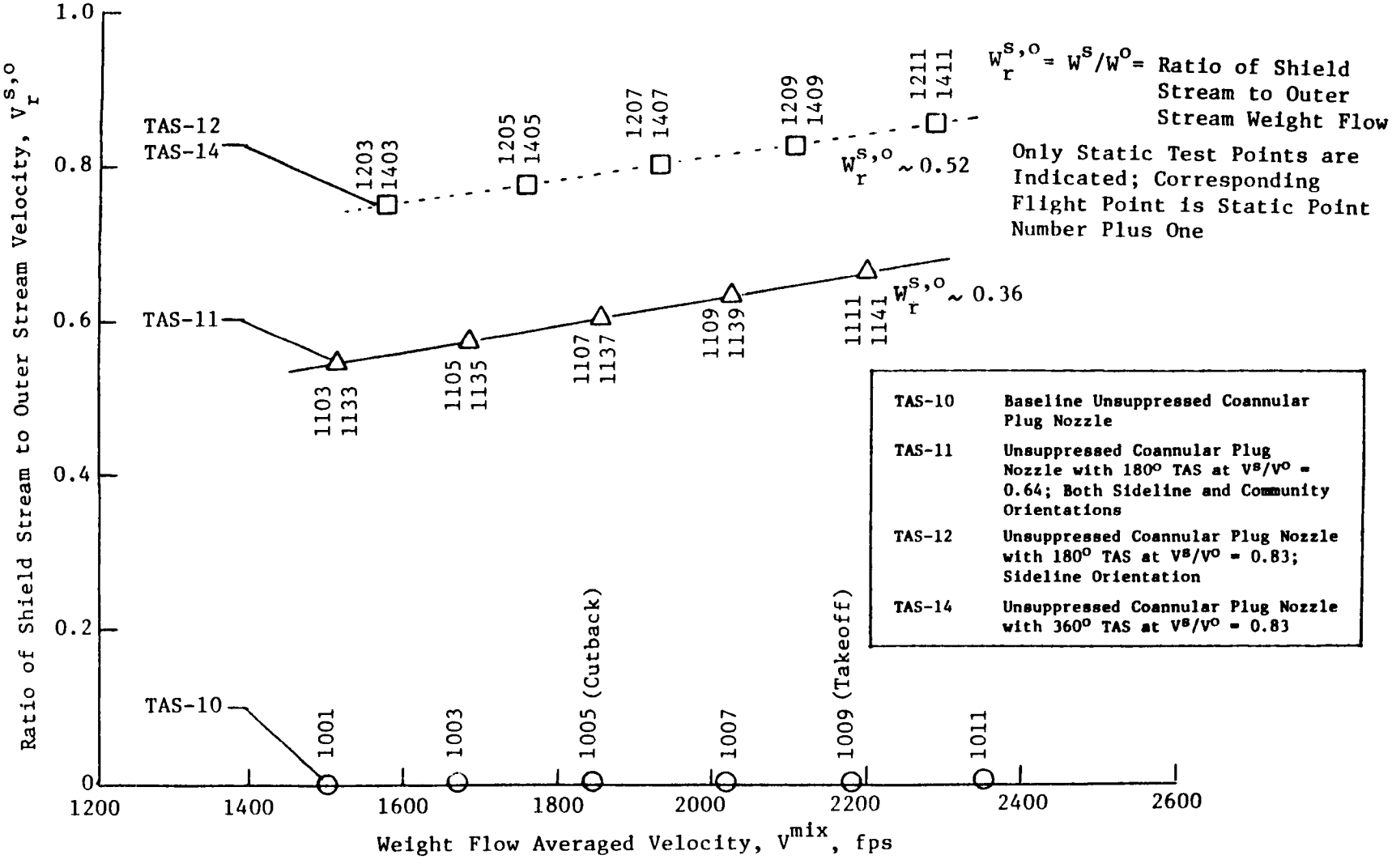

Figure 25. Description of Acoustic Tests as a Function of Weight Flow Averaged Velocity: Unsuppressed Coannular Plug Nozzles.

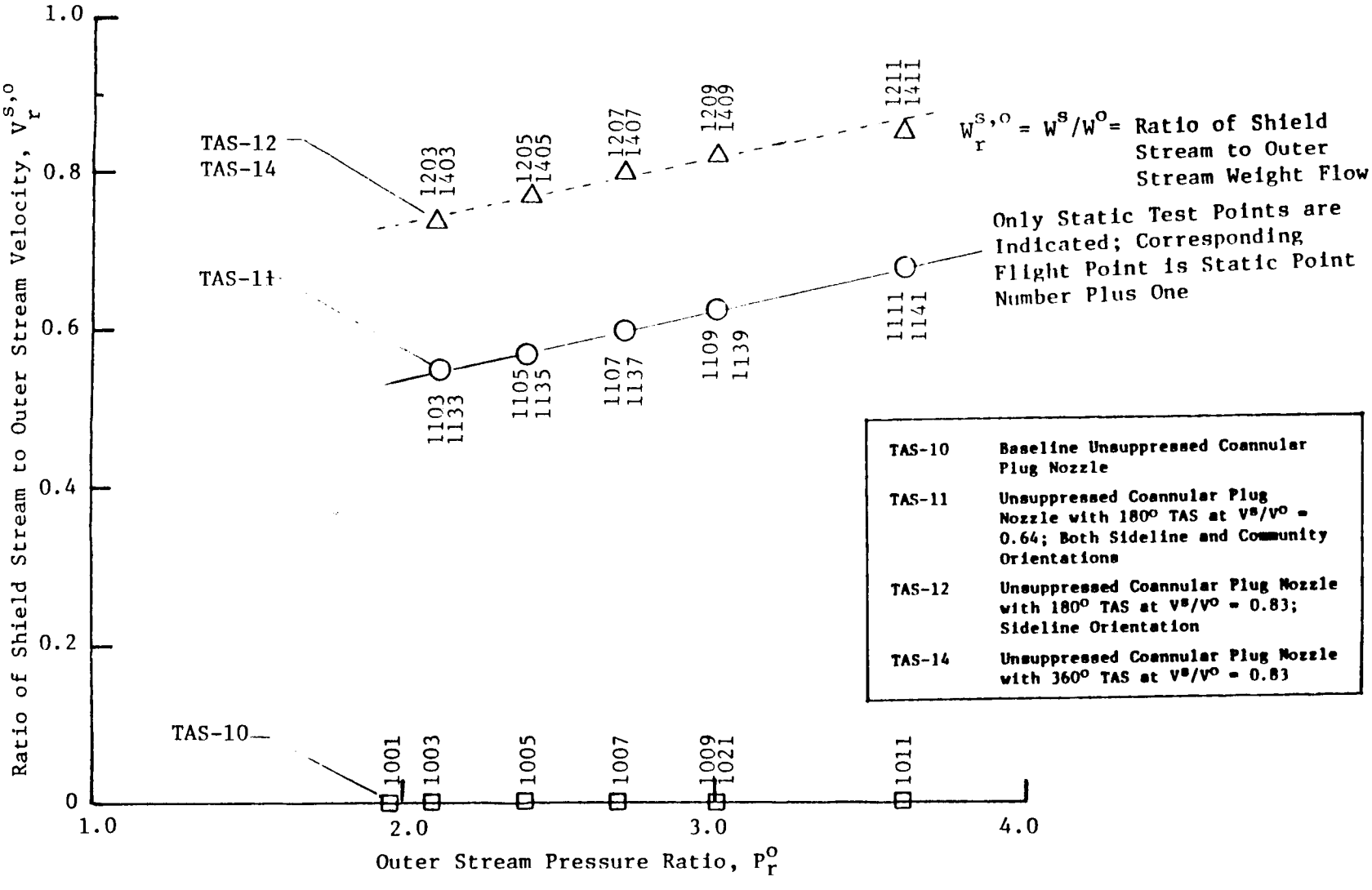

Figure 26. Description of Acoustic Tests as a Function of Outer Stream Pressure Ratio: Unsuppressed Coannular Plug Nozzles.

b. V^{mix} of static Test Points 1103/1133, 1105/1135, 1107/1137, 1109/1139, and 1111/1141 match reasonably well with those of 1001, 1003, 1005, 1007, and 1021 of the unshielded baseline coannular nozzle (TAS-10), respectively. Similarly, V^{mix} of corresponding flight points of TAS-11 and TAS-10 match one another.

c. Test Points 1203 through 1212 of TAS-12 simulate typical engine operating conditions with the 180° shield in sideline orientation.

d. Typical takeoff Test Point 1209/1210 of TAS-12 has $V^i/V^o \approx 0.65$ and $V^s/V^o \approx 0.83$. The inner stream of this test point was modified during Test Point 1221/1222 to yield $V^i/V^o \approx 0.83$ such that the effect of equal shear by the shield and inner streams on the primary outer stream can be determined.

Test Matrix for Unsuppressed Coannular Plug Nozzle with 360° Shield (TAS-14)

Configuration TAS-14 employs a full 360° thermal acoustic shield of 0.5 in. thickness on the baseline coannular plug nozzle (TAS-10). The shield flow area of this configuration is equal to that of the 0.97-in.-thick, 180° partial shield of TAS-11 and TAS-12. This configuration was tested with the choke plates identical to those used with TAS-12 so that the shield to outer stream velocity and weight flow ratios of TAS-12 and TAS-14 are comparable. A comparison of the acoustic data of these two configurations should indicate the benefit of a partial thick shield over a thinner full shield of equal area.

The test matrix of this configuration is presented in Table VII. The distribution of the test points is as follows:

a. Test Points 1403-1412 simulate typical engine operating conditions with a shield to outer stream velocity ratio of 0.83 at takeoff.

b. Typical takeoff Test Point 1409/1410 has $V^i/V^o \approx 0.65$ and $V^s/V^o \approx 0.83$. The inner stream was modified for Test Point 1421/1422 to yield $V^i/V^o \approx V^s/V^o \approx 0.83$.

3.1.2 Test Matrices of Suppressed Coannular Plug Nozzles

A total of 69 acoustic test points were completed on the mechanically suppressed coannular plug nozzle with and without thermal acoustic shields. The test configurations consisted of:

a. The baseline coannular configuration with the 20 chute suppressor in the outer stream (TAS-15).

b. The baseline TAS-15 with the 0.97-inch-thick 180° shield and the choke plates selected to give V^s/V^o of 0.64, 0.83, and 0.48 (TAS-16, -17, and -18) at a typical takeoff condition.

c. The baseline TAS-15 with 0.50-inch-thick 360° shield (TAS-19) with the choke plates identical to those of TAS-17 to give V^s/V^o of 0.83.

Figures 27 and 28 describe the scope of acoustic tests on an engine operating line in terms of shield to outer stream velocity ratios as a function of mass averaged velocity, V^{mix} and outer stream pressure ratio p_r^o.

Test Matrix for Baseline Suppressed Coannular Plug Nozzle (TAS-15)

Table VIII summarizes the test matrix for the baseline suppressed coannular plug configuration. The test points simulate typical engine operating conditions under static and simulated flight.

Test Matrix for Suppressed Coannular Plug Nozzle With 180° Shield (TAS-16, -17, and -18)

As described in Table III, the suppressed coannular plug nozzle with 180° thermal acoustic shield was tested at shield to outer stream velocity ratio, $V_r^{s,o}$, of 0.64 (TAS-16), 0.83 (TAS-17), and 0.48 (TAS-18) to investigate the sensitivity of $V_r^{s,o}$ on the acoustic benefit of the thermal acoustic shield. Tables IX, X, and XI summarize the test matrices for TAS-16, TAS-17, and TAS-18, respectively. The distribution of the test points is as follows:

a. Test Points 1603 through 1612 and 1633 through 1642 of TAS-16 simulate typical engine operating conditions with the shield in sideline and community orientation, respectively. Test Points 1651, 1639, and 1645 yield variation in P_r^i (1.71, 2.28, and 3.03) for a fixed P_r^o ($\approx$ 3.04). The objective of these three test points is to determine the benefit, if any, of subsonic inner stream on front quadrant shock associated noise.

b. Test Points 1703 through 1712 of TAS-17 simulate typical engine operating conditions with shield in community orientation. The typical takeoff Test Point 1709/1720 of this configuration has $V^i/V^o \approx 0.64$ and $V^s/V^o \approx 0.83$. The inner stream of this test point was modified during Test Point 1721/1722 to yield $V^i/V^o \approx V^s/V^o \approx 0.83$ such that the effect of equal stress by the shield and inner streams on the primary outer stream can be determined.

c. Test Points 1803 through 1812 of TAS-18 simulate typical engine operating conditions with shield in community orientation.

Test Matrix for Suppressed Coannular Plug Nozzle With 360° Shield (TAS-19)

Configuration TAS-19 employs a full 360° thermal acoustic shield of 0.5-inch thickness on the baseline suppressed coannular plug nozzle (TAS-15). The

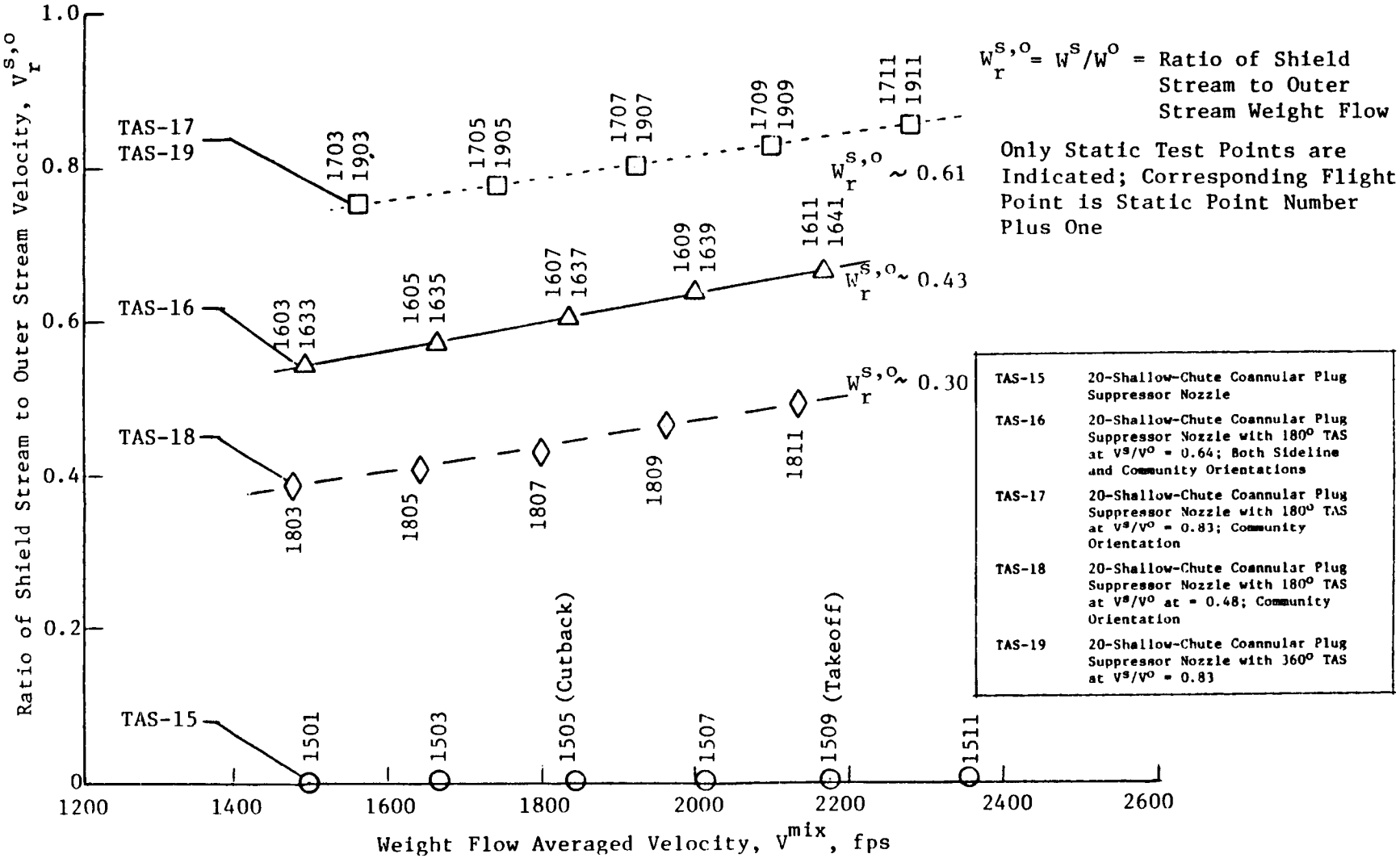

Figure 27. Description of Acoustic Tests as a Function of Weight Flow Averaged Velocity: Suppressed Coannular Plug Nozzles.

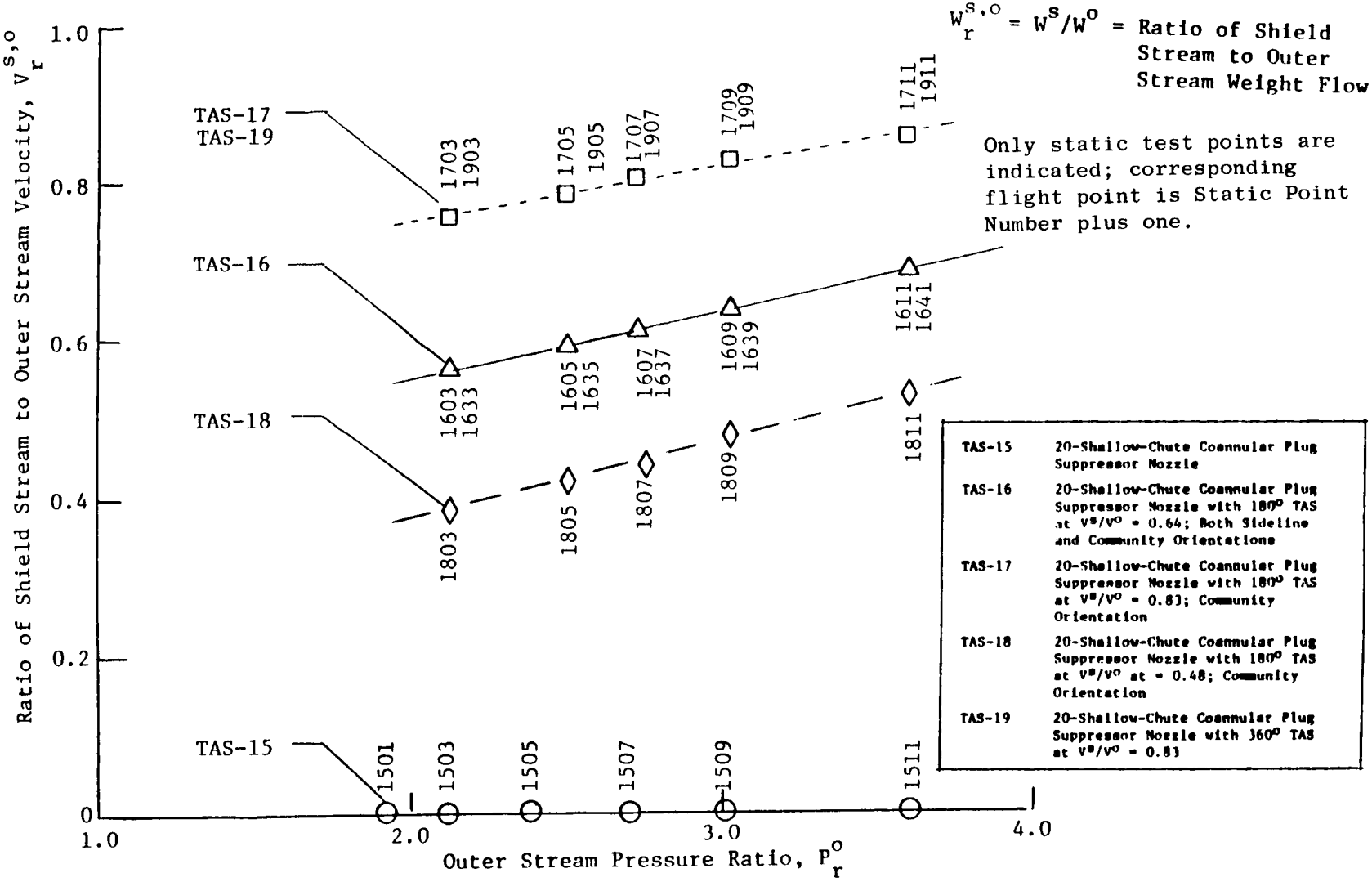

Figure 28. Description of Acoustic Tests as a Function of Outer Stream Pressure Ratio: Suppressed Coannular Plug Nozzles.

shield flow area of this configuration is equal to that of the 0.97-inch-thick 180° partial shield of TAS-16 through TAS-18. This configuration was tested with the choke plates identical to those used with TAS-17 so that the shield to outer stream velocity and weight flow ratios of TAS-17 and TAS-19 are comparable.

The test matrix of this configuration is presented in Table XII. The distribution of the test points is as follows:

a. Test Points 1903 through 1912 simulate typical engine operating conditions with shield to outer stream velocity ratio of 0.83 at takeoff.

b. Typical takeoff Test Point 1909/1910 has $V^i/V^o \approx 0.65$ and $V^s/V^o \approx 0.83$. The inner stream was modified for Test Point 1921/1922 to yield $V^i/V^o \approx V^s/V^o \approx 0.83$.

3.2 LASER VELOCIMETER TESTS

Aerodynamic flow conditions that define the LV test points are presented in Table XIII. The test points consist of:

a. One static and one simulated flight point (LV Test Points 1 and 2) of Configuration TAS-11 (unsuppressed coannular plug nozzle with 180° shield of 0.97 inch thickness operating with $V^s/V^o \approx 0.64$) at a typical takeoff aerodynamic flow condition.

b. One static and one simulated flight point (LV Test Points 3 and 4) of Configuration TAS-16 (20-chute coannular plug nozzle with 180° shield of 0.97 inch thickness, operating with $V^s/V^o \approx 0.64$) at a typical takeoff aerodynamic flow condition.

The experimentally obtained acoustic and LV data are presented in detail in the Comprehensive Data Report of this study (Reference 27).

Table XIII. Aerodynamic Conditions of Laser Velocimeter Tests on Unsuppressed and Suppressed Coannular Plug Nozzle with Partial Thermal Acoustic Shield.

Configuration	Description of Configuration	LV Test Point	Match. Acoust. Test Point	V_{ac} (fps)	Inner Stream			Outer Stream			Shield Stream			Mixed Stream			$V_r^{i,o} =$	$V_t^{s,o} =$
					P_r^i	T_T^i (°R)	V^i (fps)	P_r^o	T_T^o (°R)	V^o (fps)	P_r^s	T_T^s (°R)	V^s (fps)	P_r^{mix}	T_T^{mix} (°R)	V^{mix} (fps)	Vi/Vo	Vs/Vo
TAS-11	Unsuppressed Coannular Plug Nozzle with 180° TAS	1	1139	0	2.28	905	1512	3.01	1632	2314	1.49	1617	1447	2.36	1533	2011	0.65	0.63
		2	1140	400	2.28	943	1540	3.02	1642	2325	1.51	1607	1473	2.37	1545	2025	0.66	0.63
TAS-16	20 Shallow-Chute Coannular Plug Nozzle with 180° TAS	3	1639	0	2.29	901	1510	3.04	1651	2338	1.53	1628	1497	2.34	1550	2012	0.64	0.64
		4	1640	400	2.31	899	1516	3.07	1672	2362	1.56	1629	1537	2.36	1563	2032	0.64	0.65

4.0 ACOUSTIC AND DIAGNOSTIC TEST RESULTS

The acoustic and diagnostic laser velocimeter test results obtained from the model configurations described in Section 2.3 at the aerodynamic conditions summarized in Section 3.0 are analyzed and presented in this section.

This section is subdivided into two major subsections that discuss, respectively, the influence of the various thermal acoustic shields on the acoustic and mean velocity data of baseline unsuppressed high radius-ratio coannular plug nozzle (TAS-10) and the baseline suppressed coannular plug nozzle with the 20-chute (TAS-15) suppressor in the outer stream.

Under each of the subsections, the general acoustic characteristics of the baseline coannular nozzles are presented first and compared to the data of a convergent circular nozzle in order to demonstrate their acoustic benefit. The relative effectiveness and influence of the various thermal acoustic shields studied under this dual-flow study are presented and discussed next.

Unless otherwise stated, the acoustic results presented are measured data scaled to a typical product size of A^T = 0.903 square meters (1,400 square inches) and extrapolated to a sideline of 731.5 meters (2,400 feet) and corrected to a standard day [15° C (59° F) and 80% relative humidity] atmospheric attenuation (Shields and Bass method, Reference 17).

4.1 UNSUPPRESSED COANNULAR PLUG NOZZLE DATA

This section summarizes the acoustic and diagnostic data of the baseline unsuppressed coannular plug nozzle (TAS-10) and unsuppressed coannular plug nozzle with 0.50 in. thick partial shield (TAS-11 and TAS-12) and with 0.97 in. thick full shield (TAS-14). The scope of the acoustic tests with these four configurations was presented earlier in Table III and Figures 25 and 26. The diagnostic laser velocimeter measurements were limited to a static plume of TAS-11 at a typical takeoff condition (refer to Table XIII for flow conditions).

4.1.1 Baseline Coannular Plug Nozzle

The acoustic benefit of coannular nozzles relative to a convergent circular nozzle has been established in References 21, 22, 28, and 29 by systematic acoustic and wind tunnel aerodynamic performance measurements on scale model nozzles. The measured data identified the mixed stream velocity Vmix, outer stream radius ratio R_r^o, inner-to-outer stream velocity ratio $V_r^{i,o}$, and the inner-to-outer stream area ratio $A_r^{i,o}$ as the parameters that had significant influence on the measured jet noise data. A typical high-radius-ratio coannular plug nozzle with an outer stream radius ratio of 0.853 and an inner-to-outer stream area ratio of 0.2 was determined to give an acoustic perceived noise level benefit, relative to a convergent circular nozzle, of (a) 6 and 5.5 dB at peak jet noise angle of θ_j = 130° and (b) 6.5 and 6 dB at a forward

quadrant angle of $\theta_i = 60°$ under static and simulated flight (V_{ac} = 400 fps), conditions, respectively. These results, obtained from scale model data extrapolated to a typical supersonic cruise engine size of 1400 in^2 at a 2400 ft sideline distance, are for a typical AST/VCE takeoff cycle condition of $V^{mix} \sim 2300$ fps. Engine acoustic results obtained with a geometrically similar coannular plug nozzle on the YJ101 engine (Reference 1) confirmed the static results of the scale model studies.

The unsuppressed baseline coannular plug nozzle (TAS-10) of this study has an outer stream radius ratio of 0.85 and an inner-to-outer stream area ratio of 0.197. This configuration (A_o = 23.4 in^2 and A_i = 4.6 in^2) was tested over a range of flow variables that simulate typical AST/VCE operating conditions. The peak angle jet noise data obtained under static and simulated flight (V_{ac} = 400 fps) conditions are presented in Figures 29 and 30, respectively. In these figures, the normalized perceived noise levels at $\theta_i = 130$ are presented as functions of mixed jet velocity parameter 10 log (V^{mix}/a_{amb}). The measured aft-quadrant data are compared in each of these figures to the data of the convergent circular nozzle (References 21 and 22). A similar set of forward-quadrant data are presented in Figures 31 and 32. In these figures, the preceived noise levels at a typical forward quadrant angle of $\theta_i = 60°$ are plotted as a function of the effective shock strength parameter, 10 log β^{eff}. The PNL acoustic benefit with the unsuppressed coannular plug nozzle (TAS-10), at typical takeoff condition and relative to a convergent circular nozzles, is observed to be 6.5 and 5.5 dB at the peak jet noise angle of $\theta_i = 130°$ and 5.0 and 7.0 dB at a typical forward quadrant angle of $\theta_i = 60°$ for the static and simulated flight cases, respectively.

The static and simulated flight baseline coannular plug nozzle jet noise spectral data are compared with the corresponding results of a convergent circular nozzle in Figures 33 and 34, respectively, for typical takeoff and cutback cycle conditions. The data indicate significant coannular nozzle benefit over most of the frequency bands in the aft quadrant sound pressure levels that are dominated by jet mixing noise.

During each of the acoustic test points, on-line narrow band data were gathered with the unshielded and shielded coannular configurations using a Spectral Dynamics (SD-345) analyzer to identify screech, if any, in the measured data. While the majority of the acoustic test points were identified to be screech-free, distinct screech was identified with Test Point 1009 of the baseline coannular configuration (TAS-10). This is illustrated in Figure 35(a). The aerodynamic flow conditions of this test point correspond to a typical takeoff condition on the AST/VCE cycle. Efforts were made to eliminate the screech by changing the set inner pressure ratios (P_r^i) for the given outer pressure ratio of $P_r^o \sim 3.02$. It was observed that the screech was eliminated by changing the inner pressure ratio to 2.27 instead of the set condition of 2.07. The on-line data obtained under the modified conditions (Test Point

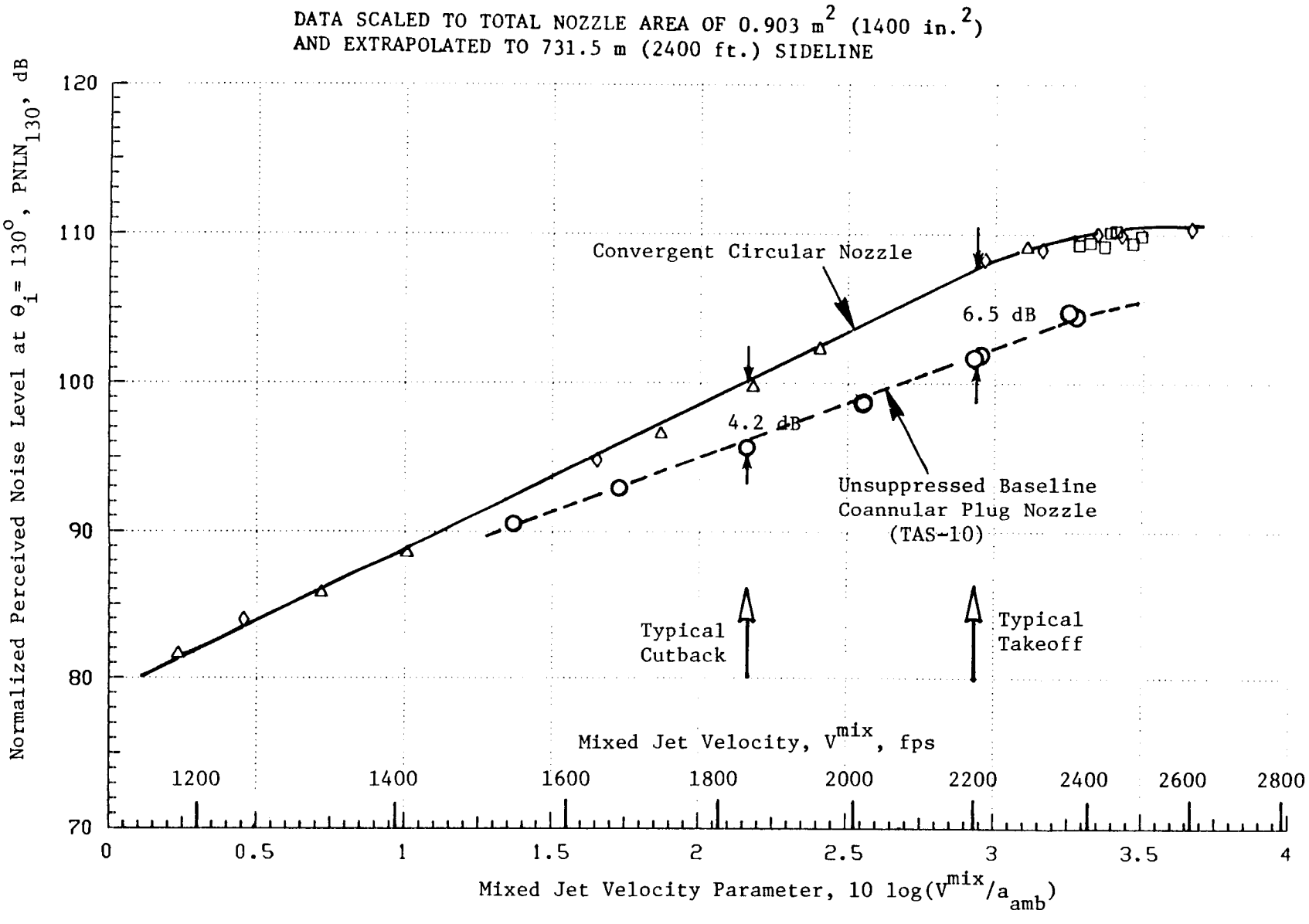

Figure 29. Comparison of Typical Aft-Quadrant Normalized Perceived Noise Level Data of Unsuppressed Baseline Coannular Plug Nozzle (TAS-10) with Those of Convergent Circular Nozzle (Static).

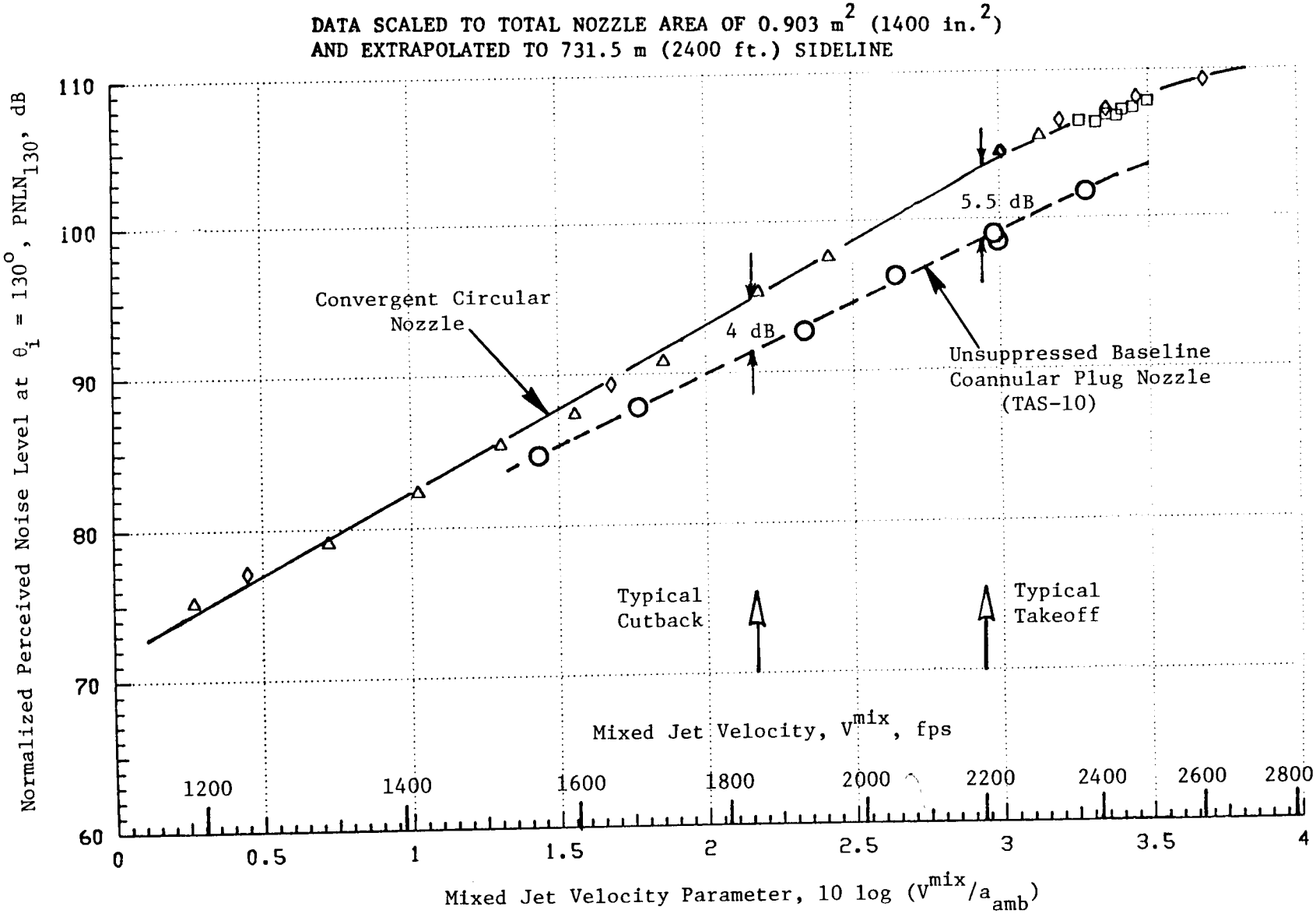

Figure 30. Comparison of Typical Aft-Quadrant Perceived Noise Level Data of Unsuppressed Coannular Plug Nozzle (TAS-10) with Those of Convergent Circular Nozzle (Simulated Flight).

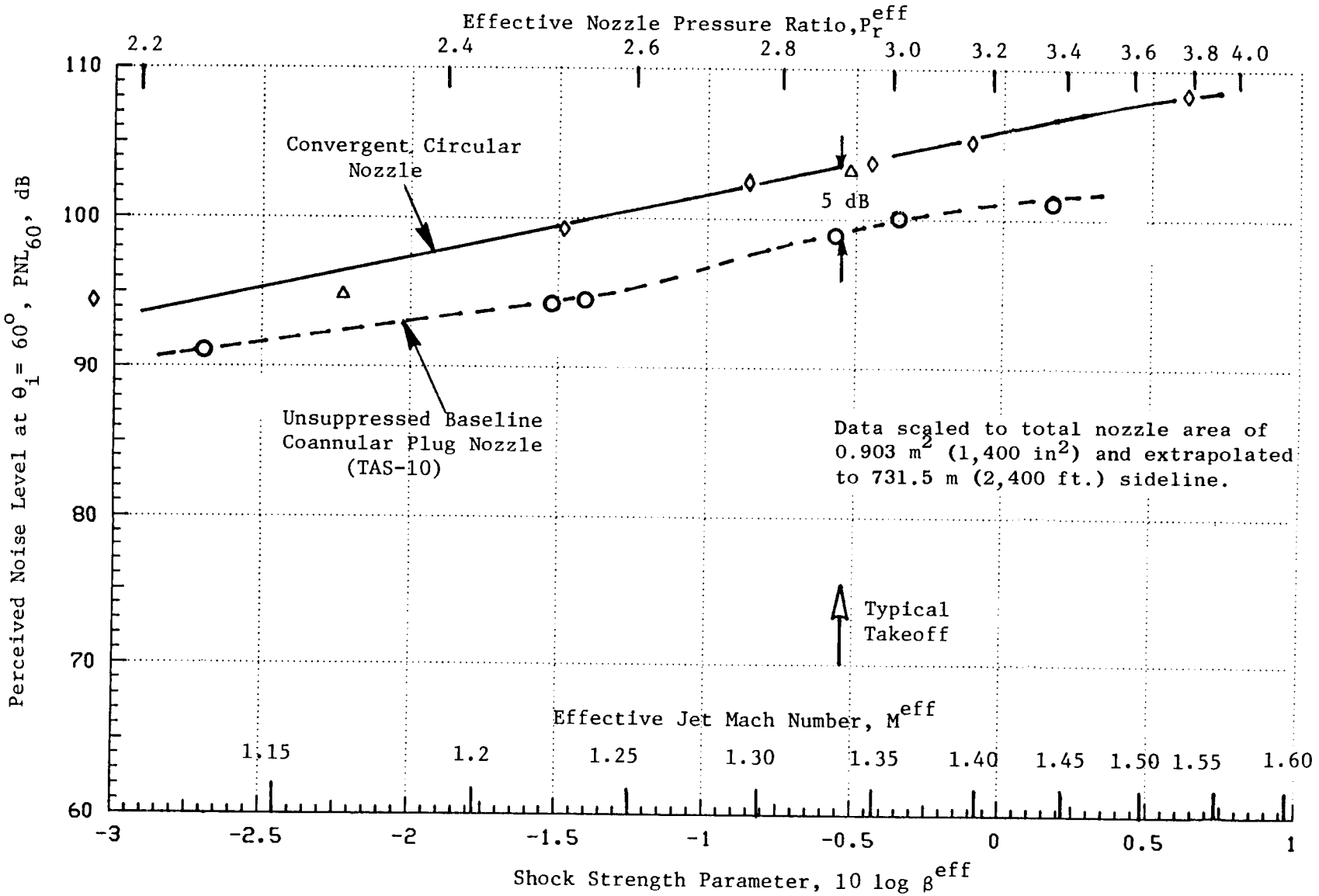

Figure 31. Comparison of Typical Forward-Quadrant Perceived Noise Level Data of Unsuppressed Coannular Plug Nozzle (TAS-10) with Those of Convergent Circular Nozzle (Static).

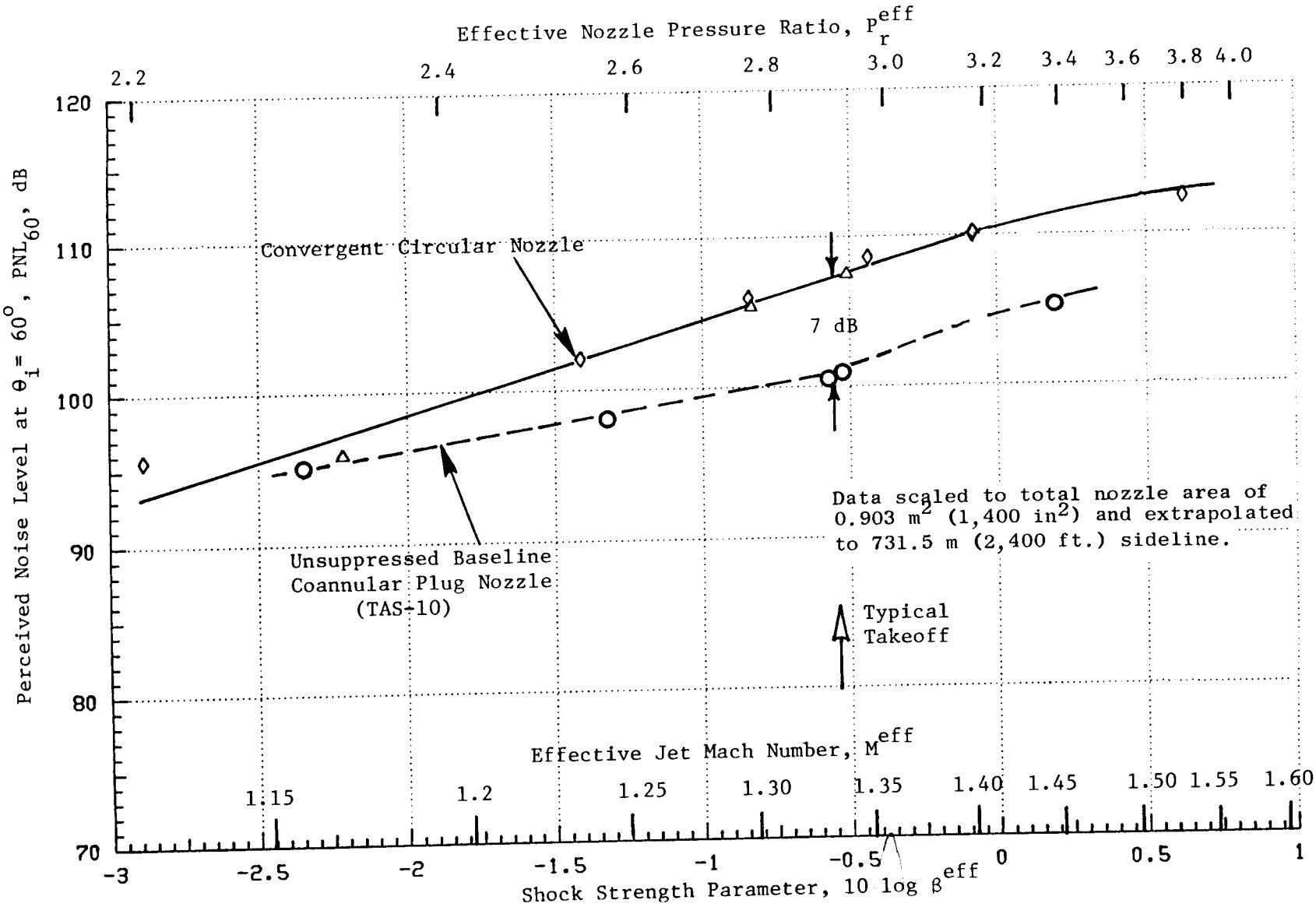

Figure 32. Comparison of Typical Forward-Quadrant Perceived Noise Level Data of Unsuppressed Coannular Plug Nozzle (TAS-10) with Those of Convergent Circular Nozzle (Simulated Flight).

	SYMBOL	TEST POINT	V_{ac}	INNER STREAM P_r^i	INNER STREAM T_T^i	INNER STREAM V^i	OUTER STREAM P_r^o	OUTER STREAM T_T^o	OUTER STREAM V^o	MIXED CONDITIONS P_r^{mix}	MIXED CONDITIONS T_T^{mix}	MIXED CONDITIONS V^{mix}	$V_r^{i,o}$	NF, dB
STATIC	◇	504	0	-	-	-	2.51	1675	2170	2.51	1675	2170	-	-5.1
	○	1021	0	2.28	900	1500	3.01	1620	2310	2.86	1500	2170	.65	-6.7
FLIGHT	◇	506	400	-	-	-	2.53	1675	2180	2.53	1675	2180	-	-5.1
	○	1022	400	2.30	870	1480	3.04	1665	2350	2.88	1530	2200	.63	-6.7

(T_T-°R; V-fps)

DATA SCALED TO TOTAL NOZZLE AREA OF 0.903 m^2 (1400 in^2)
AND EXTRAPOLATED TO 731.5 m (2400 ft) SIDELINE.

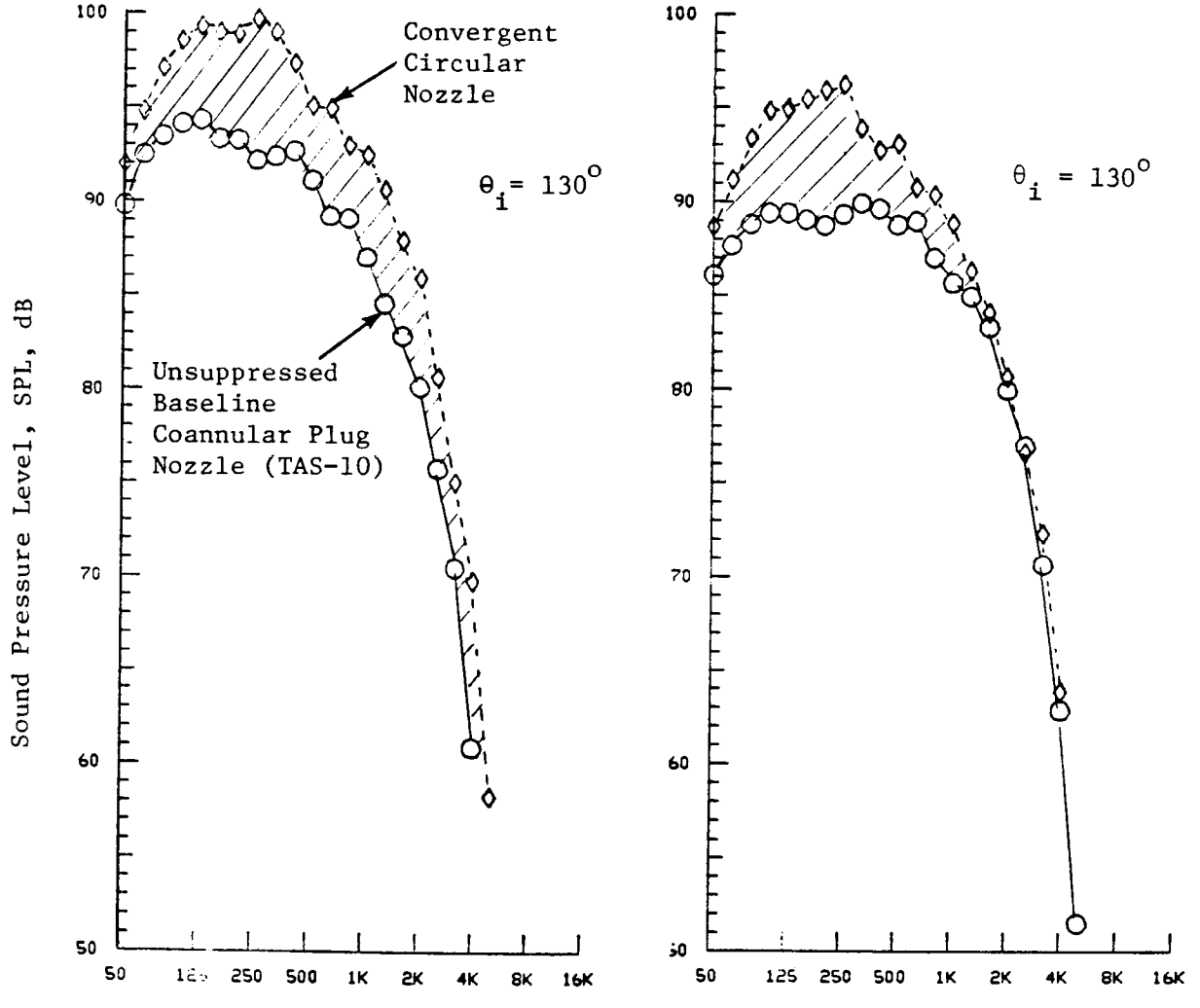

a) Static

b) Simulated Flight
(V_{ac} = 122 mps or 400 fps)

Figure 33. Comparison of Aft-Quadrant Sound Pressure Levels of Unsuppressed Baseline Coannular Plug Nozzle (TAS-10) with Those of Convergent Circular Nozzle at a Typical Takeoff Condition.

(T_T-°R; V-fps)

	SYMBOL	TEST POINT	V_{ac}	INNER STREAM P_r^i	INNER STREAM T_T^i	INNER STREAM V^i	OUTER STREAM P_r^o	OUTER STREAM T_T^o	OUTER STREAM V^o	MIXED CONDITIONS P_r^{mix}	MIXED CONDITIONS T_T^{mix}	MIXED CONDITIONS V^{mix}	$V_r^{i,o}$	NF, dB
STATIC	◇	561	0	-	-	-	2.16	1470	1875	2.16	1470	1875	-	-4.9
	○	1005	0	1.75	810	1200	2.33	1475	1460	2.21	1360	1830	.61	-5.2
FLIGHT	◇	562	400	-	-	-	2.16	1465	1870	2.16	1465	1870	-	-4.9
	○	1006	400	1.76	855	1240	2.40	1530	2030	2.28	1415	1895	.61	-5.2

DATA SCALED TO TOTAL NOZZLE AREA OF 0.903 m^2 (1400 in^2)
AND EXTRAPOLATED TO 731.5 m (2400 ft) SIDELINE.

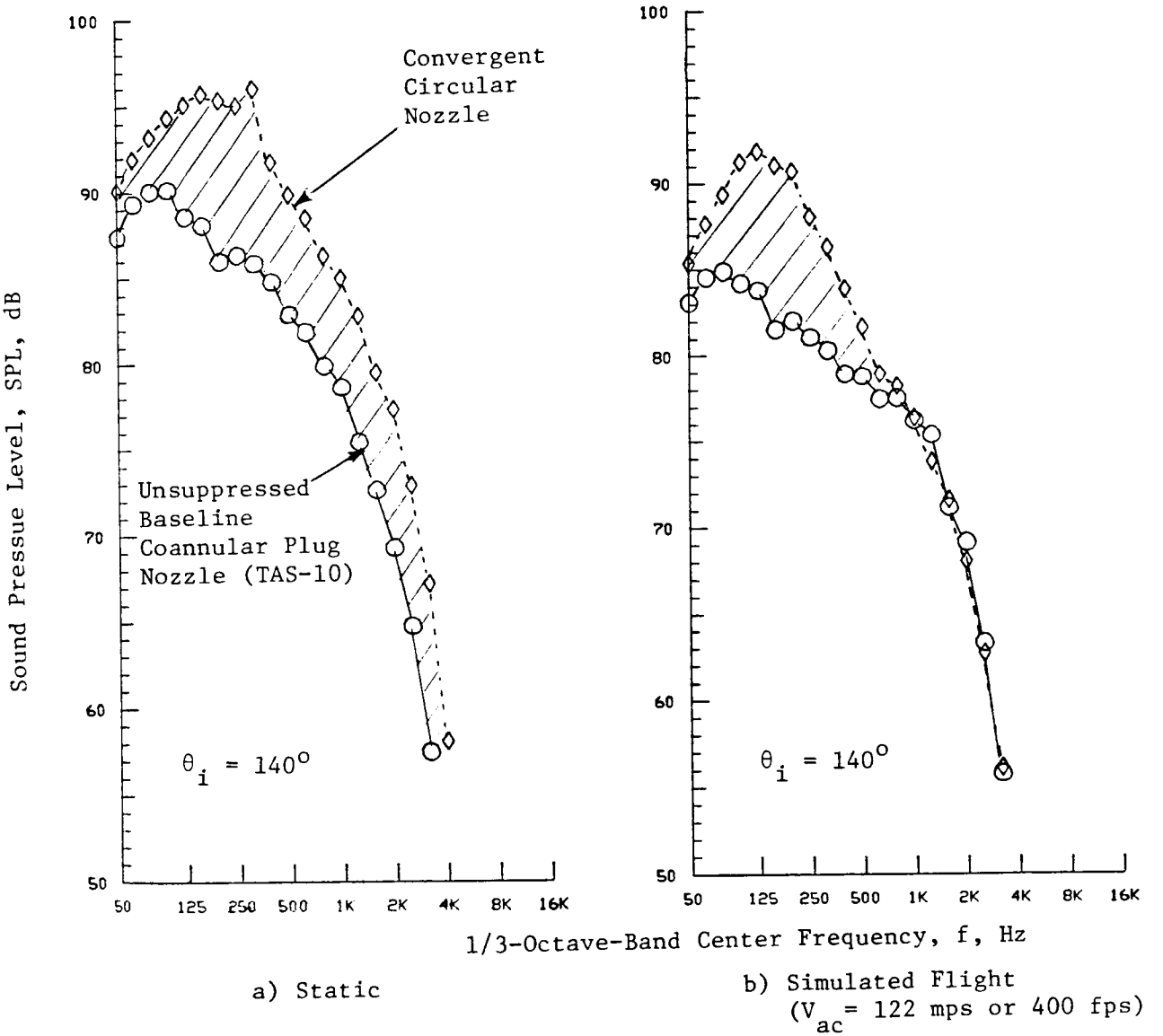

a) Static

b) Simulated Flight (V_{ac} = 122 mps or 400 fps)

Figure 34. Comparison of Aft-Quadrant Sound Pressure Levels of Unsuppressed Baseline Coannular Plug Nozzle (TAS-10) with Those of Convergent Circular Nozzle at a Typical Cutback Condition.

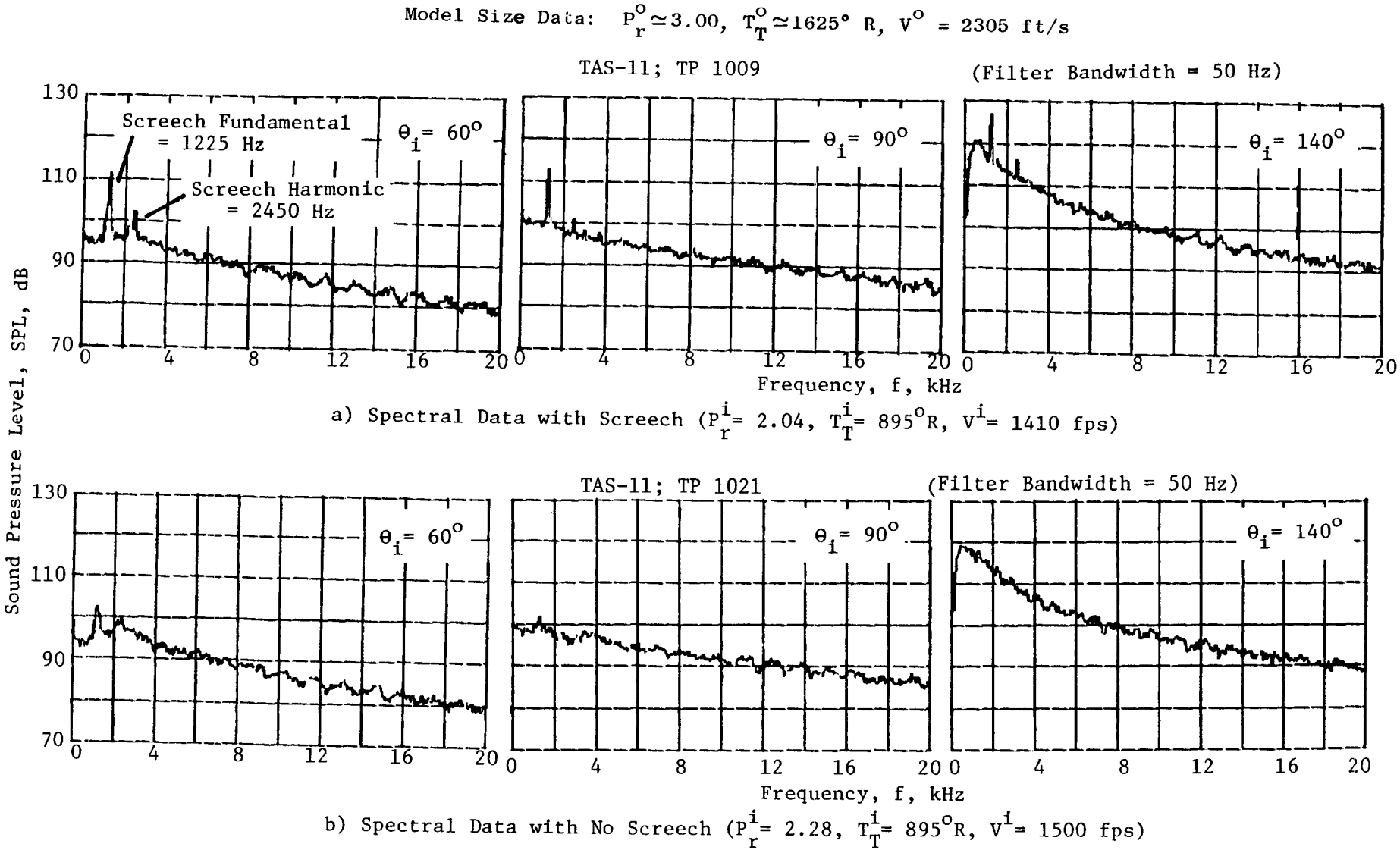

Figure 35. On-Line Narrowband Spectra that Demonstrates Elimination of Screech by a Small Modification in the Inner Stream Condition.

1021) are illustrated in Figure 35(b). To illustrate the effect of the screech on the scaled and extrapolated acoustic results, the data obtained from these two test points, which have identical outer streams and slightly different inner streams, are presented in Figures 36 and 37. The spectral comparison of Figure 36 indicates that the two sets of data agree with each other except at the screech frequency, which itself is observed to be invariant with the measurement angle. The effect of the screech on the PNL - and OASPL - directivities is illustrated in Figure 37. The increase in PNL and OASPL levels with screech is of the order of 2 to 3 dB. In all of the comparisons henceforth presented that employ the data of the baseline coannular plug nozzle at the typical takeoff condition, the data that correspond to the screech free Test Point 1021 have been used.

From studies conducted on scale model convergent coplanar coaxial nozzles, it is concluded in Reference 30 that for a fixed underexpanded outer stream pressure ratio there exists an inner stream pressure at which the OAPWL and the front quadrant noise of a coannular nozzle is a minimum. To ascertain whether such front quadrant noise reduction can be obtained with the baseline coannular plug nozzle of this study (TAS-10), static acoustic tests were conducted with the outer stream held constant at $P_r^o \sim 3.02$ and the inner stream varied over a range of $1.75 < P_r^i < 3.02$. Front quadrant data measured at $\theta_i = 60°$ during these tests are summarized in Figure 38. The data presented include the overall sound pressure levels, peak sound pressure levels of the shock-cell associated broadband, and the perceived noise levels. The data indicate that for the underexpanded fixed outer stream condition, an optimum underexpanded inner stream condition exists at $P_r^o \sim 2.6$, at which the front quadrant noise data is a minimum. At this optimum condition, the front quadrant PNL is observed to be 2 dB less than that of the typical engine operating line data.

4.1.2 Effect of Shield-to-Outer-Stream Velocity Ratio with Partial Thermal Acoustic Shield

As described in Section 2.3.1, the unsuppressed coannular plug nozzle (TAS-10) was tested with the 0.97 in. thick, 180° thermal acoustic shield using two different sets of choke plates. The plates were selected to give, over a typical engine operating line, a range of shield-to-outer stream velocity ratios of 0.55 to 0.68 for TAS-11 and 0.74 to 0.86 for TAS-12. At a typical takeoff condition, the shield-to-outer stream velocity ratios $V_r^{s,o}$, for TAS-11 and TAS-12 were 0.64* and 0.83* respectively. The objective of this test series, conducted per the test matrices presented in Section 3.1.1, was to investigate the influence of shield-to-outer stream velocity ratio, $V_r^{s,o}$, on the acoustic characteristics of the unsuppressed

*For convenience, these values of $V_r^{s,o}$, at takeoff will be identified as the shield-to-outer stream velocity ratios of these two configurations.

SYMBOL	CONFIG	TEST POINT	V_{ac}	INNER STREAM P_r^i	INNER STREAM T_T^i	INNER STREAM V^i	OUTER STREAM P_r^o	OUTER STREAM T_T^o	OUTER STREAM V^o	MIXED CONDITIONS P_r^{mix}	MIXED CONDITIONS T_T^{mix}	MIXED CONDITIONS V^{mix}	$V_r^{i,o}$	$V_r^{s,o}$	NF, dB
○	TAS-10	1009	0	2.04	893	1408	2.99	1629	2305	2.81	1514	2165	.61	0	-6.6
△	TAS-10	1021	0	2.28	897	1503	3.01	1620	2306	2.86	1497	2170	.65	0	-6.7

(T_T-°R; V- fps)

DATA SCALED TO TOTAL NOZZLE AREA OF 0.903 m^2 (1400 in^2) AND EXTRAPOLATED TO 731.5 m (2400 ft.) SIDELINE.

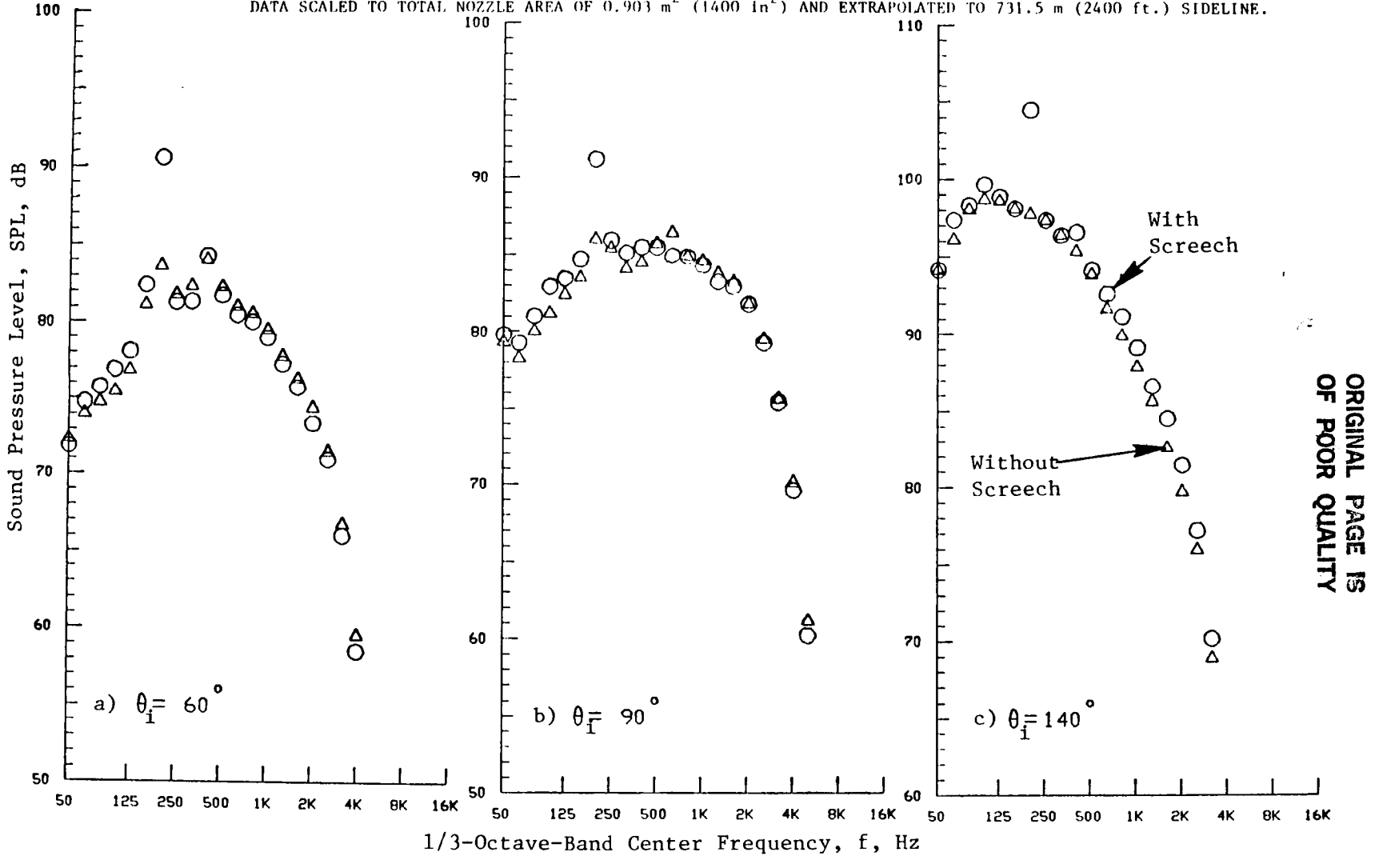

Figure 36. Typical Spectra of Unsuppressed Coannular Plug Nozzle at Takeoff Condition, With and Without Screech, Static.

See Figure 36 for aerodynamic conditions.

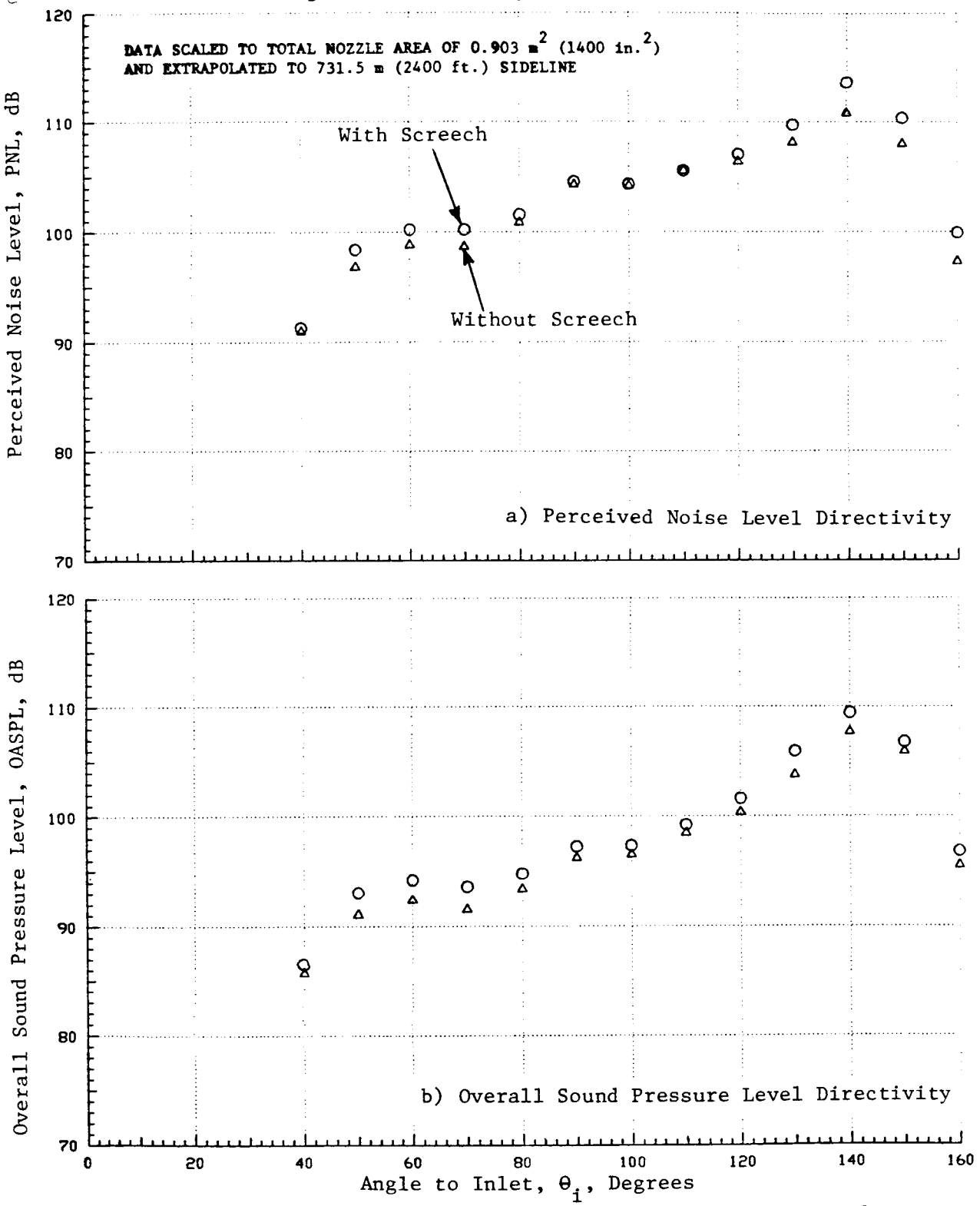

Figure 37. PNL and OASPL Directivities of the Unsuppressed Baseline Coannular Plug Nozzle at Typical Takeoff Condition, With and Without Screech.

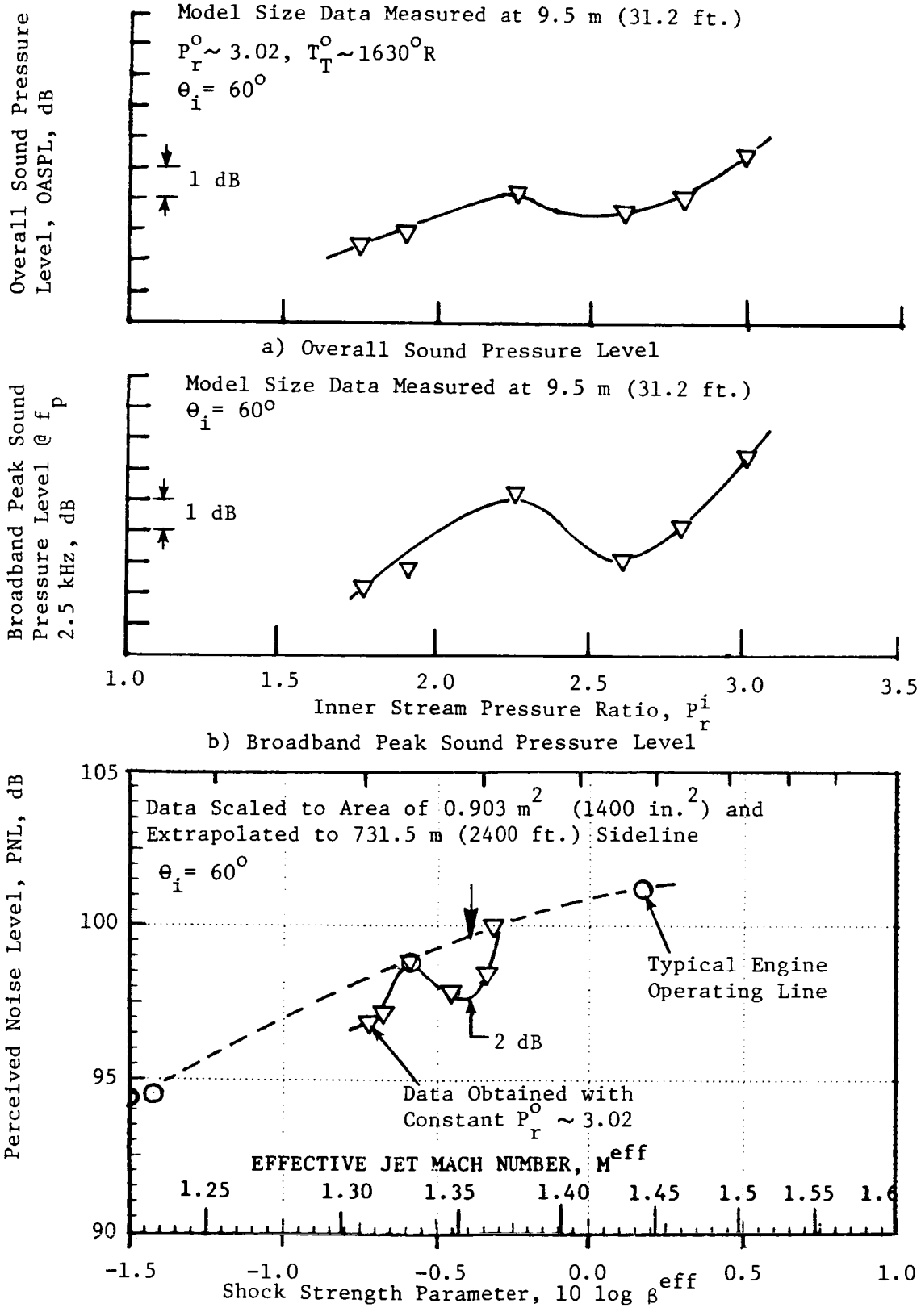

Figure 38. Variation in Front Quadrant Noise of Unsuppressed Baseline Coannular Nozzle Over a Range of Inner Stream Pressure Ratios for a Given Supersonic Outer Stream.

coannular plug nozzle. The inner and outer stream conditions were such that the inner-to-outer stream velocity ratio, $V_r^{i,o}$, was maintained approximately equal to 0.6 over the test range. The acoustic data obtained with the partial shield in the sideline orientation relative to the microphones are presented in this subsection. The presented data include the PNL directivities and selected front- and aft-quadrant spectral data of TAS-11 and TAS-12 at typical takeoff and cutback conditions. The data are compared with the corresponding acoustic characteristics of the baseline unsuppressed coannular plug nozzle, TAS-10.

The simulated flight PNL-directivities of TAS-11 and TAS-12 at a typical takeoff condition are compared with that of TAS-10 in Figure 39. The data indicates a PNL reduction of 0.3 dB at all observer angles up to $\theta_i = 120°$ with the TAS-11 configuration ($V_r^{s,o}$ = 0.64). At the peak noise angles of $\theta_i = 130°$ and 140°, the PNL reductions with the shielded configurations are observed to be minimal. However, the spectral data at these angles, presented in Figures 40 and 41, indicate high-frequency noise reduction by both shielded configurations with TAS-11 ($V_r^{s,o}$ = 0.64) yielding the lowest measured high frequency sound pressure levels. Since the low and middle frequency spectra dominate at these aft angles, the effect of the high frequency reduction with the shields on the calculated PNL data is not significant. In addition, the low and middle frequency spectral levels are observed to increase with shield velocity. At the forward quadrant angles, while no increases in sound pressure levels at low and middle frequency ranges are noted, equal reductions are observed at middle and high frequencies with the shielded configurations.

The simulated flight PNL-directivities of TAS-11 and TAS-12 at a typical cutback condition are presented in Figure 42 and compared with that of the baseline unsuppressed coannular plug nozzle. The data indicate a PNL reduction with the shields at all observer angles. At the peak noise angle of θ_i = 120°, a maximum PNL reduction of 4.0dB is obtained with the TAS-11 configuration $V_\gamma^{s,o}$ = 0.58). The corresponding PNL reduction with the TAS-11 at θ_i = 90° and 60° is observed to be 3.5 dB. In addition, the influence of $V_r^{s,o}$, on the measured PNL data is observed to be minimal at all angles for the cutback case. Spectral characteristics of TAS-11 and TAS-12 corresponding to the simulated cutback condition of Figure 42 are presented in Figures 43 and 44. While only the data at $\theta_i = 90°$ and maximum noise angle of $\theta_i = 130°$ are presented in Figure 43, a set of data at three front and three aft quadrant angles is presented in Figure 44. The aft-quadrant cutback spectral data exhibit high frequency noise reduction similar to that at takeoff condition, along with the predomination of low and middle frequency levels with the shielded configurations. At the forward quadrant angles, equal reductions are observed with the shielded configurations for all values of $f > 500$ Hz.

4.1.3 Influence of Partial Thermal Acoustic Shield Orientation

The acoustic data of the unsuppressed coannular plug nozzle with the 180° shield in sideline orientation, presented in the previous section, are compared

SYMBOL	CONFIG.	TEST POINT	V_{ac}	INNER STREAM P_r^i	INNER STREAM T_T^i	INNER STREAM V^i	OUTER STREAM P_r^o	OUTER STREAM T_T^o	OUTER STREAM V^o	SHIELD STREAM P_r^s	SHIELD STREAM T_T^s	SHIELD STREAM V^s	MIXED CONDITIONS P_r^{mix}	MIXED CONDITIONS T_T^{mix}	MIXED CONDITIONS V^{mix}	$V_r^{i,o}$	$V_r^{s,o}$	NF, dB
○	TAS-10	1022	400	2.30	865	1485	3.04	1665	2350	-	-	-	2.88	1525	2200	0.63	-	-6.7
□	TAS-11	1110	400	2.29	940	1540	3.04	1650	2340	1.52	1615	1490	2.39	1555	2040	0.66	0.64	-5.2
◇	TAS-12	1210	400	2.29	930	1535	3.03	1650	2335	2.08	1620	1925	2.59	1555	2120	0.66	0.83	-5.8

(T_T-°R; V- fps)

DATA SCALED TO TOTAL NOZZLE AREA OF 0.903 m^2 (1400 in^2) AND EXTRAPOLATED TO 731.5 m (2400 ft.) SIDELINE.

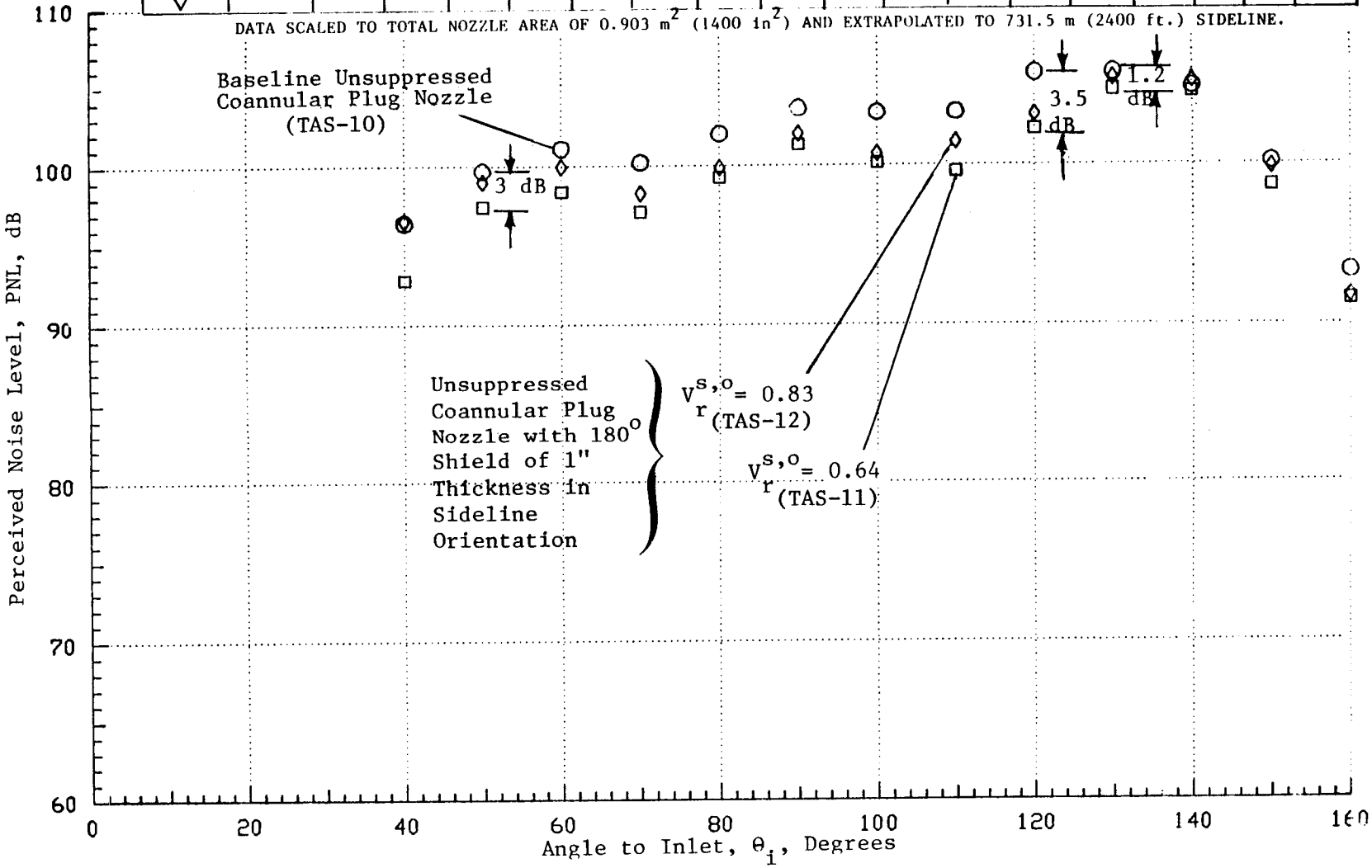

Figure 39. Effect of Shield-to-Outer Stream Velocity Ratio on the PNL-Directivity of the Unsuppressed Coannular Plug Nozzle with Partial Shield at Takeoff Conditions (Simulated Flight).

(Refer to Figure 39 for aerodynamic flow conditions.)

Data scaled to total nozzle area of 0.903 m^2 (1,400 in^2) and extrapolated to 731.5 m (2,400 ft.) sideline.

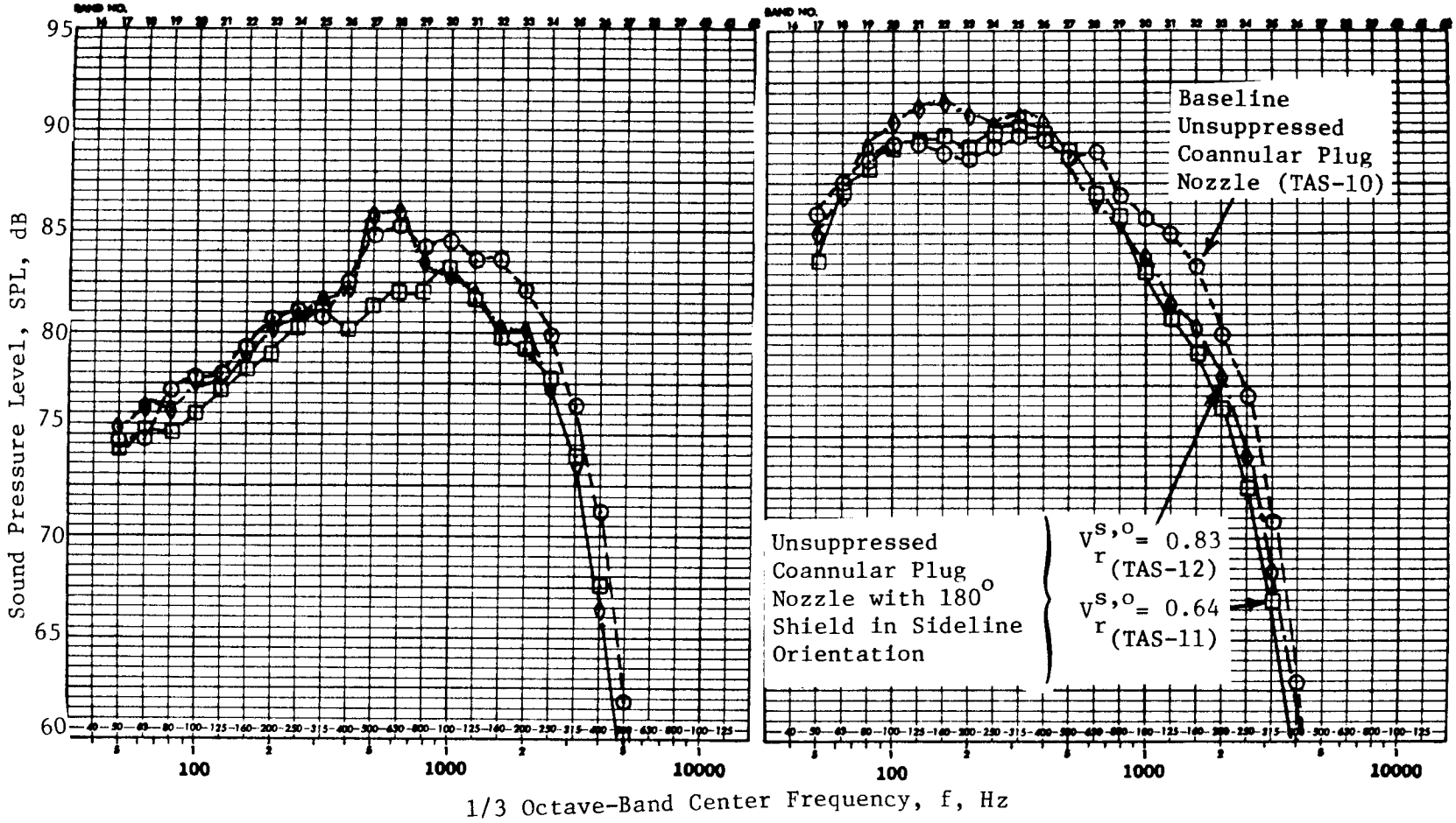

a) Directivity Angle $\theta_i = 90^o$

b) Directivity Angle $\theta_i = 130^o$

Figure 40. Effect of Shield-to-Outer Stream Velocity Ratio on Typical Spectra of Unsuppressed Coannular Plug Nozzle with Partial Shield at Takeoff Condition (Simulated Flight).

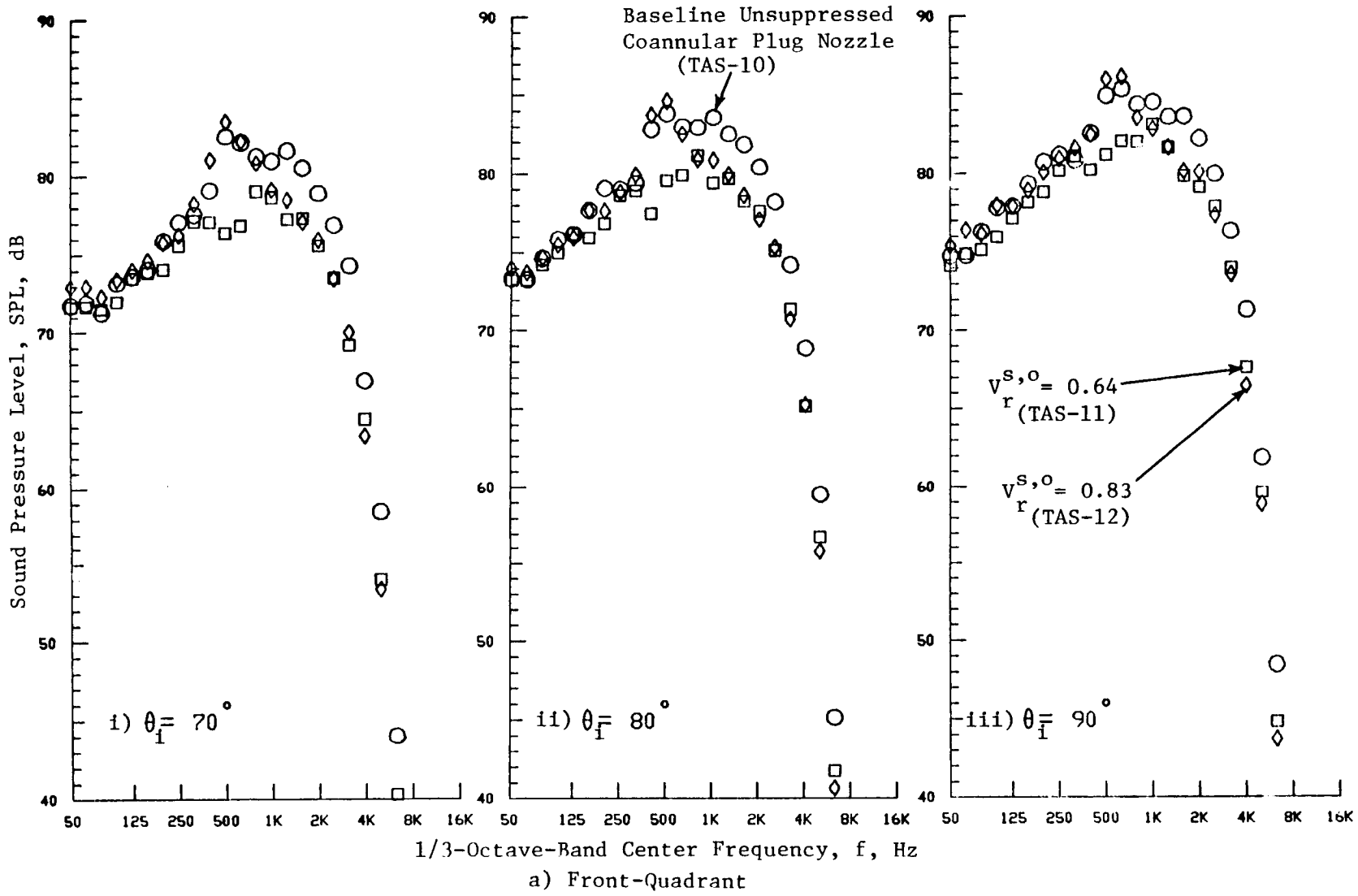

a) Front-Quadrant

Figure 41. Effect of Shield-to-Outer Stream Velocity Ratio on Selected Front and Aft Quadrant Spectra of Unsuppressed Plug Nozzle with Partial Shield at Takeoff Conditions (Simulated Flight).

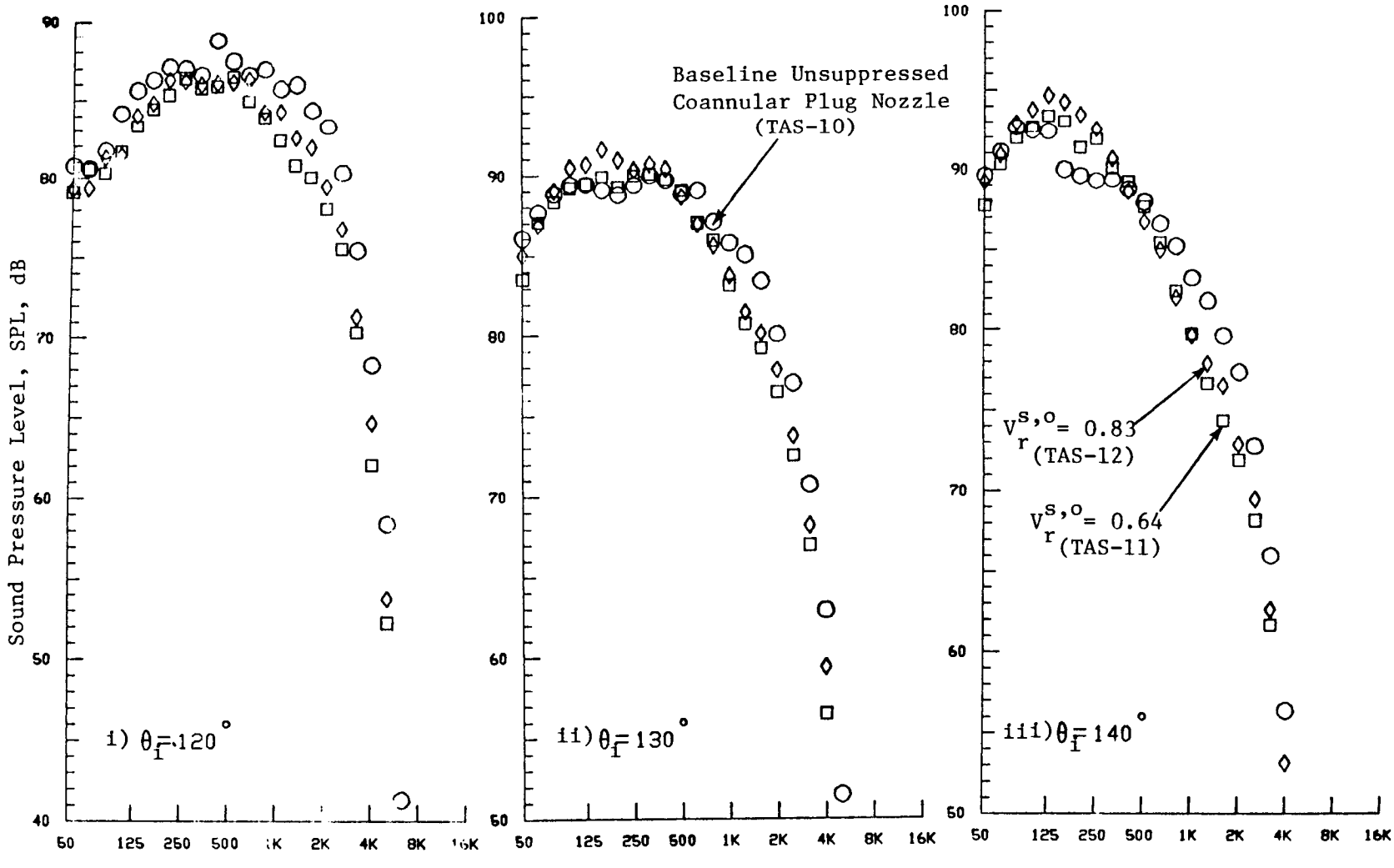

b) Aft-Quadrant

Figure 41. Effect of Shield-to-Outer Stream Velocity Ratio on Selected Front and Aft Quadrant Spectra of Unsuppressed Plug Nozzle with Partial Shield at Takeoff Conditions (Simulated Flight) (Concluded).

SYMBOL	CONFIG.	TEST POINT	V_{ac}	INNER STREAM P_r^i	INNER STREAM T_T^i	INNER STREAM V^i	OUTER STREAM P_r^o	OUTER STREAM T_T^o	OUTER STREAM V^o	SHIELD STREAM P_r^s	SHIELD STREAM T_T^s	SHIELD STREAM V^s	MIXED CONDITIONS P_r^{mix}	MIXED CONDITIONS T_T^{mix}	MIXED CONDITIONS V^{mix}	$V_r^{i,o}$	$V_r^{s,o}$	NF, dB
○	TAS-10	1006	400	1.76	855	1240	2.40	1530	2030	-	-	-	2.28	1415	1895	0.61	-	-5.2
□	TAS-11	1106	400	1.75	835	1220	2.38	1480	1980	1.32	1445	1150	1.92	1390	1690	0.62	0.58	-3.9
◇	TAS-12	1206	400	1.75	830	1210	2.40	1485	1995	1.67	1460	1550	2.04	1400	1770	0.61	0.78	-4.5

DATA SCALED TO TOTAL NOZZLE AREA OF 0.903 m^2 (1400 in^2) AND EXTRAPOLATED TO 731.5 m (2400 ft.) SIDELINE.

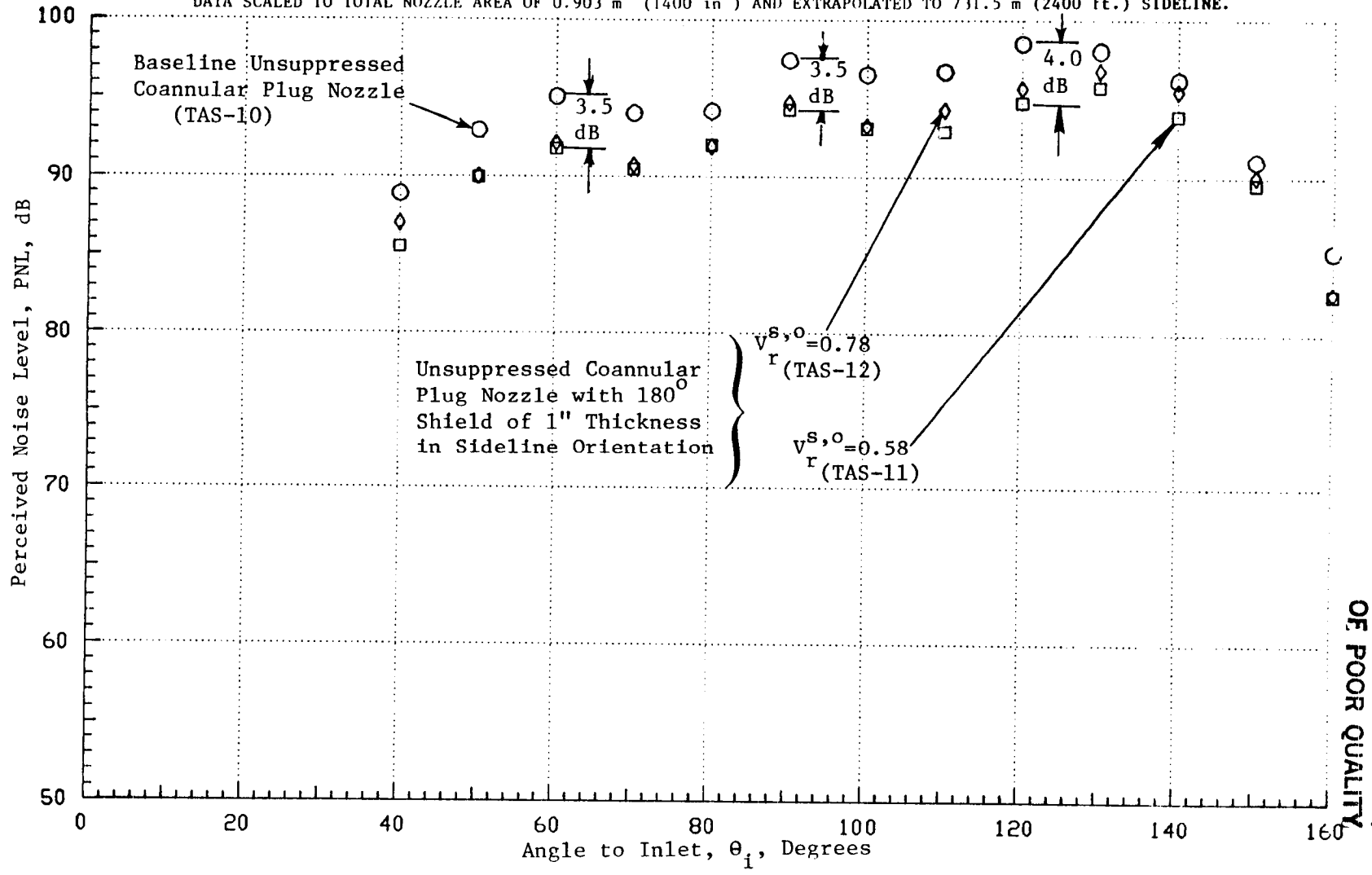

Figure 42. Effect of Shield-to-Outer Stream Velocity Ratio on the PNL-Directivity of Unsuppressed Coannular Plug Nozzle with Partial Shield at Cutback Condition (Simulated Flight).

(Refer to Figure 42 for aerodynamic flow conditions.)

Data scaled to total nozzle area of 0.903 m^2 (1,400 in^2) and extrapolated to 731.5 m (2,400 ft.) sideline.

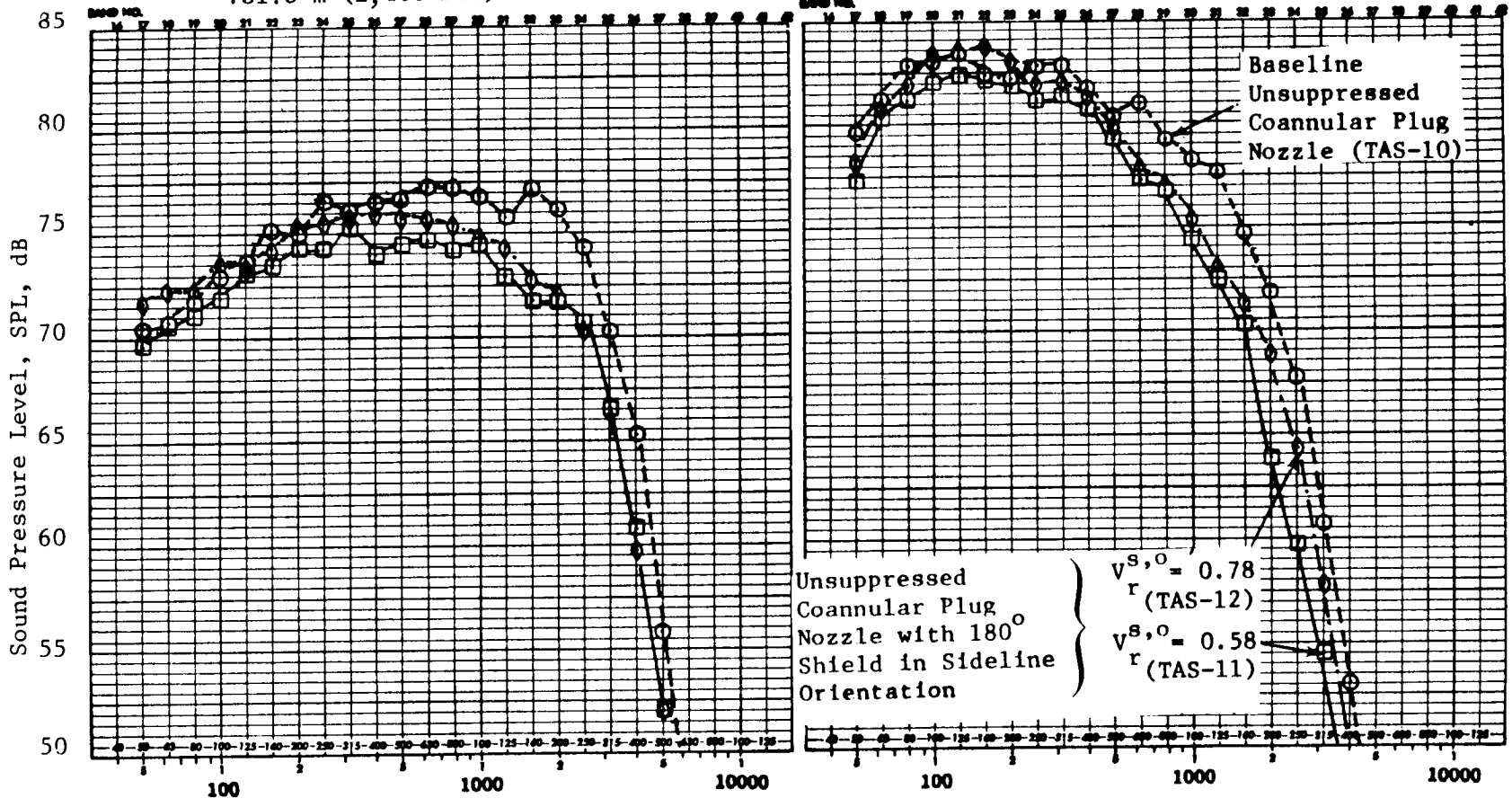

a) Directivity Angle θ_i = 90°

b) Directivity Angle θ_i = 130°

Figure 43. Effect of Shield-to-Outer Stream Velocity Ratio on Typical Spectra of Unsuppressed Coannular Plug Nozzle with Partial Shield at Cutback Condition (Simulated Flight).

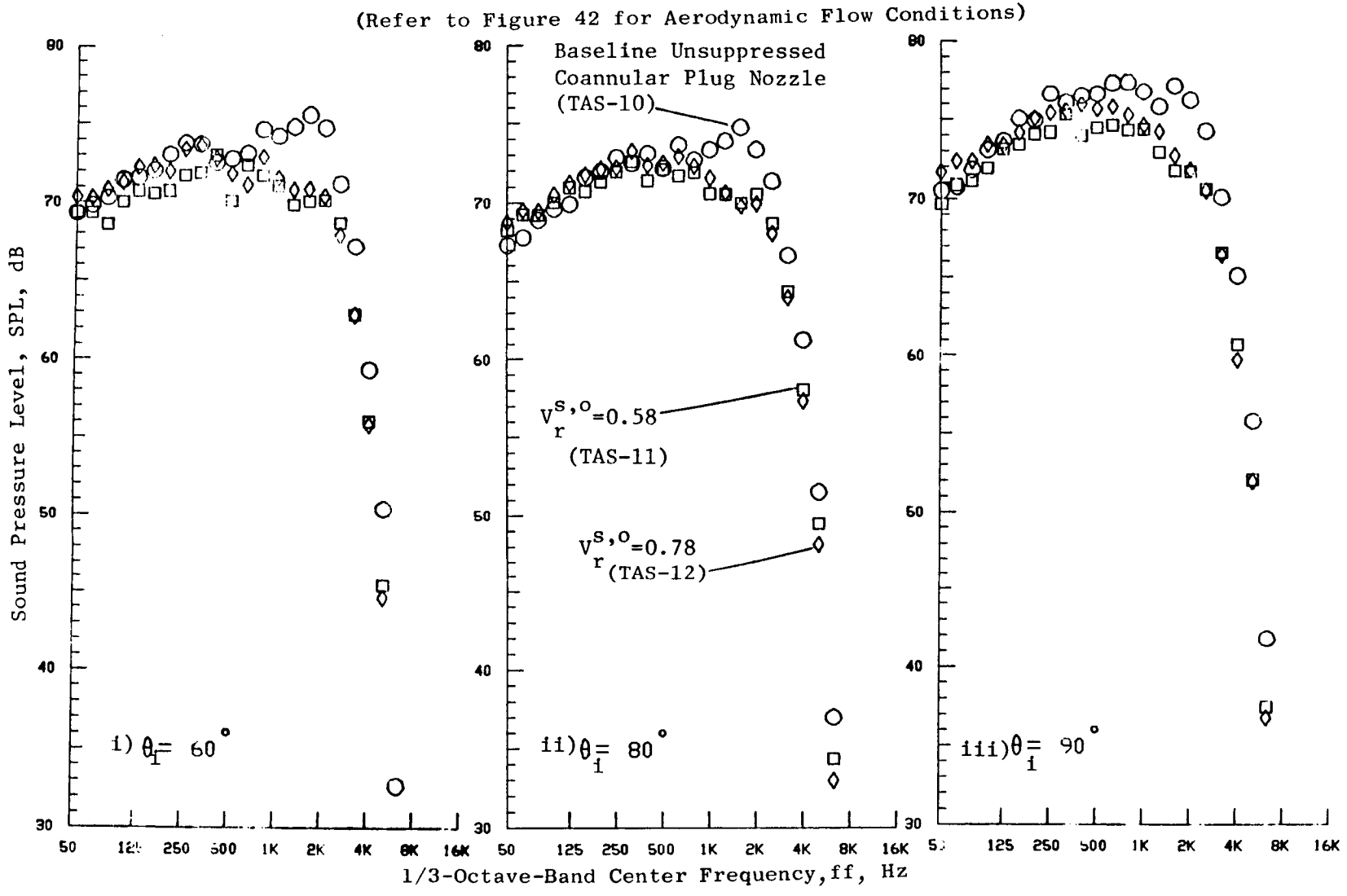

a) Front-Quadrant

Figure 44. Effect of Shield-to-Outer Stream Velocity Ratio on Selected Front and Aft Quadrant Spectra of Unsuppressed Coannular Plug Nozzle with Partial Shield at Cutback Condition (Simulated Flight).

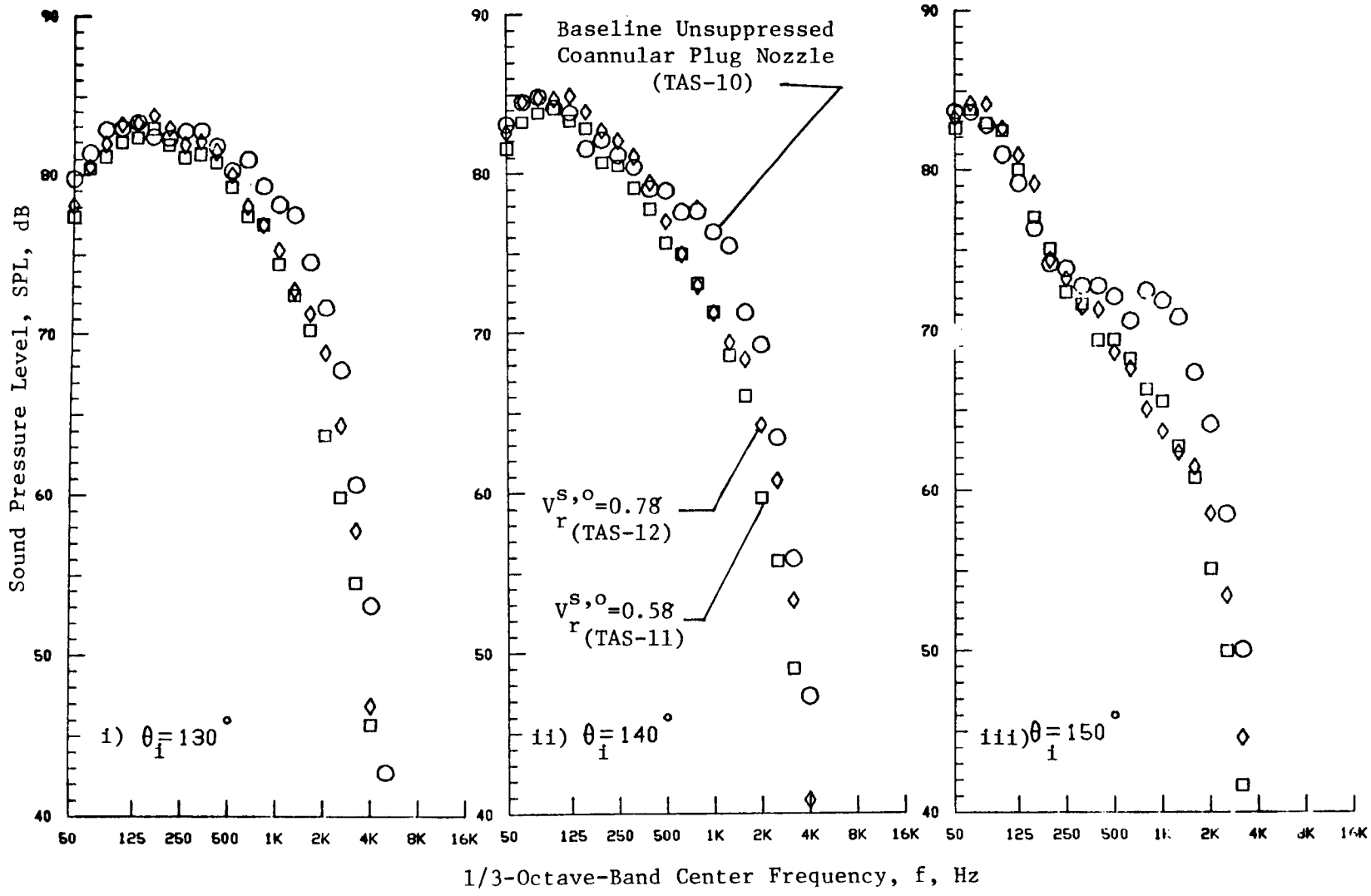

b) Aft-Quadrant

Figure 44. Effect of Shield-to-Outer Stream Velocity Ratio on Selected Front and Aft Quadrant Spectra of Unsuppressed Coannular Plug Nozzle with Partial Shield at Cutback Condition (Simulated Flight) (Concluded).

with data obtained with the partial shield in community orientation relative to the microphones. This test series was conducted as shown in Table V (TAS-11) with the set of choke plates that resulted in a shield-to-outer stream velocity ratio $V_r^{s,o}$, of 0.64 at a takeoff condition. The aft-quadrant static perceived noise level data obtained at θ_i = 120 through 150°, over typical engine operating cycle conditions, are presented in Figure 45. The results indicate that, for given nozzle flow conditions, the aft-quadrant PNL data measured with the shield in community orientation are lower than the corresponding data obtained with the same shield in the sideline orientation. Over the range of test conditions, the influence of the partial shield orientation from community to sideline configuration on the azimuthal assymetric acoustic field is observed to be about 2 dB at the indicated aft-quadrant angles.

The static PNL-directivities of configuration TAS-11 with the shield in community and sideline orientations and at takeoff flow conditions are presented in Figure 46. The data indicate that at all aft-quadrant angles, the perceived noise levels measured with the shield in the community orientation are lower than those measured with the shield in the sideline configuration. The corresponding aft-quadrant static spectral data are presented in Figure 47. The data indicate significantly lower sound pressure levels at high frequencies with the shield in community orientation. Since the high frequency noise sources are near the nozzle exit, the observed higher sound pressure levels asymmetry with the sideline orientation are due to the asymmetry in the flow and source distributions. The effect of shield orientation on low frequency noise is observed to be minimal as this component is from downstream sources in the merged single jet.

4.1.4 Comparison of Partial and Full Thermal Acoustic Shield Data

Configuration TAS-14 employs a 360° thermal acoustic shield of 0.5 in. thickness around the baseline unsuppressed coannular nozzle (TAS-10). The shield flow area of this full shield has been designed to be equal to that of the 0.97 in. thick, 180° shield of configuration TAS-11 and TAS-12. This yields equal mass flow rates through the two shields for a given set of shield flow conditions. Acoustic tests were conducted with the 360° shielded unsuppressed configuration (TAS-14) with choke plates identical to those used with TAS-12 (180° shield in sideline orientation) to give a shield-to-outer stream velocity ratio of 0.83 at a typical takeoff condition. The acoustic data of TAS-14 are compared in this section with those of TAS-12 in order to identify the benefit of the thicker and partial thermal acoustic shield.

The normalized perceived noise level data of TAS-12 (with 180° shield in sideline orientation) and TAS-14 (with 360° shield) at selected aft-quadrant angles and measured under static and simulated flight conditions are presented in Figures 48 and 49. The data are plotted as a function of the mixed jet velocity parameter. The data demonstrate, in general, the aft-quadrant acoustic benefit of a thicker partial shield over the 360° shielded configuration for a given set of flow conditions. The acoustic benefit is observed to be in the range of 1 to 2 dB over the cycle conditions.

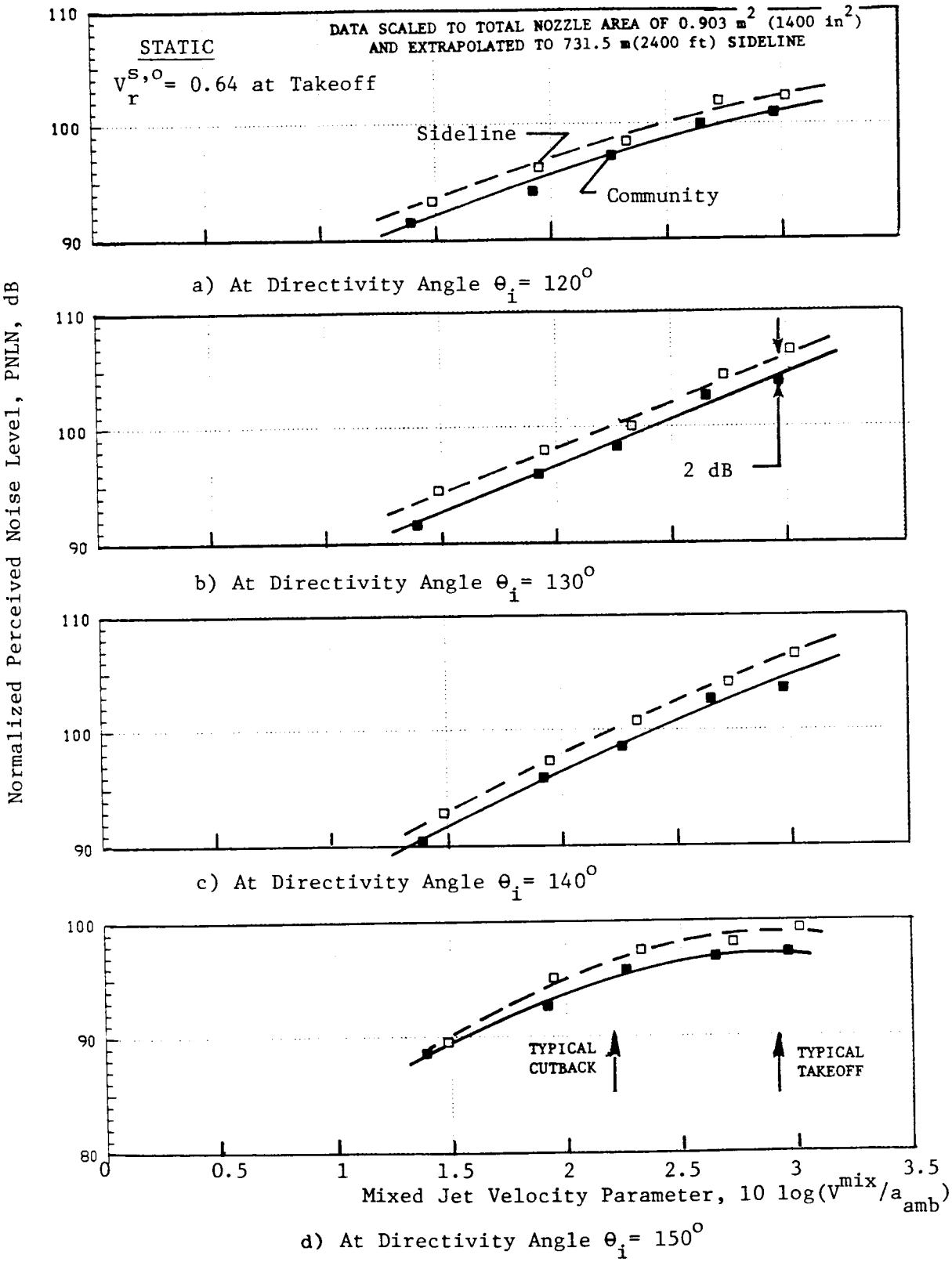

Figure 45. Effect of Shield Orientation on the Aft Quadrant Normalized Perceived Noise of Unsuppressed Coannular Plug Nozzle with 180° Shield (TAS-11).

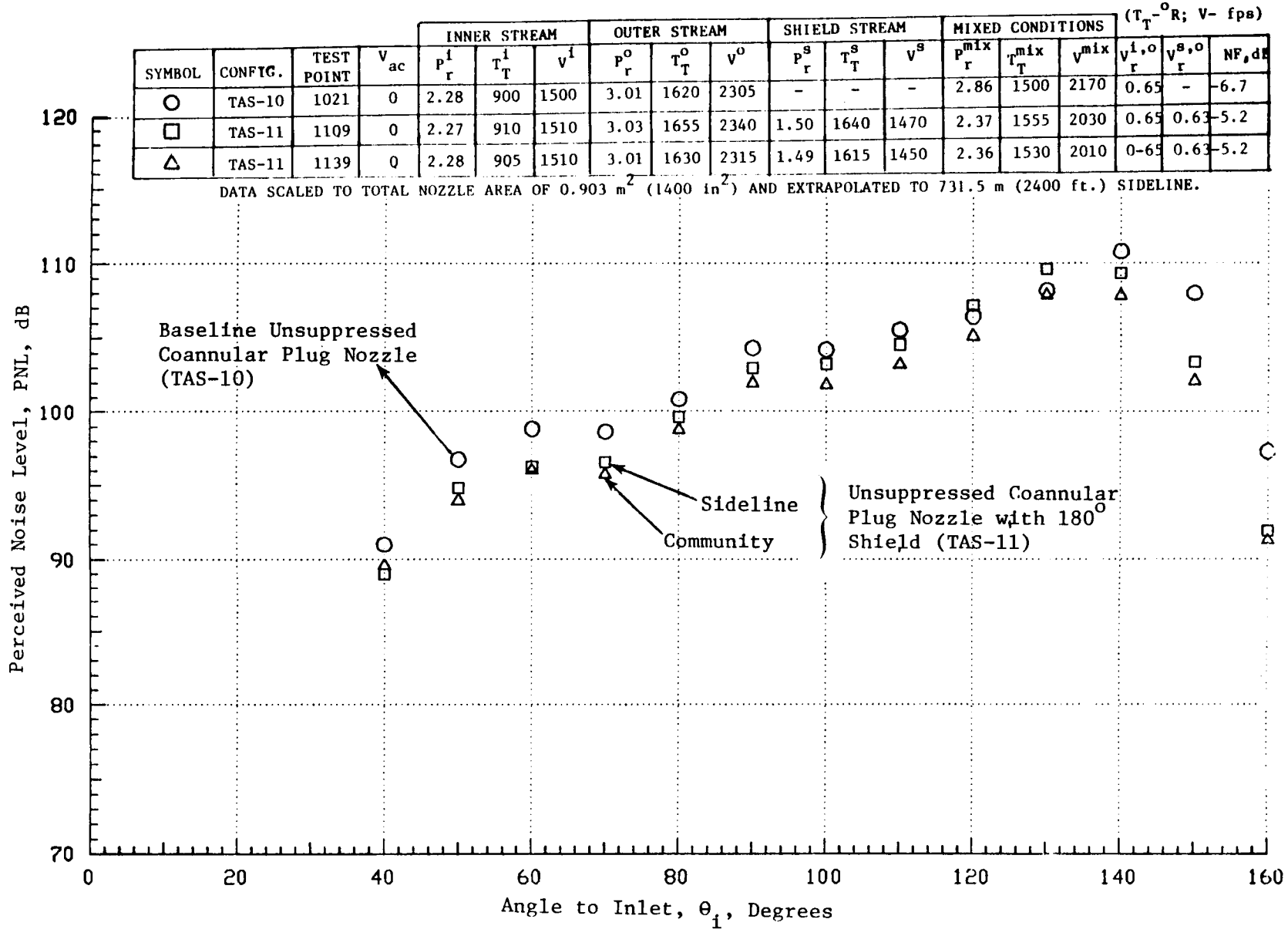

Figure 46. Effect of Shield Orientation on the PNL-Directivity of Unsuppressed Coannular Plug Nozzle with 180° Shield (TAS-11) at Takeoff Condition (Static).

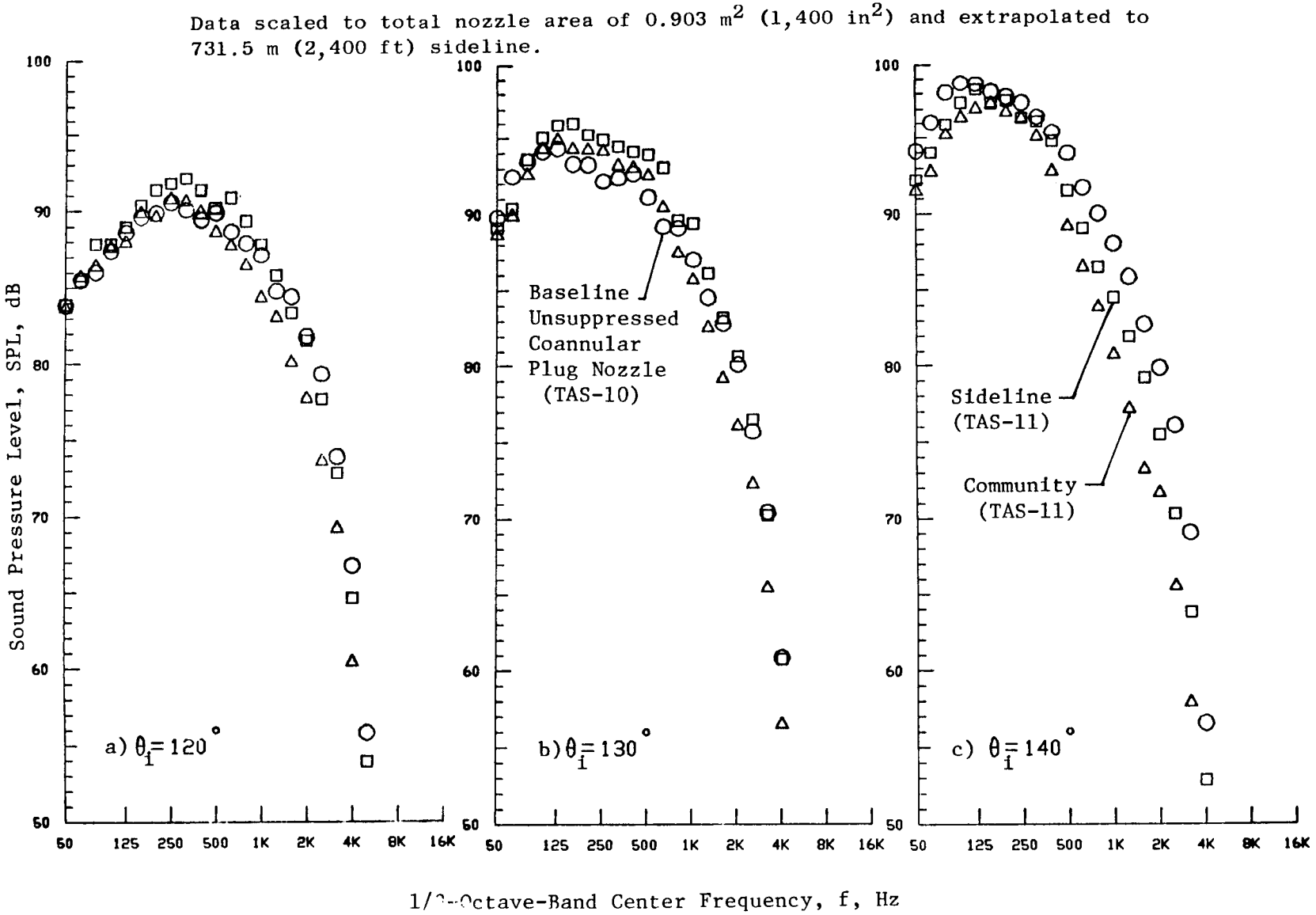

Figure 47. Effect of Shield Orientation on the Aft Quadrant Spectra of Unsuppressed Coannular Plug Nozzle with 180° Shield (TAS-11) at Takeoff Condition (Static).

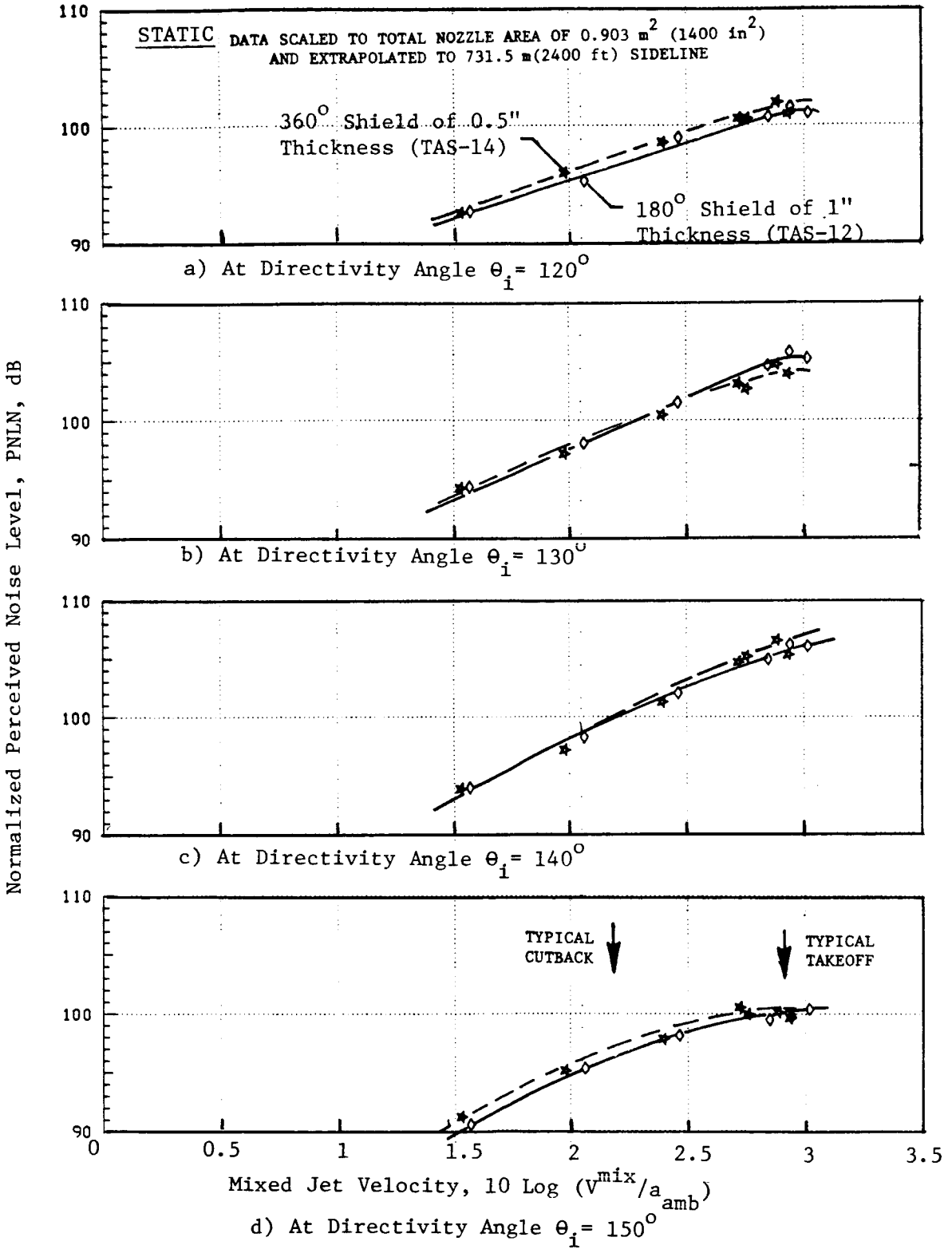

Figure 48. Aft Quadrant Normalized Perceived Noise Level Static Data of Unsuppressed Coannular Plug Nozzle with 180° and 360° Shields ($V_r^{s,o}$ = 0.83 at Takeoff).

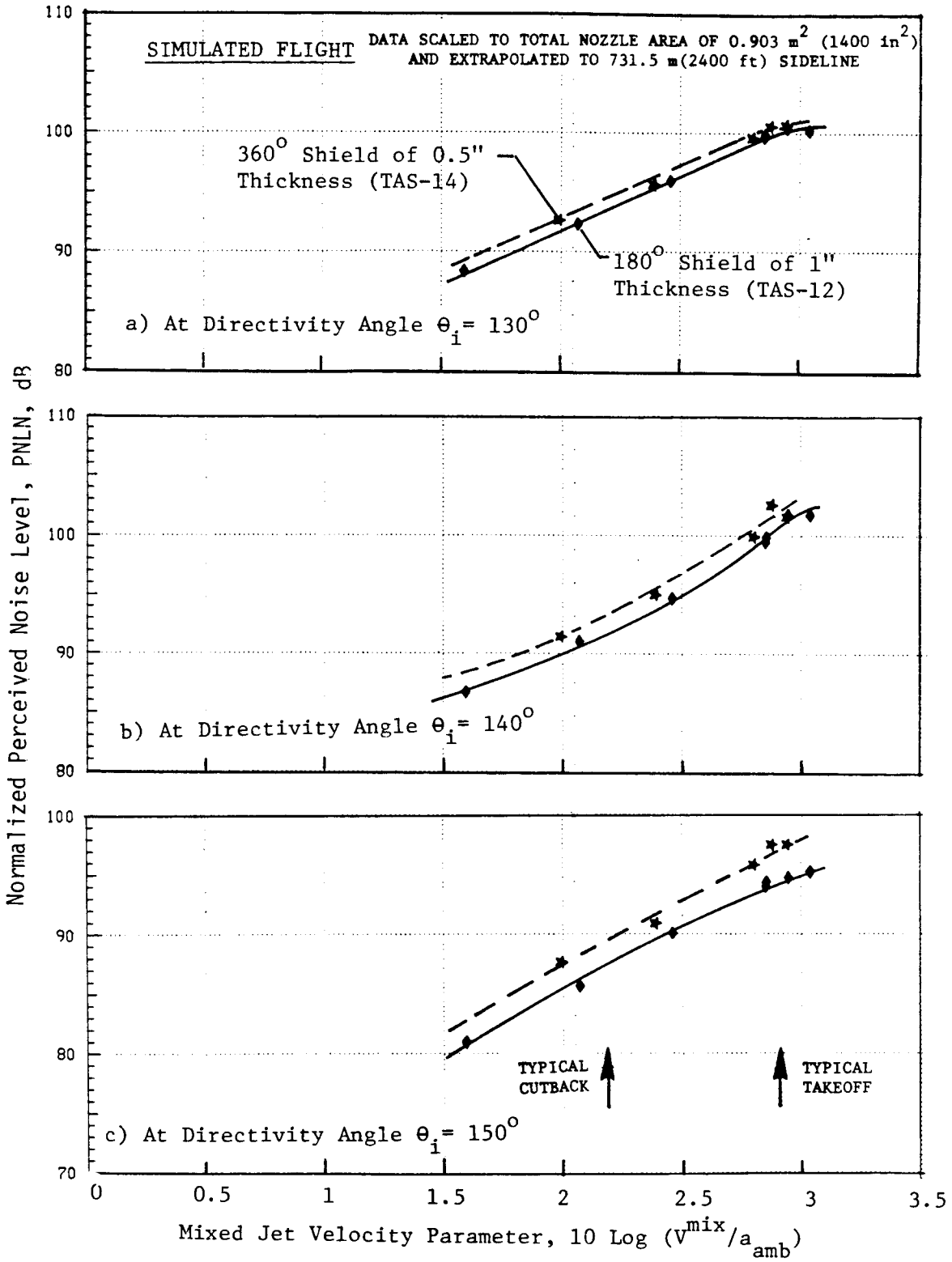

Figure 49. Aft Quadrant Normalized Perceived Noise Level Simulated Flight Data of Unsuppressed Coannular Plug Nozzle with 180° and 360° Shields ($V_r^{s,o}$ = 0.83 at Takeoff).

C-2

This section is concluded by presenting typical comparisons between sound power level spectra of the baseline unsuppressed coannular plug nozzle (TAS-10) and those of the 360° shielded unsuppressed coannular plug nozzle (TAS-14). The static data obtained at takeoff and cutback conditions are presented in Figure 50. The data indicate significant reduction in the measured sound power levels at high frequencies for the shielded configuration. This indicates that the noise sources of the coannular jet that are close to the nozzle exit have been shielded by the full shield flow. However, on the basis of overall power level corrected for equal thrust, there is no power reduction with the shielded configuration. No significant changes are observed in the low and middle frequency power spectra. The corresponding spectra of a convergent circular nozzle (References 21 and 22) are also presented in Figure 50 to indicate the benefit of a baseline coannular plug nozzle relative to a convergent circular nozzle. The observed high frequency turn up in the power spectra of the convergent circular nozzle is attributed to an anomaly in the instrumentation.

4.1.5 Flow Field Characteristics with Partial Thermal Acoustic Shield

The mean and turbulent velocity profiles obtained during axial traverses in the static plume of the unsuppressed coannular nozzle with the 180° thermal acoustic shield (that is, LV Plume 1 of Table XIII) are presented in Figure 51. The data compare axial mean and turbulent velocity variations along nozzle centerline with the corresponding data obtained during axial traverses at radial locations of $R/R_t^s = 0.5$ on the shielded and unshielded sides. The aerodynamic flow conditions correspond to a typical takeoff condition. An examination of the static measured axial velocity data indicate that:

a. Two weak shock-cell structures are formed downstream of the plug along the nozzle centerline.

b. The presence of the partial shield results in an asymmetry in the axial variation of the mean velocities between the shielded and unshielded side (traverses B and C). Axial traverse data taken at $R/R_t^s = 0.5$ on the shielded and unshielded sides indicate higher mean velocity on shielded side up to an $X/D_{eq} \sim 8.0$. This is due to reduction in shearing of baseline nozzle flow as a result of the existence of the shield flow.

c. The normalized turbulent velocity along the centerline is within 8% up to an $X/D_{eq} \simeq 10$ with the mean velocity remaining approximately constant (and reaching its maximum value at $X/D_{eq} \sim 10$) indicating the presence of a potential core.

d. The presence of the shield also results in an asymmetry in the turbulent velocities (traverses B and C) between the shielded and unshielded side data. Axial traverse turbulent data taken at $R/R_t^s = 0.5$ in the shielded and unshielded side indicate lower turbulent velocities for $X/D_{eq} < 4$ on the shield side due to reduction of

	SYMBOL	CONFIG.	TEST POINT	V_{ac}	INNER STREAM P_r^i	INNER STREAM T_T^i	INNER STREAM V^i	OUTER STREAM P_r^o	OUTER STREAM T_T^o	OUTER STREAM V^o	SHIELD STREAM P_r^s	SHIELD STREAM T_T^s	SHIELD STREAM V^s	MIXED CONDITIONS P_r^{mix}	MIXED CONDITIONS T_T^{mix}	MIXED CONDITIONS V^{mix}	$V_r^{i,o}$	$V_r^{s,o}$	NF_s, dB	F, lb	OAPWL, dB
					(T_T-°R; V- fps)																
FIG. a)	◇	CONIC	504	0	-	-	-	2.51	1675	2170	-	-	-	2.51	1675	2170	-	-	-5.1	43900	184.2
	○	TAS-10	1021	0	2.28	900	1500	3.01	1620	2310	-	-	-	2.86	1500	2170	0.65	-	-6.7	53600	183.3
	△	TAS-14	1409	0	2.28	880	1490	2.94	1660	2310	2.07	1640	1930	2.53	1560	2100	0.65	0.84	-5.6	44600	182.6
FIG. b)	◇	CONIC	561	0	-	-	-	2.16	1470	1875	-	-	-	2.16	1470	1875	-	-	-5.4	35100	179.9
	○	TAS-10	1005	0	1.75	810	1200	2.33	1475	1460	-	-	-	2.21	1360	1830	0.61	-	-5.2	36700	175.4
	△	TAS-14	1405	0	1.75	850	1230	2.31	1510	1970	1.65	1490	1550	1.99	1420	1750	0.62	0.79	-4.1	30900	175.8

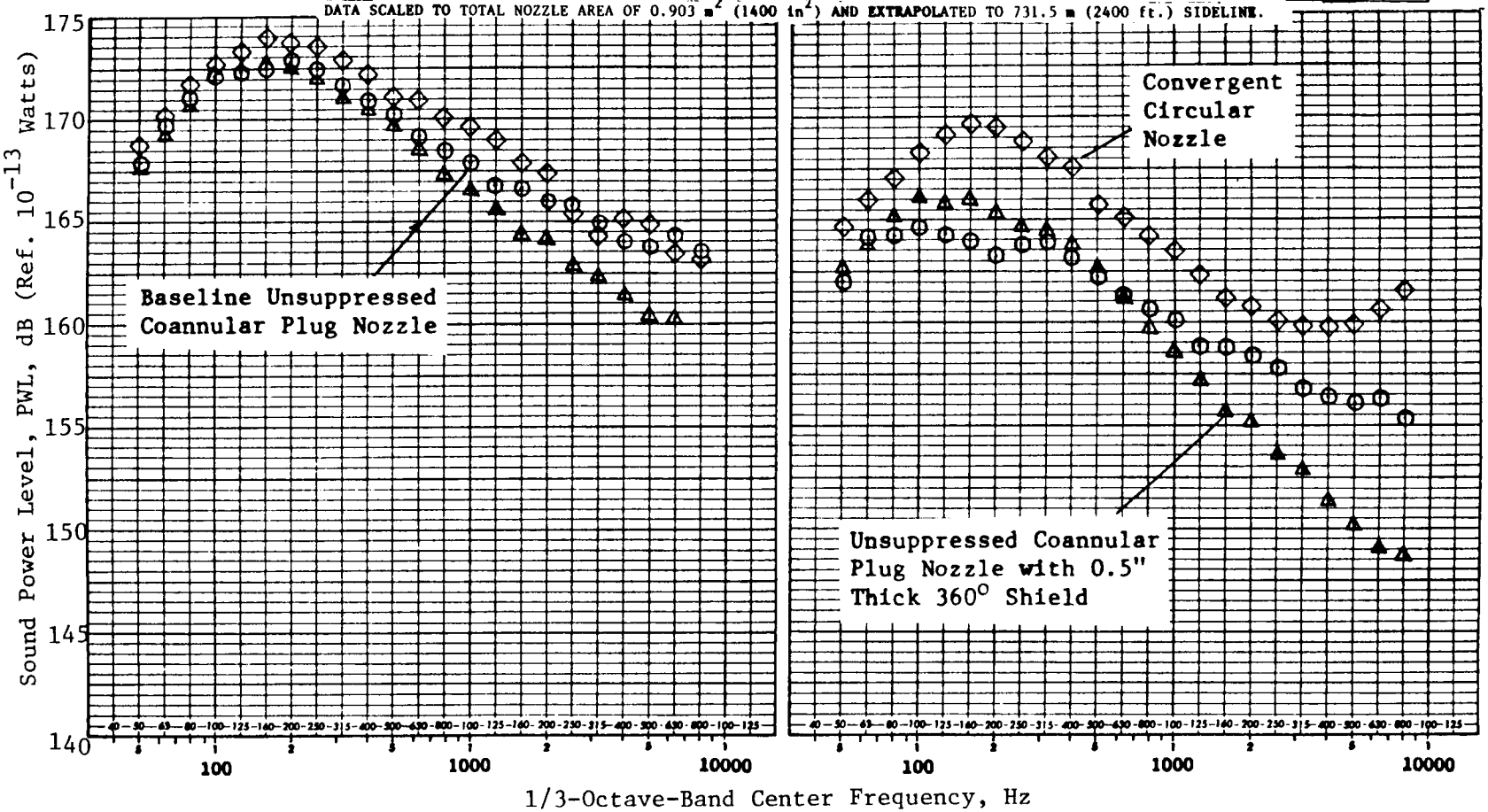

a) At Typical Takeoff b) At Typical Cutback

Figure 50. Sound Power Level Comparison Between the Unshielded and 360° Shielded Unsuppressed Coannular Plug Nozzle at Typical Takeoff and Cutback Conditions.

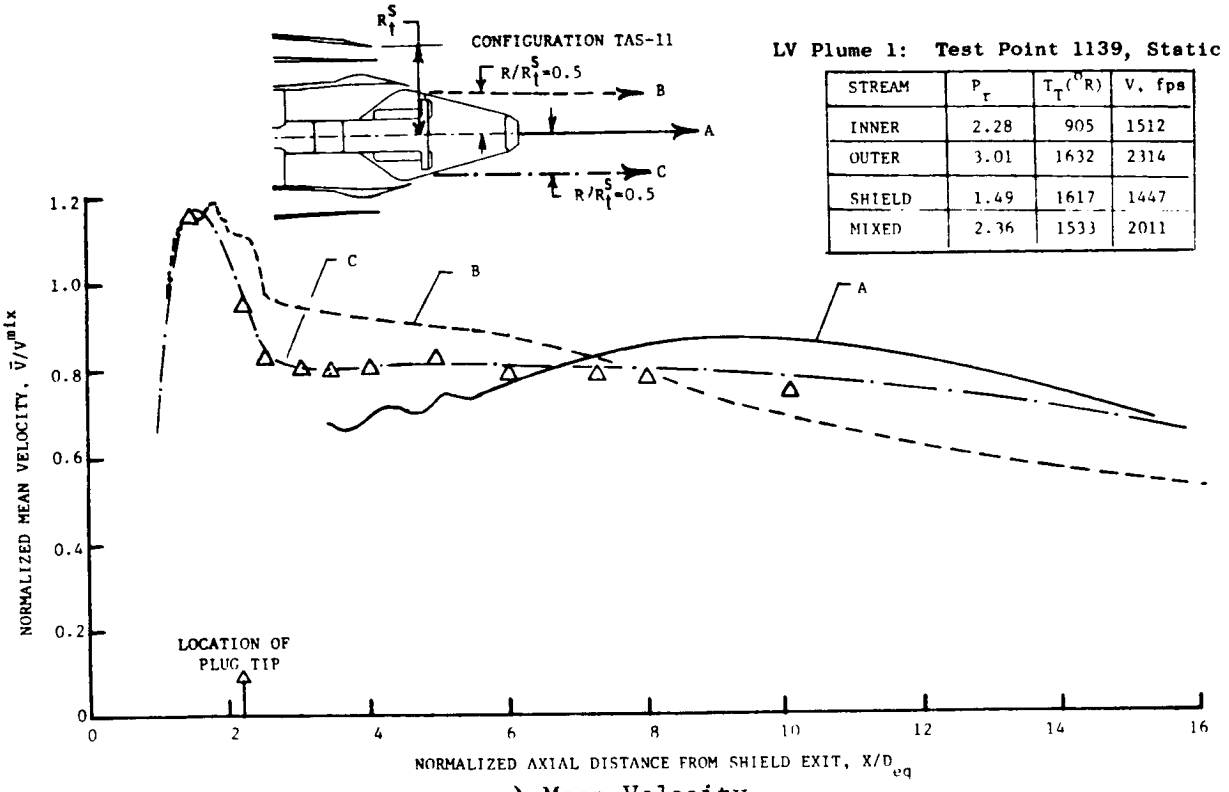

STREAM	P_r	T_T(°R)	V, fps
INNER	2.28	905	1512
OUTER	3.01	1632	2314
SHIELD	1.49	1617	1447
MIXED	2.36	1533	2011

a) Mean Velocity

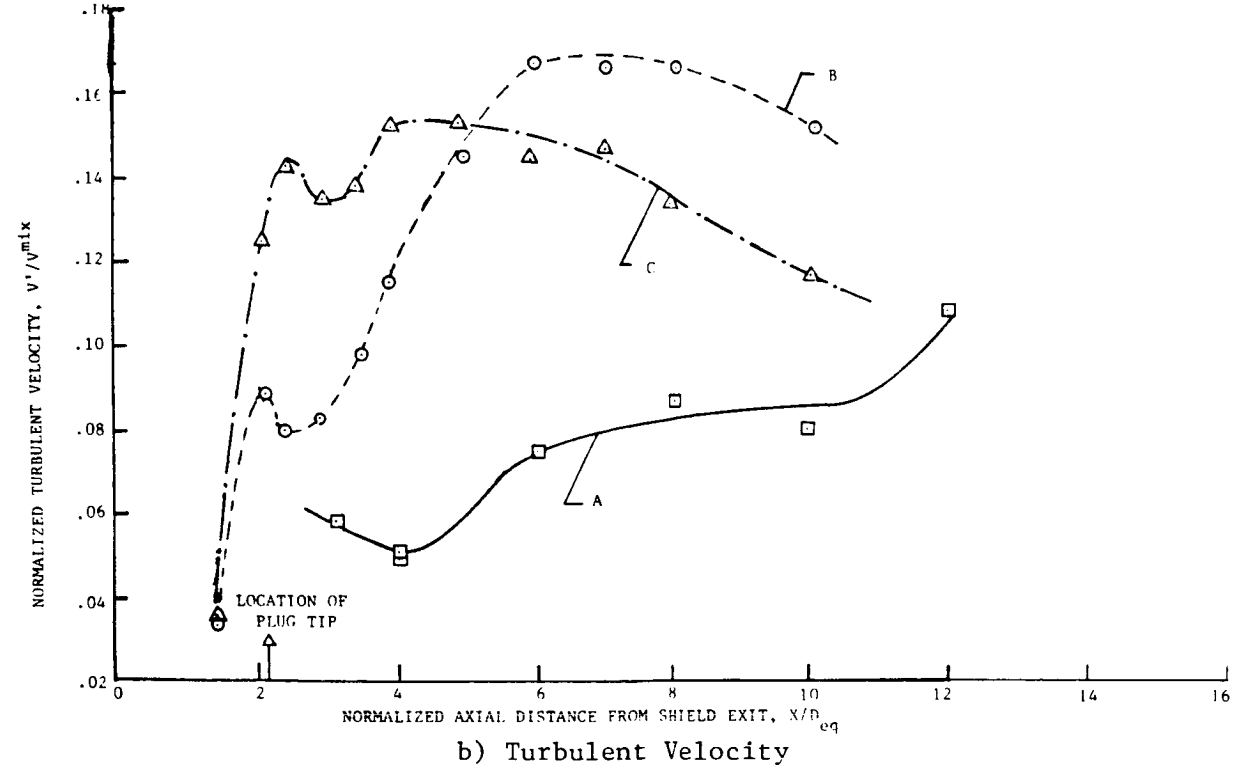

b) Turbulent Velocity

Figure 51. Axial Variation of Mean and Turbulent Velocities (Axial Components) in the Plume of Unsuppressed Coannular Plug Nozzle with 180° Shield at Takeoff Condition.

shearing of the baseline nozzle flow because of the presence of the shield flow. For $X/D_{eq} > 4$ the turbulent velocities on the shield side are higher, with a maximum of 16.5% of V^{max} at $X/D_{eq} \sim 7$.

The asymmetry in the mean and turbulent velocities between the shielded and unshielded sides can also be noted from the sets of radial traverse data that are presented in Figures 52 and 53, respectively. The radial mean velocity data in the pre-merged region (refer to data obtained at traverse J) indicate the distinct presence of the shield flow. At this location, the peak mean velocity on the shield side is lower than that on the unshielded side. The corresponding turbulent velocity profile indicates the location of mixing regions in between the inner and outer streams, outer and shield streams, and shield and ambient environment. For all regions up to an $X/D_{eq} \sim 5.0$ the turbulent velocity on the shielded side (refer to Figure 51) is observed to be lower compared to that on the unshielded side, indicating decreased shear of the nozzle flow due to the presence of shield. Further downstream and up to an $X/D_{eq} \sim 10.0$, the peak mean velocity of the shielded side is noted to be higher than that on the unshielded side due to the slower mean velocity decay rate, indicating a stretching of the jet on the shield side. The dips observed in the radial mean velocity profiles near the nozzle centerline are due to the flow separation at the base region of the plug truncation.

The laser velocimeter measured static data, presented earlier in Figures 51 and 52, are compared in Figures 54 through 56 to the corresponding data obtained under simulated flight conditions. This is to demonstrate the effect of simulated flight (V_{ac} = 400 ft/s) on the axial variation of mean and turbulent velocities, and on the radial variation of mean velocity. Because of the reduction of shear stresses due to the presence of the free-jet, the turbulent velocities measured for $X/D_{eq} < 10$ during simulated flight are lower than the corresponding static data. This, in general, results in the observed slower decay of the jet plume in simulated flight. The effect of free-jet on the flow-field characteristics of unsuppressed coannular plug nozzle with partial shield is discussed further in Section 5.2.

The acoustic data measured with the 180° shielded unsuppressed coannular plug configuration at aerodynamic flow conditions that correspond to the above static LV data were presented earlier in Section 4.1.3. The measured PNL-directivity data are repeated in Figure 57 and compared to the corresponding baseline unsuppressed coannular plug nozzle (TAS-10) data to show the noise suppression due to the partial shield. In addition, the 180° shield effectiveness on the directivity of the various 1/3-octave-band frequencies is presented in Figure 58. The aft quadrant data of this figure indicate increased suppression with increase in frequency. In addition, similar to the shielded annular nozzle data of Figures 6 through 8, the fluid shielding results in a significant attenuation of the high frequency noise for $\theta_i > 130°$. For example, for frequencies $\geq$ 1000 Hz, the maximum suppression at $\theta_i = 150°$ is observed to be about 12 dB. The suppression of $\leq$ 4 dB noted in the front quadrant is attributed to modifications in the velocity gradients by the shield flow.

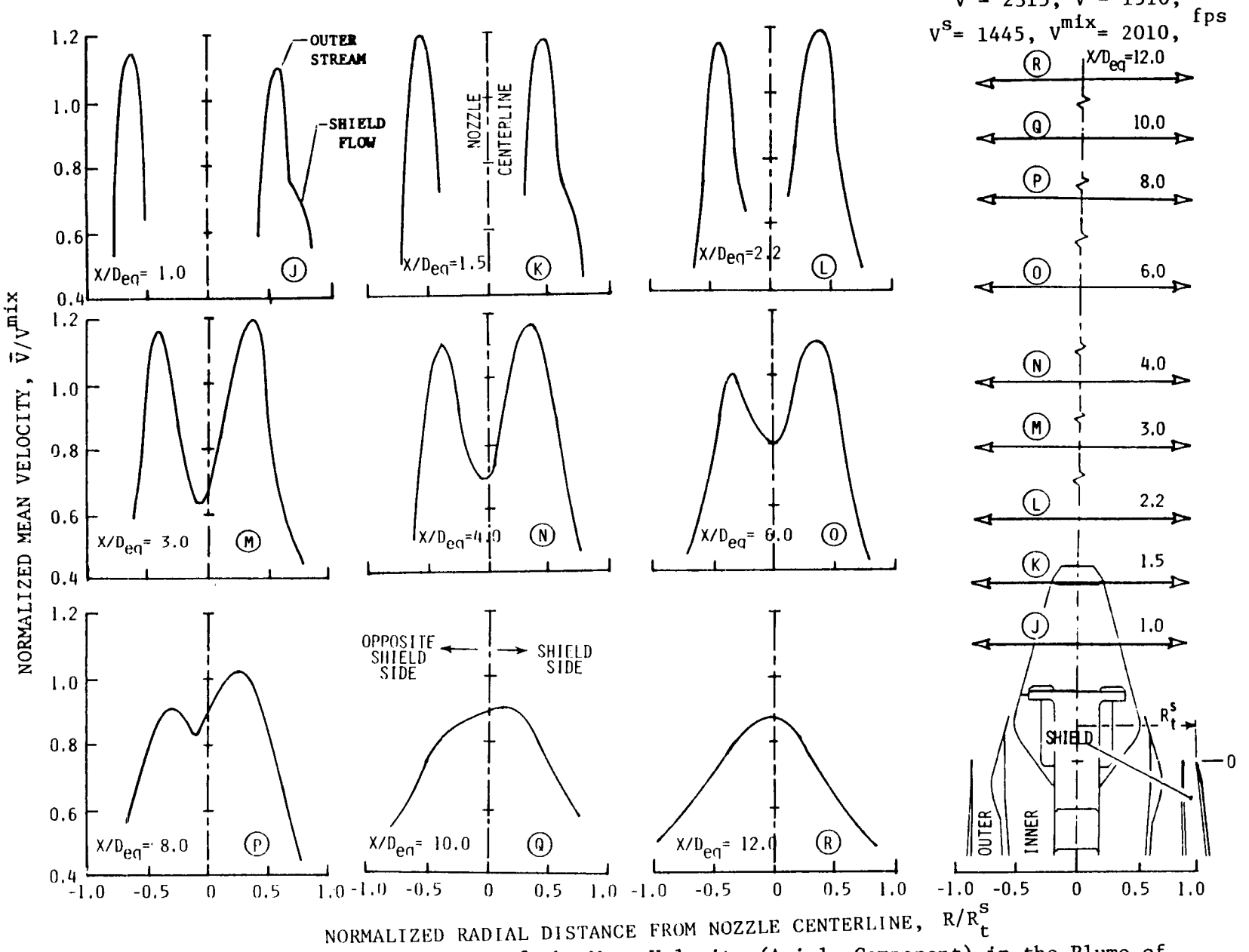

Figure 52. Radial Variation of the Mean Velocity (Axial Component) in the Plume of Unsuppressed Coannular Plug Nozzle with 180° Shield at Takeoff Condition.

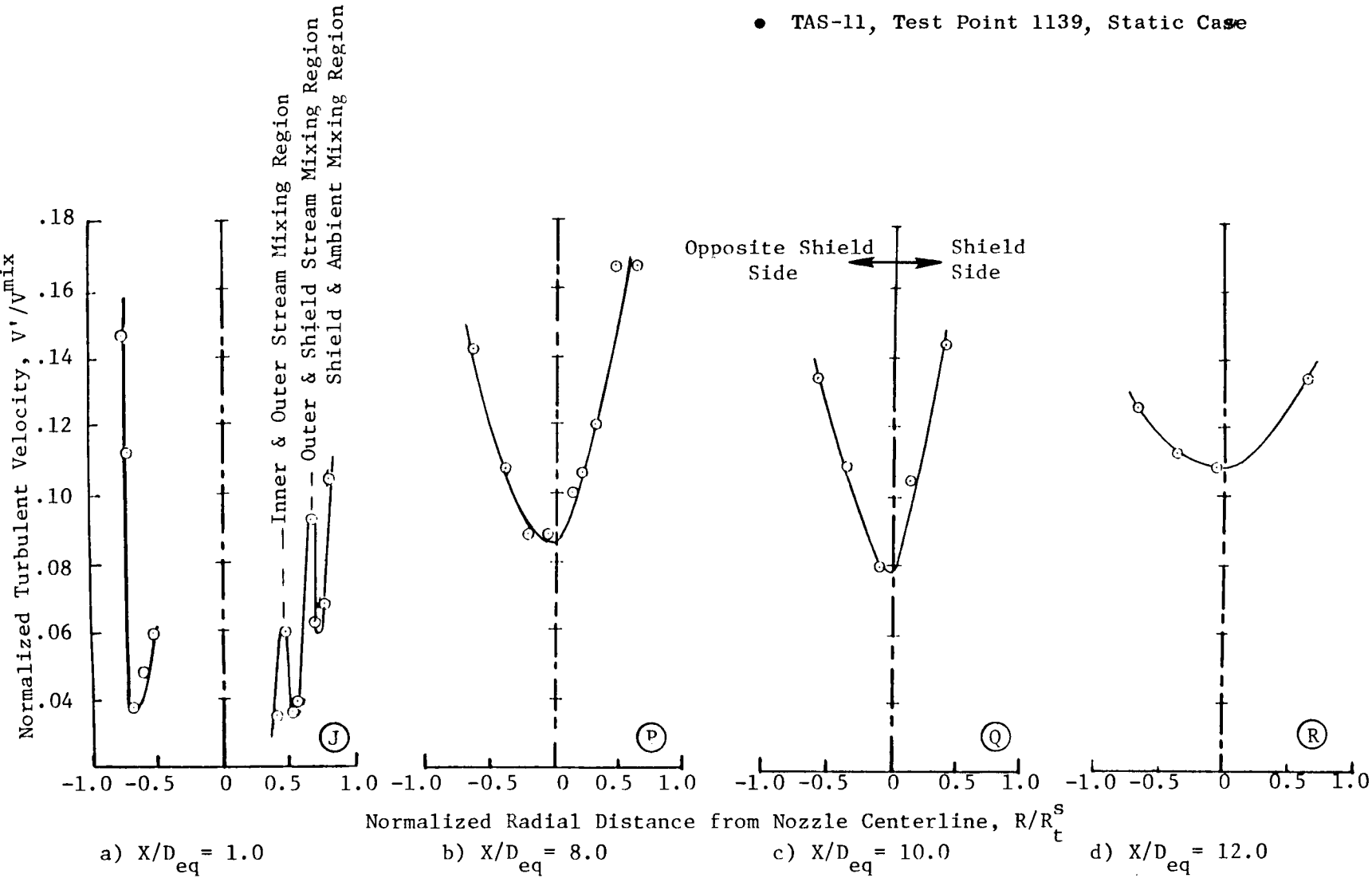

Figure 53. Radial Variation of the Turbulent Velocity (Axial Component) in the Plume of Unsuppressed Coannular Plug Nozzle with 180° Shield at Takeoff Condition.

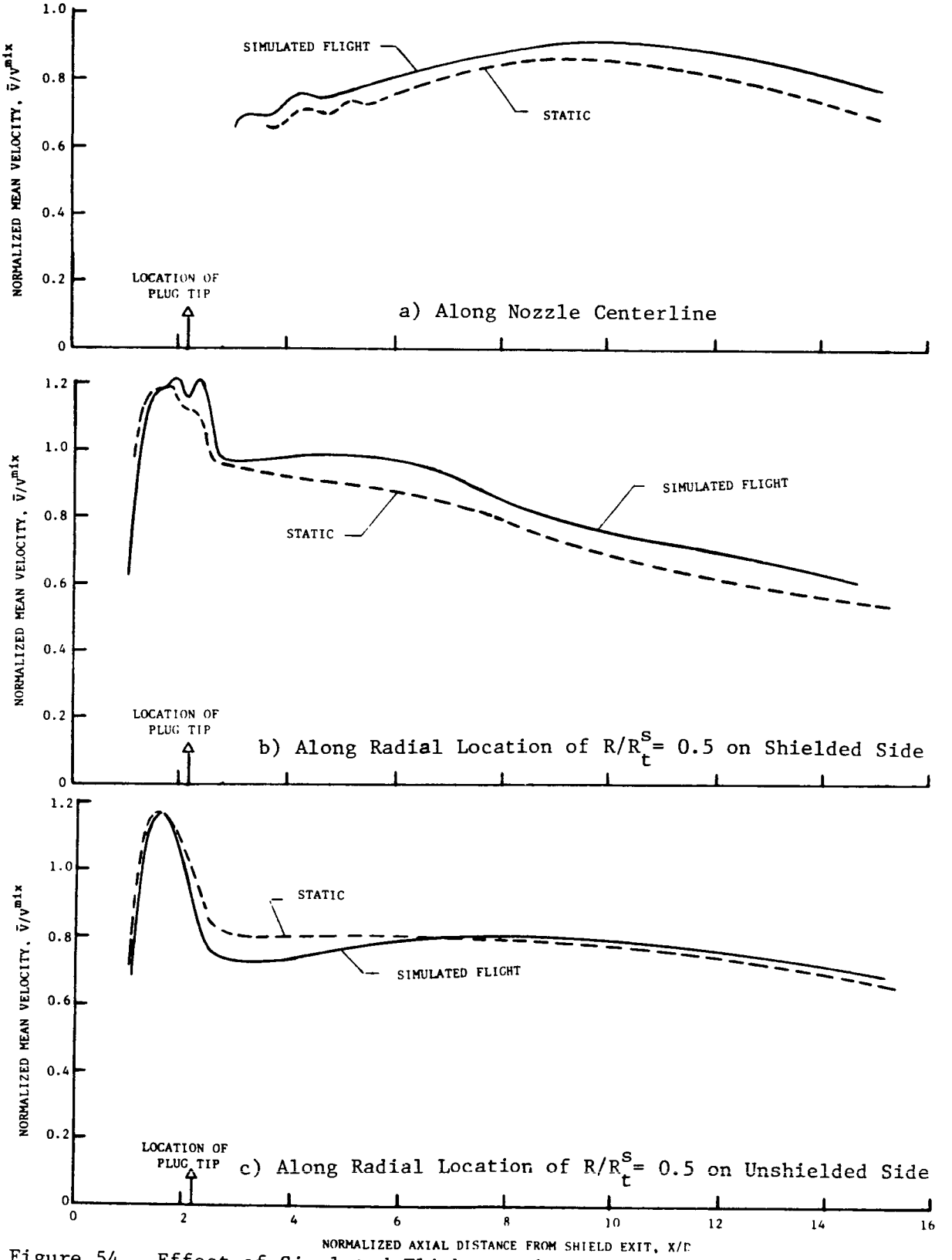

Figure 54. Effect of Simulated Flight on the Axial Variation of Mean Velocity Along the Centerline, Shielded and Unshielded Side of Unsuppressed Coannular Plug Nozzle with 180° Shield (TAS-11) at Takeoff Condition.

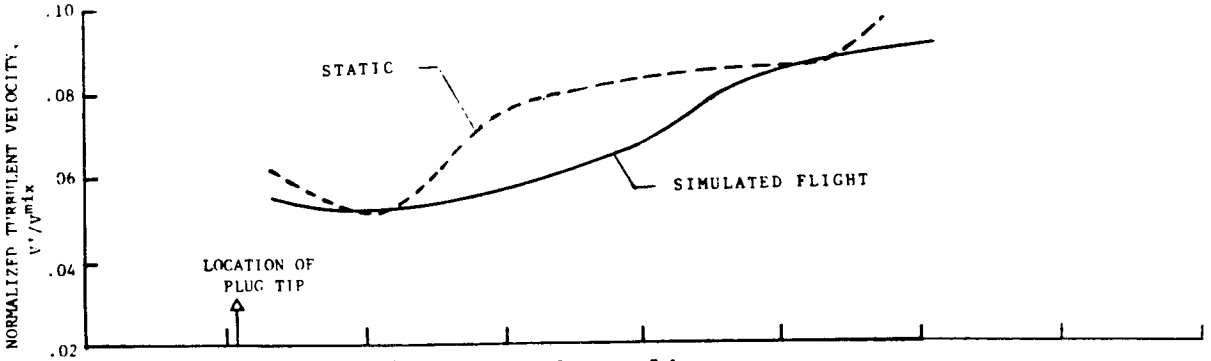

a) Along Nozzle Centerline

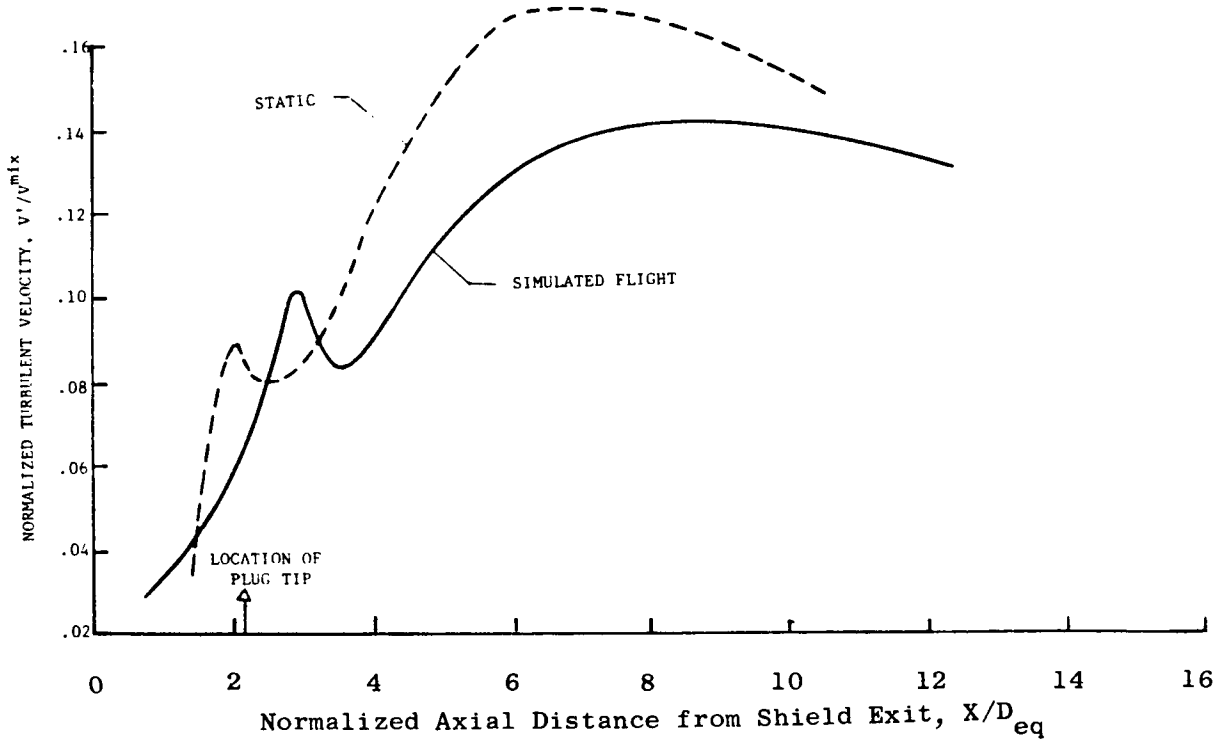

b) Along Radial Location of $R/R_t^s = 0.5$ on Shielded Side

Figure 55. Effect of Simulated Flight on the Axial Variation of Turbulent Velocity Along the Centerline, Shielded and Unshielded Side of Unsuppressed Coannular Plug Nozzle with 180° Shield (TAS-11) at Takeoff Condition.

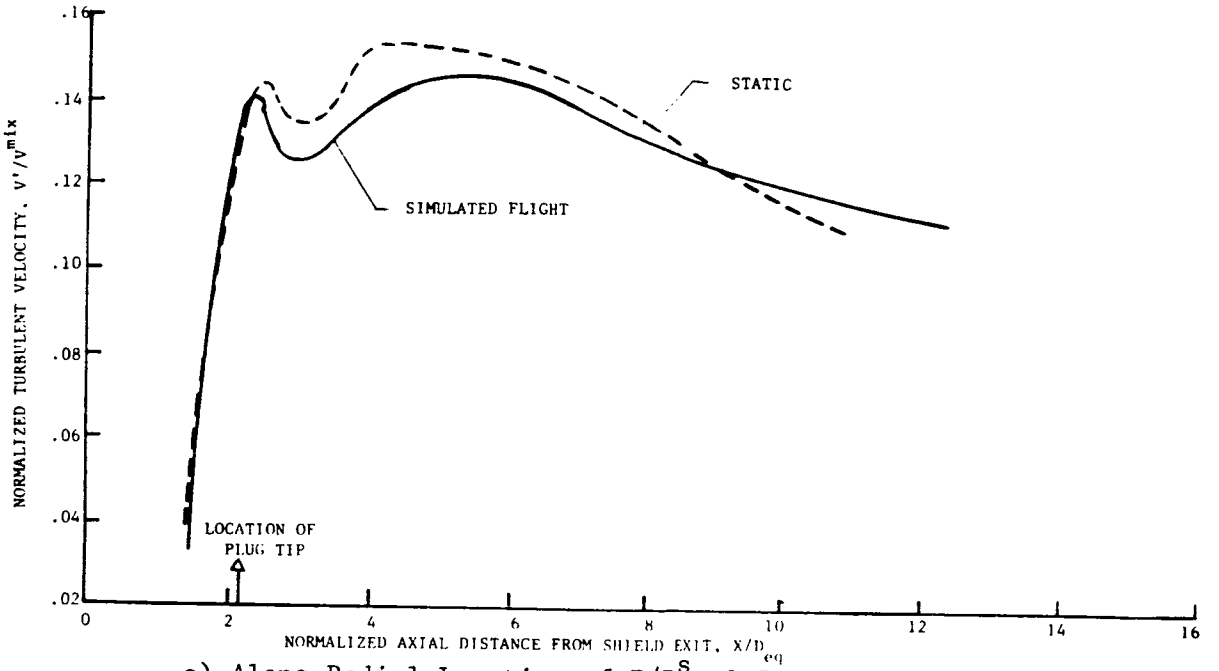

c) Along Radial Location of $R/R_t^s = 0.5$ on Unshielded Side

Figure 55. Effect of Simulated Flight on the Axial Variation of Turbulent Velocity Along the Centerline, Shielded and Unshielded Side of Unsuppressed Coannular Plug Nozzle with 180° Shield (TAS-11) at Takeoff Condition (Concluded).

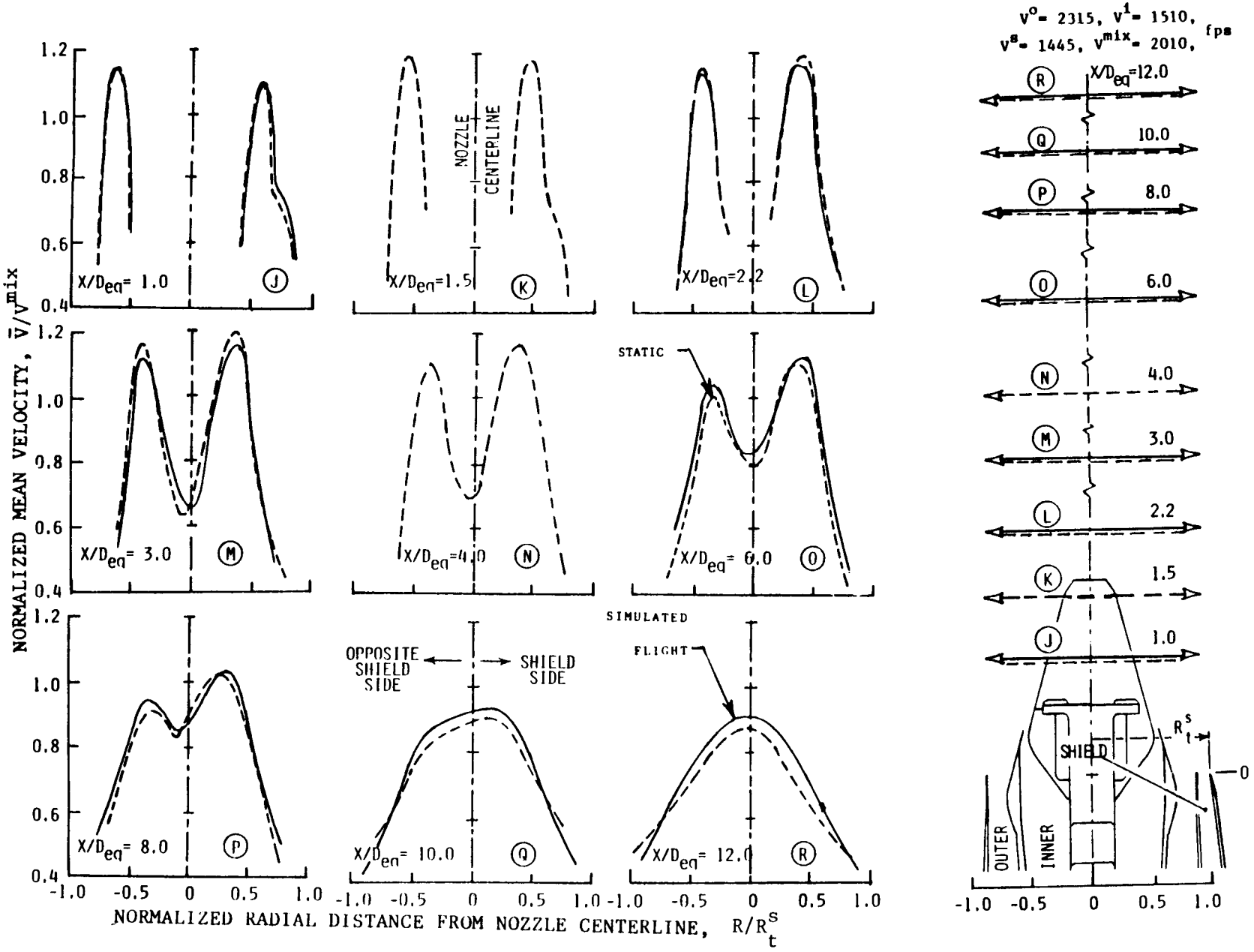

Figure 56. Effect of Simulated Flight on the Radial Variation of the Mean Velocity of the Plume of Unsuppressed Coannular Plug Nozzle with 180° Shield (TAS-11) at Takeoff Condition.

SYMBOL	CONFIG	TEST POINT	V_{ac}	INNER STREAM P_r^i	INNER STREAM T_T^i	INNER STREAM V^i	OUTER STREAM P_r^o	OUTER STREAM T_T^o	OUTER STREAM V^o	SHIELD STREAM P_r^s	SHIELD STREAM T_T^s	SHIELD STREAM V^s	MIXED CONDITIONS P_r^{mix}	MIXED CONDITIONS T_T^{mix}	MIXED CONDITIONS V^{mix}	$V_r^{i,o}$	$V_r^{s,o}$	NF, dB
○	TAS-10	1021	0	2.28	900	1500	3.01	1620	2305	-	-	-	2.86	1500	2170	0.65	-	-6.7
△	TAS-11	1139	0	2.28	905	1510	3.01	1630	2315	1.49	1615	1450	2.36	1530	2010	0.65	0.63	-5.2

(T_T-°R; V- fps)

DATA SCALED TO TOTAL NOZZLE AREA OF 0.903 m^2 (1400 in^2) AND EXTRAPOLATED TO 731.5 m (2400 ft.) SIDELINE.

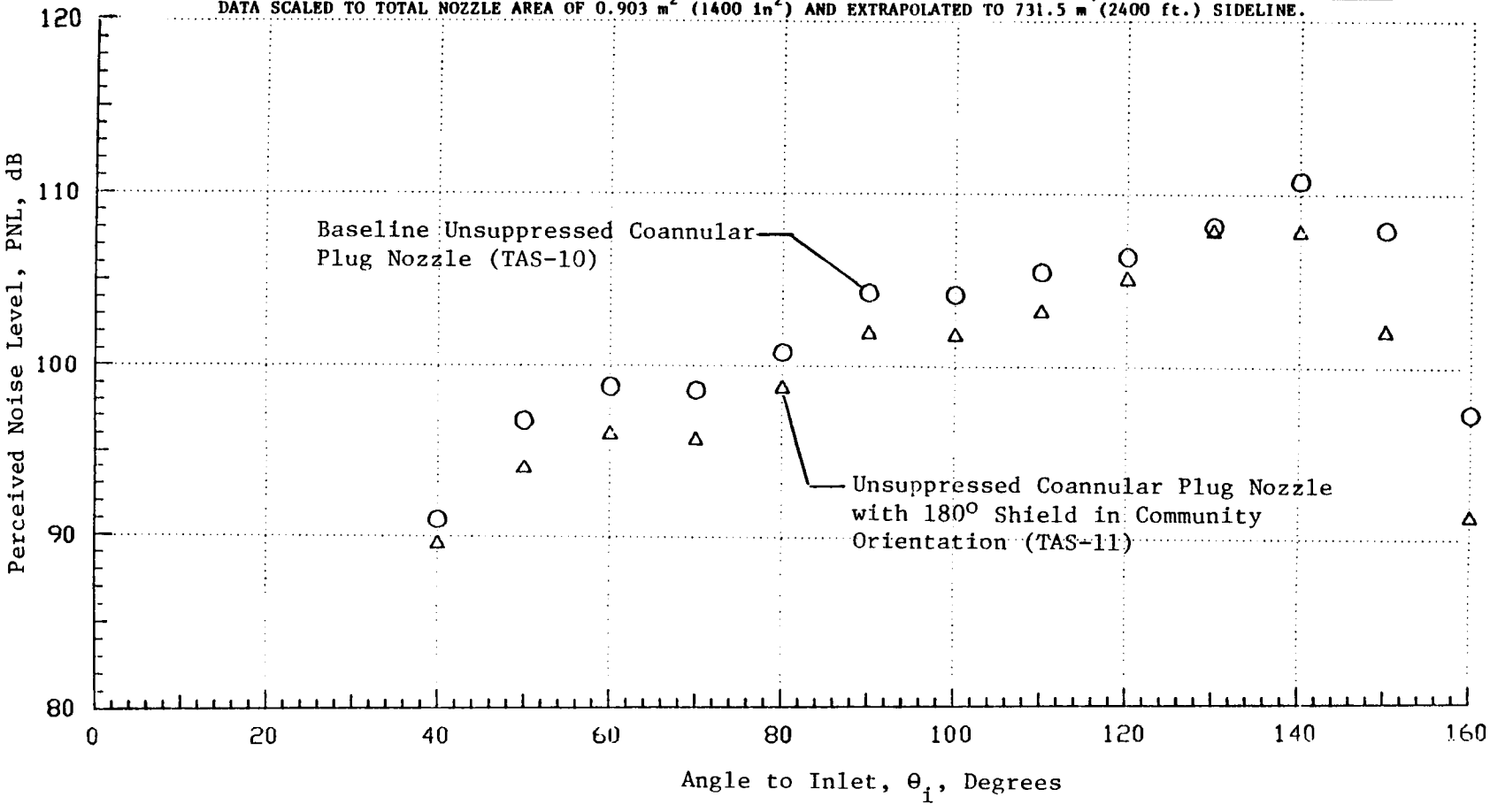

Figure 57. Effect of 180° Shield in Community Orientation of the PNL-Directivity of Unsuppressed Coannular Plug Nozzle at Takeoff Condition (Static).

(Refer to Figure 57 for aerodynamic flow conditions.)

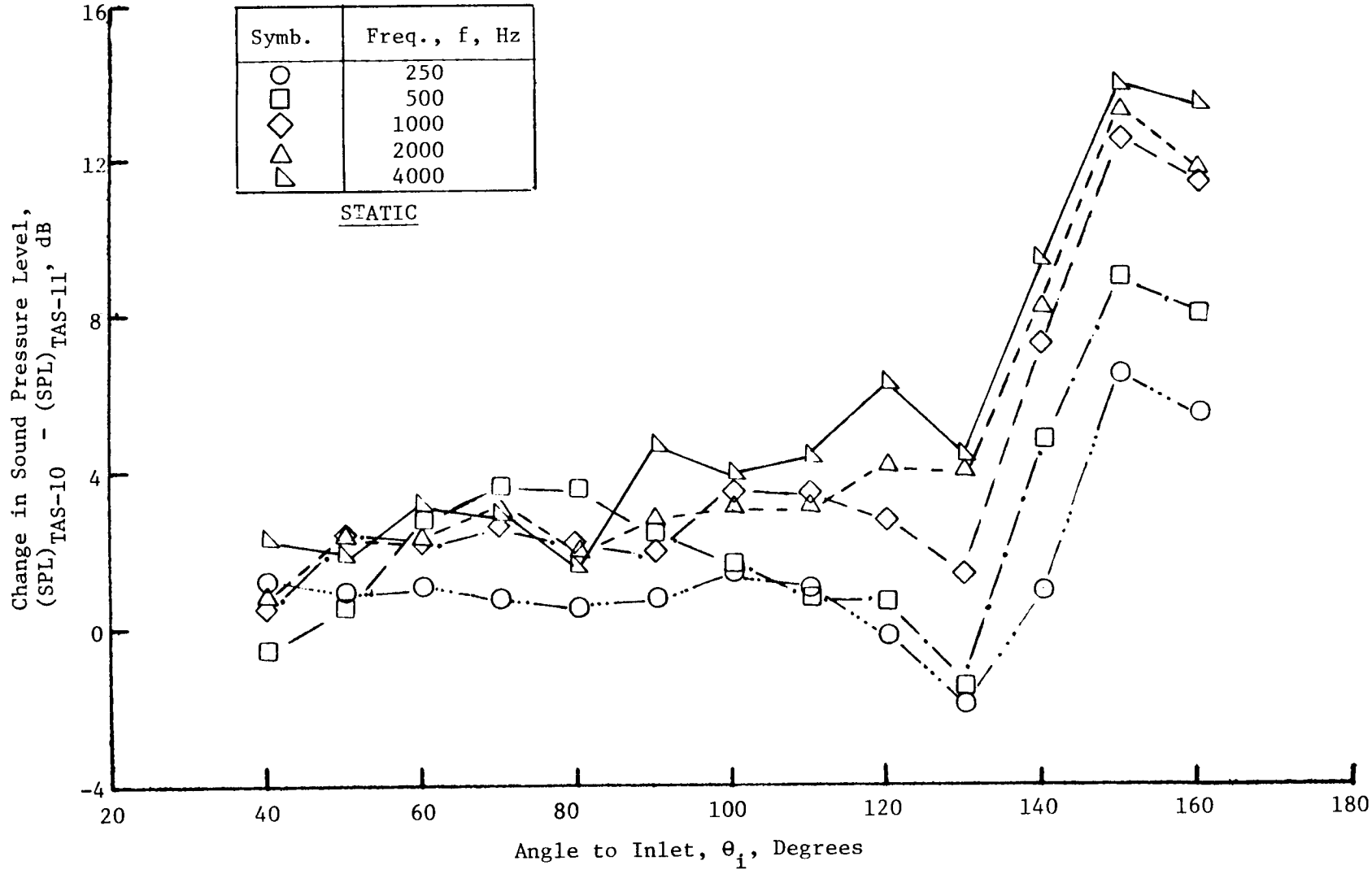

Figure 58. Influence of 180° Shield in Community Orientation on the Directivity of Various One-Third-Octave Band Frequencies of Unsuppressed Coannular Plug Nozzle at Takeoff Condition.

4.2 SUPPRESSED COANNULAR PLUG NOZZLE DATA

This section summarizes the acoustic and diagnostic data of the baseline suppressed coannular plug nozzle (TAS-15) and suppressed coannular plug nozzle with partial shield (TAS-16, TAS-17, and TAS-18) and full shield (TAS-19). The scope of acoustic tests with these five configurations was presented earlier in Table III and Figures 27 and 28. The diagnostic laser velocity measurements were limited to a static and simulated flight plume of TAS-16 at a typical takeoff condition (refer to Table XIII for flow conditions).

4.2.1 Baseline Suppressed Configuration

The baseline unshielded configuration of this study is the suppressed coannular plug nozzle with a convergent 20-element suppressor in the outer stream and a convergent annular inner stream (TAS-15). This configuration has been tested on Model 10-1 during an earlier NASA Lewis supported program (Reference 22). To broaden the data base of this baseline suppressed coannular configuration, it was tested during this program as shown in the test matrix presented in Table VIII. Normalized perceived noise level data measured at static and simulated flight (V_{ac} = 400 fps) conditions at an aft quadrant angle of θ_i = 130° are presented in Figures 59 and 60. The data are plotted as a function of mixed jet velocity parameter. The corresponding perceived noise level data at a forward quadrant angle of θ_i = 60° are presented in Figures 61 and 62. The forward quadrant data are plotted as a function of the effective shock strength parameter. The repeatability of the data is demonstrated in these figures by comparing the data obtained during this program with those obtained from the previous test (Reference 22).

The suppressed baseline coannular plug nozzle data are compared in Figures 59 through 62 with the static and simulated flight data of a convergent circular nozzle (Reference 21 and 22). The comparison shows that at a mixed jet velocity of 2200 fps (typical AST takeoff condition) the suppressed configuration shows 11.5 dB and 7 dB reduction in the PNL at θ_i = 130° below that of a convergent circular nozzle under static and simulated flight conditions. This static-to-flight suppressor loss is observed at all mass-averaged velocities greater than 1600 fps. Similar trends in the flight PNL data were observed at all aft angles.

The typical forward quadrant (θ_i = 60°) PNL data presented in Figures 61 and 62 indicate a noise reduction of 4.2 dB and 5.0 dB at a typical takeoff condition under static and simulated flight conditions, respectively. Also, for a given β^{eff}, the PNL data of the suppressed configuration at θ_i = 60° are equal or higher than those of the unsuppressed coannular nozzle (presented earlier in Figures 31 and 32). This indicates that the suppressor configuration is not very effective in reducing the shock-cell noise.

The static and simulated flight spectral data of the baseline suppressed coannular plug nozzle, at a typical takeoff condition, are compared with the corresponding results for the convergent circular nozzle in Figures 63 and 64, respectively. The front quadrant spectral data of Figures 63(a) and 64(a) reveal a shift in the shock-cell associated peak frequency to a higher value

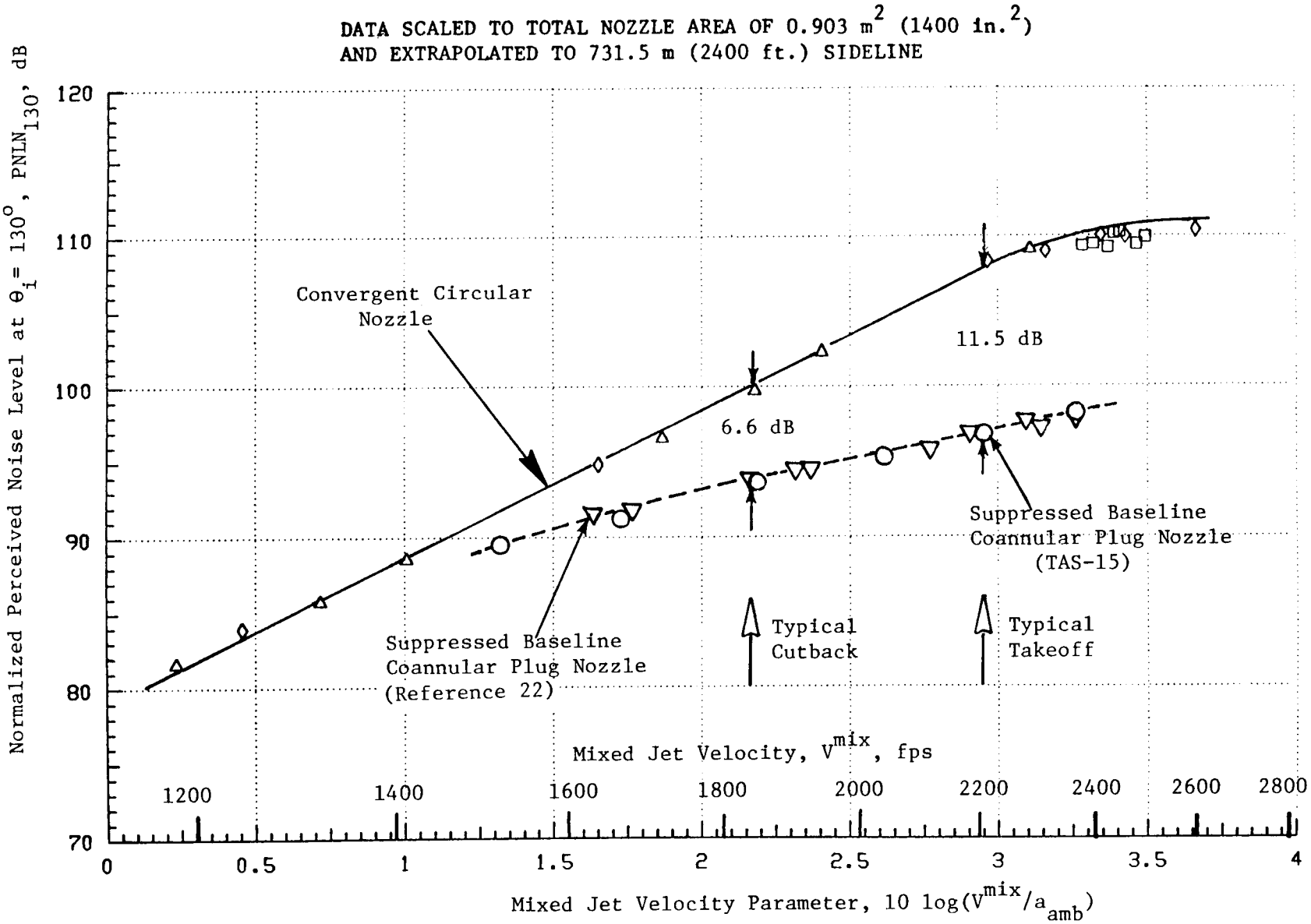

Figure 59. Comparison of Typical Aft-Quadrant Normalized Perceived Noise Level Data of Suppressed Baseline Coannular Plug Nozzle (TAS-15) with Those of Convergent Circular Nozzle (Static).

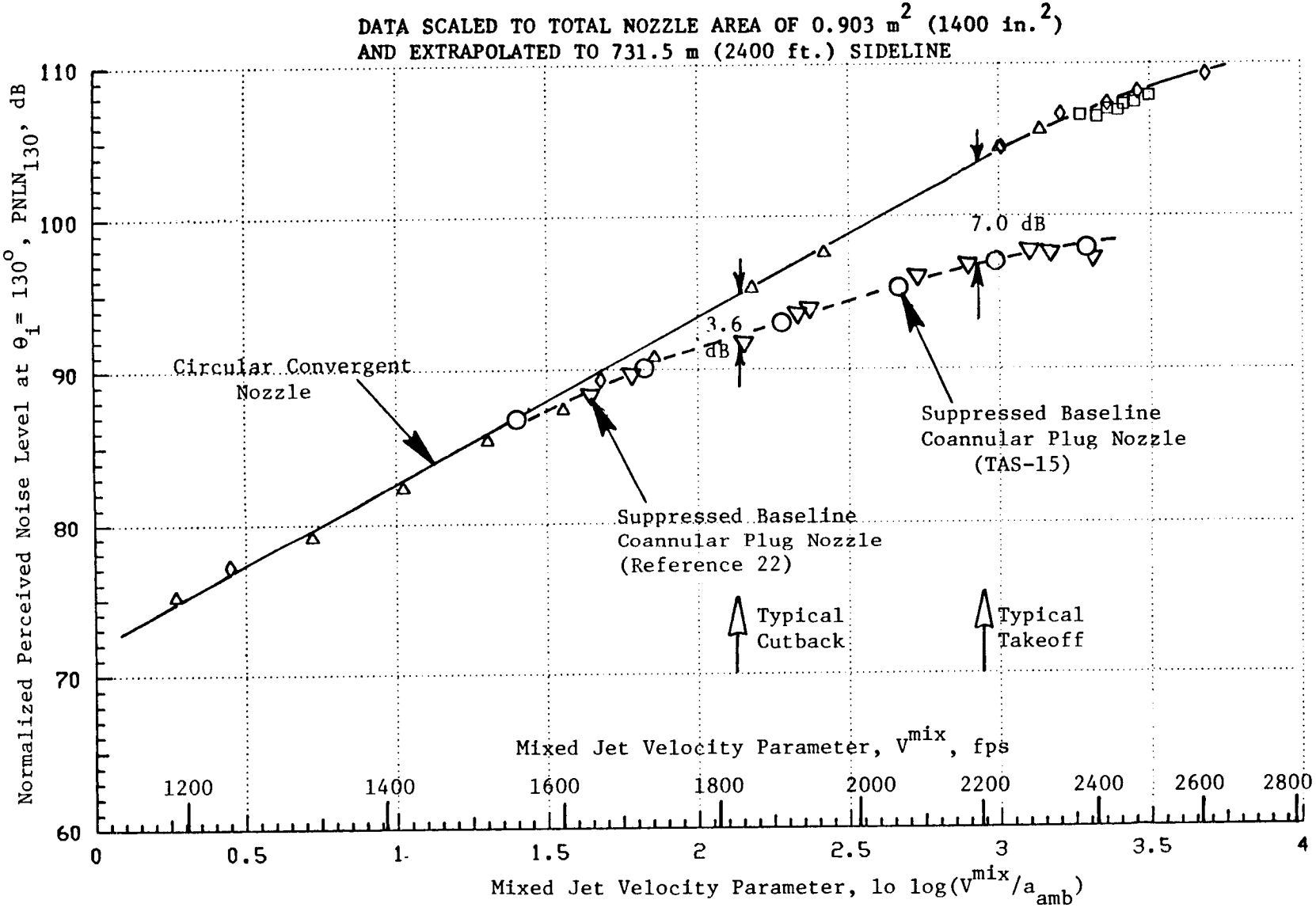

Figure 60. Comparison of Typical Aft-Quadrant Normalized Perceived Noise Level Data of Suppressed Baseline Coannular Plug Nozzle (TAS-15) with Those of Convergent Circular Nozzle (Simulated Flight).

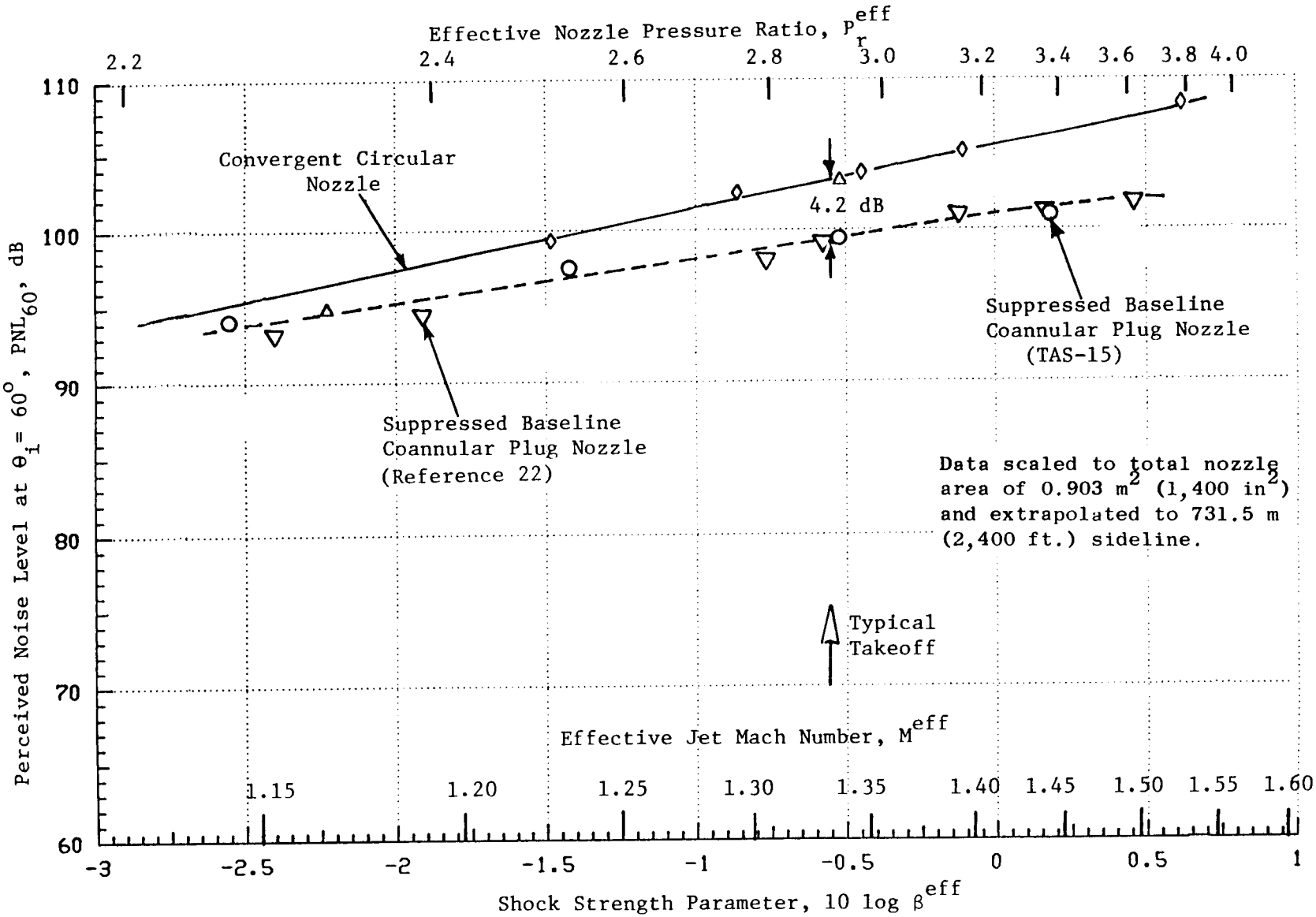

Figure 61. Comparison of Typical Forward-Quadrant Perceived Noise Level Data of Suppressed Baseline Coannular Plug Nozzle (TAS-15) with Those of Convergent Circular Nozzle (Static).

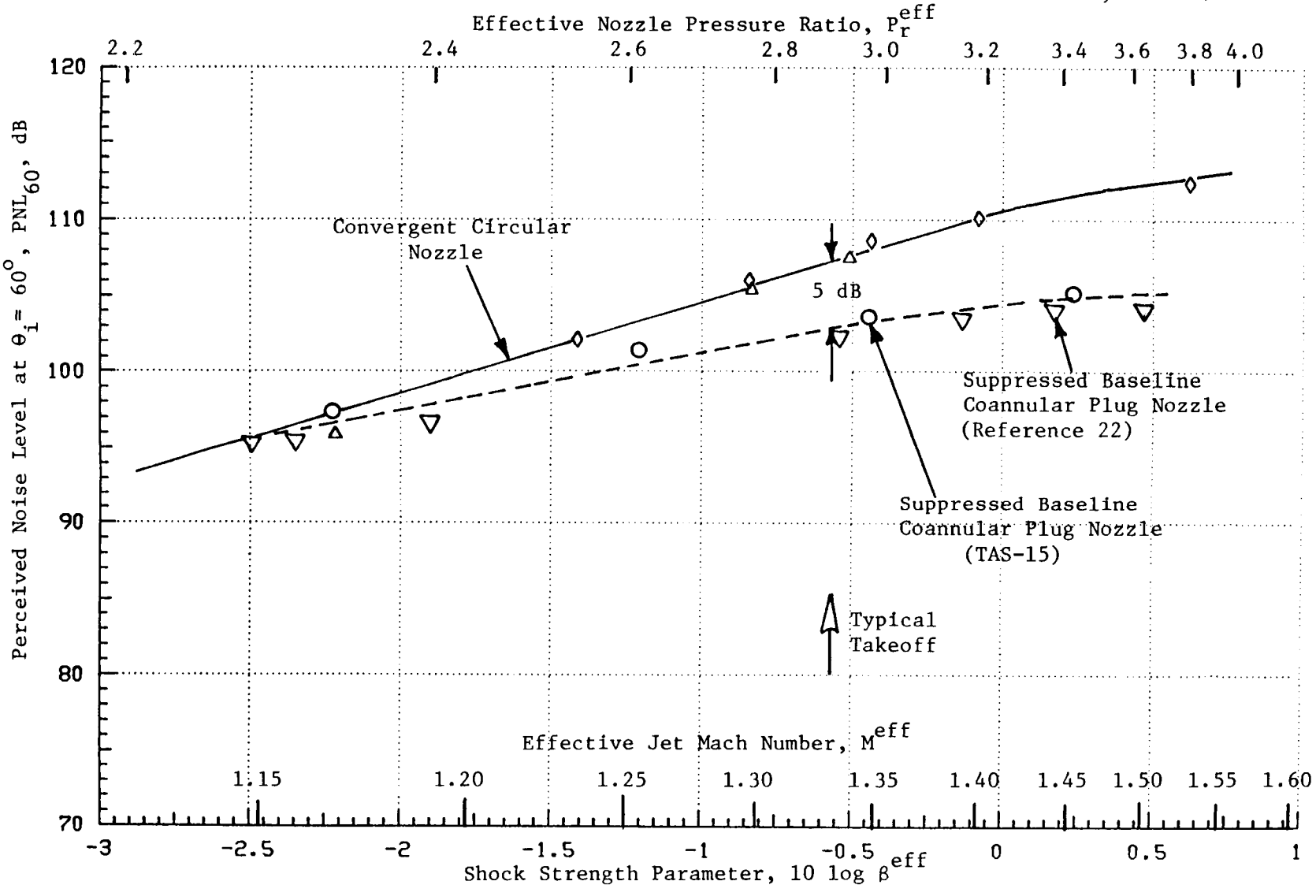

Figure 62. Comparison of Typical Forward-Quadrant Percieved Noise Level of Suppressed Coannular Plug Nozzle (TAS-15) with Those of Convergent Circular Nozzle (Simulated Flight).

SYMBOL	TEST POINT	V_{ac}	INNER STREAM P_r^i	INNER STREAM T_T^i	INNER STREAM V^i	OUTER STREAM P_r^o	OUTER STREAM T_T^o	OUTER STREAM V^o	MIXED CONDITIONS P_r^{mix}	MIXED CONDITIONS T_T^{mix}	MIXED CONDITIONS V^{mix}	$V_r^{i,o}$	NF_θ, dB
◇	504	0	-	-	-	2.51	1675	2170	2.51	1675	2170	-	-5.1
○	1509	0	2.33	900	1520	3.03	1640	2340	2.88	1510	2190	.65	-6.8

(T_T-°R; V-fps)

DATA SCALED TO TOTAL NOZZLE AREA OF 0.903 m^2 (1400 in^2) AND EXTRAPOLATED TO 731.5 m (2400 ft) SIDELINE.

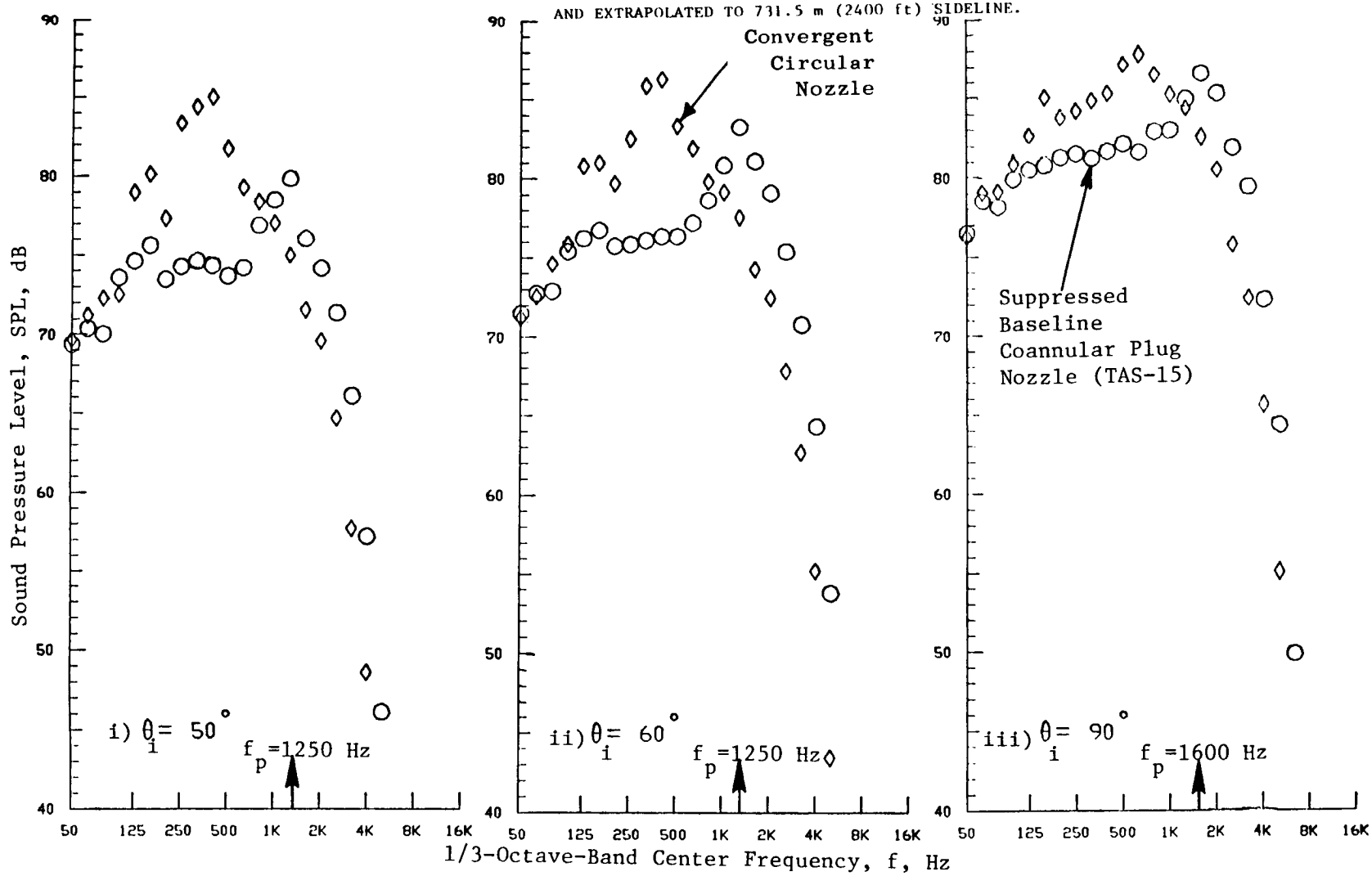

a) Front-Quadrant

Figure 63. Comparison of Sound Pressure Levels of Suppressed Baseline Coannular Plug Nozzle (TAS-15) with Those of Convergent Circular Nozzle at a Typical Takeoff Condition (Static).

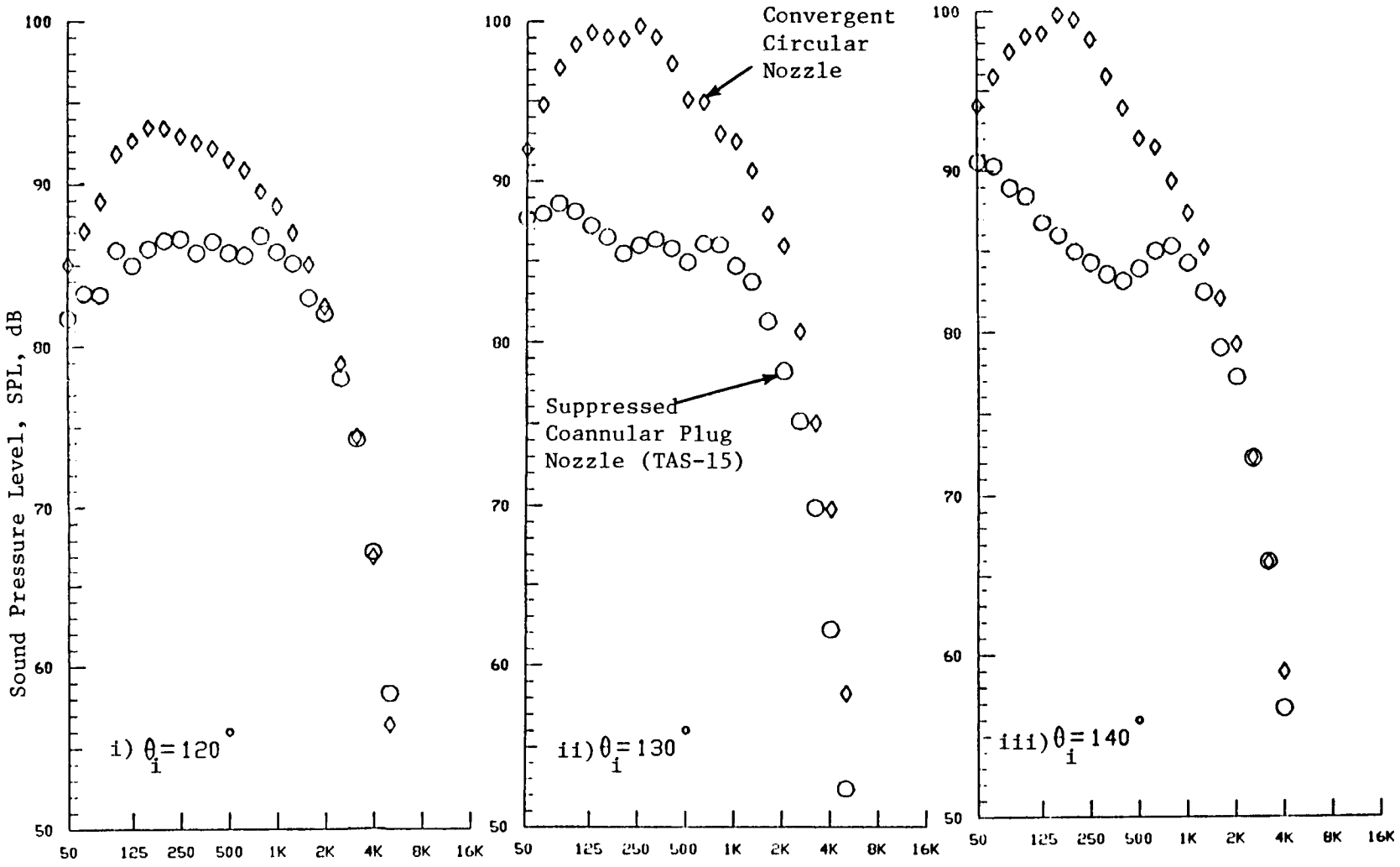

b) Aft Quadrant

Figure 63. Comparison of Sound Pressure Levels of Suppressed Baseline Coannular Plug Nozzle (TAS-15) with Those of Convergent Circular Nozzle at a Typical Takeoff Condition (Static). (Concluded)

SYMBOL	TEST POINT	V_{ac}	INNER STREAM P_r^i	INNER STREAM T_T^i	INNER STREAM V^i	OUTER STREAM P_r^o	OUTER STREAM T_T^o	OUTER STREAM V^o	MIXED CONDITIONS P_r^{mix}	MIXED CONDITIONS T_T^{mix}	MIXED CONDITIONS V^{mix}	$V_r^{i,o}$	NF, dB
◇	506	400	-	-	-	2.53	1675	2180	2.53	1675	2180	-	-5.1
○	1510	400	2.32	910	1530	3.09	1640	2340	2.93	1520	2205	.65	-6.8

(T_T-°R; v-fps)

DATA SCALED TO TOTAL NOZZLE AREA OF 0.903 m^2 (1400 in^2)
AND EXTRAPOLATED TO 731.5 m (2400 ft) SIDELINE.

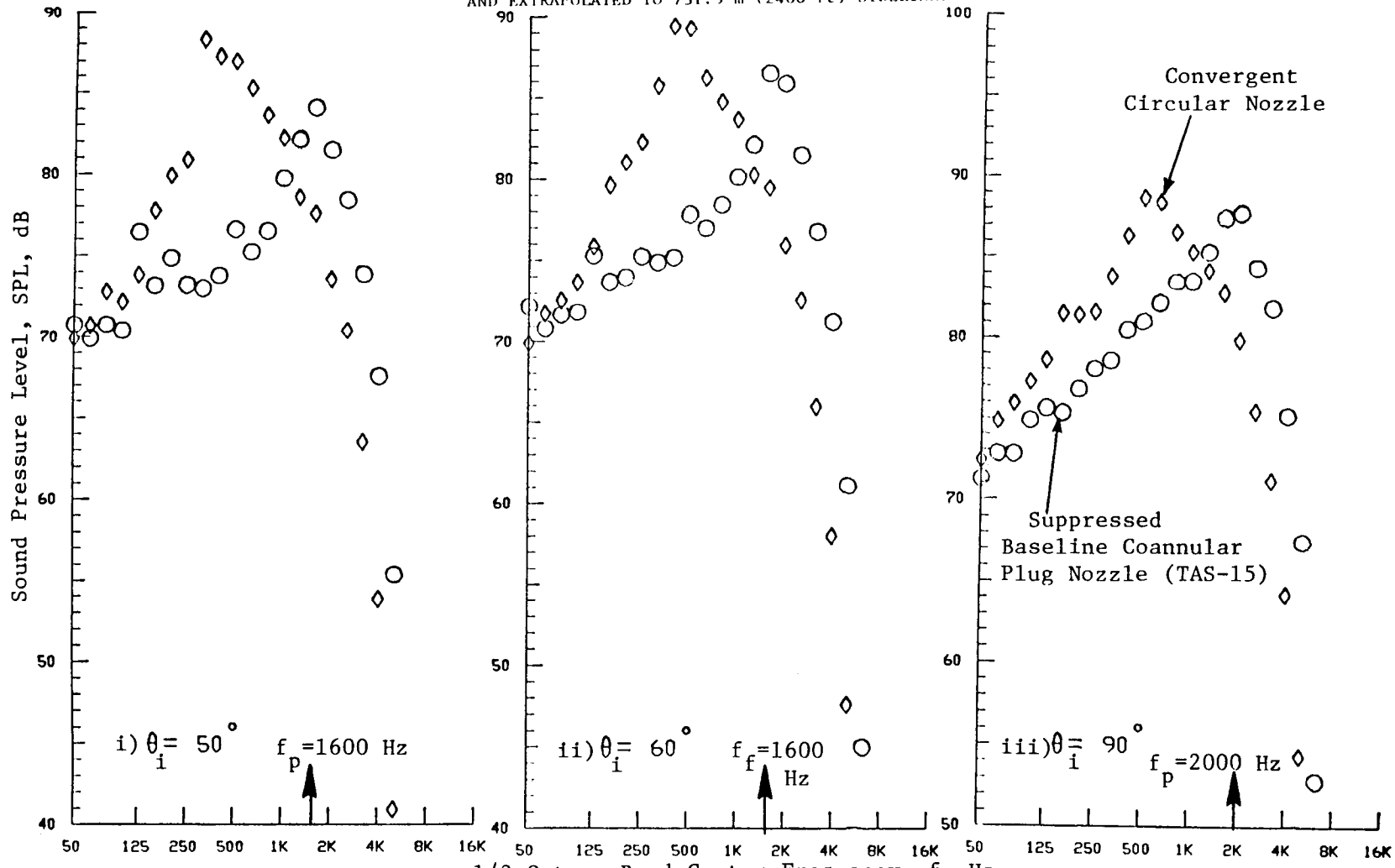

a) Front-Quadrant

Figure 64. Comparison of Sound Pressure Levels of Suppressed Baseline Coannular Plug Nozzle (TAS-15) with Those of Convergent Circular Nozzle at a Typical Takeoff Condition (Simulated Flight).

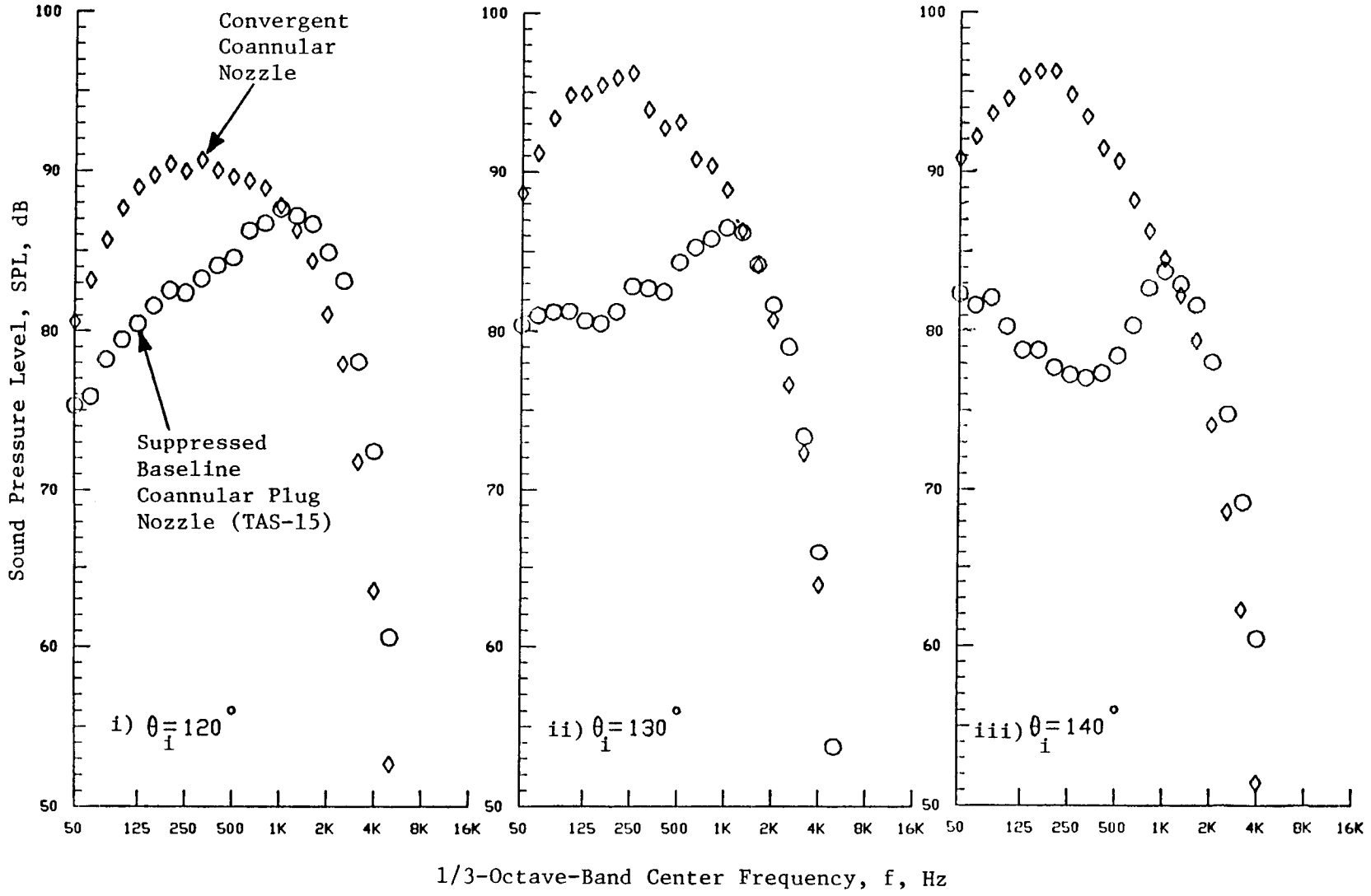

b) Aft-Quadrant

Figure 64. Comparison of Sound Pressure Levels of Suppressed Baseline Coannular Plug Nozzle (TAS-15) with Those of Convergent Circular Nozzle at a Typical Takeoff Condition (Simulated Flight). (Concluded)

for the suppressor configuration. As described in Reference 24, detailed diagnostic data obtained with the suppressed configuration in the vicinity of the plug and at flow conditions close to the flow conditions of Figure 63 indicated:

a. the presence of at least 8 shock-cells on the plug and in front of each of the suppressor flow elements

b. the average shock-cell spacing, L_{avg}, on the plug is 1.03 inches

c. subsonic flow region and hence no shock-cell structure downstream of the plug.

In order to characterize the frequency associated with the shock-cells on the plug, the shock-cell related broadband peak frequencies for the static test were calculated using the following equation (Reference 31).

$$(f_p)_{static} = \frac{U_c}{L_{avg}\,(1 + M_c \cos \theta_i)} \tag{14}$$

In the above equation U_c is the convection velocity of the eddy that is taken as equal to 0.65 x jet velocity V, $M_c = U_c/a_{amb}$ with a_{amb} being the ambient sound speed and θ_i the observer angle with respect to upstream axis. The jet velocity associated with the shock-cells on the plug was taken to be the outer stream velocity V^o. The shock broadband peak frequency corresponding to a flight Mach number M_{ac} was calculated by applying the Doppler shift to the predicted static data as follows:

$$(f_p)_{flight} = \frac{(f_p)_{static}}{1 - M_{ac} \cos \theta_i} \tag{15}$$

The static broadband peak frequencies are then predicted to be 9,460, 10,550, and 17,720 Hz at θ_i = 50°, 60°, and 90°, respectively. These frequencies are within the 1/3-octave-bands having center frequencies of 10, 10, and 16 kHz, respectively. When these are extrapolated to the typical product size of 1400 in^2, the associated broadband peak frequencies at θ_i = 50°, 60°, and 90° correspond respectively to 1/3-octave-bands having center frequencies of 1.25, 1.25, and 2.0 kHz for the static case and 1.6, 1.6, and 2.0 kHz for the flight case. These predicted peak frequencies are observed to be in agreement with the corresponding measured values, indicated in Figures 63(a) and 64(a).

An examination of the suppressed coannular nozzle aft-quadrant spectral data of Figures 63(b) and 64(b) indicates a significant amount of reduction in the low and middle frequency SPL levels relative to those of the convergent circular nozzle. Also, because of the pronounced high frequency content of the suppressor configuration, there is no significant benefit at high frequencies compared to the convergent circular nozzle. By comparing the laser velocimeter measured axial mean and turbulent velocity profiles, it has been shown

in Reference 22 that the supersonic exhaust from the suppressor flow elements decay rapidly to a subsonic flow in all regions downstream of the plug. This is in contrast to the convergent circular nozzle which maintains a supersonic flow up to a distance ten times the diameter of the nozzle. The enhanced mixing rate achieved by the increased total surface area of the mechanical suppressor jet leads to the observed rapid decay of the plume, and hence the reduction in the sound pressure levels at low and middle frequency ranges. The high frequency noises are from sources in the supersonic flow located on the plug and near the nozzle exit.

The perceived noise level directivity and selected spectra obtained under static tests for the typical takeoff, cutback, and approach conditions are presented in Figure 65. The spectral data indicate the significant high frequency noise that is associated with the suppressor configuration. The spectra of the 32-chute suppressor (TAS-6) of the single flow thermal acoustic shield study (Reference 12) were observed also to have a pronounced high frequency content.

4.2.2 Effect of Shield-to-Outer-Stream Velocity Ratio with Partial Thermal Acoustic Shield

As described in Section 3.1.2, the suppressed baseline coannular plug nozzle (TAS-15) was tested with the 0.97 in. thick, 180° thermal acoustic shield using three different sets of choke plates that were selected to give, over a typical engine operating line, a range of shield-to-outer stream velocity ratios of 0.56 to 0.69 for TAS-16, 0.75 to 0.86 for TAS-17, and 0.37 to 0.53 for TAS-18. At a typical takeoff condition, the shield-to-outer steam velocity ratios for TAS-16, -17, and -18 were 0.64, 0.83, and 0.48, respectively. For convenience, these values of $V_r^{s,o}$ at takeoff will be identified as the shield-to-outer stream velocity ratios of these three configurations. The objective of this test series, conducted as in the matrices presented in Tables IX through XI, was to investigate the influence of shield-to-outer stream velocity ratio, $V_r^{s,o}$, on the noise characteristics of the suppressed coannular plug nozzle operating with a given set of inner and outer stream conditions. As indicated in Section 3.1.2, the inner and outer stream conditions were chosen such that the inner-to-outer stream velocity ratio $V_r^{i,o}$ was approximately 0.6 over the entire test range. The acoustic data measured with the shield in the community orientation to the microphones are employed in this study.

The normalized perceived noise level data of TAS-16 through 18, at aft quadrant angles of θ_i = 120° and 130°, are summarized in Figure 66. The data are plotted as a function of the mixed jet velocity parameter. The shielded suppressor data are compared in this figure with the corresponding acoustic data of the suppressed baseline coannular plug nozzle (TAS-15). An examination of the data indicates that at the peak angle of θ_i = 120°, PNL is reduced 5 dB below the suppressed baseline coannular plug nozzle with the

SYMBOL	CONFIG.	TEST POINT	V_{ac}	INNER STREAM P_r^i	INNER STREAM T_T^i	INNER STREAM V^i	OUTER STREAM P_r^o	OUTER STREAM T_T^o	OUTER STREAM V^o	MIXED CONDITIONS P_r^{mix}	MIXED CONDITIONS T_T^{mix}	MIXED CONDITIONS V^{mix}	$V_r^{i,o}$	$V_r^{s,o}$	NF_θ dB
○	TAS-15	1501	0	1.58	827	1102	1.93	1203	1574	1.86	1141	1496	.70	0	-4.7
□	TAS-15	1505	0	1.89	817	1277	2.33	1468	1954	2.24	1349	1830	.65	0	-5.4
◇	TAS-15	1509	0	2.33	899	1522	3.03	1642	2328	2.88	1512	2187	.65	0	-6.8

(T_T-°R; V- fps)

DATA SCALED TO TOTAL NOZZLE AREA OF 0.903 m^2 (1400 in^2) AND EXTRAPOLATED TO 731.5 m (2400 ft.) SIDELINE.

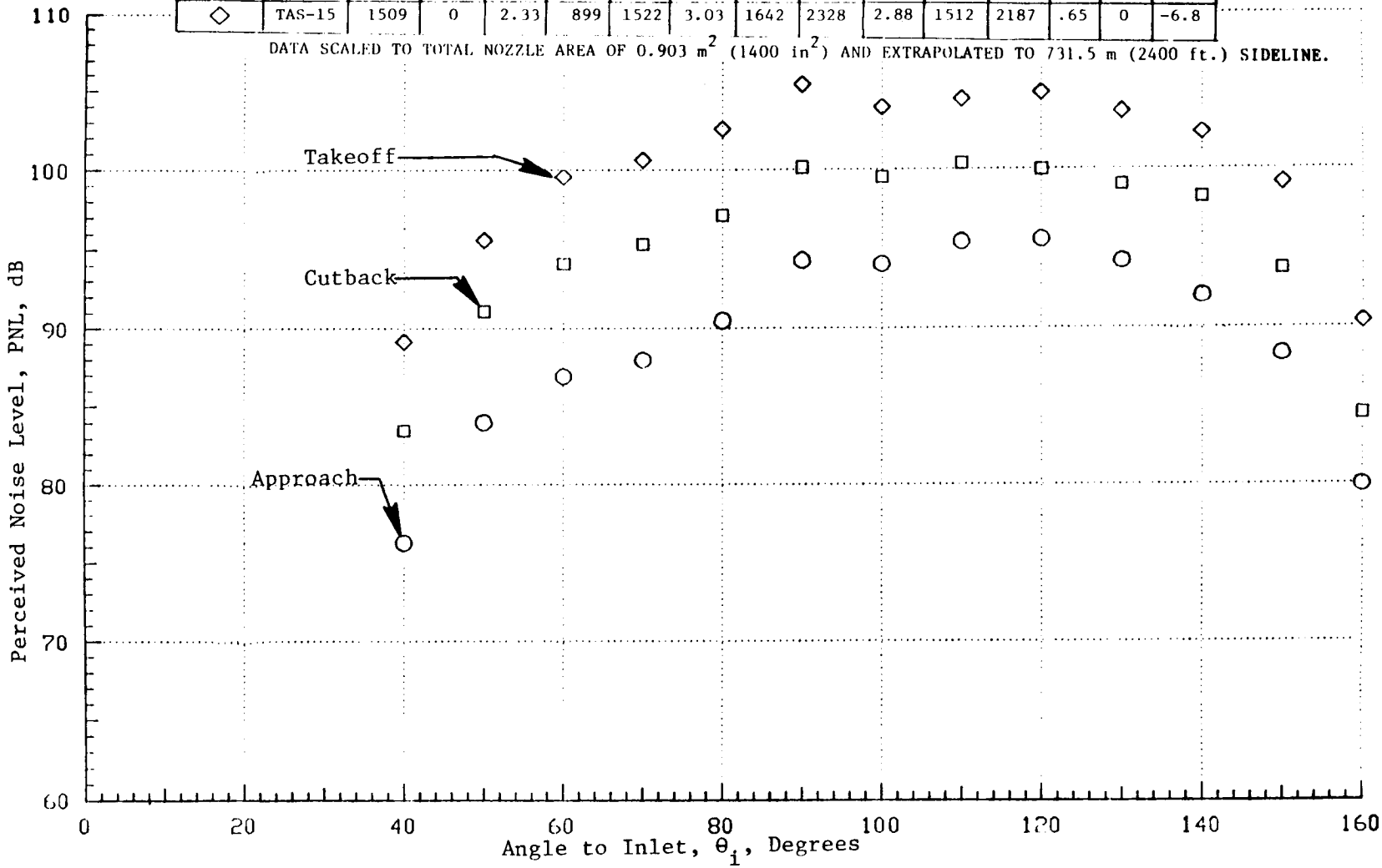

a) Perceived Noise Level

Figure 65. Perceived Noise Level Directivity and Selected Spectra of Suppressed Baseline Coannular Plug Nozzle at Typical Takeoff, Cutback, and Approach Conditions.

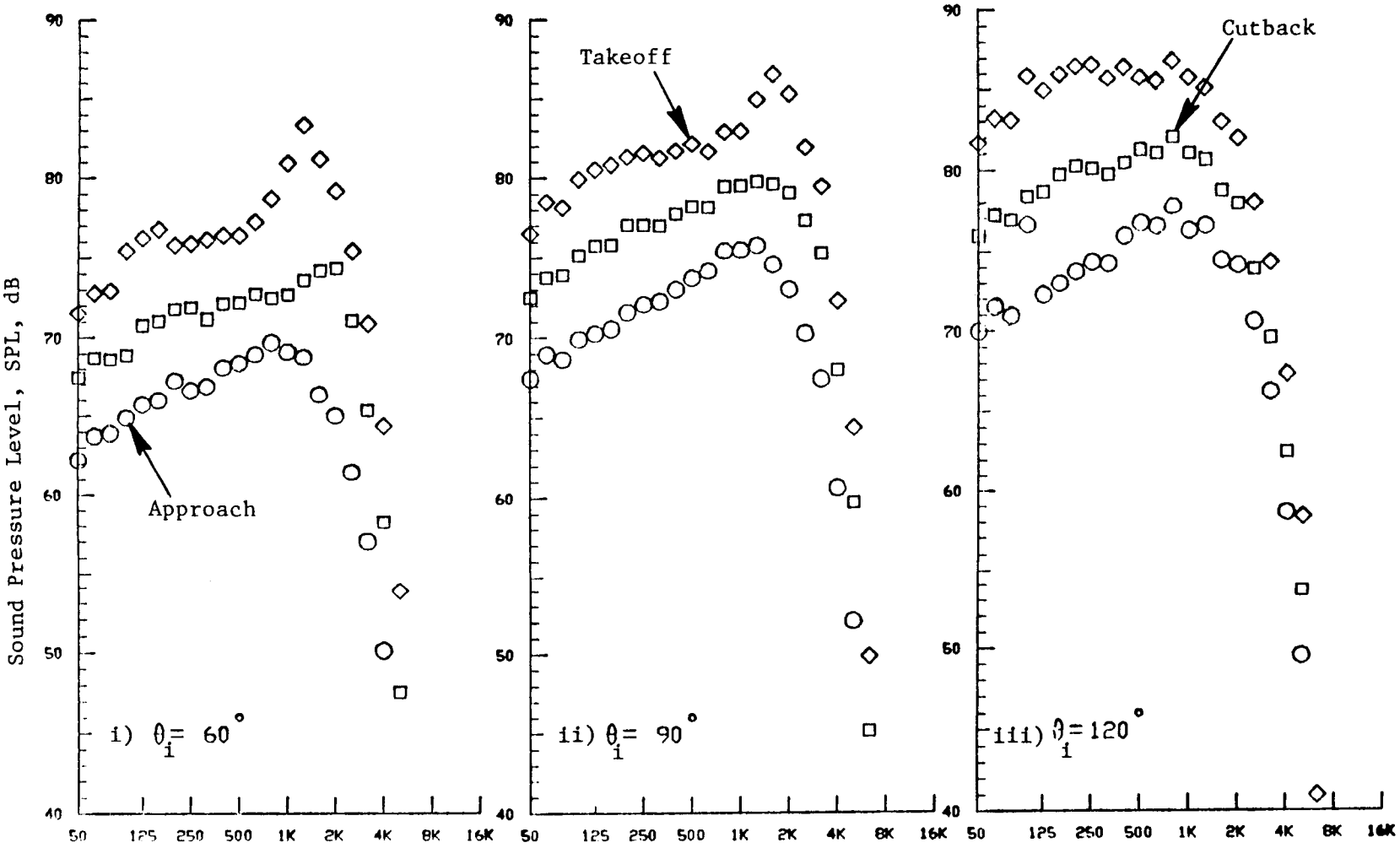

b) Spectra at θ_i= 60°, 90°, 120°

Figure 65. Perceived Noise Level Directivity and Selected Spectra of Suppressed Baseline Coannular Plug Nozzle at Typical Takeoff, Cutback, and Approach Conditions. (Concluded)

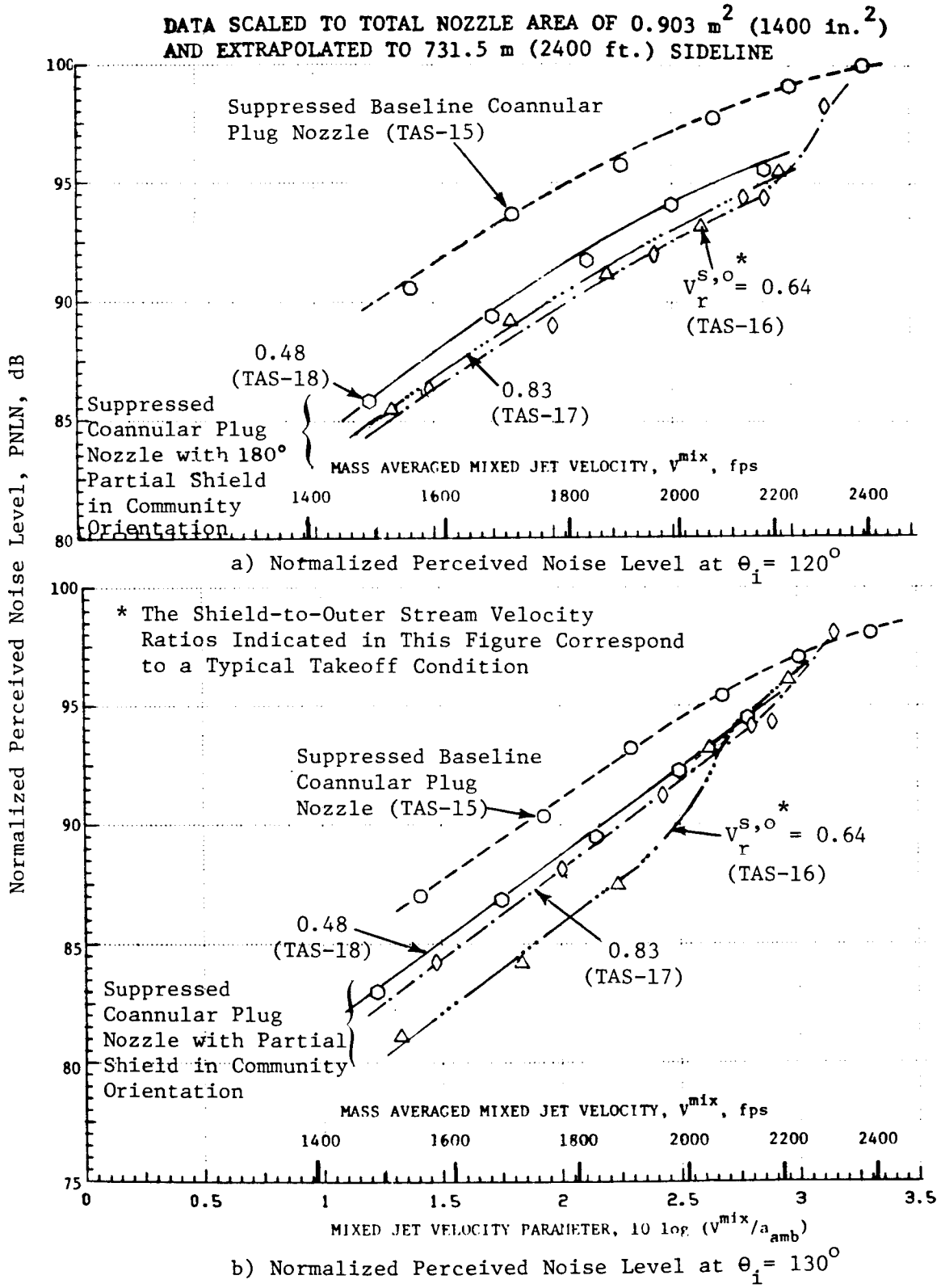

Figure 66. Effect of Shield-to-Outer Stream Velocity Ratio on the Aft-Quadrant Simulated Flight Perceived Noise Level.

TAS-16 ($V_r^{s,o}$ = 0.64) and TAS-18 ($V_r^{s,o}$ = 0.83), and 3.5 dB below the TAS-17 ($V_r^{s,o}$ = 0.48) over the engine operating cycle. However, the corresponding data at θ_i = 130° indicate the significant acoustic benefit obtained with $V_r^{s,o}$ = 0.64 (TAS-16) compared to those obtained with TAS-17 and TAS-18, except at mixed velocities greater than 2,100 fps.

The PNL directivities and selected front- and aft-quadrant spectral data obtained with the three partial shielded configurations of this study (TAS-16 through -18), under both static and simulated flight conditions, are presented next in this subsection in order to demonstrate the influence of the various thermal acoustic shields. The data, at typical takeoff and cutback conditions, are compared with the corresponding data of the suppressed baseline coannular nozzle TAS-15.

Figure 67 compares the simulated flight PNL-directivities of TAS-16, -17, and -18 with those of TAS-15 at a typical takeoff condition. The data indicate, in general, the acoustic benefit of the shields at all observer angles. At the peak noise angle of θ_i = 120°, a maximum PNL reduction of 8.8 dB is obtained with TAS-16 ($V_r^{s,o}$ = 0.64). The corresponding PNL reduction, with TAS-16 at θ_i = 90° and 60°, is observed to be 5.5 dB. In addition, the influence of $V_r^{s,o}$ on the measured PNL data is minimal at all angles up to 120°. Beyond this angle, only the shielded configurations with $V_r^{s,o}$ = 0.48 and 0.64 yield significant acoustic benefit relative to the suppressed baseline coannular plug nozzle.

Spectral characteristics corresponding to the simulated flight takeoff condition of Figure 67 are presented in Figures 68 and 69. While only the data at θ_i = 90° and 120° are presented in Figure 68, a set of data at three front and three aft quadrant angles is presented in Figure 69. An examination of the spectral data at θ_i = 90° indicates that, for all values of f > 400 Hz, sound pressure levels are significantly reduced for the shielded configurations relative to the suppressed baseline coannular nozzle. A maximum SPL reduction of 9 dB is noted at f = 1,600 Hz with the TAS-16 configuration ($V_r^{s,o}$ = 0.64). As noted in the earlier single-flow study of this investigation (Reference 12), this SPL reduction at θ_i = 90° and at the higher frequencies is attributed to the alteration in source strength and distribution near the suppressor exit by the shield flow. The spectral characteristics of the shielded and unshielded suppressor coannular configurations at other forward quadrant angles (refer to Figure 69) are noted to be similar to those at θ_i = 90°.

An examination of the spectral characteristics at the aft-angle of θ_i = 120° (see Figure 68) reveals that the shielded configurations suppress the noise of the baseline nozzle significantly at the prominent middle frequencies and at high frequencies. Out of the three partial configurations tested during this study, TAS-16 with $V_r^{s,o}$ = 0.64 is observed to have the lowest measured sound pressure levels at all frequencies greater than 315 Hz. A maximum SPL reduction of 13 dB is noted at f = 1600 Hz. At the baseline nozzle peak frequency of f = 1,000 Hz, a SPL reduction of 8.5 is indicated. For

				INNER STREAM			OUTER STREAM			SHIELD STREAM			MIXED CONDITIONS					
SYMBOL	CONFIG.	TEST POINT	V_{ac}	P_r^i	T_T^i	V^i	P_r^o	T_T^o	V^o	P_r^s	T_T^s	V^s	P_r^{mix}	T_T^{mix}	V^{mix}	$V_r^{i,o}$	$V_r^{s,o}$	NF, dB
○	TAS-15	1510	400	2.32	910	1530	3.09	1640	2340	-	-	-	2.93	1520	2205	0.65	0.00	-6.8
△	TAS-16	1640	↓	2.31	900	1520	3.07	1670	2360	1.56	1630	1540	2.36	1550	2030	0.64	0.65	-5.1
◇	TAS-17	1710		2.30	910	1520	3.06	1660	2350	2.13	1620	1950	2.59	1560	2120	0.65	0.83	-5.8
⬡	TAS-18	1810		2.30	860	1480	3.06	1680	2360	1.27	1620	1140	2.27	1550	1985	0.63	0.48	-4.8

(T_T-°R; V- fps)

DATA SCALED TO TOTAL NOZZLE AREA OF 0.903 m^2 (1400 in^2) AND EXTRAPOLATED TO 731.5 m (2400 ft.) SIDELINE.

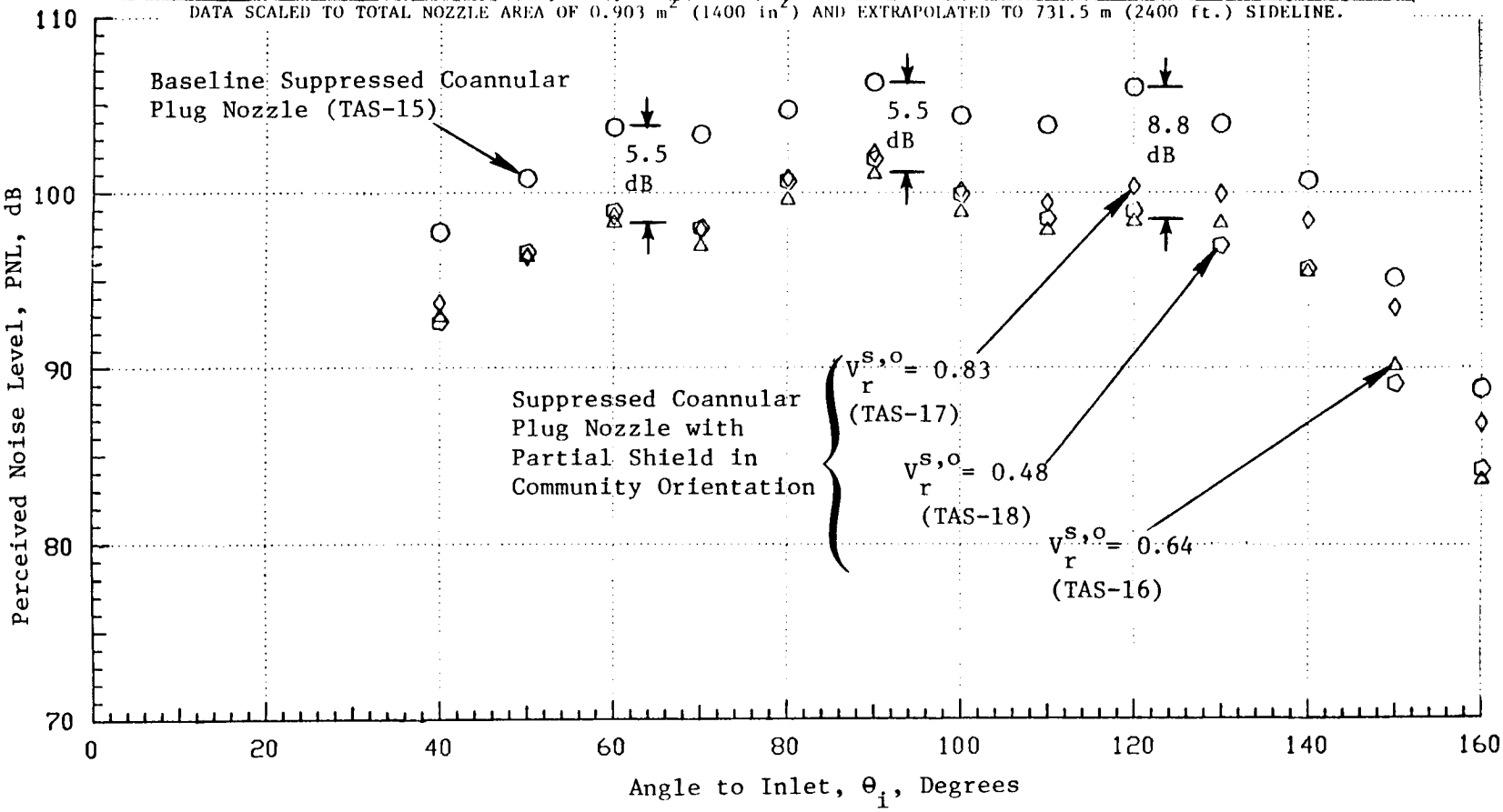

Figure 67. Effect of Shield-to-Outer Stream Velocity Ratio on the PNL-Directivity of the Suppressed Coannular Plug Nozzle with Partial Shield at Takeoff Condition (Simulated Flight).

(Refer to Figure 67 for aerodynamic flow conditions.)

DATA SCALED TO TOTAL NOZZLE AREA OF 0.903 m^2 (1400 $in.^2$)
AND EXTRAPOLATED TO 731.5 m (2400 ft.) SIDELINE

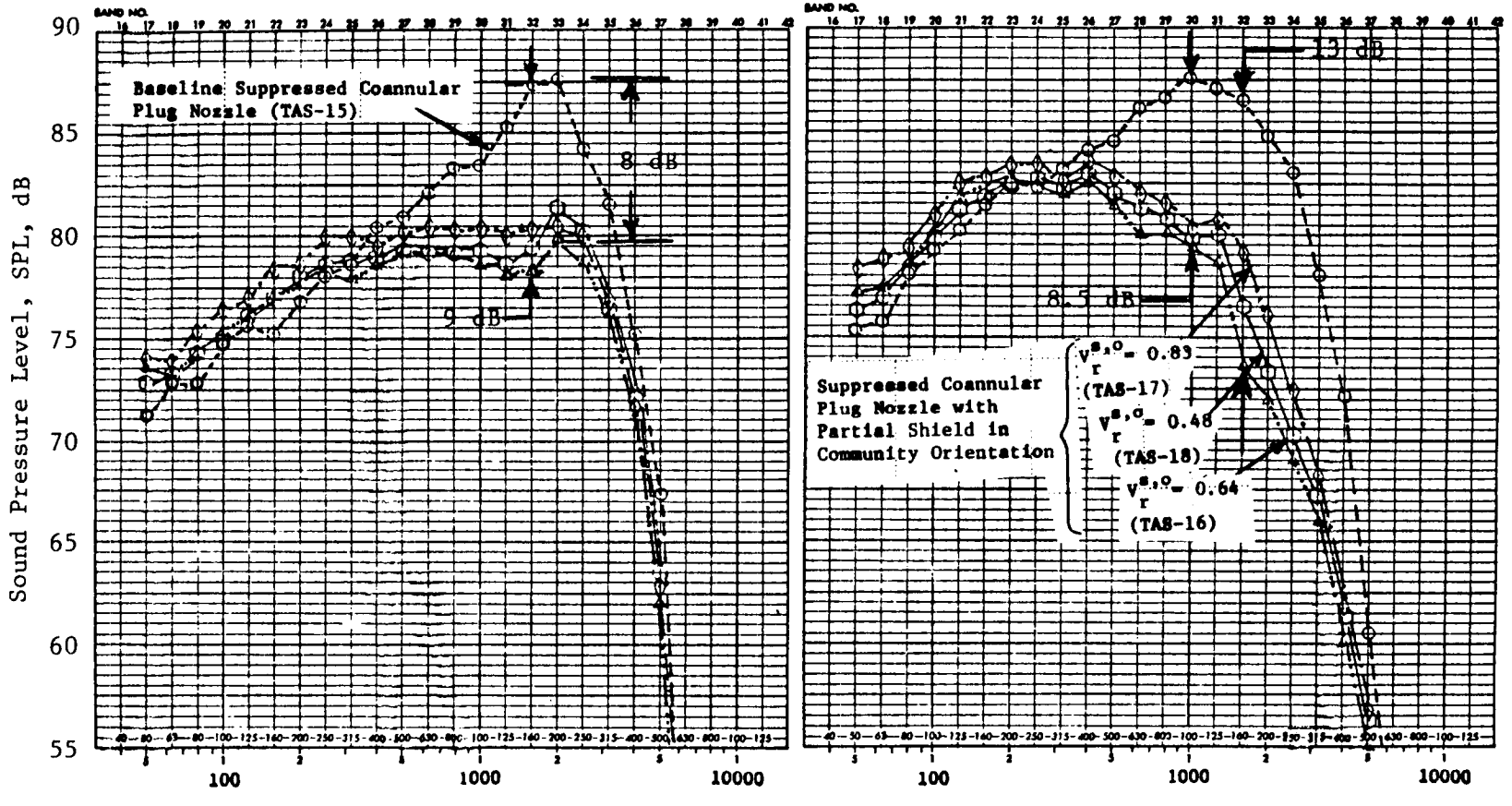

a) Directivity Angle θ_i = 90°

b) Directivity Angle θ_i = 120°

Figure 68. Effect of Shield-to-Outer Stream Velocity Ratio on Typical Spectra of the Suppressed Coannular Plug Nozzle with Partial Shield at Takeoff Condition (Simulated Flight).

(Refer to Figure 67 for aerodynamic conditions.)

Data scaled to total nozzle area of 0.903 m^2 (1,400 in^2) and extrapolated to 731.5 m (2,400 ft.) sideline.

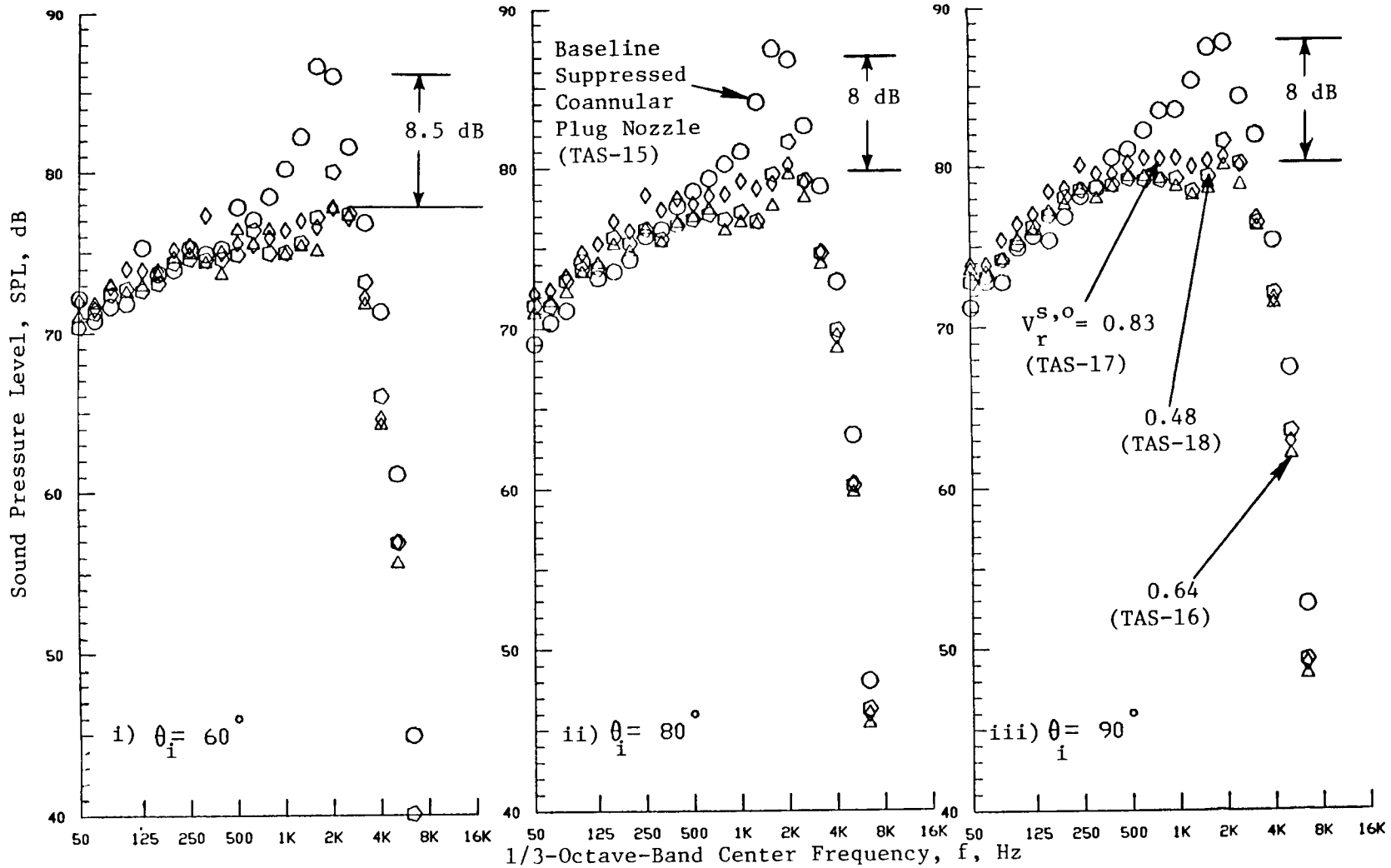

a) Front-Quadrant

Figure 69. Effect of Shield-to-Outer Stream Velocity Ratios on Selected Front and Aft Quadrant Spectra of the Suppressed Coannular Plug Nozzle with Partial Shield at Takeoff Condition (Simulated Flight).

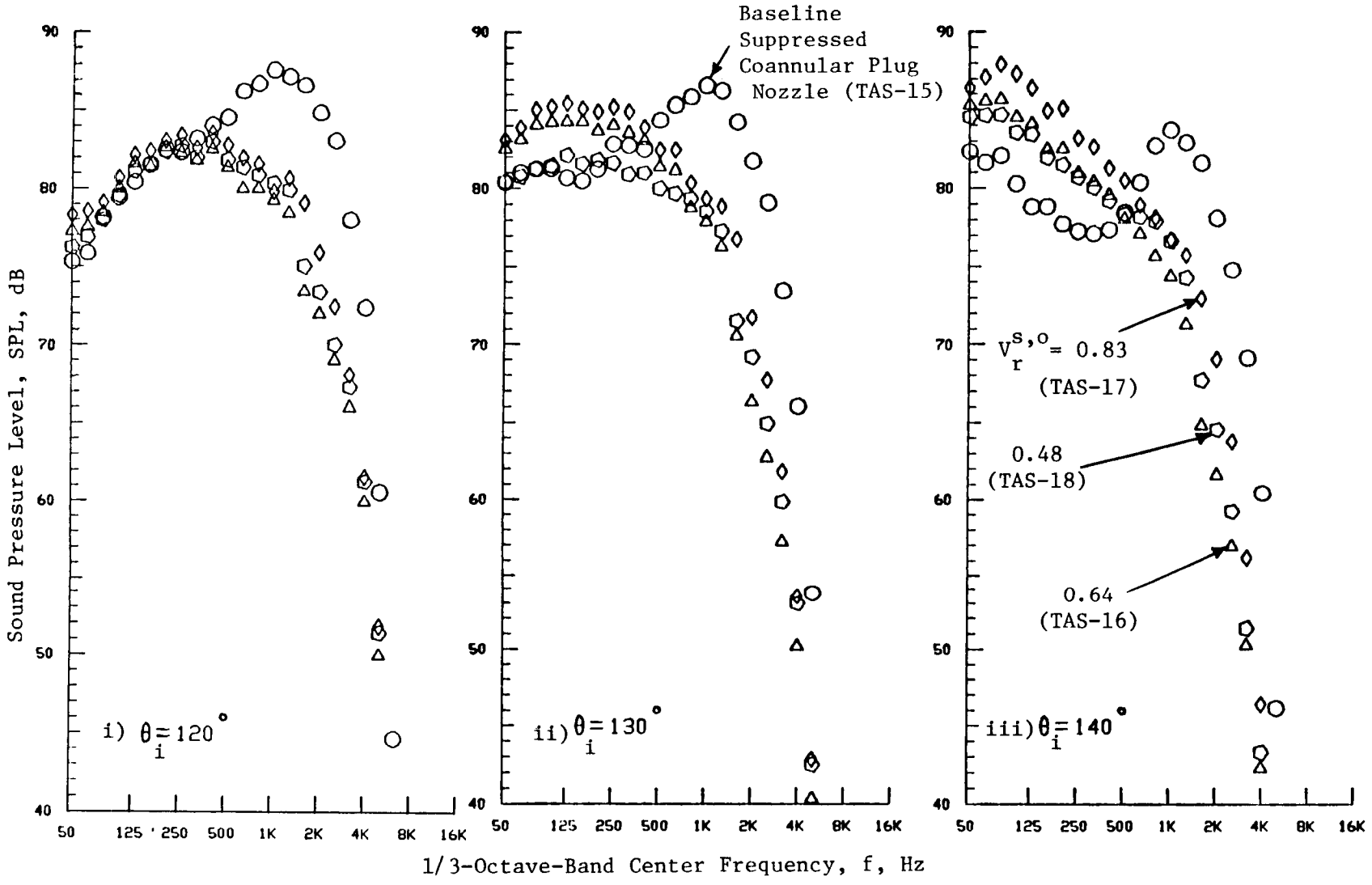

b) Aft-Quadrant

Figure 69. Effect of Shield-to-Outer Stream Velocity Ratios on Selected Front and Aft Quadrant Spectra of the Suppressed Coannular Plug Nozzle with Partial Shield at Takeoff Condition (Simulated Flight). (Concluded)

frequencies less than 315 Hz, the sound pressure levels of the shielded configurations are observed to be higher than those of the unshielded baseline nozzle, and are observed also to increase with $V_r^{s,o}$. At all angles $\leq 120°$, this increase in sound pressure levels at low frequencies and with the shielded configurations is found to be limited to 2 dB relative to the unshielded baseline suppressed nozzle. However, at microphone locations of $\theta_i \geq 130°$, this increase in SPL at low frequencies is significant, and reaches 8 dB at θ_i = 140°. The increase in low frequency SPL associated with the shielded configurations more than offsets the decrease in high frequency SPL in the PNL calculation. This decreases the PNL benefit due to shielded nozzles at these shallow angles. This observation is clearly noted in the PNL directivity plot of TAS-17 nozzle operating with $V_r^{s,o}$ = 0.83 (see Figure 67).

Acoustic data measured during static tests with the nozzle flow conditions at the typical takeoff and corresponding to the simulated flight data of Figures 67 through 69, are presented in Figures 70 through 72. An examination of the PNL directivity data of Figure 70 with the TAS-16 configuration operating with $V_r^{s,o}$ = 0.64 shows that at the peak noise angle of θ_i = 120°, a maximum PNL reduction of 4.2 dB is obtained. The corresponding PNL reductions with TAS-16 at θ_i = 90° and 60° are observed to be 4.5 dB and 5 dB, respectively. However, at high shallow angles in the aft quadrant, the perceived noise levels of the shielded configurations are equal to or greater than those of the baseline suppressed coannular plug nozzle.

An examination of the static spectral data of Figure 71 indicates that at θ_i = 90°, reductions in sound pressure levels due to the source alteration near the suppressor exit are measured with the shielded configurations for all values of $f > 315$ Hz. Also, a maximum SPL reduction of 8 dB is noted at the baseline nozzle peak noise frequency of f = 1600 Hz. In addition, as with the simulated flight data, varying the values of $V_r^{s,o}$ has minimal influence on the front quadrant spectra and perceived noise levels of the three shielded nozzles. An examination of the static aft-quadrant spectral data shows that the TAS-16 configuration with $V_r^{s,o}$ = 0.64 has the lowest measured sound pressure levels at high frequencies.

PNL-directivity and selected spectral data of TAS-16 through TAS-18, obtained during the static and simulated flight tests at the cutback cycle conditions, are presented in Figures 73 through 76. Examination of these figures showed general trends in acoustic data similar to those at takeoff. Also, the data indicate that at aft-angles of $\theta_i \geq 130°$, TAS-16 has the lowest measured sound pressure levels at high frequencies.

4.2.3 Influence of Partial Thermal Acoustic Shield Orientation

The acoustic data of the suppressed coannular plug nozzle with the 180° shield in community orientation are compared in this section to data obtained

SYMBOL	CONFIG.	TEST POINT	V_{ac}	INNER STREAM P_r^i	INNER STREAM T_T^i	INNER STREAM V^i	OUTER STREAM P_r^o	OUTER STREAM T_T^o	OUTER STREAM V^o	SHIELD STREAM P_r^s	SHIELD STREAM T_T^s	SHIELD STREAM V^s	MIXED CONDITIONS P_r^{mix}	MIXED CONDITIONS T_T^{mix}	MIXED CONDITIONS V^{mix}	$V_r^{i,o}$	$V_r^{s,o}$	NF, dB
○	TAS-15	1509	0	2.33	900	1520	3.03	1640	2340	-	-	-	2.88	1510	2190	0.65	-	-6.8
△	TAS-16	1639	↓	2.29	900	1510	3.04	1650	2340	1.53	1630	1500	2.34	1550	2010	0.65	0.64	-5.0
◇	TAS-17	1709	↓	2.29	900	1510	3.06	1670	2360	2.07	1650	1940	2.56	1575	2120	0.64	0.82	-5.7
⬡	TAS-18	1809	↓	2.27	880	1490	3.02	1660	2340	1.26	1635	1115	2.26	1550	1970	0.64	0.48	-4.8

(T_T-°R; V- fps)

DATA SCALED TO TOTAL NOZZLE AREA OF 0.903 m^2 (1400 in^2) AND EXTRAPOLATED TO 731.5 m (2400 ft.) SIDELINE.

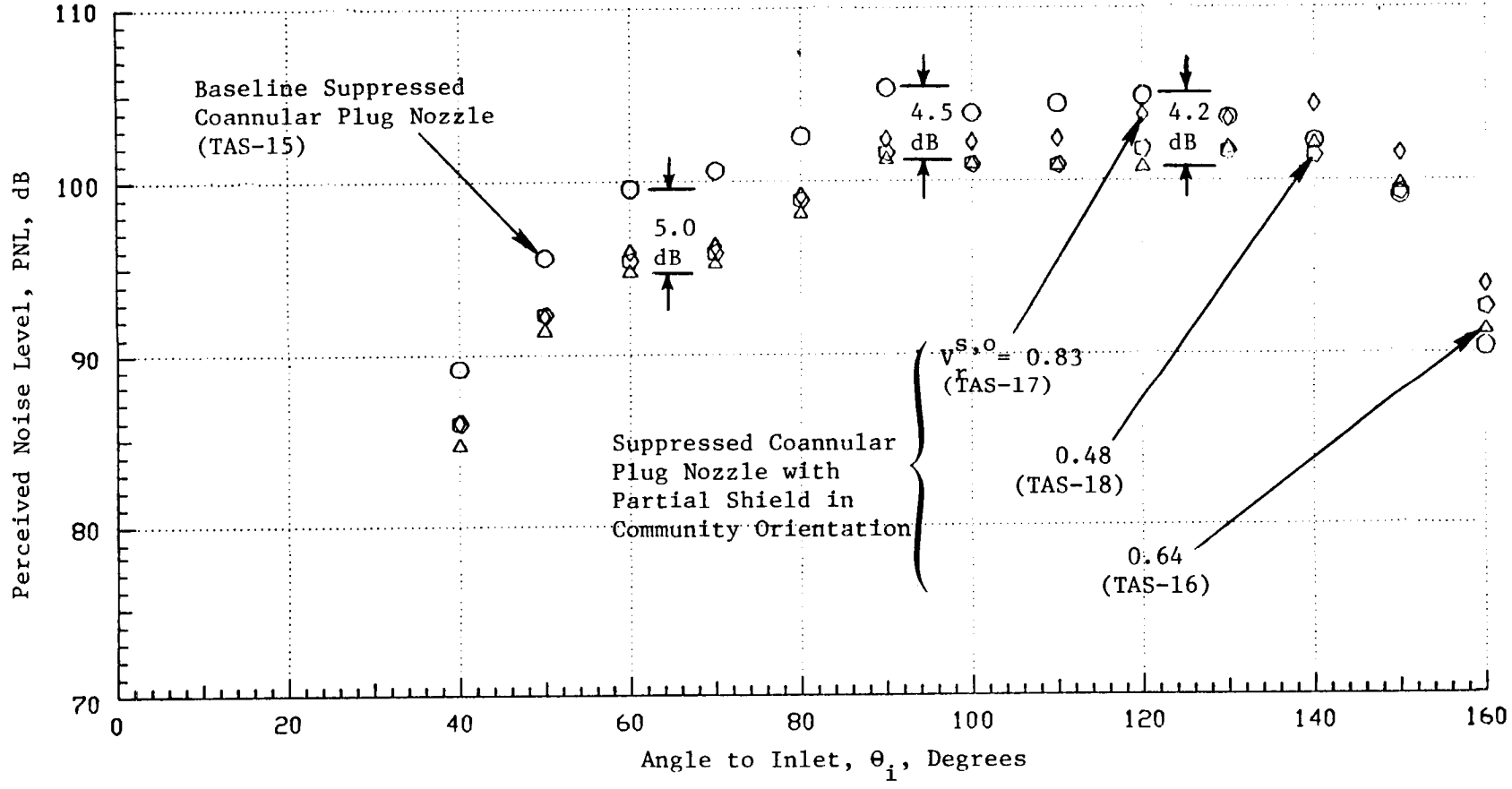

Figure 70. Effect of Shield-to-Outer Stream Velocity Ratio on the PNL-Directivity of the Suppressed Coannular Plug Nozzle with Partial Shield at Takeoff Condition (Static).

(Refer to Figure 70 for aerodynamic conditions.)

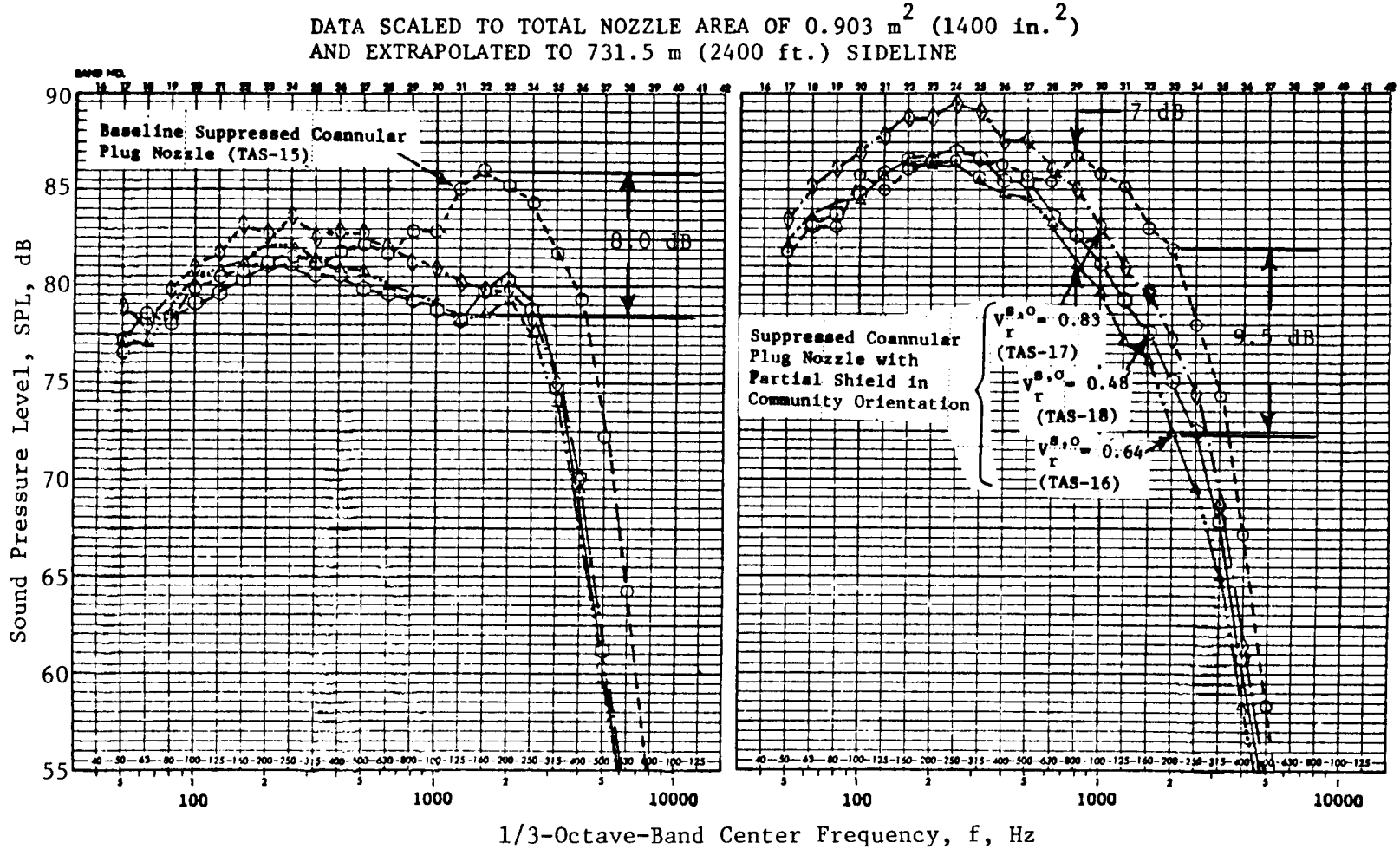

a) Directivity Angle θ_i = 90°

b) Directivity Angle θ_i = 120°

Figure 71. Effect of Shield-to-Outer Stream Velocity Ratio on Typical Spectra of the Suppressed Coannular Plug Nozzle with Partial Shield in Community Orientation at Takeoff Condition (Static).

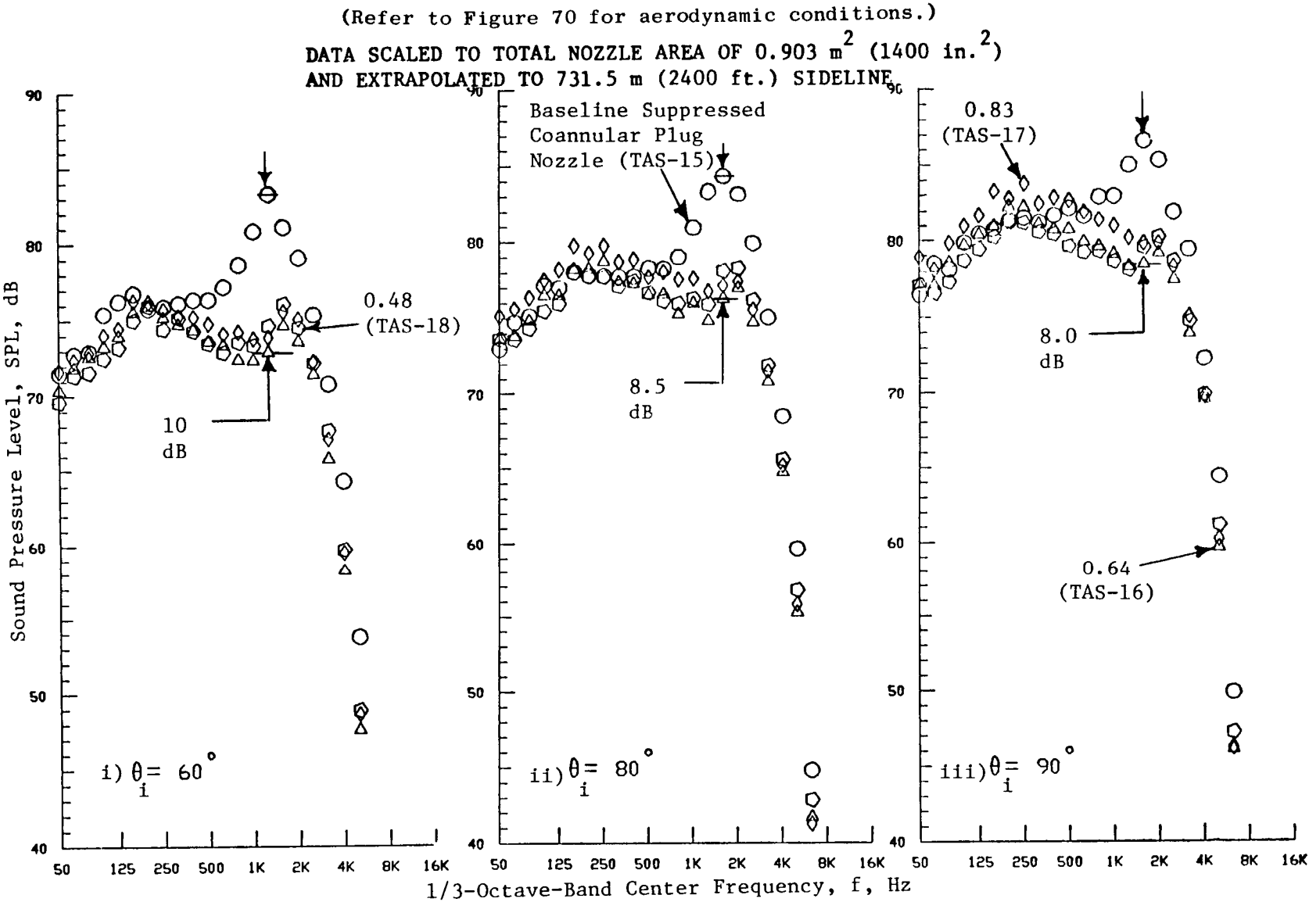

a) Front-Quadrant

Figure 72. Effect of Shield-to-Outer Stream Velocity Ratio on Selected Front and Aft Quadrant Spectra of the Suppressed Coannular Plug Nozzles with Partial Shield at Takeoff Condition (Static).

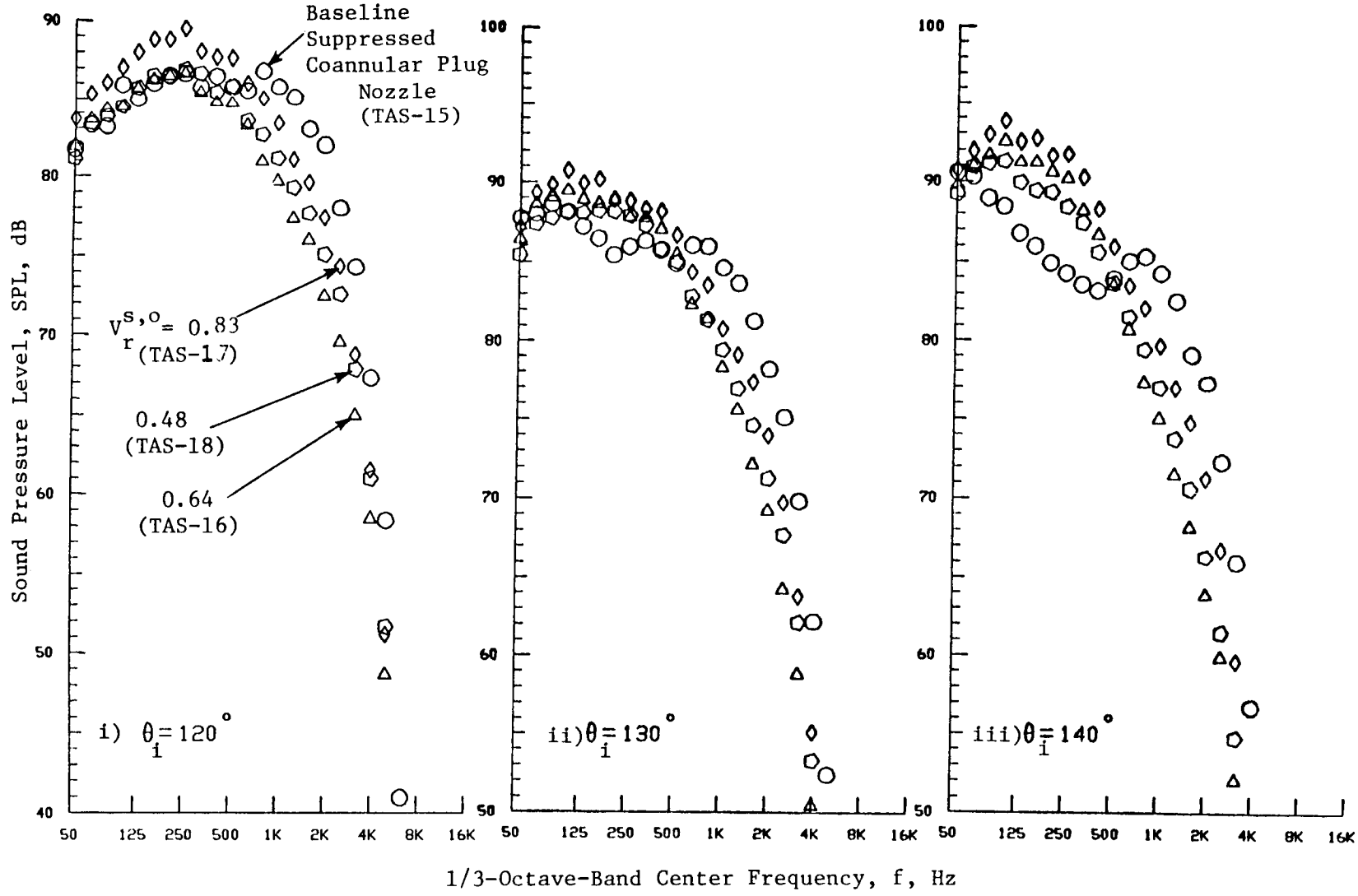

b) Aft-Quadrant

Figure 72. Effect of Shield-to-Outer Stream Velocity Ratio on Selected Front and Aft Quadrant Spectra of the Suppressed Coannular Plug Nozzles with Partial Shield at Takeoff Condition (Static). (Concluded)

SYMBOL	CONFIG.	TEST POINT	V_{ac}	INNER STREAM P_r^i	INNER STREAM T_T^i	INNER STREAM V^i	OUTER STREAM P_r^o	OUTER STREAM T_T^o	OUTER STREAM V^o	SHIELD STREAM P_r^s	SHIELD STREAM T_T^s	SHIELD STREAM V^s	MIXED CONDITIONS P_r^{mix}	MIXED CONDITIONS T_T^{mix}	MIXED CONDITIONS V^{mix}	$V_r^{i,o}$	$V_r^{s,o}$	NF, dB
○	TAS-15	1505	0	1.89	815	1275	2.33	1470	1955	-	-	-	2.24	1350	1830	0.65	-	-5.4
△	TAS-16	1635	0	1.76	840	1225	2.38	1495	1990	1.32	1475	1170	1.89	1410	1675	0.61	0.59	-3.7
◇	TAS-17	1705	0	1.75	850	1225	2.40	1530	2025	1.66	1515	1570	2.01	1450	1780	0.61	0.77	-4.1
⬡	TAS-18	1805	0	1.75	820	1205	2.36	1490	1985	1.14	1475	815	1.85	1395	1650	0.61	0.41	-3.7

(T_T-°R; V- fps)

DATA SCALED TO TOTAL NOZZLE AREA OF 0.903 m^2 (1400 in^2) AND EXTRAPOLATED TO 731.5 m (2400 ft.) SIDELINE.

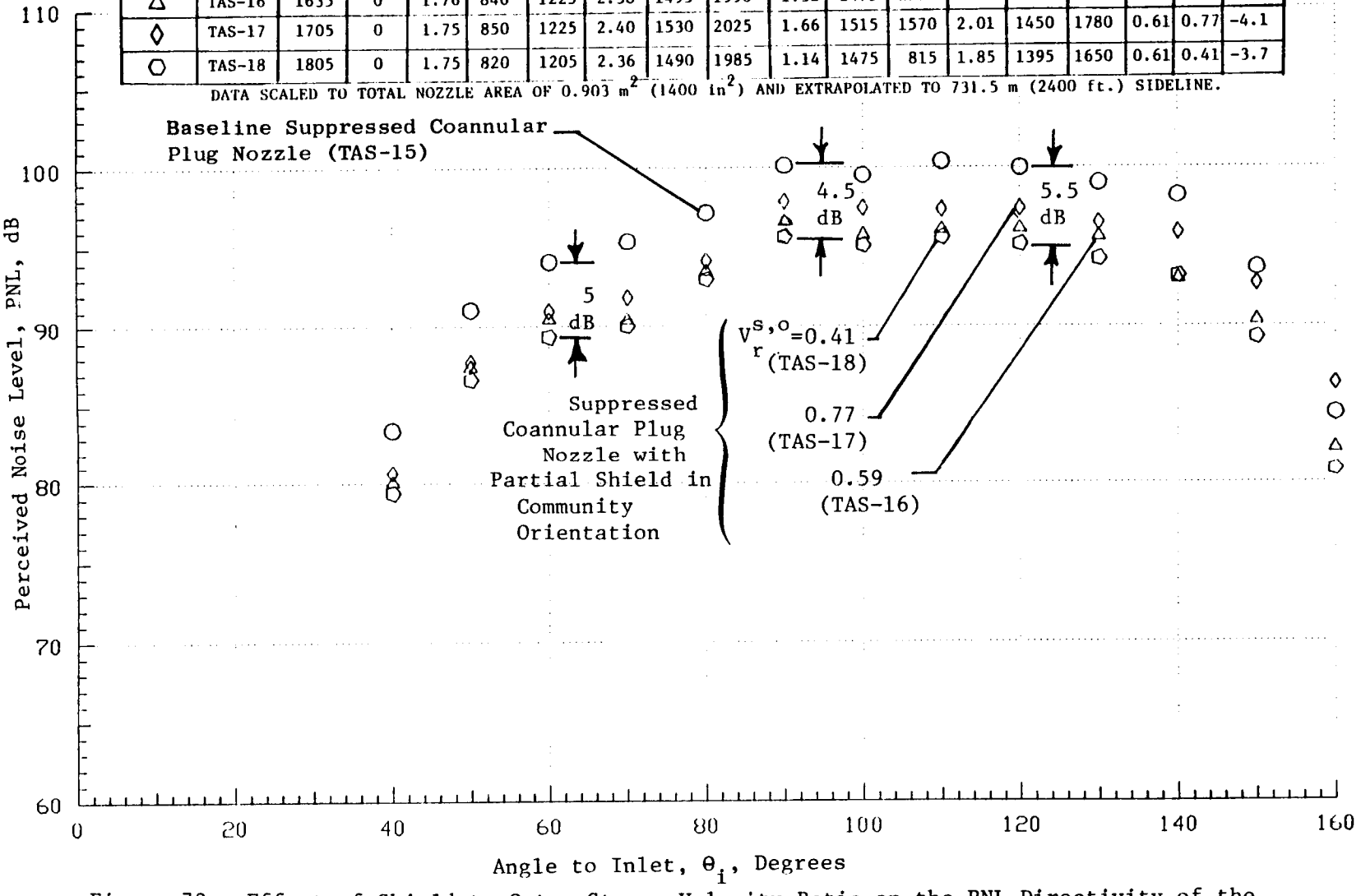

Figure 73. Effect of Shield-to-Outer Stream Velocity Ratio on the PNL-Directivity of the Suppressed Coannular Plug Nozzles with Partial Shield at Cutback Conditions (Static).

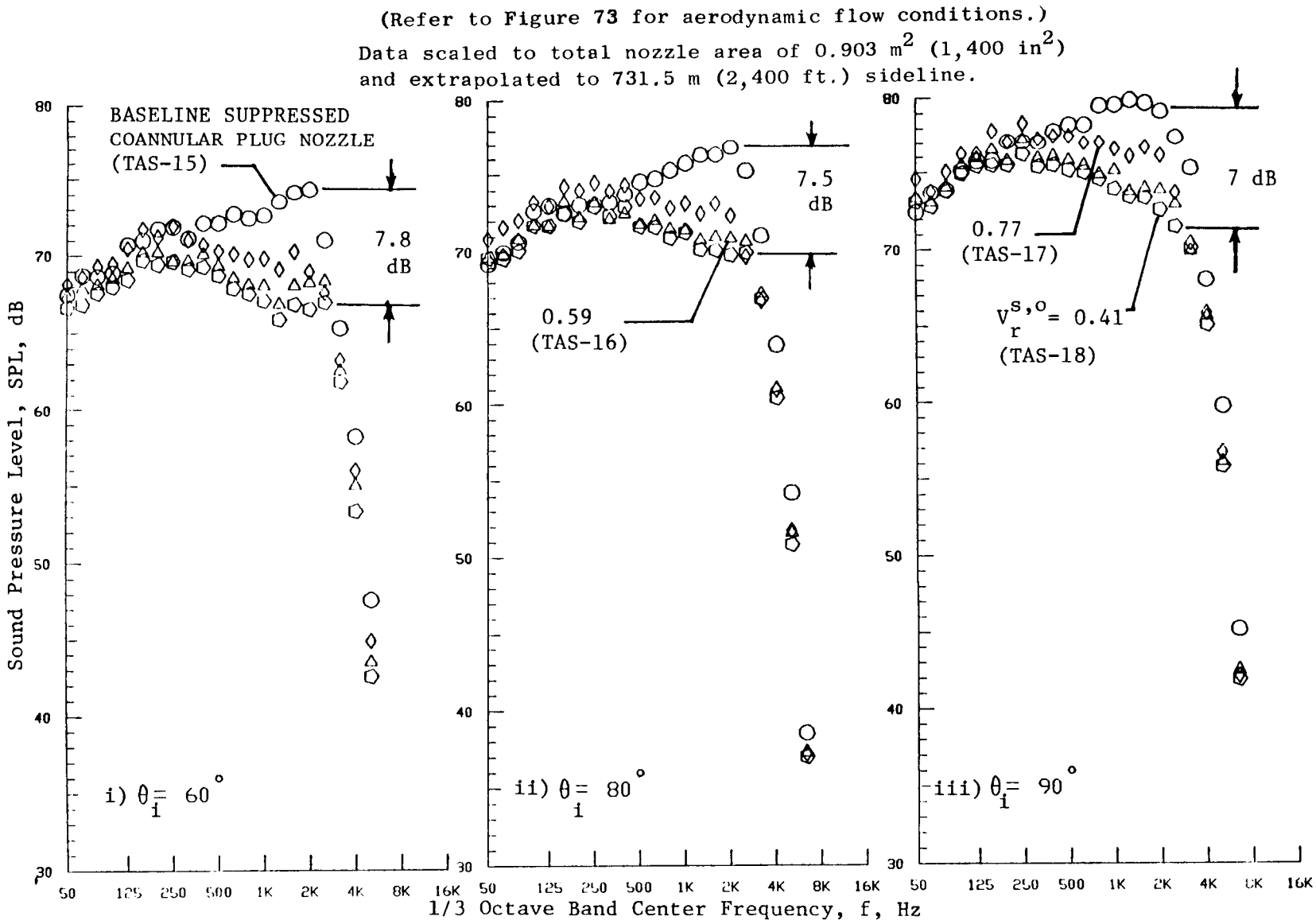

a) FRONT QUADRANT

Figure 74. Effect of Shield-to-Outer Stream Velocity Ratio on Selected Front and Aft Quadrant Spectra of the Suppressed Coannular Plug Nozzles with Partial Shield at Cutback Conditions (Static).

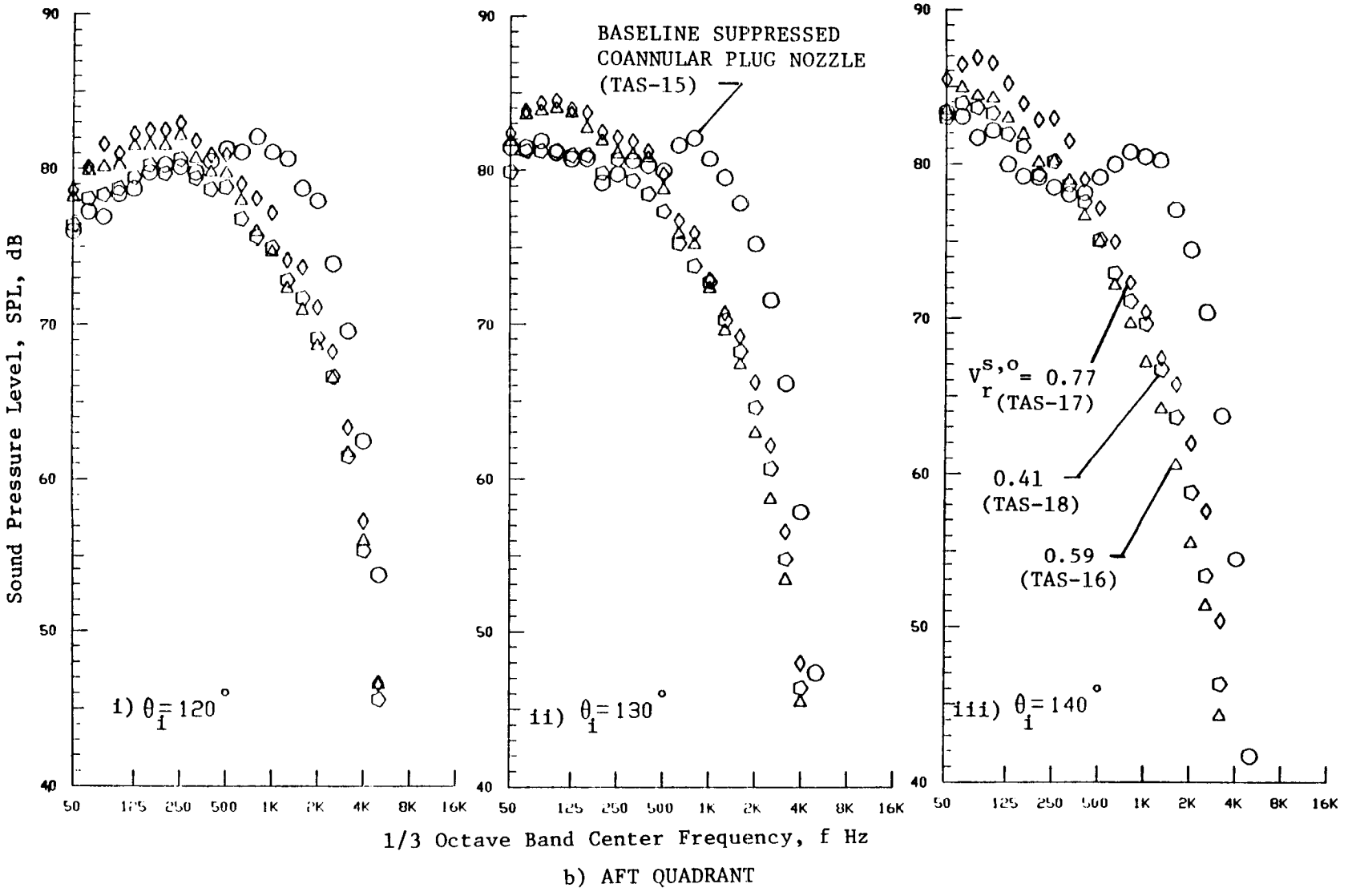

Figure 74. Effect of Shield-to-Outer Stream Velocity Ratio on Selected Front and Aft Quadrant Spectra of the Suppressed Coannular Plug Nozzles with Partial Shield at Cutback Conditions (Static). (Concluded)

SYMBOL	CONFIG.	TEST POINT	V_{ac}	INNER STREAM P_r^i	INNER STREAM T_T^i	INNER STREAM V^i	OUTER STREAM P_r^o	OUTER STREAM T_T^o	OUTER STREAM V^o	SHIELD STREAM P_r^s	SHIELD STREAM T_T^s	SHIELD STREAM V^s	MIXED CONDITIONS P_r^{mix}	MIXED CONDITIONS T_T^{mix}	MIXED CONDITIONS V^{mix}	$V_r^{i,o}$	$V_r^{s,o}$	NF, dB
○	TAS-15	1506	400	1.79	820	1225	2.43	1490	2010	-	-	-	2.30	1375	1875	0.61	-	-5.4
△	TAS-16	1636	400	1.76	840	1230	2.41	1515	2015	1.35	1470	1200	1.90	1420	1700	0.61	0.60	-3.7
◇	TAS-17	1706	400	1.76	840	1225	2.39	1485	1990	1.69	1450	1565	2.02	1400	1755	0.62	0.79	-4.3
○	TAS-18	1806	400	1.77	855	1245	2.40	1505	2010	1.16	1445	860	1.87	1410	1670	0.62	0.43	-3.6

(T_T-°R; V- fps)

DATA SCALED TO TOTAL NOZZLE AREA OF 0.903 m^2 (1400 in^2) AND EXTRAPOLATED TO 731.5 m (2400 ft.) SIDELINE.

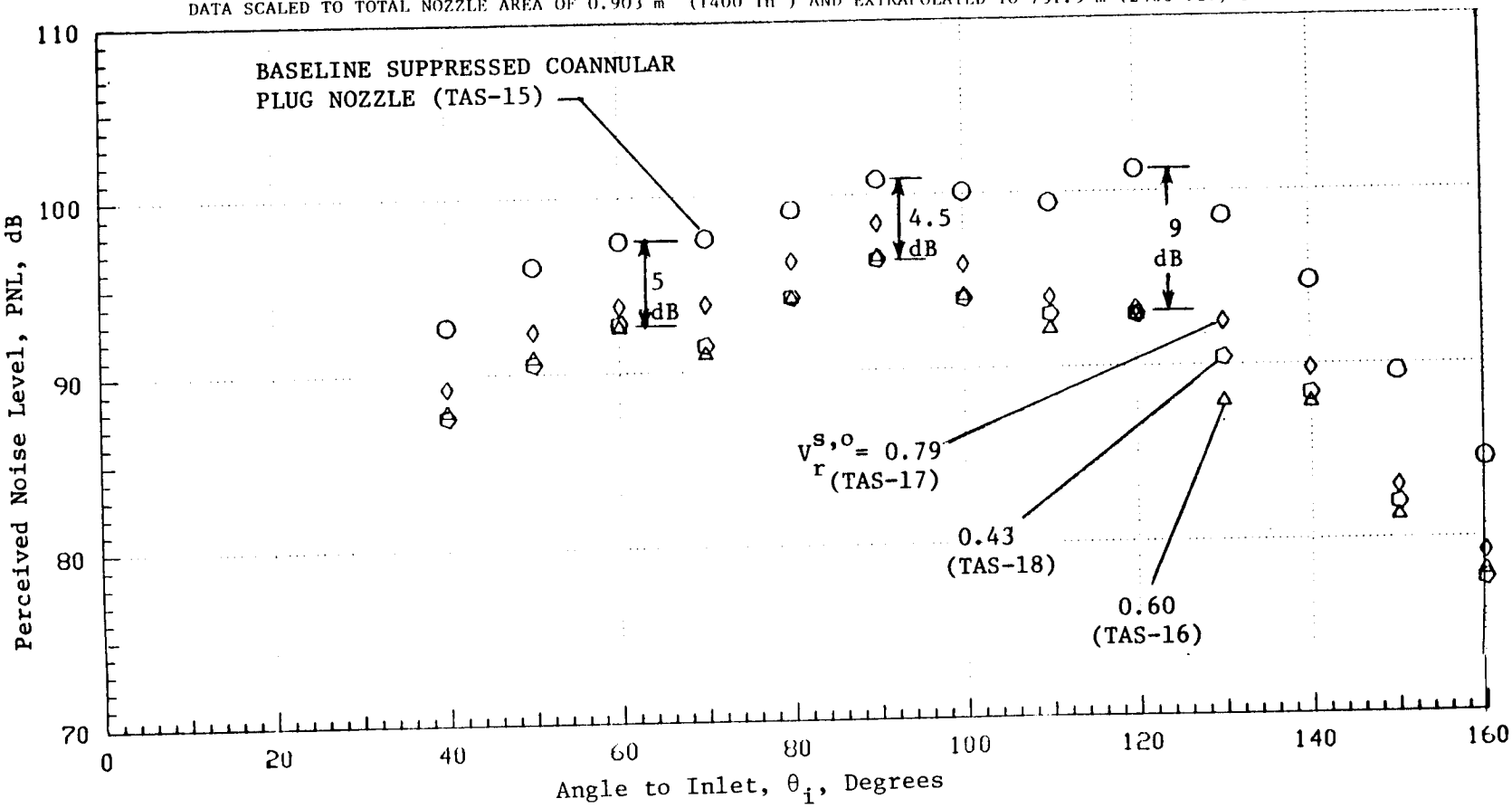

Figure 75. Effect of Shield-to-Outer Stream Velocity Ratio on the PNL-Directivity of the Suppressed Coannular Plug Nozzles with Partial Shield at Cutback Conditions (Simulated Flight).

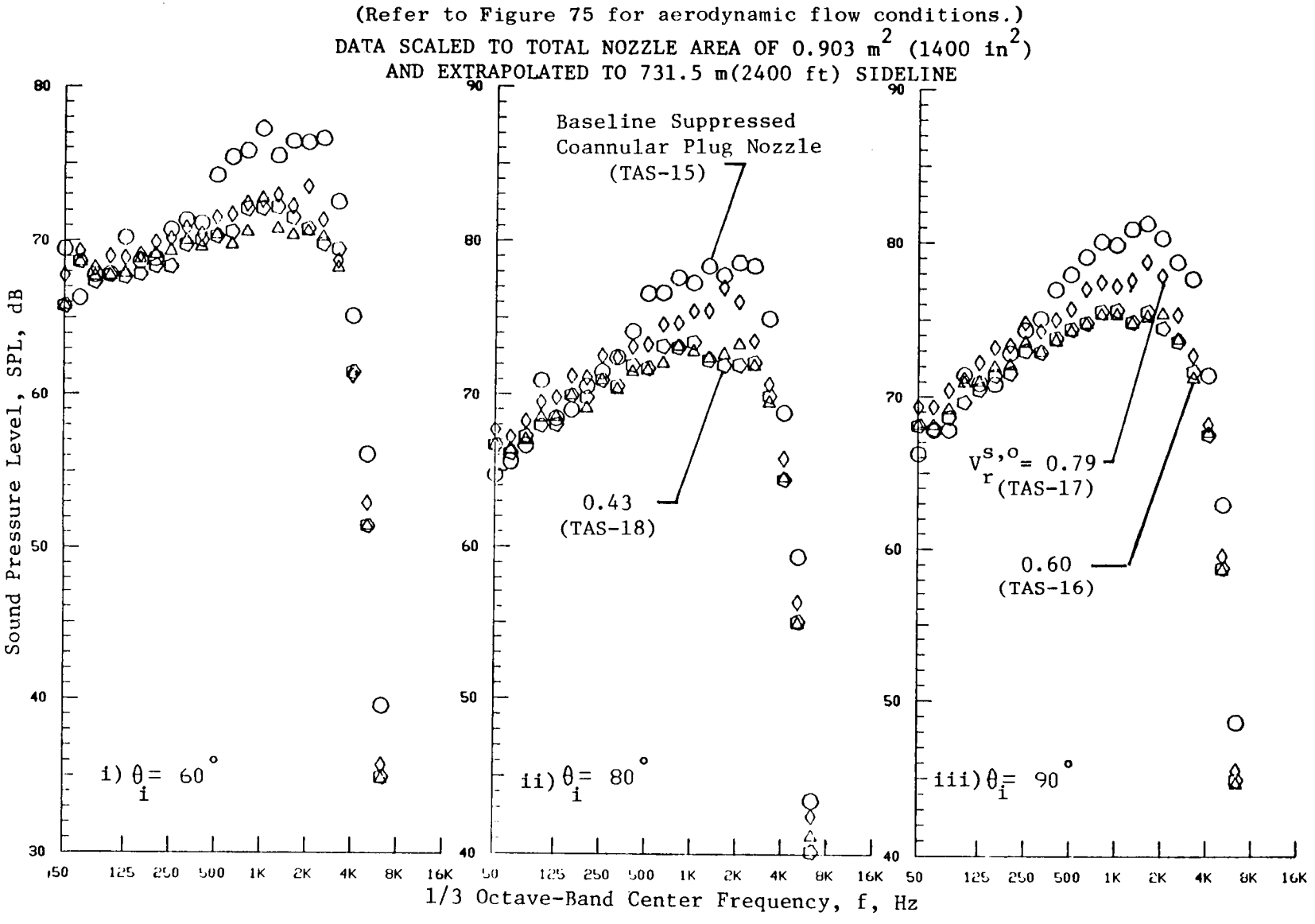

a) FRONT QUADRANT

Figure 76. Effect of Shield-to-Outer Stream Velocity Ratio on Selected Front and Aft Quadrant Spectra of the Suppressed Coannular Plug Nozzle with Partial Shield at Cutback Cycle Conditions (Simulated Flight).

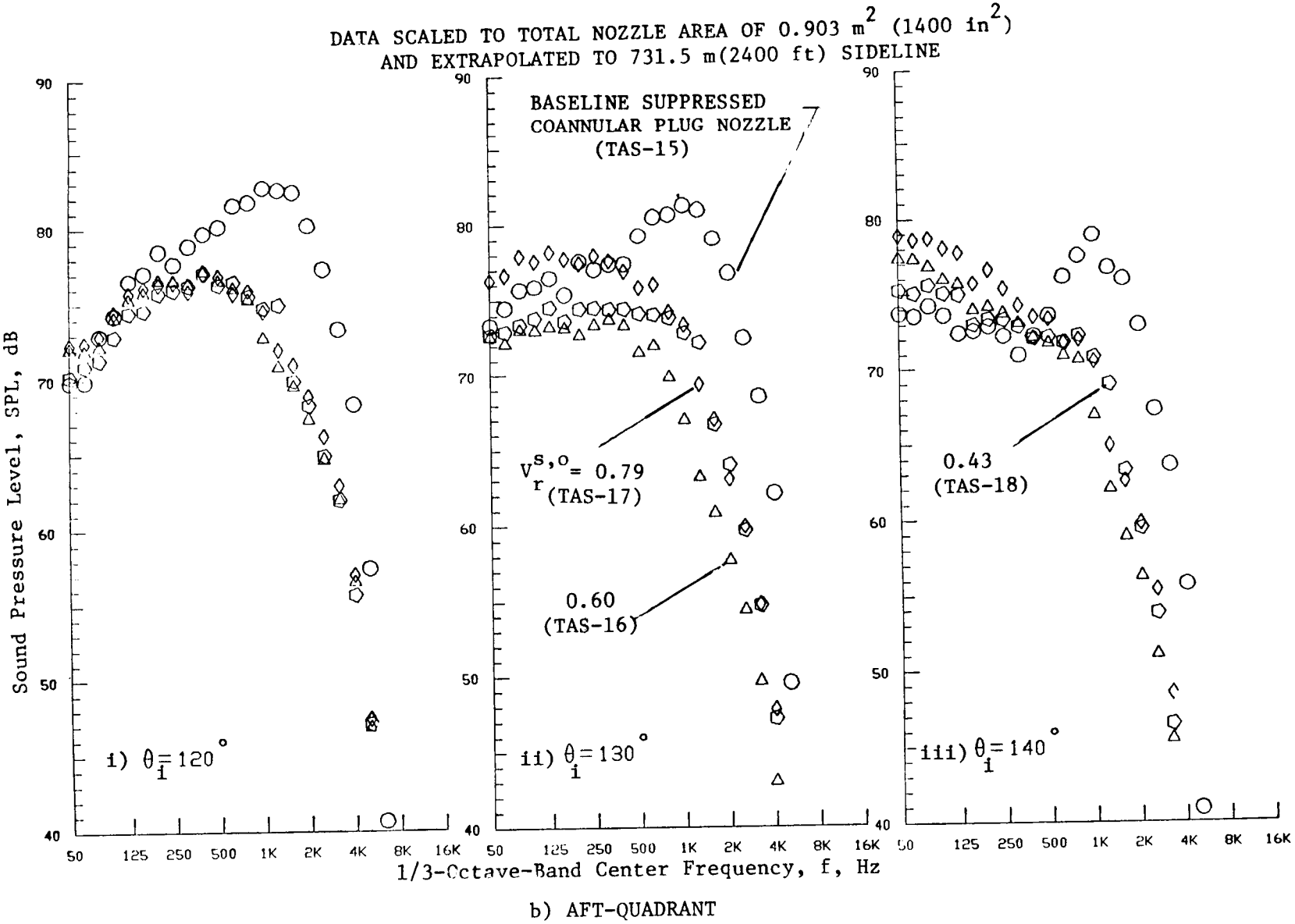

b) AFT-QUADRANT

Figure 76. Effect of Shield-to-Outer Stream Velocity Ratio on Selected Front and Aft Quadrant Spectra of the Suppressed Coannular Plug Nozzle with Partial Shield at Cutback Cycle Conditions (Simulated Flight). (Concluded)

with the partial shield in sideline orientation. This test series was conducted, as in Table IX (TAS-16), with a set of choke plates yielding a shield-to-outer stream velocity ratio, $V_r^{s,o}$, of 0.64 at takeoff. The aft quadrant static data obtained at θ_i = 130° and 140° over typical engine operating cycle conditions are summarized in Figure 77. The data indicate that, for given nozzle flow conditions, the aft quadrant PNL with the shield in the sideline orientation is higher than the corresponding level with the same shield in the community orientation. Over the range of test conditions, the influence on the azimuthal asymmetric acoustic field of the partial shield orientation from a sideline to a community configuration is observed to range from 2.5 dB at typical approach conditions to approximately 1.0 dB at a typical takeoff.

Figure 78 presents PNL-directivities of configuration TAS-16 with the shield in community and sideline orientations for a typical takeoff condition. The data indicate that, except at large shallow angles, the perceived noise levels measured with the shield in sideline orientation are higher than the noise levels measured with the shield in community setup. At large shallow angles, the data are equal. Aft-quadrant spectral data corresponding to the flow conditions of Figure 78 are presented in Figure 79. Since the low frequency noise is from a downstream region where the flow streams have merged into a single jet, the effect of the shield orientation for given flow conditions is least at low frequencies. Also since the high frequency noise is generated near the nozzle exit, the higher observed SPL levels with the shield in the sideline orientation are due to the unsymmetrical flow and source distributions in this region and the associated unsymmetric shielding effect.

4.2.4 Comparison of Partial and Full Thermal Acoustic Shield Nozzle Data

Configuration TAS-19 employs a 360° thermal acoustic shield of 0.5 in. thickness around the baseline suppressor coannular nozzle (TAS-15). The shield flow area of this full shield has been designed to be equal to that of the 0.97 in. thick, 180° shield (Configurations TAS-16 through -18) such that the mass flow rates through the two shields are equal for given shield flow conditions. Acoustic tests were conducted with the full shielded configuration with choke plates identical to those used with TAS-17 (partial shield in community orientation) to yield a shield-to-outer stream velocity ratio $V_r^{s,o}$ of approximately 0.83 at a typical takeoff condition. In this section the measured data of TAS 19 are compared to the data of TAS-17 to show the benefit of the thicker partial thermal acoustic shield.

The normalized perceived noise level data of TAS-17 (180° shield) and TAS-19 (360° shield) at aft-quadrant angles of θ_i = 130°, 140° and 150° are presented in Figures 80 and 81. The data measured under static and simulated flight conditions, respectively, are plotted as a function of the mixed jet

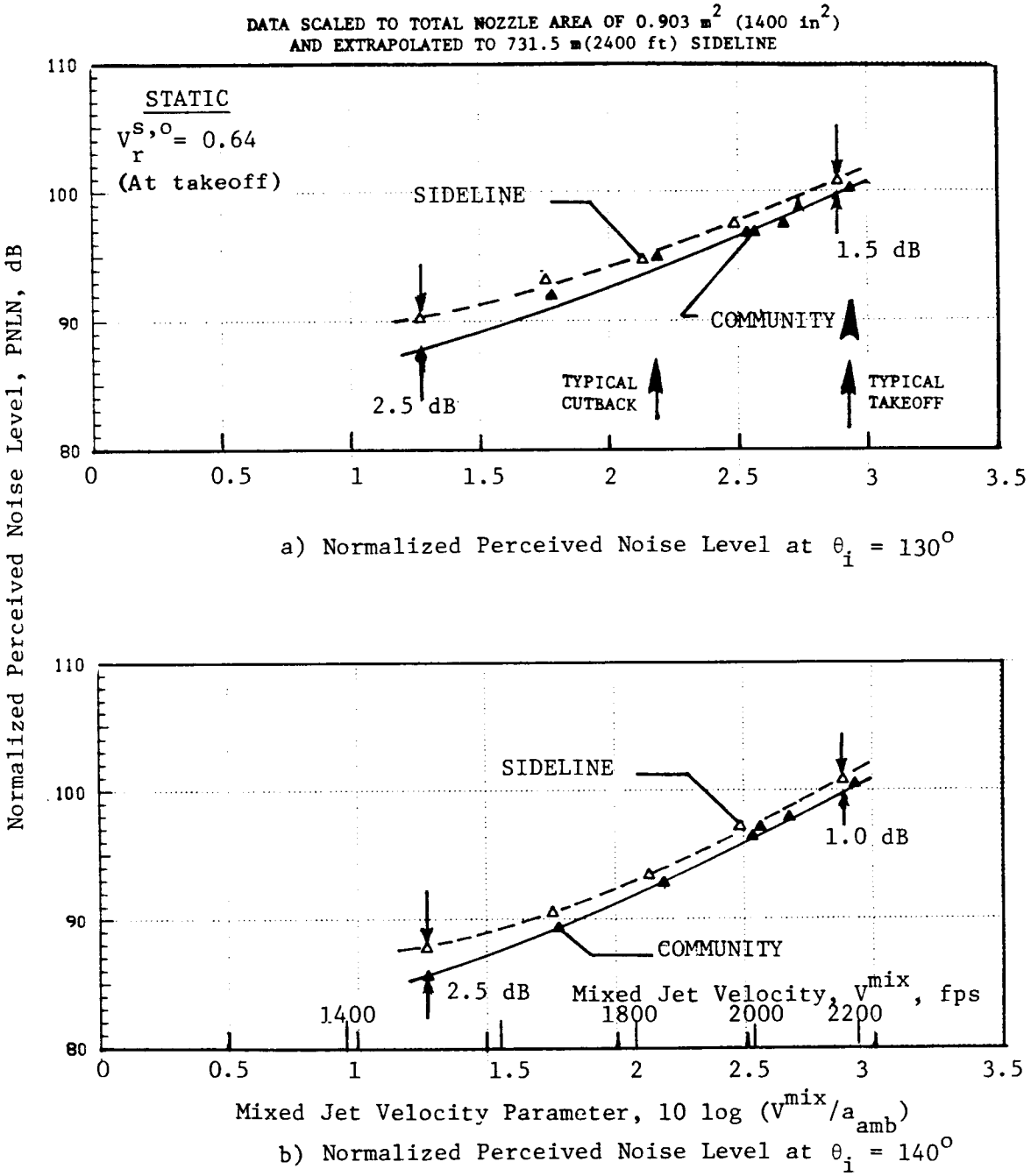

Figure 77. Effect of Shield Orientation on the Aft Quadrant Normalized Perceived Noise Level of Suppressed Coannular Plug Nozzle with 180° Shield (TAS-16).

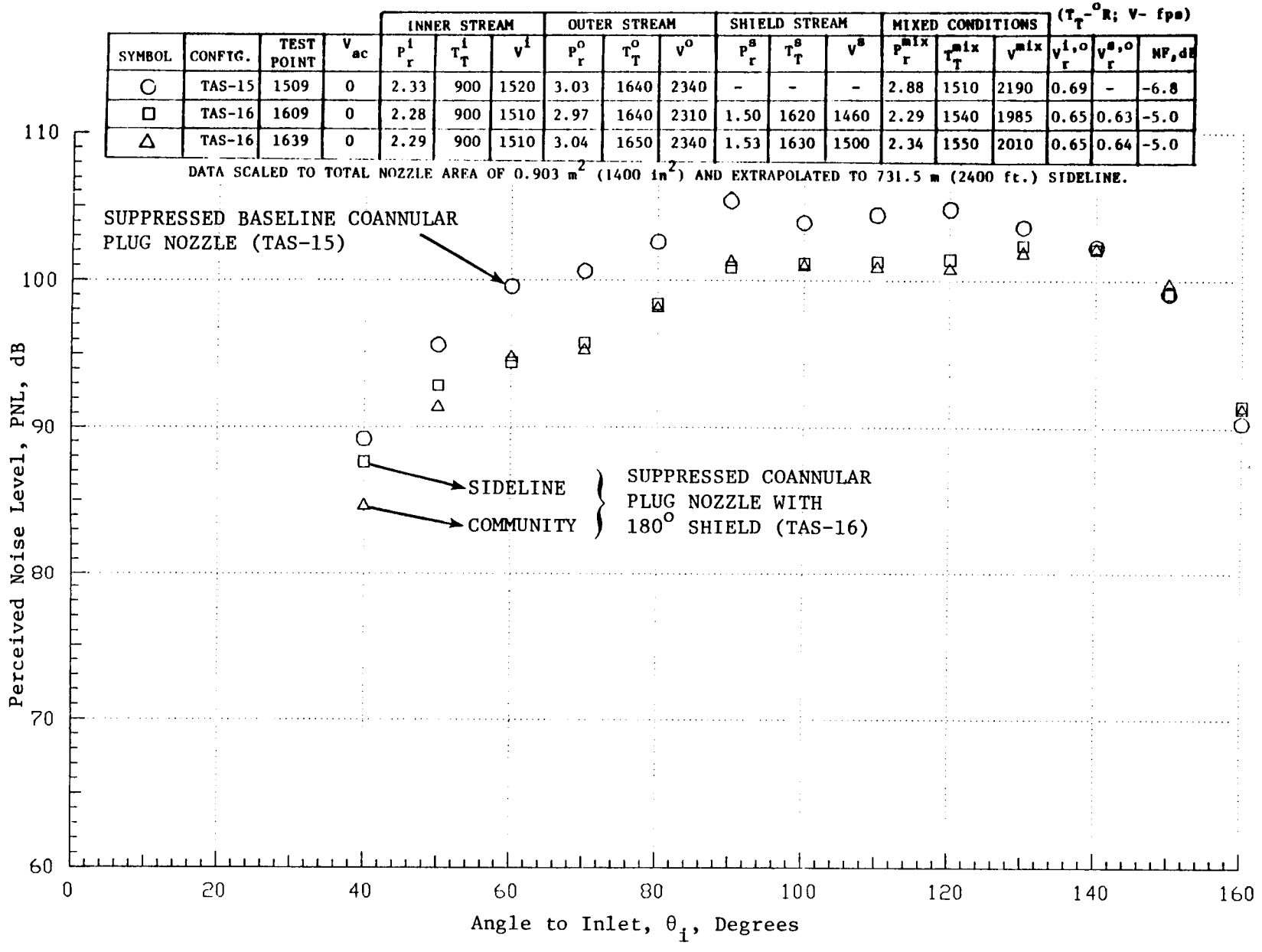

				INNER STREAM			OUTER STREAM			SHIELD STREAM			MIXED CONDITIONS					
SYMBOL	CONFIG.	TEST POINT	V_{ac}	P_r^i	T_T^i	V^i	P_r^o	T_T^o	V^o	P_r^s	T_T^s	V^s	P_r^{mix}	T_T^{mix}	V^{mix}	$V_r^{i,o}$	$V_r^{s,o}$	NF, dB
○	TAS-15	1509	0	2.33	900	1520	3.03	1640	2340	-	-	-	2.88	1510	2190	0.69	-	-6.8
□	TAS-16	1609	0	2.28	900	1510	2.97	1640	2310	1.50	1620	1460	2.29	1540	1985	0.65	0.63	-5.0
△	TAS-16	1639	0	2.29	900	1510	3.04	1650	2340	1.53	1630	1500	2.34	1550	2010	0.65	0.64	-5.0

Figure 78. Effect of Shield Orientation on the PNL-Directivity of Suppressed Coannular Plug Nozzle with 180° Shield at Takeoff Condition (TAS-16).

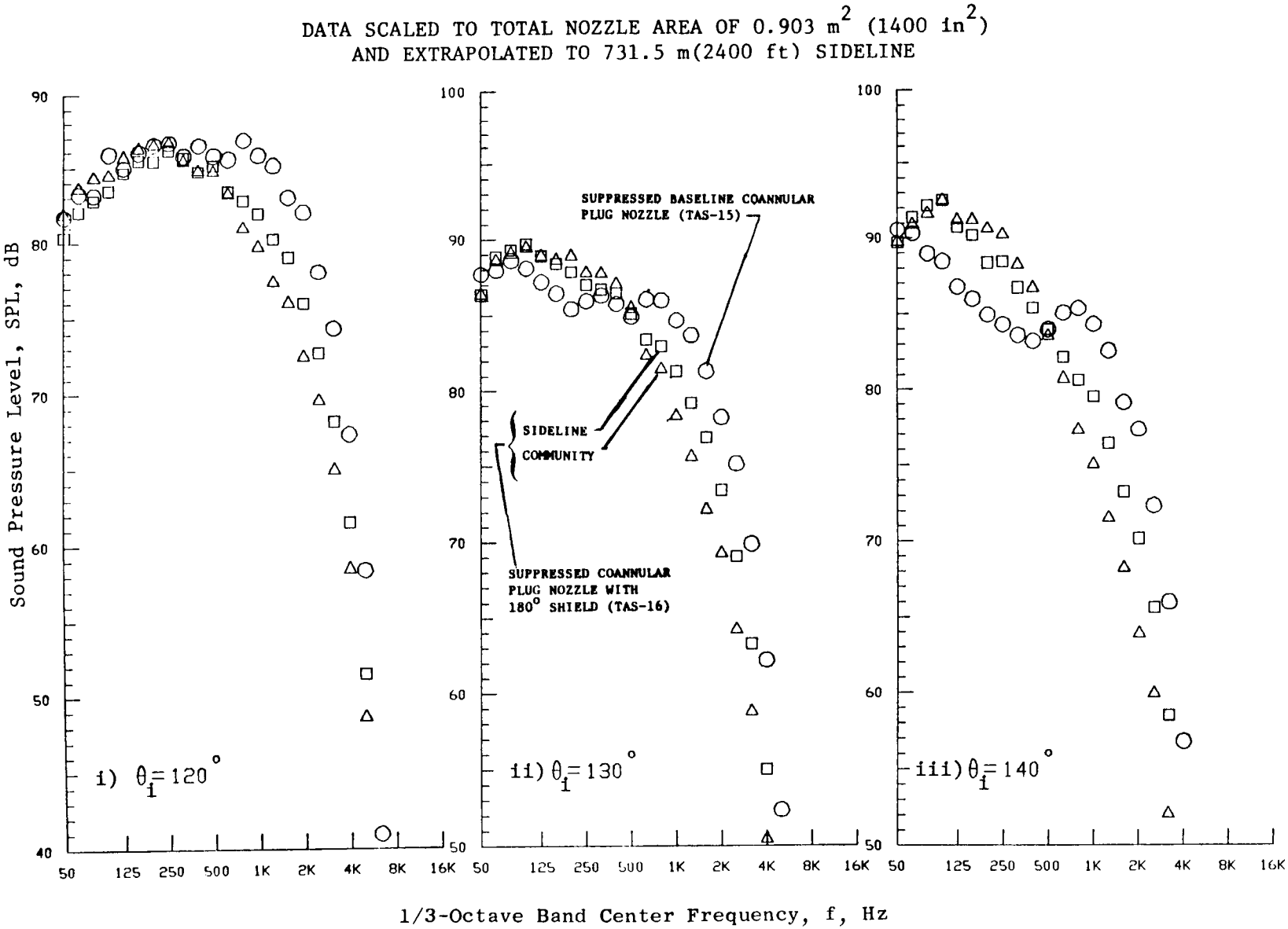

Figure 79. Effect of Shield Orientation on the Aft Quadrant Spectra of Suppressed Coannular Plug Nozzle with 180° Shield (TAS-16) at Takeoff Condition.

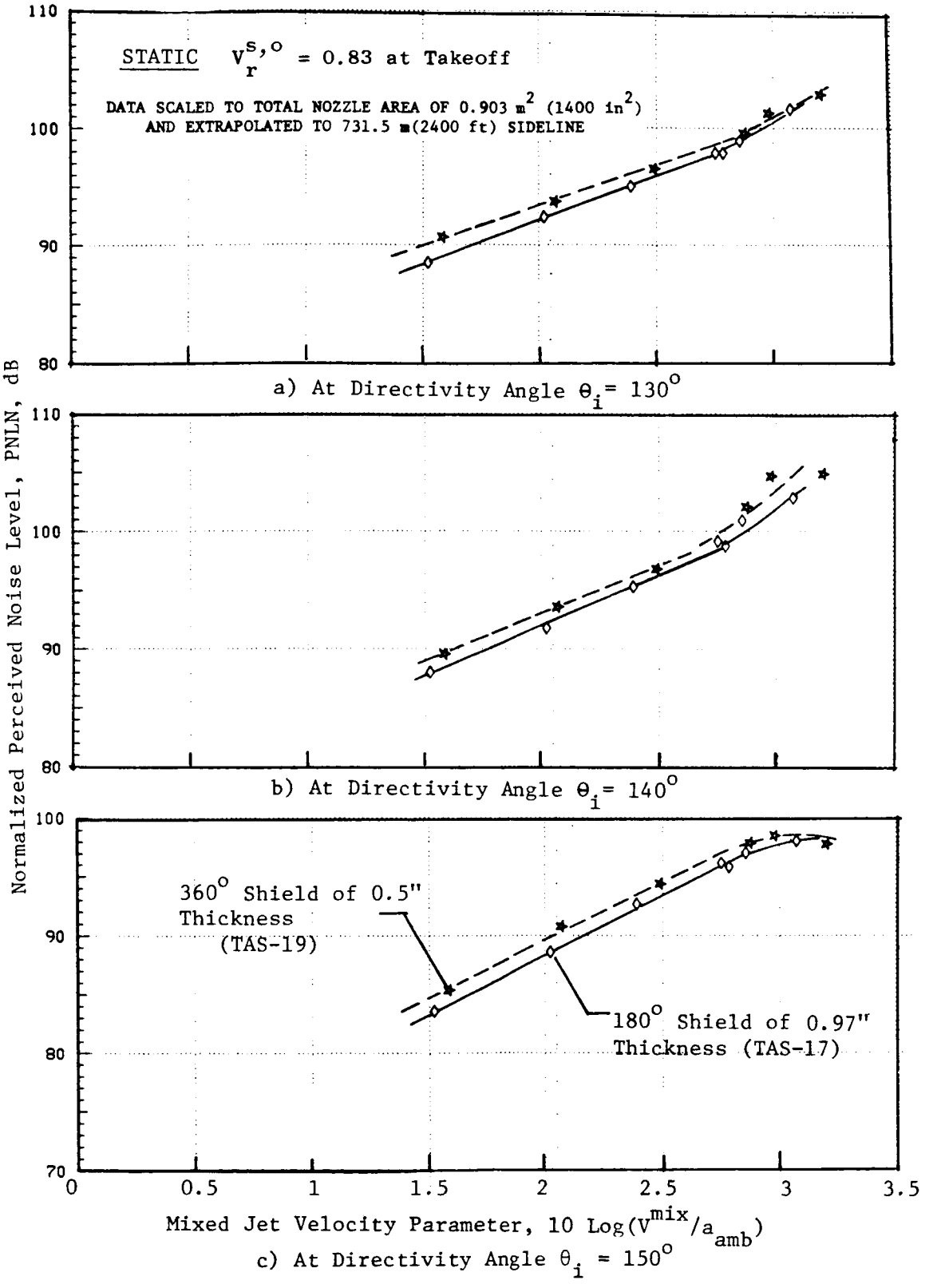

Figure 80. Aft Quadrant Normalized PNL Static Data of Suppressed Coannular Plug Nozzle with 180° and 360° Shield.

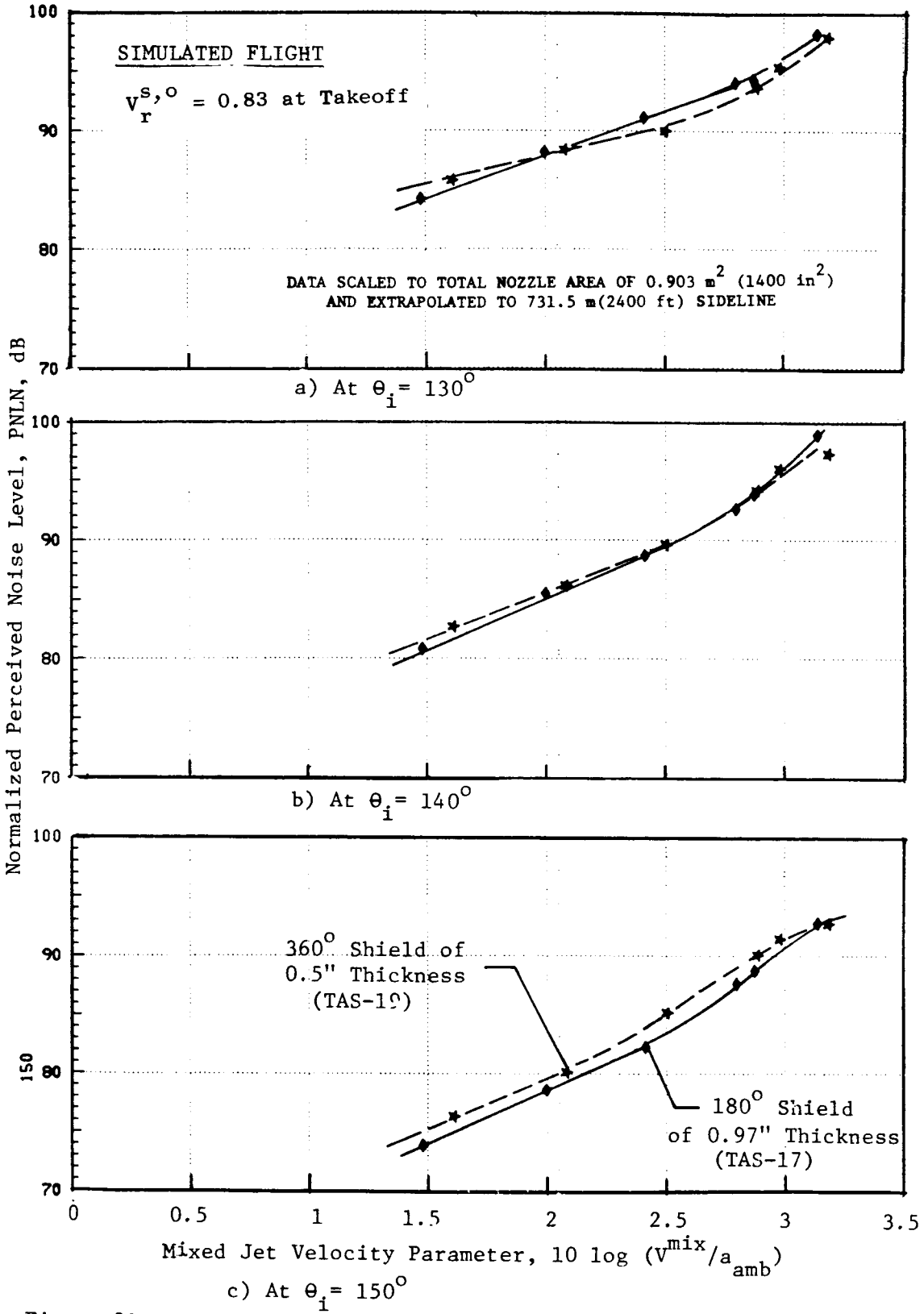

Figure 81. Aft Quadrant Normalized PNL Simulated Flight Data of Suppressed Coannular Plug Nozzle with 180° and 360° Shield.

velocity parameter. The data indicate that, for given shield flow conditions, the normalized perceived noise level data of the full shield (0.5 in. thick) configuration are higher than the corresponding data of the 180° shield (0.97 in. thick) configuration. This is particularly explicit for the static test data. Also, this difference decreases with an increase in the mixed jet velocity.

Aft-quadrant static spectral data at typical takeoff conditions are presented in Figure 82. The data show no significant spectral differences between the partial and full shield configurations data up to an aft quadrant angle of $\theta_i = 120°$. At directivity angles greater than 120°, the sound pressure levels associated with the partial shielded configuration are lower at all frequencies than those of full shielded configurations. Relative to the unshielded baseline suppressor nozzle, the partial shield configuration yields a larger suppression at higher frequencies, while the full shield configuration yields a significant increase in the low frequency spectra. Corresponding selected aft quadrant spectra obtained during simulated flight tests are presented in Figure 83. Observations similar to those of the static data are noted; however, no significant spectral differences between the partial and full shield configurations are indicated up to $\theta_i = 130°$.

Selected aft quadrant static and simulated flight spectral data at typical cutback conditions are presented in Figures 84 and 85, respectively. Selected aft-quadrant static spectra at approach condition are presented in Figure 86. Observations similar to those made earlier for the takeoff data can be applied to those test conditions also. The low frequency sound pressure levels are seen to increase. Therefore, though the shields significantly suppressed the high frequency noise at these angles, because of this increase the overall perceived noise levels were not reduced by the shields. This is indicated by the typical takeoff of PNL-directivity data presented in Figure 87.

This section is concluded by comparing the typical sound power spectra of unshielded and 360° shielded suppressed coannular plug nozzles to those of the convergent circular nozzle. The static spectra obtained at typical takeoff and cutback conditions are presented in Figure 88. This figure shows the significant sound power level reduction obtained with the baseline suppressor configuration (TAS-15) relative to the convergent circular nozzle at all low and middle frequencies. This is a result of the significantly higher mixing rate associated with the suppressor configuration. The increased mixing rate is achieved through an increase in surface area of the suppressor jet that is available for shear with the surrounding ambient air. However, no benefit is noted at high frequencies for sources near the nozzle exit. Introducing the full shield around the suppressor yields the observed power level reductions in the high frequency data due to shielding of the high frequency sources near the nozzle exit. However, the presence of the shield flow decreases the decay rate of the suppressor jet. This leads to the increase in the low and middle frequency power levels. The mean velocity data that describe the effect of shield flow on the decay rate of the suppressor jet are presented in the next section.

SYMBOL	CONFIG.	TEST POINT	V_{ac}	INNER STREAM P_r^i	INNER STREAM T_T^i	INNER STREAM V^i	OUTER STREAM P_r^o	OUTER STREAM T_T^o	OUTER STREAM V^o	SHIELD STREAM P_r^s	SHIELD STREAM T_T^s	SHIELD STREAM V^s	MIXED CONDITIONS P_r^{mix}	MIXED CONDITIONS T_T^{mix}	MIXED CONDITIONS V^{mix}	$V_r^{i,o}$	$V_r^{s,o}$	NF, dB
○	TAS-15	1509	0	2.33	900	1520	3.03	1640	2340	-	-	-	2.88	1510	2190	0.65	-	-6.8
◇	TAS-17	1709	0	2.29	900	1510	3.06	1670	2360	2.07	1650	1940	2.56	1575	2120	0.64	0.82	-5.7
⬡	TAS-19	1909	0	2.28	905	1510	3.03	1650	2335	2.14	1630	1970	2.57	1560	2115	0.65	0.84	-5.8

(T_T-°R; V- fps)

DATA SCALED TO TOTAL NOZZLE AREA OF 0.903 m^2 (1400 in^2) AND EXTRAPOLATED TO 731.5 m (2400 ft.) SIDELINE.

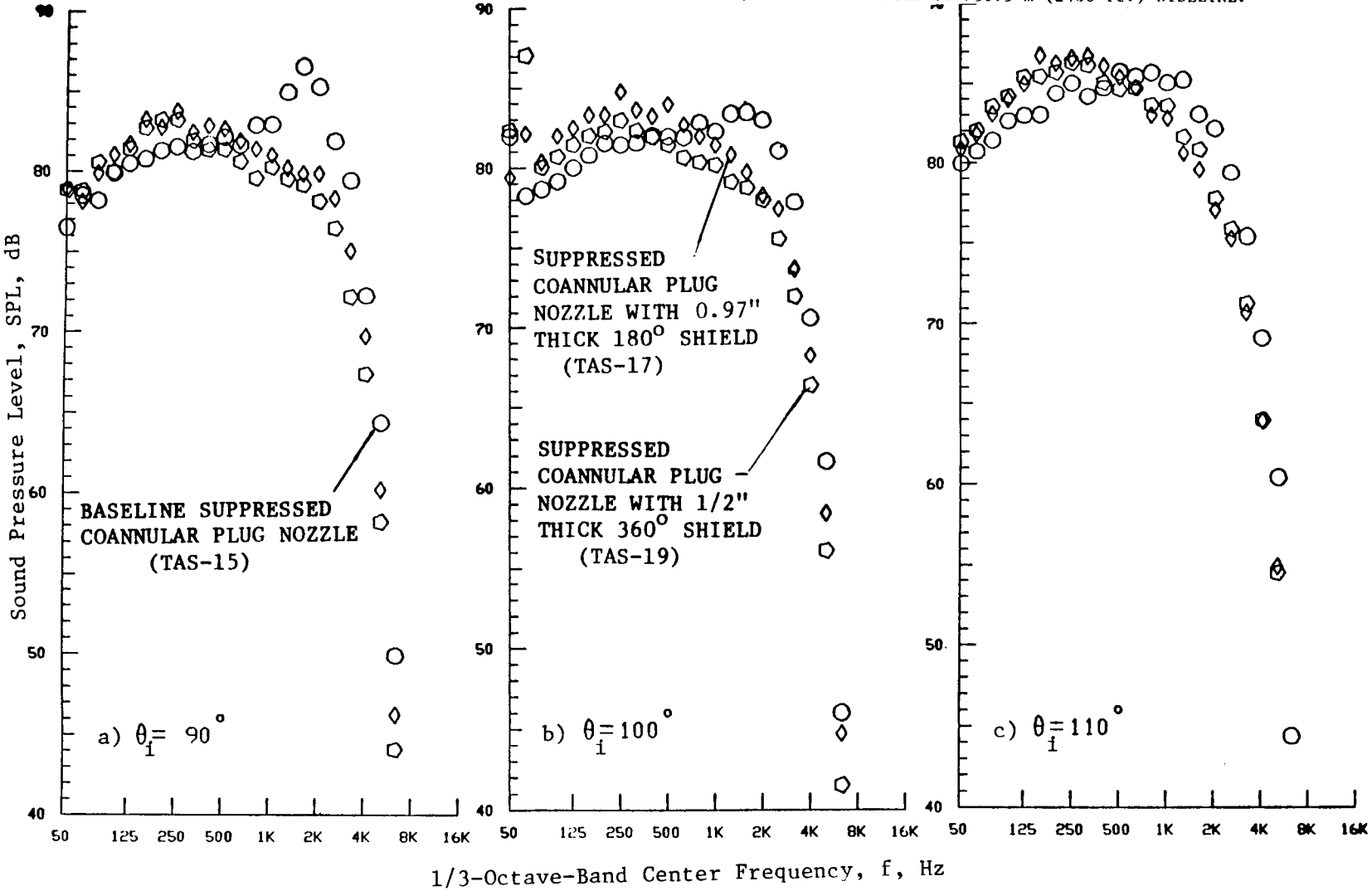

Figure 82. Aft Quadrant Static Spectral Data of Suppressed Coannular Plug Nozzle with 180° and 360° Shields at Typical Takeoff Condition.

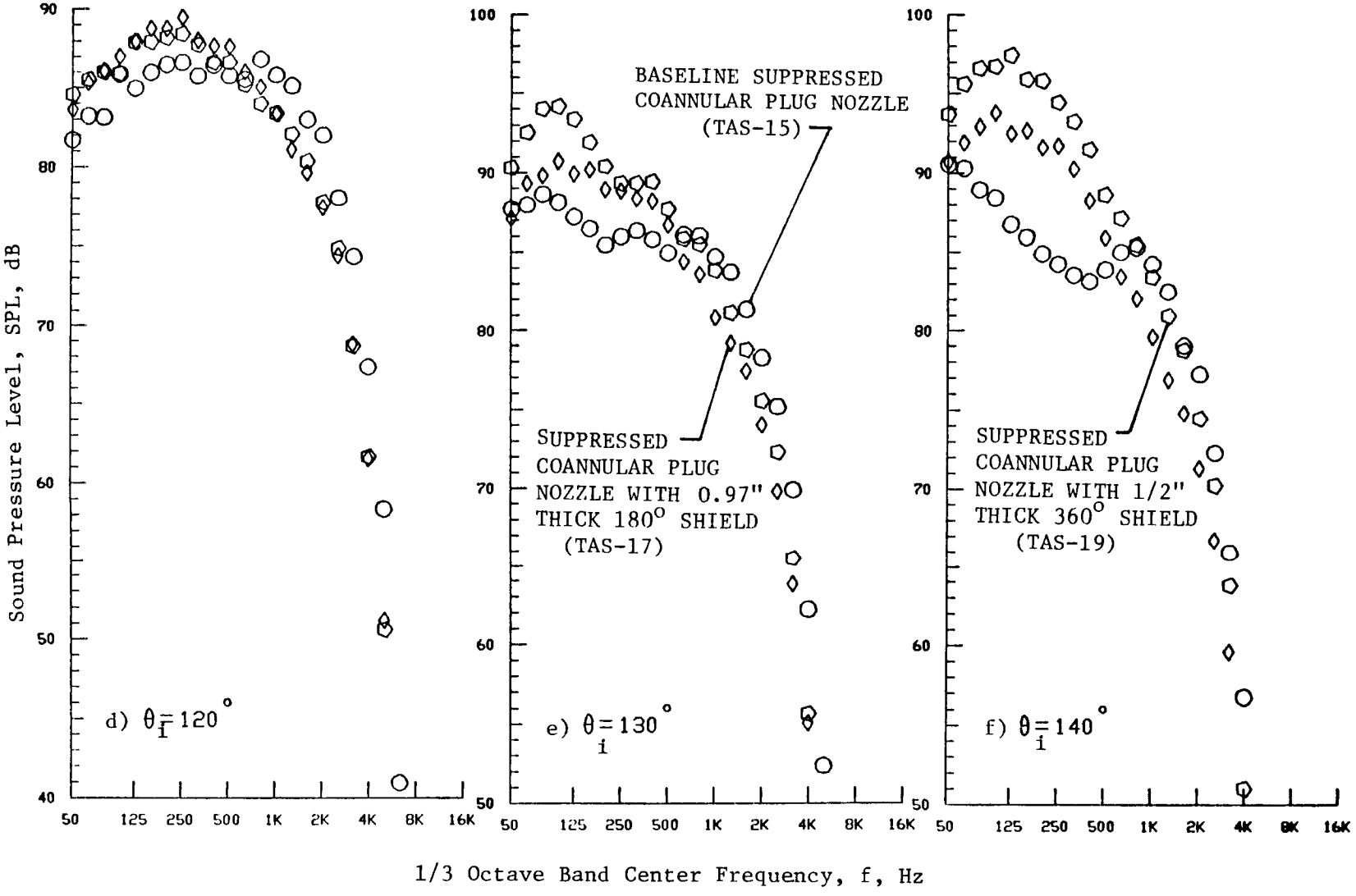

Figure 82. Aft Quadrant Static Spectral Data of Suppressed Coannular Plug Nozzle with 180° and 360° Shields at Typical Takeoff Condition. (Concluded)

SYMBOL	CONFIG.	TEST POINT	V_{ac}	INNER STREAM P_r^i	INNER STREAM T_T^i	INNER STREAM V^i	OUTER STREAM P_r^o	OUTER STREAM T_T^o	OUTER STREAM V^o	SHIELD STREAM P_r^s	SHIELD STREAM T_T^s	SHIELD STREAM V^s	MIXED CONDITIONS P_r^{mix}	MIXED CONDITIONS T_T^{mix}	MIXED CONDITIONS V^{mix}	$V_r^{i,o}$	$V_r^{s,o}$	NF_s, dB
○	TAS-15	1510	400	2.32	910	1530	3.09	1640	2340	-	-	-	2.93	1520	2205	0.65	0.00	-6.8
◇	TAS-17	1710	↓	2.30	910	1520	3.06	1660	2350	2.13	1620	1950	2.59	1560	2120	0.65	0.83	-5.8
⬡	TAS-19	1910		2.28	895	1500	3.04	1650	2335	2.19	1615	1980	2.60	1550	2120	0.64	0.85	-5.8

(T_T-°R; V- fps)

DATA SCALED TO TOTAL NOZZLE AREA OF 0.903 m^2 (1400 in^2) AND EXTRAPOLATED TO 731.5 m (2400 ft.) SIDELINE.

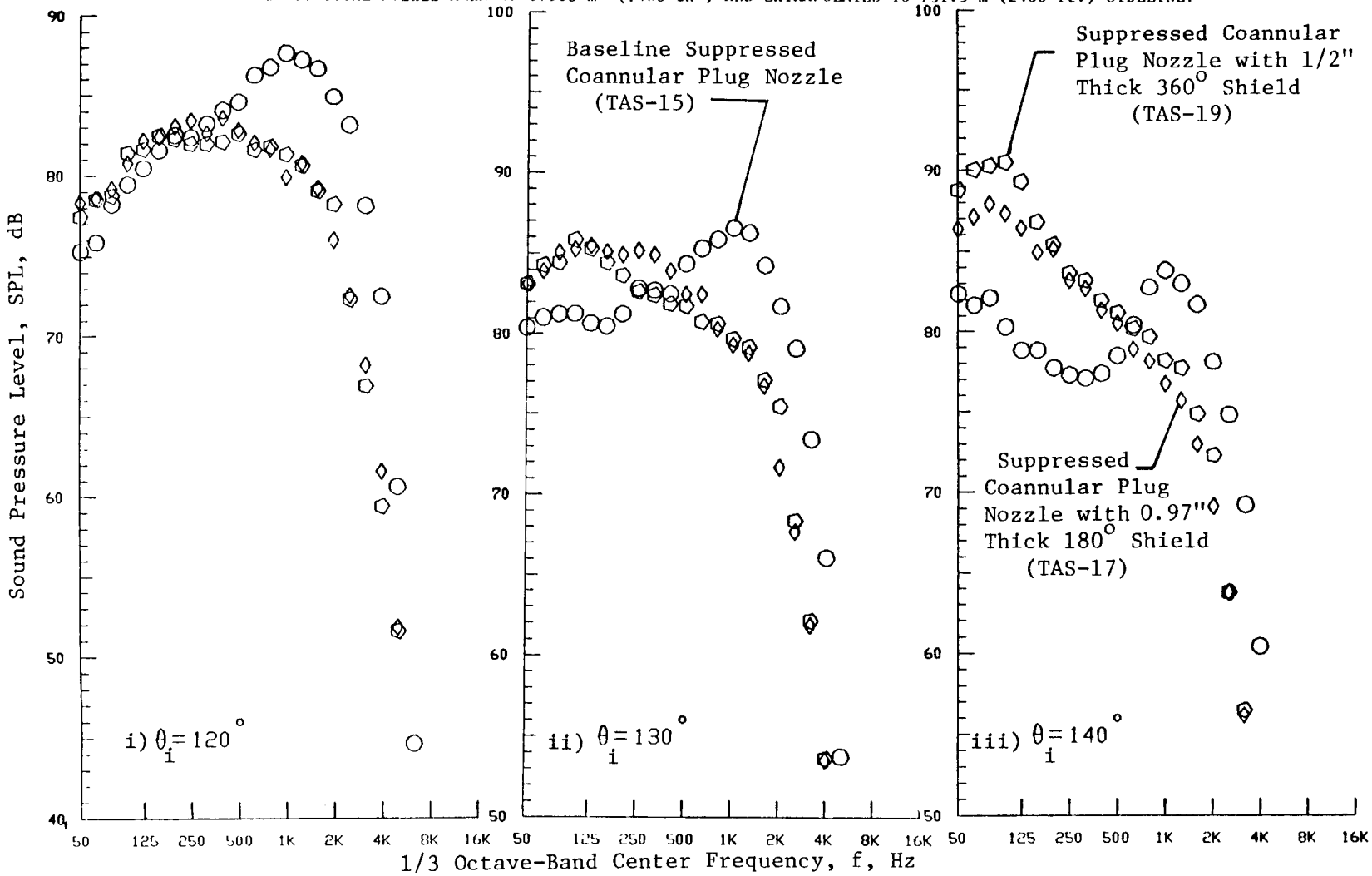

Figure 83. Aft Quadrant Simulated Flight Spectral Data of Suppressed Coannular Plug Nozzle with 180° and 360° Shields at Typical Takeoff Conditions.

SYMBOL	CONFIG.	TEST POINT	V_{ac}	INNER STREAM P_r^i	INNER STREAM T_T^i	INNER STREAM V^i	OUTER STREAM P_r^o	OUTER STREAM T_T^o	OUTER STREAM V^o	SHIELD STREAM P_r^s	SHIELD STREAM T_T^s	SHIELD STREAM V^s	MIXED CONDITIONS P_r^{mix}	MIXED CONDITIONS T_T^{mix}	MIXED CONDITIONS V^{mix}	$V_r^{i,o}$	$V_r^{s,o}$	NF, dB
○	TAS-15	1505	0	1.89	820	1280	2.33	1470	1955	-	-	-	2.24	1350	1830	0.65	-	-5.4
◇	TAS-17	1705	0	1.75	850	1230	2.34	1530	2025	1.66	1515	1570	2.01	1450	1780	0.61	0.77	-4.1
⬡	TAS-19	1905	0	1.75	830	1215	2.38	1475	1980	1.70	1465	1580	2.02	1400	1755	0.61	0.80	-4.3

(T_T-°R; V- fps)

DATA SCALED TO TOTAL NOZZLE AREA OF 0.903 m^2 (1400 in^2) AND EXTRAPOLATED TO 731.5 m (2400 ft.) SIDELINE.

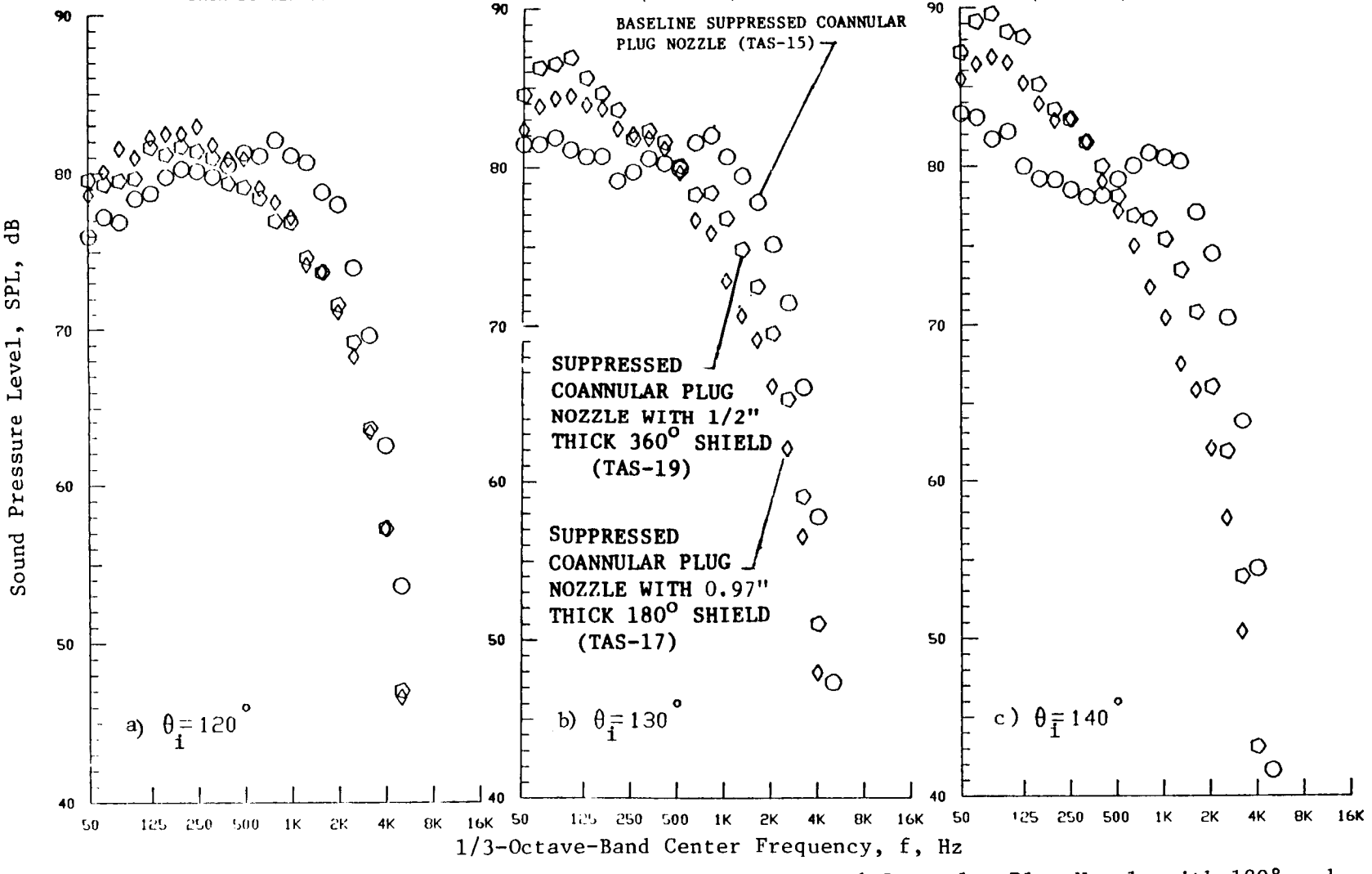

Figure 84. Aft Quadrant Static Spectral Data of Suppressed Coannular Plug Nozzle with 180° and 360° Shields at Typical Cutback Conditions.

(T_T-°R; V- fps)

SYMBOL	CONFIG.	TEST POINT	V_{ac}	INNER STREAM P_r^i	INNER STREAM T_T^i	INNER STREAM V^i	OUTER STREAM P_r^o	OUTER STREAM T_T^o	OUTER STREAM V^o	SHIELD STREAM P_r^s	SHIELD STREAM T_T^s	SHIELD STREAM V^s	MIXED CONDITIONS P_r^{mix}	MIXED CONDITIONS T_T^{mix}	MIXED CONDITIONS V^{mix}	$V_r^{i,o}$	$V_r^{s,o}$	NF_s, dB
○	TAS-15	1506	400	1.79	820	1225	2.43	1490	2010	-	-	-	2.30	1375	1875	0.61	-	-5.4
◇	TAS-17	1706	400	1.76	840	1225	2.39	1485	1990	1.69	1450	1565	2.02	1400	1760	0.62	0.79	-4.3
⬡	TAS-19	1906	400	1.75	820	1205	2.38	1490	1990	1.73	1460	1595	2.03	1400	1760	0.61	0.80	-4.3

DATA SCALED TO TOTAL NOZZLE AREA OF 0.903 m^2 (1400 in^2) AND EXTRAPOLATED TO 731.5 m (2400 ft.) SIDELINE.

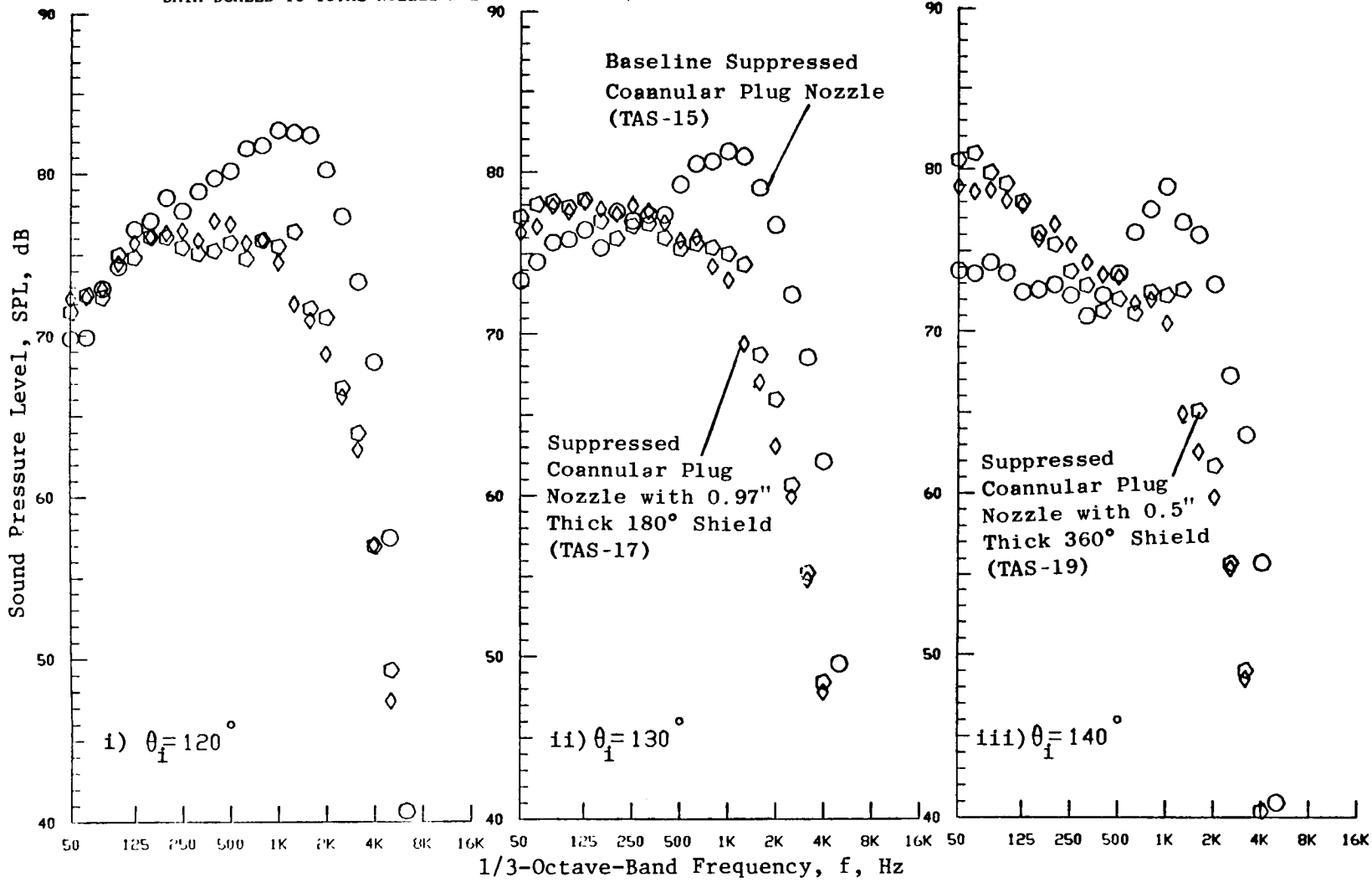

Figure 85. Aft Quadrant Simulated Flight Spectral Data of Suppressed Coannular Plug Nozzle with 180° and 360° Shields and at Typical Cutback Condition.

SYMBOL	CONFIG.	TEST POINT	V_{ac}	INNER STREAM P_r^i	INNER STREAM T_T^i	INNER STREAM V^i	OUTER STREAM P_r^o	OUTER STREAM T_T^o	OUTER STREAM V^o	SHIELD STREAM P_r^s	SHIELD STREAM T_T^s	SHIELD STREAM V^s	MIXED CONDITIONS P_r^{mix}	MIXED CONDITIONS T_T^{mix}	MIXED CONDITIONS V^{mix}	$V_r^{i,o}$	$V_r^{s,o}$	NF, dB
○	TAS-15	1503	0	1.57	820	1095	2.12	1310	1745	-	-	-	2.02	1235	1645	0.63	-	-4.9
◇	TAS-17	1703	0	1.57	850	1115	2.10	1430	1820	1.49	1415	1360	1.79	1365	1585	0.61	0.75	-3.5
⬡	TAS-19	1903	0	1.58	815	1095	2.10	1380	1785	1.53	1370	1375	1.80	1315	1570	0.61	0.77	-3.7

(T_T-°R; V- fps)

DATA SCALED TO TOTAL NOZZLE AREA OF 0.903 m^2 (1400 in^2) AND EXTRAPOLATED TO 731.5 m (2400 ft.) SIDELINE.

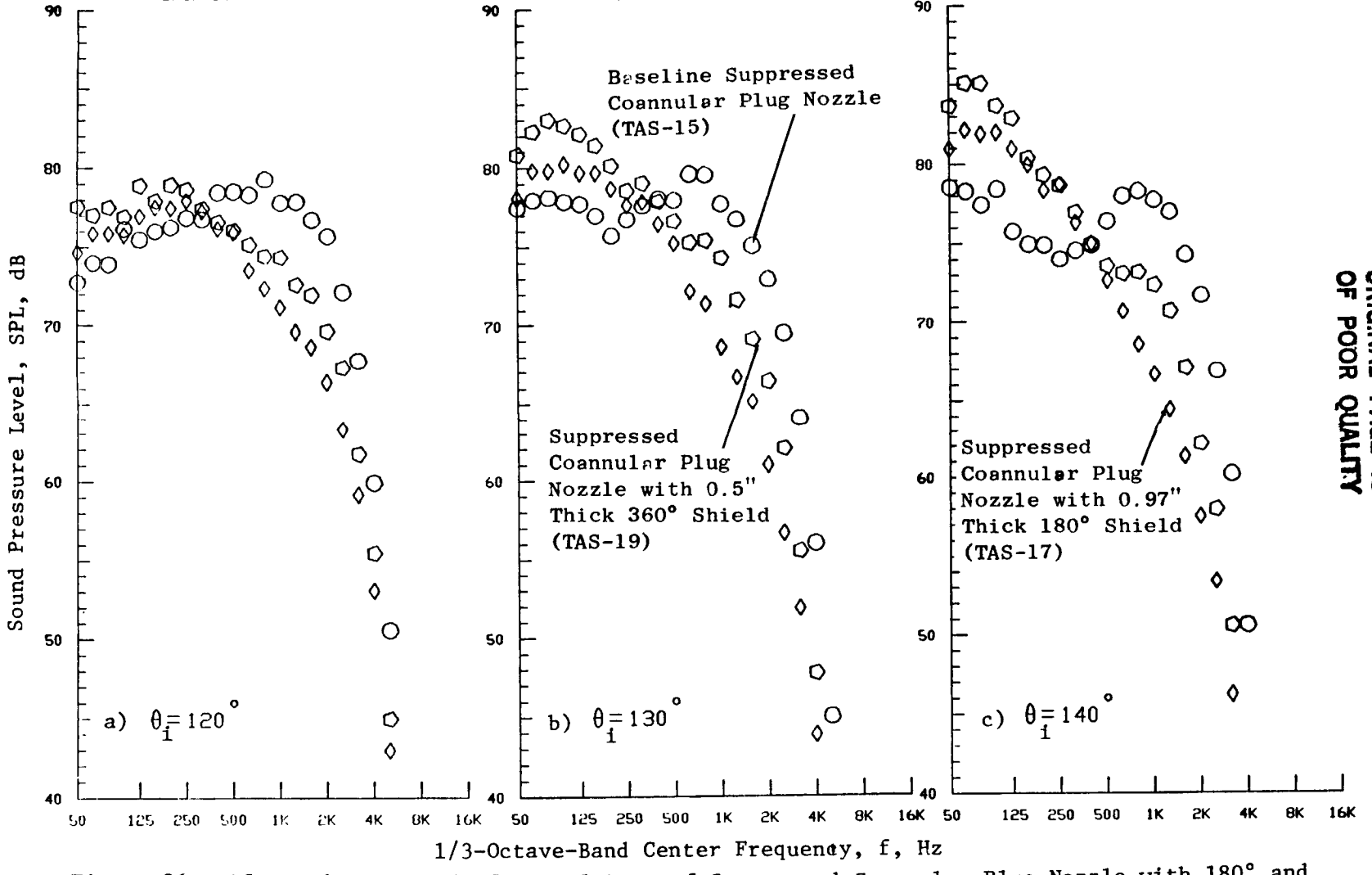

Figure 86. Aft Quadrant Static Spectral Data of Suppressed Coannular Plug Nozzle with 180° and 360° Shields at Typical Approach Condition.

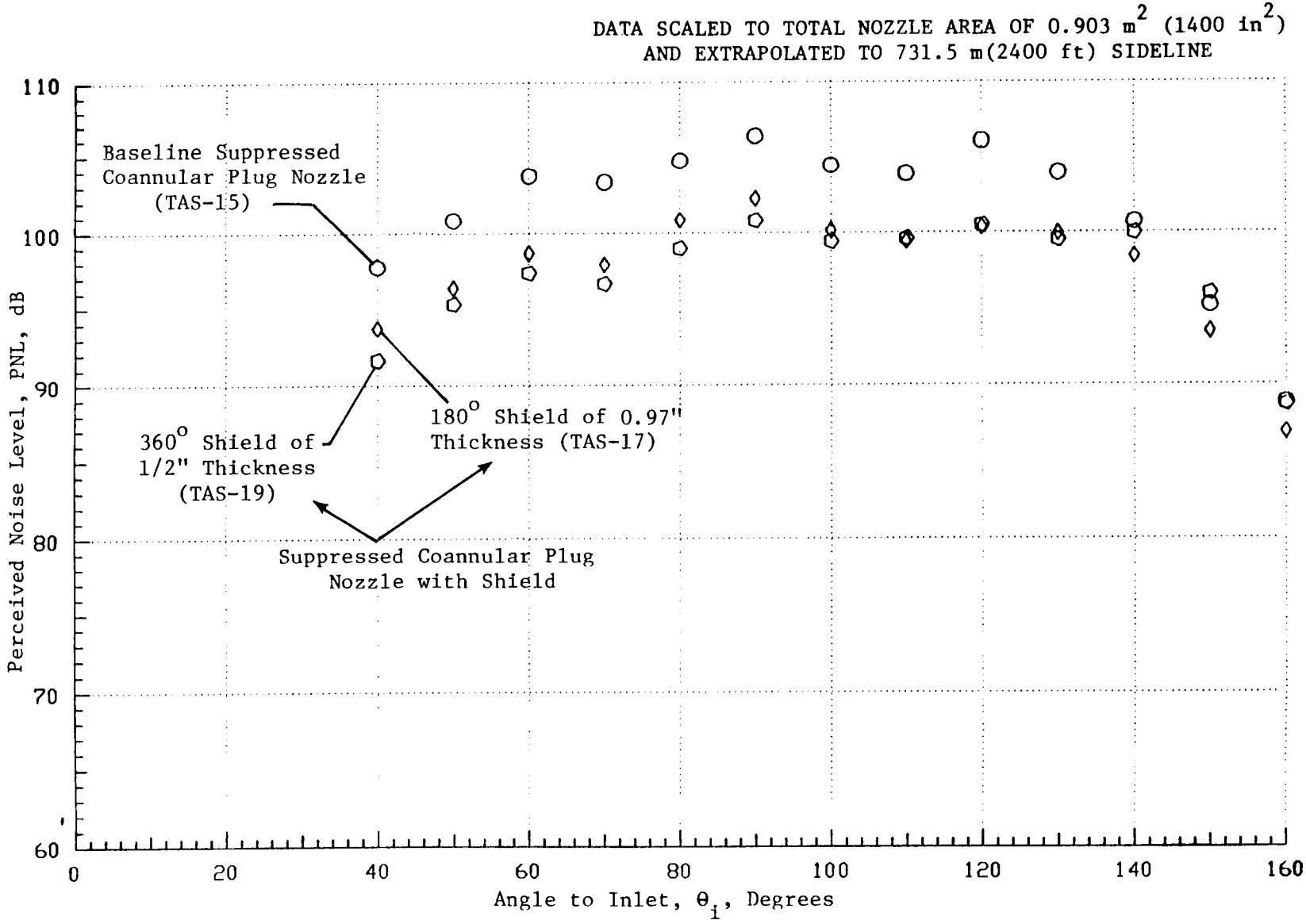

Figure 87. Simulated Flight PNL Directivity of Suppressed Coannular Plug Nozzle with 180° and 360° Shields at Takeoff Condition.

	SYMBOL	CONFIG.	TEST POINT	V_{ac}	INNER STREAM P_r^i	INNER STREAM T_T^i	INNER STREAM V^i	OUTER STREAM P_r^o	OUTER STREAM T_T^o	OUTER STREAM V^o	SHIELD STREAM P_r^s	SHIELD STREAM T_T^s	SHIELD STREAM V^s	MIXED CONDITIONS P_r^{mix}	MIXED CONDITIONS T_T^{mix}	MIXED CONDITIONS V^{mix}	$V_r^{i,o}$	$V_r^{s,o}$	NF, dB	F, lb	OAPWL, dB
					(T_T-°R; V- fps)																
FIG. a)	◇	CONIC	504	0	-	-	-	2.51	1675	2170	-	-	-	2.51	1675	2170	-	-	-5.1	43900	184.2
	○	TAS-15	1509	0	2.33	900	1520	3.03	1640	2340	-	-	-	2.88	1510	2190	0.65	-	-6.8	54600	179.1
	▷	TAS-19	1909	0	2.28	905	1510	3.03	1650	2335	2.14	1630	1970	2.57	1560	2115	0.65	0.84	-5.8	45500	180.5
FIG. b)	◇	CONIC	561	0	-	-	-	2.16	1470	1875	-	-	-	2.16	1470	1875	-	-	-4.9	35100	179.9
	○	TAS-15	1505	0	1.89	820	1280	2.33	1470	1955	-	-	-	2.24	1350	1830	0.65	-	-5.4	37600	174.3
	▷	TAS-19	1905	0	1.75	830	1215	2.38	1475	1980	1.70	1465	1580	2.02	1400	1755	0.61	0.80	-4.3	31600	173.6

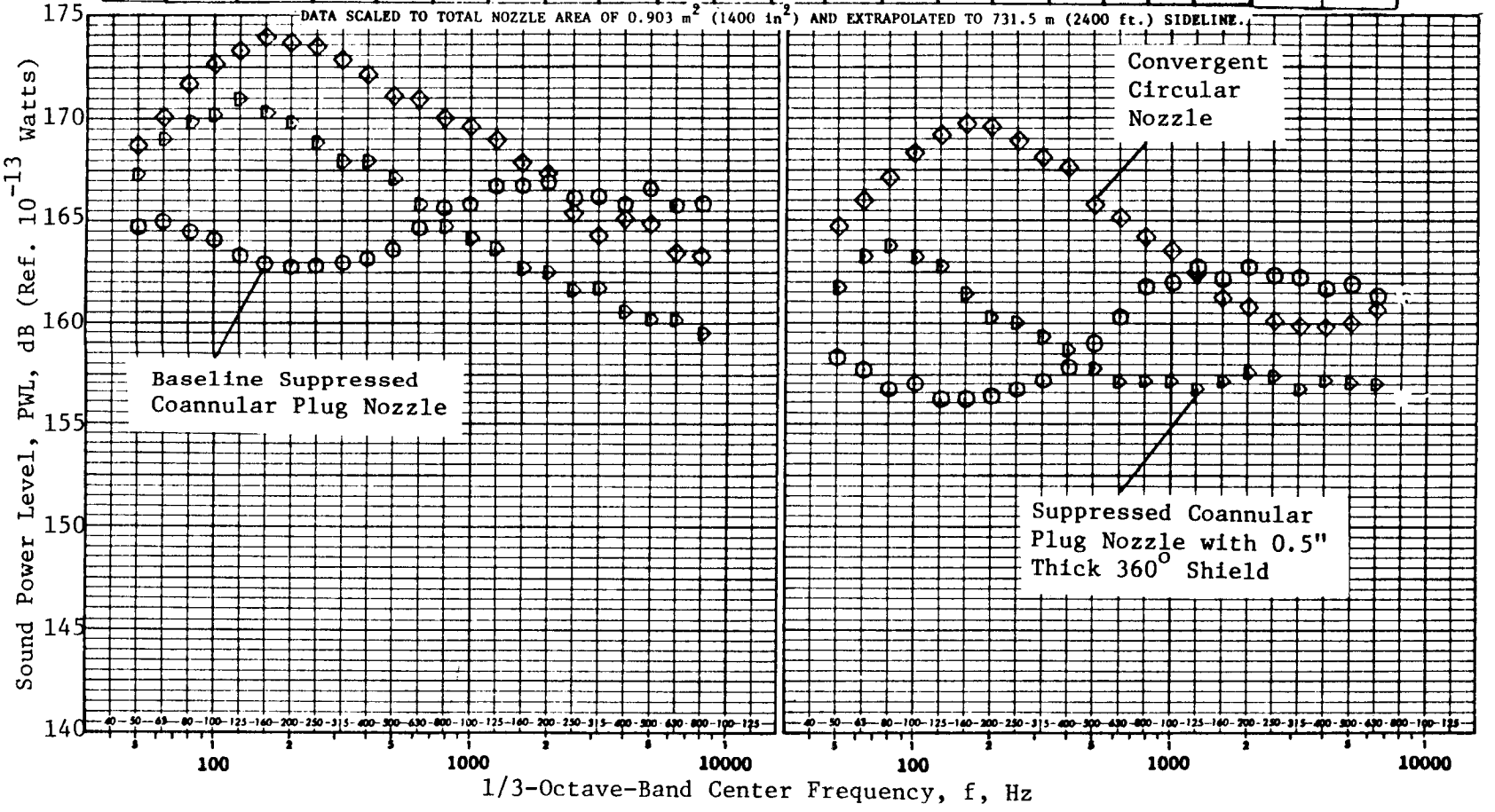

a) At Typical Takeoff

b) At Typical Cutback

Figure 88. Sound Power Level Comparison Between Unshielded and 360° Shielded Suppressed Coannular Plug Nozzle (Static).

4.2.5 Flow-Field Characteristics with Partial Thermal Acoustic Shield

The mean and turbulent velocity profiles obtained during axial traverses in the static plume of the suppressed coannular nozzle with the 180° thermal acoustic shield (that is, LV plume 3 of Table XIII) are presented in Figure 89. The data compare axial mean and turbulent velocity variations along the nozzle centerline to the corresponding data obtained during axial traverses at radial locations of $R/R_t^s = 0.5$ on the shielded and unshielded sides. The aerodynamic flow conditions are similar to those of the unsuppressed configuration and correspond to a typical takeoff condition. An examination of the static measured axial velocity data indicates that:

a. No shock structures are formed downstream of the plug.

b. The presence of the partial shield results in an asymmetry between the shielded and unshielded side axial variations of the mean velocities (traverses B and C) due to the significantly different mixing characteristics. Axial traverse data taken at $R/R_t^s = 0.5$ on the shielded and unshielded side indicate higher mean velocities on the shield side up to an $X/D_{eq} \sim 10$. The asymmetry decreases for $X/D_{eq} > 10$

c. The normalized turbulent velocity along the centerline is within 6% up to an $X/D_{eq} \approx 10$ with the mean velocity remaining approximately constant, indicating the existence of a potential core.

d. The presence of the shield also results in an asymmetry in the turbulent velocities (traverses B and C) between the shielded and unshielded side data. Axial traverse turbulent data taken at $R/R_t^s = 0.5$ on shield and unshield side indicate higher turbulent velocities (with a maximum of 12% of V^{mix}) on shield side for $X/D_{eq} > 4$. The lower turbulent velocities for $X/D_{eq} < 4$ on the shield side are the result of reduction in shearing of the baseline nozzle flow because of the presence of the shield flow near the nozzle exit.

The asymmetry in the mean velocities between the shielded and unshielded side can also be noted from the set of radial traverse data presented in Figure 90. The radial mean velocity profiles in the premerged region (refer to data obtained at traverses J and K) indicate the presence of the shield flow. At these locations, the peak mean velocity on the shielded side is lower than that on the unshielded side. Over a significant region downstream of the plug (up to an $X/D_{eq} \sim 10.0$), the peak mean velocity on the shield side is higher than that on the unshielded side. This is due to the reduced mixing with ambient air on the shield side and hence lower decay rate for the mean velocity. As with the unsuppressed configurations (refer to Figure 52), the dips observed in the radial mean velocity profiles near the nozzle centerline are due to the flow separation in the region of the plug truncation.

The laser velocimeter measured static data, presented earlier in Figures 89 and 90, are compared in Figures 91 through 93 to the corresponding data obtained under simulated flight conditions (V_{ac} = 400 fps). Because of the reduction in shear stresses due to the presence of the free jet, the turbulent

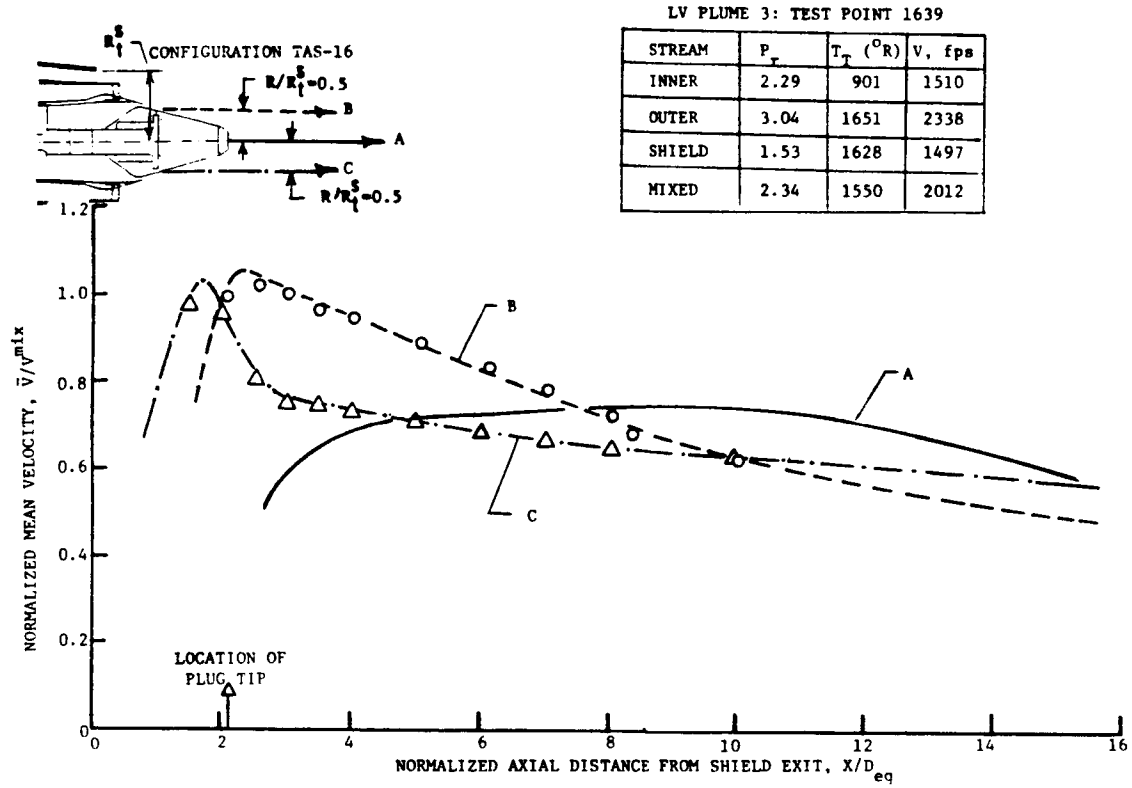

a) Mean Velocity

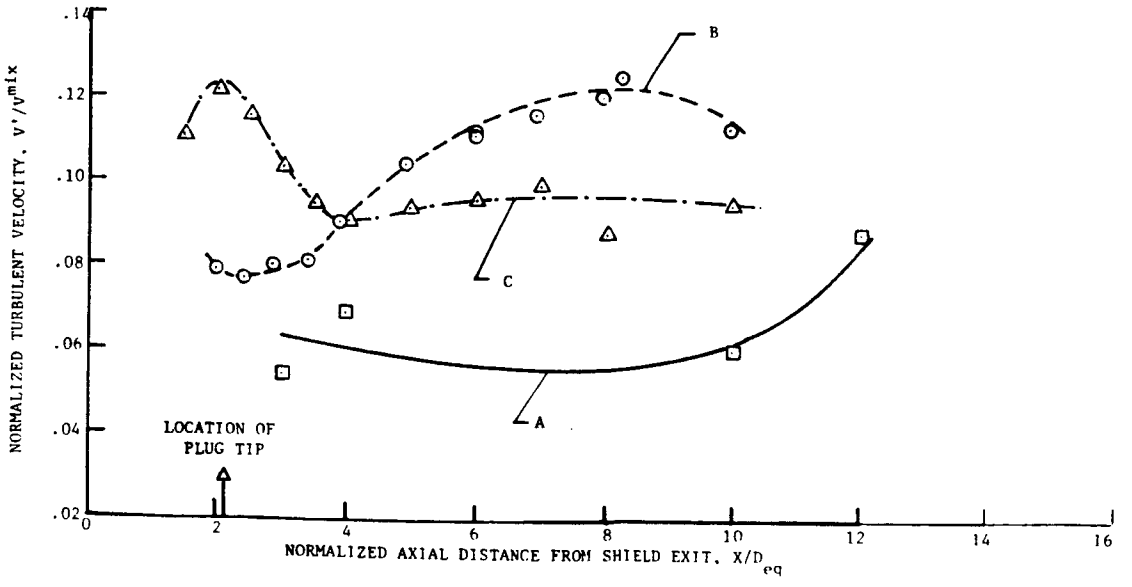

b) Turbulent Velocity

Figure 89. Axial Variation of Mean and Turbulent Velocities in the Plume of Suppressed Coannular Plug Nozzle with 180° Shield at Takeoff Condition (Static).

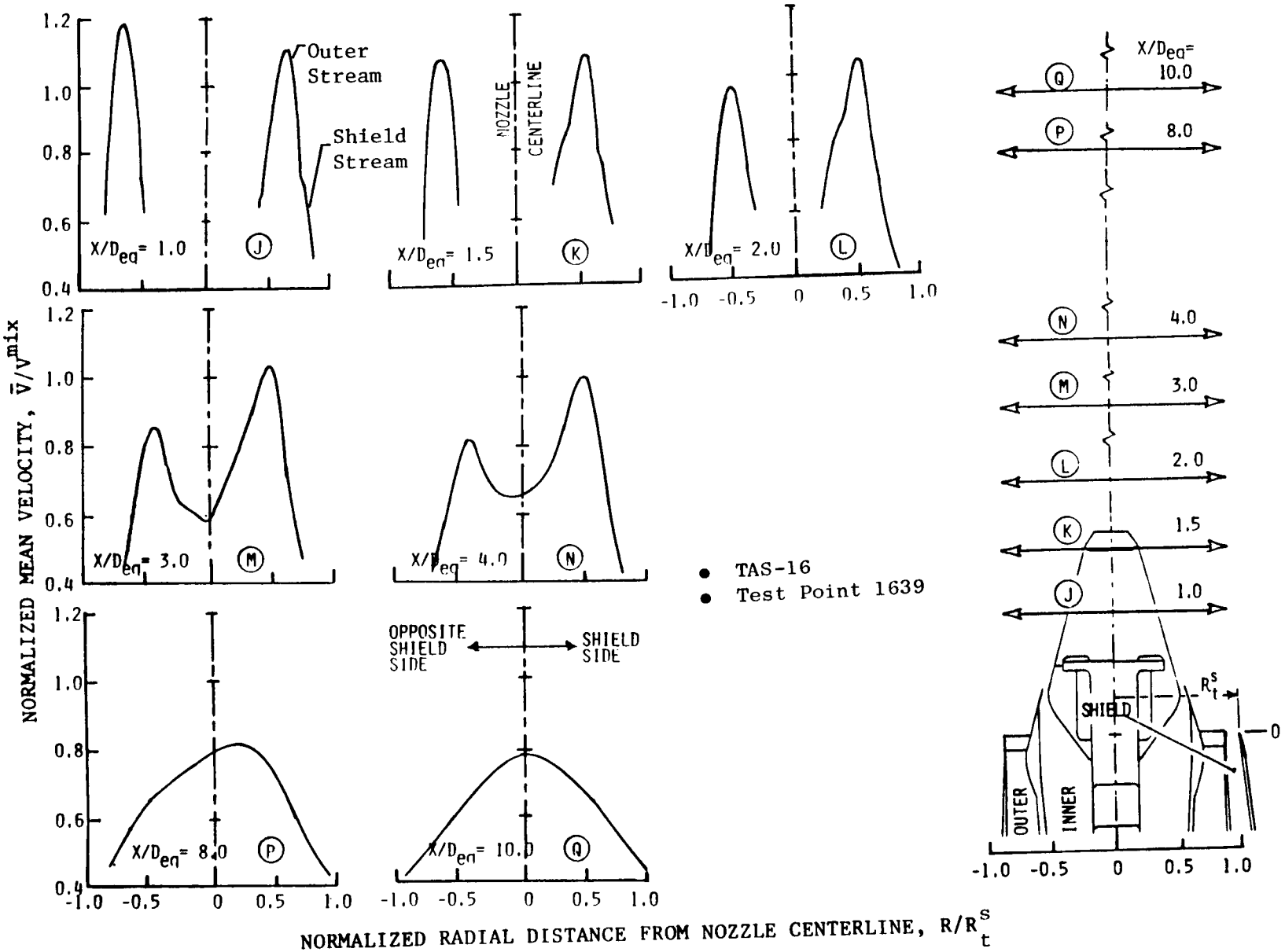

Figure 90. Radial Variation of the Mean Velocity (Axial Component) in the Plume of Suppressed Coannular Plug Nozzle with 180° Shield at Takeoff Condition (Static).

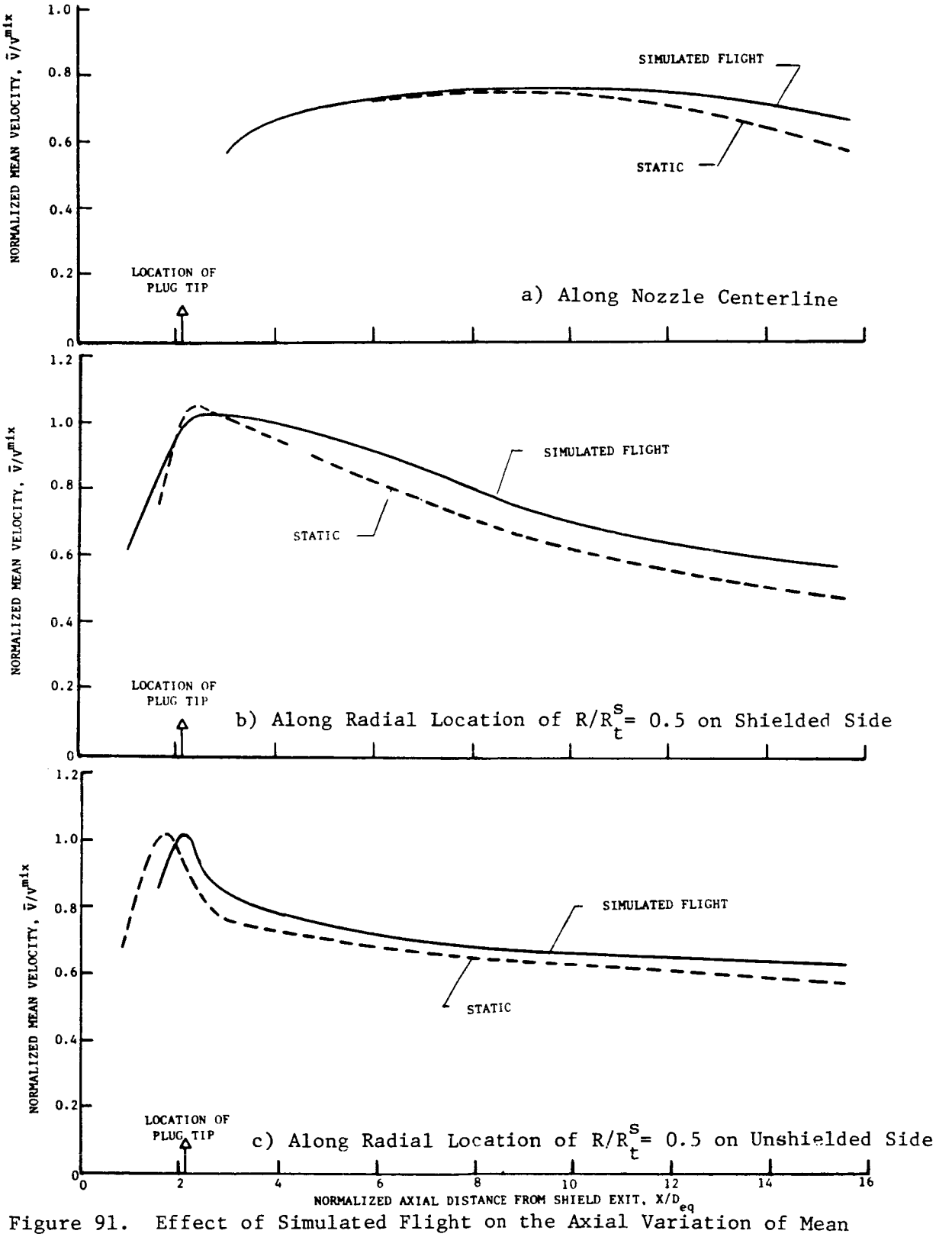

Figure 91. Effect of Simulated Flight on the Axial Variation of Mean Velocity Along Centerline and Shielded and Unshielded Sides of Suppressed Coannular Plug Nozzle with 180° Shield (TAS-16) at Takeoff Condition.

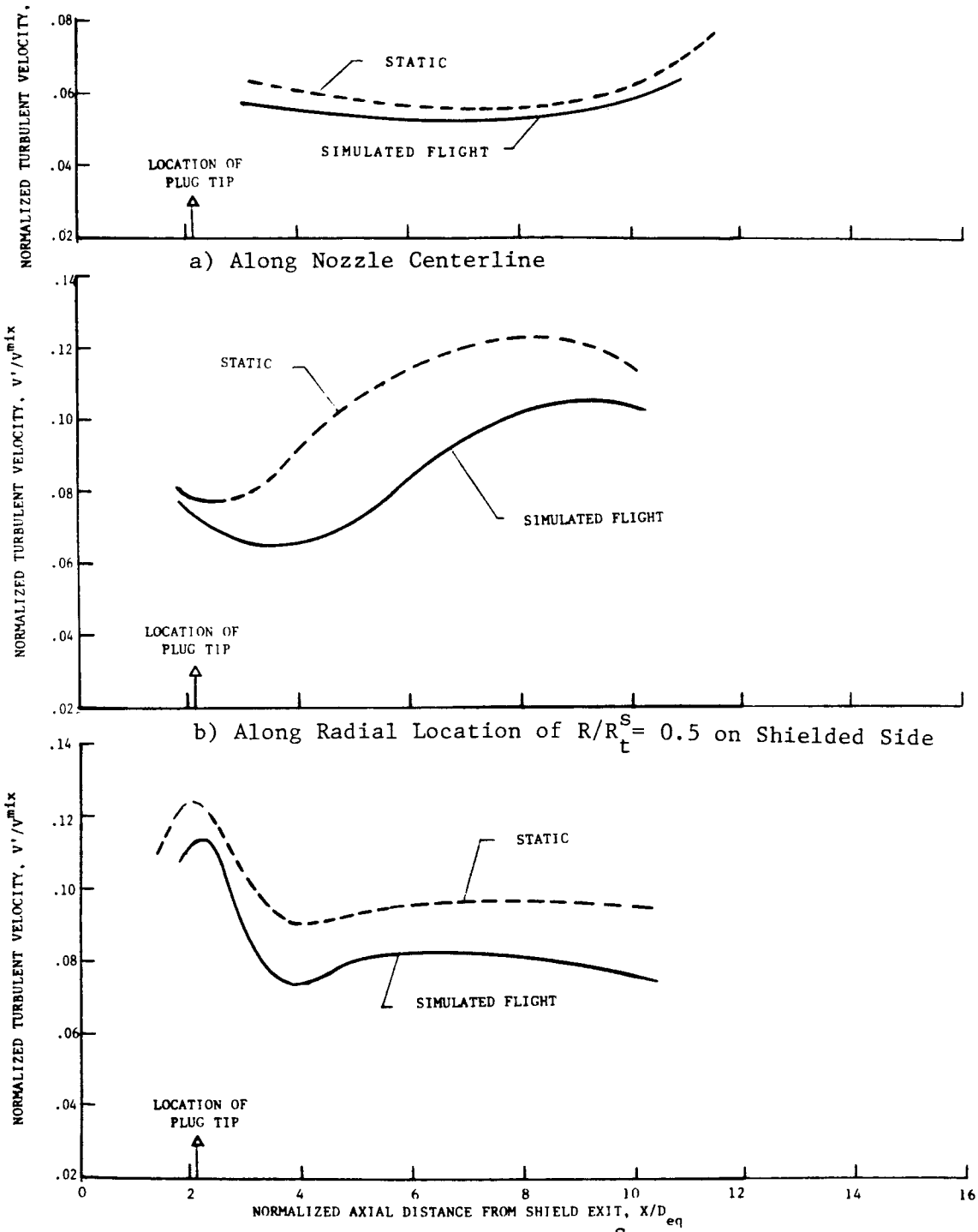

Figure 92. Effect of Simulated Flight on the Axial Variation of Turbulent Velocity on the Centerline and Shielded and Unshielded Sides of Suppressed Coannular Plug Nozzle with 180° Shield (TAS-16) at Takeoff Condition.

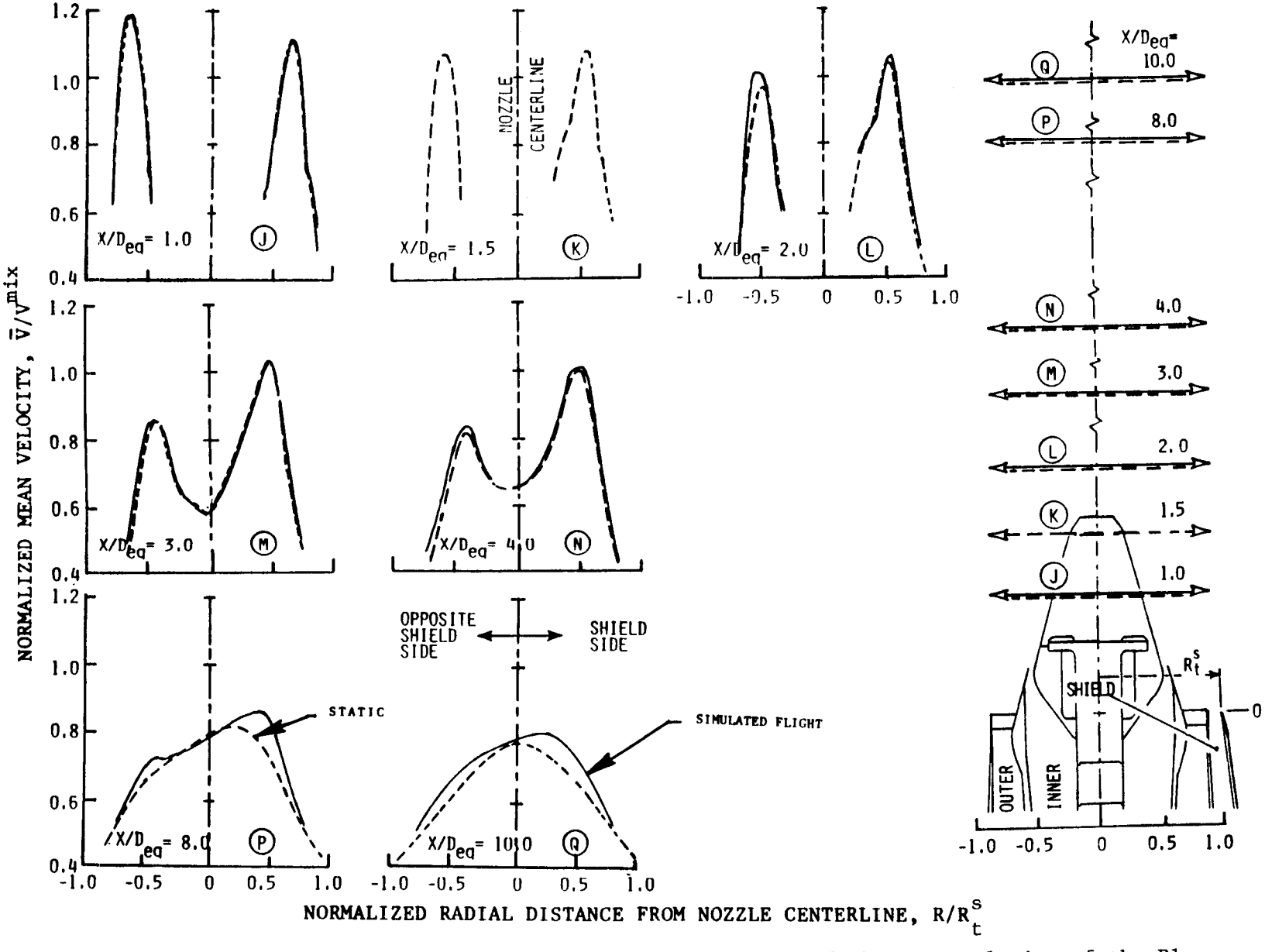

Figure 93. Effect of Simulated Flight on the Radial Variation of the Mean Velocity of the Plume of Suppressed Coannular Plug Nozzle with 180° Shield (TAS-16) at Takeoff Condition.

velocities measured during simulated flight are lower than the corresponding static data. This results in a slower decay of the jet plume and hence the observed higher mean velocity under simulated flight for any given location.

The acoustic data measured with the suppressed coannular plug nozzle with the 180° shield in community orientation were presented and discussed in detail under Section 4.2.2. Selected acoustic data from this section that correspond to the static and simulated flight LV test conditions are repeated in Figures 94 and 95 and compared with the corresponding data of the baseline suppressed coannular plug nozzle (TAS-15). The PNL-directivity data of 94 indicate a PNL reduction of 8.8 dB and 4.2 dB, respectively, at the peak noise angle of θ_i = 120° under the simulated flight and static conditions. The corresponding spectral data at θ_i = 120° presented in Figure 95 indicate that for all values of f > 250 Hz, significant reductions in sound pressure levels are observed with the shielded configuration relative to the baseline suppressed coannular plug nozzle. Also, the 180° shield effectiveness on the directivity of the various 1/3-octave-band center frequencies is presented in Figure 96. Data indicate, similarly to the shielded annular suppressor nozzle data of Figures 6 through 8, the rapid increase in noise suppression in the aft quadrant due to the shielding effect at high frequencies only. The reduction noted, particularly in the front quadrant, is due to the source alterations because of changes in the flow field characteristics by the shield flow. In addition, the stretching of the jet on the shield side due to the slower decay of the jet plume increases the low frequency noise.

4.2.6 Effect of Shield Flow on Suppressor Base Drag

The presence of the shield stream around the chutes of the mechanical suppressor is expected to reduce the base region ventilation, thereby increasing the suppressor base drag and reducing the nozzle thrust coefficient. To assess the influence of the shield stream on the suppressor base pressure from which the suppressor performance parameters can be estimated, eight static pressure taps (as pictured in Figure 21) were installed at several wall locations. Base pressure data were measured simultaneously at each of the acoustic test points of the baseline suppressed coannular plug nozzle (TAS-15) and from the suppressed coannular plug nozzles with the partial shields (TAS-16 through -18). These measurements were used to estimate a representative base pressure within the projected area of a shielded and unshielded chute, from which the change in the outer nozzle thrust coefficient resulting from the partial shield was calculated. The calculated base drag data of the 180° shielded suppressor configurations over a range of suppressor pressure ratios P_r^o and at different shield-to-outer stream velocity ratios ($V_r^{s,o}$ at typical takeoff are 0.48, 0.64, and 0.83) are compared in this section to those of the baseline suppressor nozzle to show the dependence of suppressor base drag on shield-to-outer-stream velocity ratio.

SYMBOL	CONFIG.	TEST POINT	V_{ac}	INNER STREAM P_r^i	INNER STREAM T_T^i	INNER STREAM V^i	OUTER STREAM P_r^o	OUTER STREAM T_T^o	OUTER STREAM V^o	SHIELD STREAM P_r^s	SHIELD STREAM T_T^s	SHIELD STREAM V^s	MIXED CONDITIONS P_r^{mix}	MIXED CONDITIONS T_T^{mix}	MIXED CONDITIONS V^{mix}	$V_r^{i,o}$	$V_r^{s,o}$	NF_s, dB
O	TAS-15	1509	0	2.33	900	1520	3.03	1640	2340	-	-	-	2.88	1510	2190	0.65	-	-6.8
△	TAS-16	1639	0	2.29	900	1510	3.04	1650	2340	1.53	1630	1500	2.34	1550	2010	0.65	0.64	-5.0

(T_T-°R; V- fps)

DATA SCALED TO TOTAL NOZZLE AREA OF 0.903 m^2 (1400 in^2) AND EXTRAPOLATED TO 731.5 m (2400 ft.) SIDELINE.

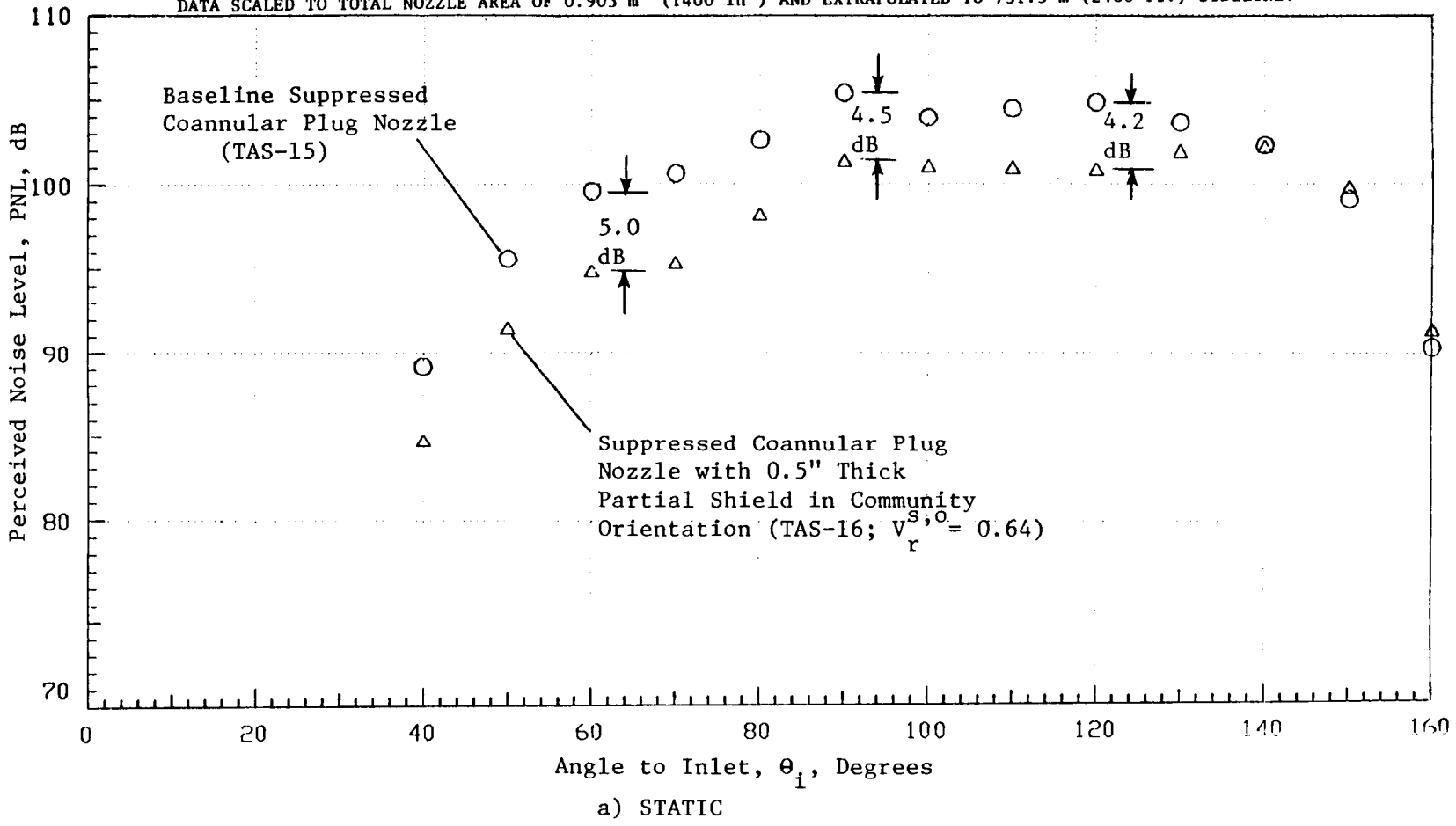

a) STATIC

ORIGINAL PAGE IS
OF POOR QUALITY

Figure 94. Effect of 180° Shield in Community Orientation on the PNL Directivity of Suppressed Coannular Plug Nozzle at LV Test Conditions.

SYMBOL	CONFIG	TEST POINT	V_{ac}	INNER STREAM P_r^i	INNER STREAM T_T^i	INNER STREAM V^i	OUTER STREAM P_r^o	OUTER STREAM T_T^o	OUTER STREAM V^o	SHIELD STREAM P_r^s	SHIELD STREAM T_T^s	SHIELD STREAM V^s	MIXED CONDITIONS P_r^{mix}	MIXED CONDITIONS T_T^{mix}	MIXED CONDITIONS V^{mix}	$V_r^{i,o}$	$V_r^{s,o}$	NF, dB
																		(T_T-°R; V- fps)
○	TAS-15	1510	400	2.32	910	1530	3.09	1640	2340	-	-	-	2.93	1520	2205	0.65	0	-6.8
△	TAS-16	1640	400	2.31	900	1520	3.07	1670	2360	1.56	1630	1540	2.36	1550	2030	0.64	0.65	-5.1

DATA SCALED TO TOTAL NOZZLE AREA OF 0.903 m^2 (1400 in^2) AND EXTRAPOLATED TO 731.5 m (2400 ft.) SIDELINE.

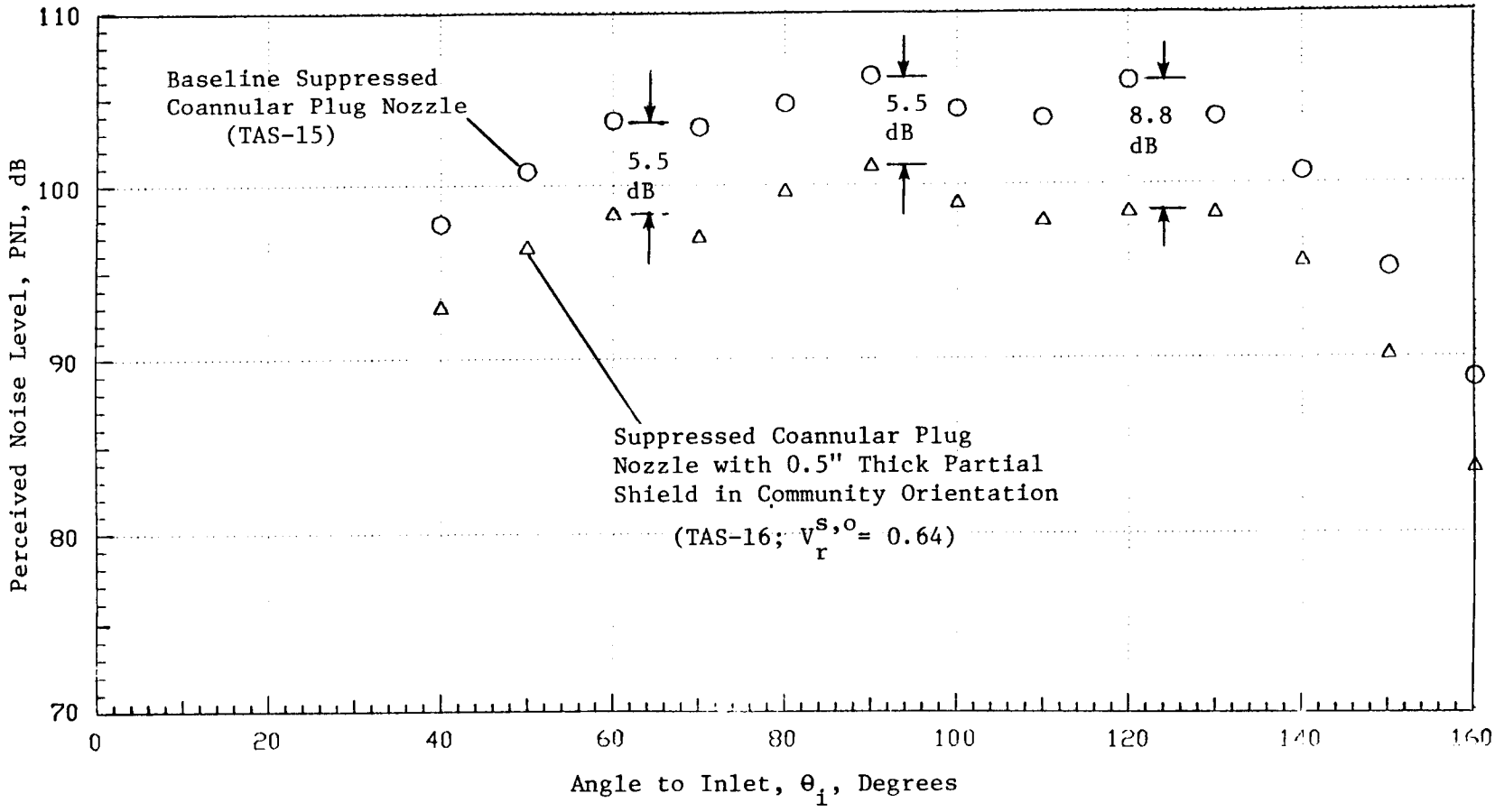

b) Simulated Flight

Figure 94. Effect of 180° Shield in Community Orientation on the PNL Directivity of Suppressed Coannular Plug Nozzle at LV Test Conditions. (Concluded)

(Refer to Figure 94 for aerodynamic conditions.)

Data Scaled to Total Nozzle Area of 0.903 m^2 (1400 in^2) and Extrapolated to 731.5 m (2400 ft.) Sideline.

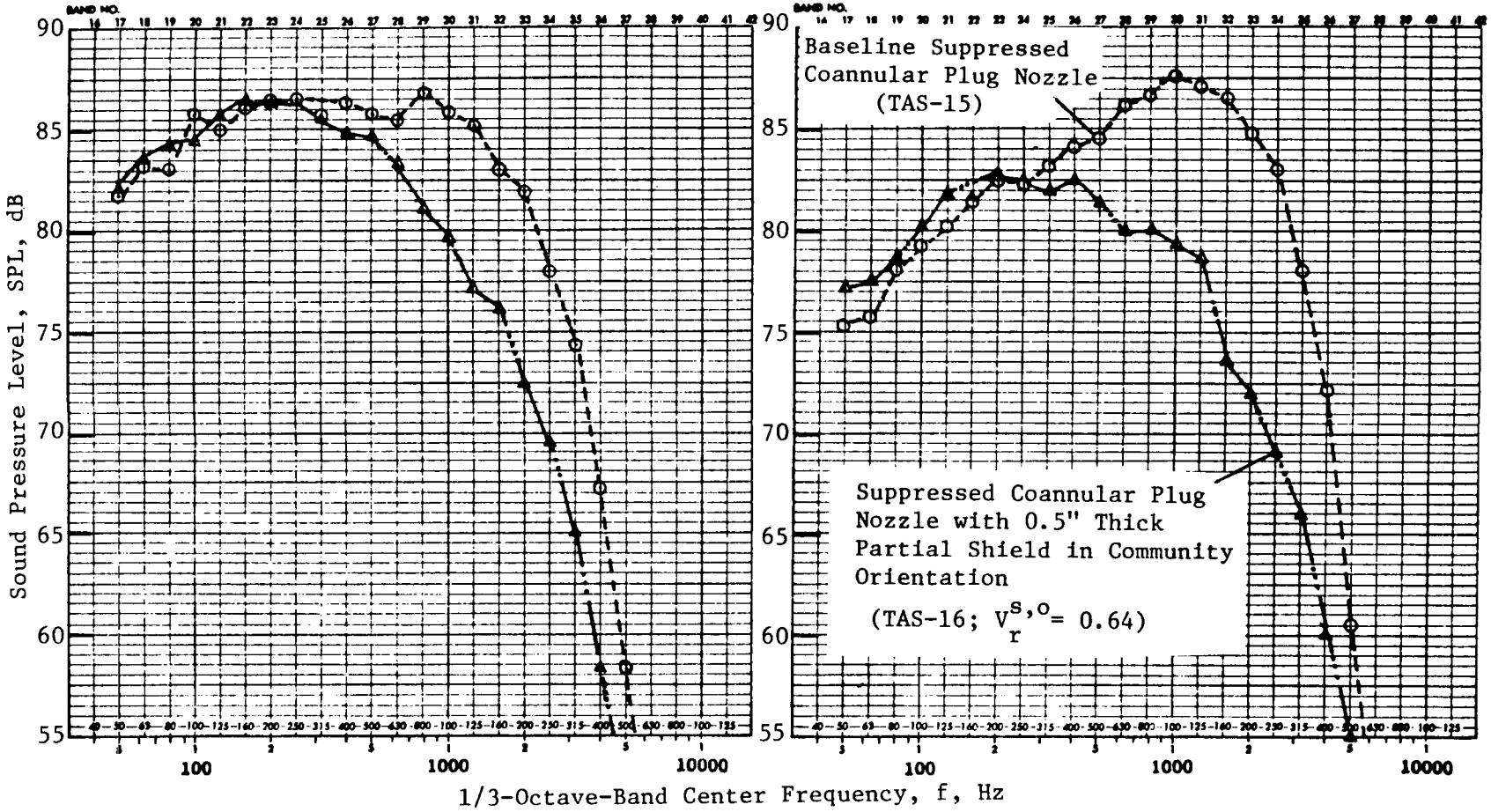

a) Static

b) Simulated Flight (V_{ac} = 400 fps)

Figure 95. Effect of 180° Shield in Community Orientation on Suppressed Coannular Plug Nozzle Spectra at θ_i = 120° at LV Test Conditions.

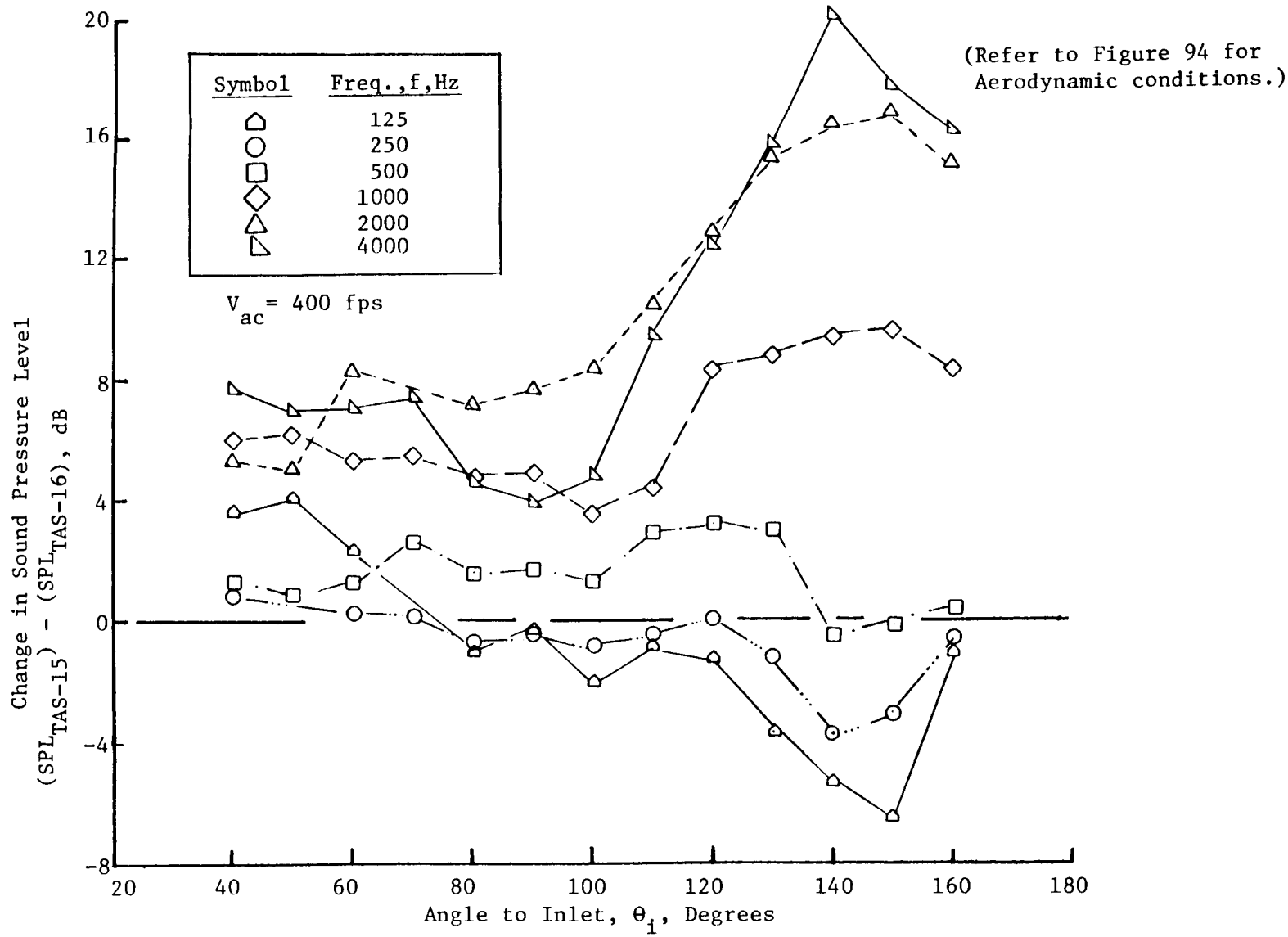

Figure 96. Influence of 180° Shield in Community Orientation on the Directivity of Various One-Third-Octave Band Frequencies of Unsuppressed Coannular Plug Nozzle at Takeoff Condition.

The locations of the eight static pressure taps in a chute region of the 20-shallow-chute suppressor nozzle are presented in Figure 97. The projected base area of each of the chutes was divided suitably into eight elements (of areas A_k defined as in Figure 97), each of which was associated with a static pressure probe. The static pressure data measured by each tap for a given nozzle condition were assumed constant over the tap's associated area. An area-weighted chute average base pressure ($\bar{P}_s$) was calculated from the measured eight static pressures $(P_s)_k$ for each of the test conditions using the following equation:

$$\bar{P}_s = \frac{\Sigma\ (P_s)_k\ A_k}{\Sigma A_k} \tag{16}$$

The base drag, F_D^{chute} associated with each of the chutes was calculated then as follows:

$$F_D^{chute} = (P_{amb} - \bar{P}_s)\ \Sigma A_k \tag{17}$$

The total base drag F_D of the 20-shallow chute suppressor nozzle (TAS-15) is given by

$$(F_D)_{TAS-15} = 20\ F_D^{chute} \tag{18}$$

For the 180° partial shielded configurations TAS-16, TAS-17, and TAS-18, the base pressure measurements were made on the shield side. On the unshield side, the base pressures are assumed to be the same as for the baseline suppressor nozzle (TAS-15) operating at identical suppressor stream conditions. The total base drag for the shielded configurations was calculated as follows:

$$\begin{matrix}(F_D)_{TAS-16} \\ TAS-17 \\ TAS-18\end{matrix} = 10\ \begin{matrix}(F_D)^{chute}_{TAS-16} \\ TAS-17 \\ TAS-18\end{matrix} + 10\ (F_D)^{chute}_{TAS-15} \tag{19}$$

The thrust loss coefficient ΔC_{fg} due to the base drag was computed finally as equal to

$$\Delta C_{fg} = \frac{F_D}{F^o} \times 100 \tag{20}$$

where $F^o = W^o V^o/g$ is the ideal thrust of the suppressor nozzle.

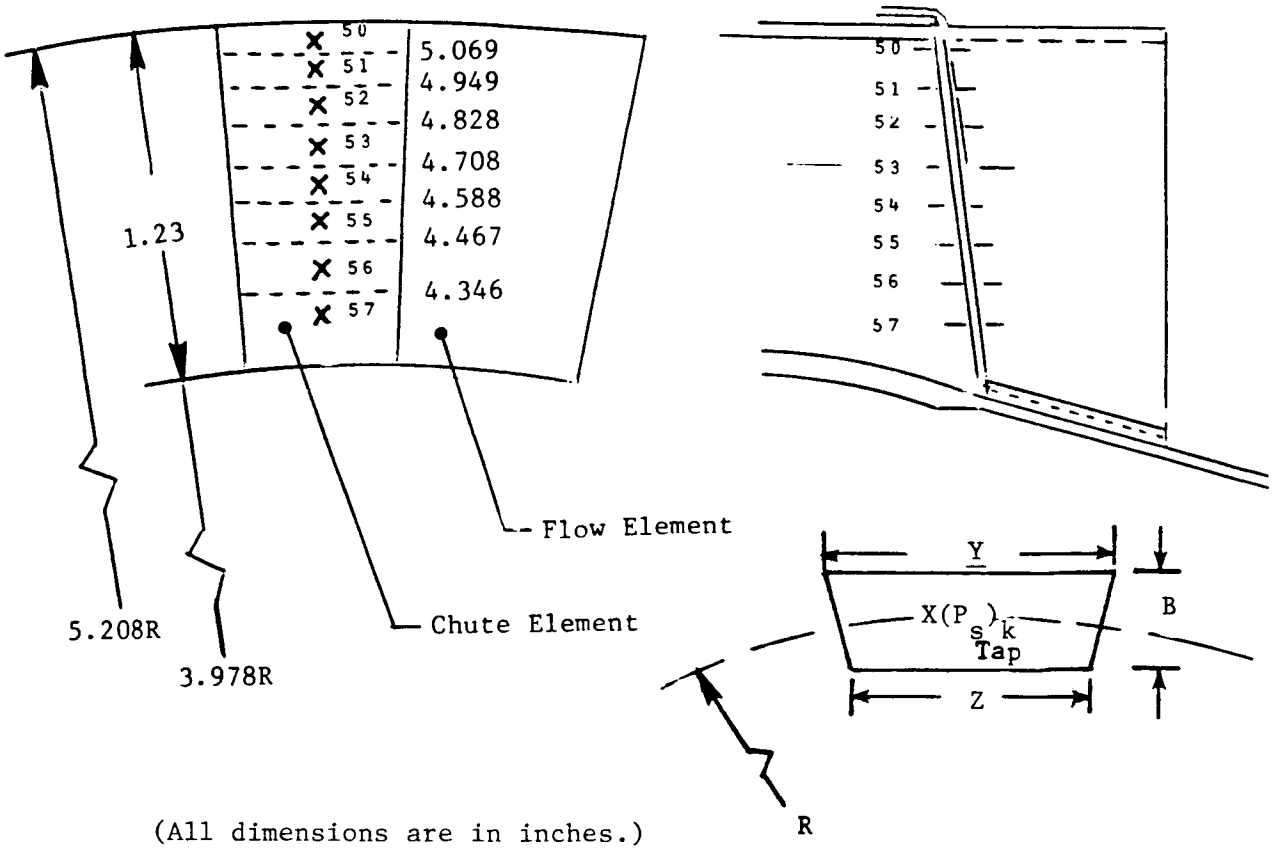

(All dimensions are in inches.)

Pressure Tap No.	Index k	R	Y	Z	B	Element (A_k) Area, In^2	A_k/A^T
Tip		5.208					
#50	1	5.129	0.692	0.678	0.139	0.0952	0.1227
#51	2	5.009	0.678	0.666	0.120	0.0806	0.1039
#52	3	4.888	0.666	0.654	0.121	0.0799	0.1030
#53	4	4.768	0.654	0.642	0.120	0.0778	0.1003
#54	5	4.648	0.642	0.630	0.120	0.0763	0.0984
#55	6	4.527	0.630	0.618	0.121	0.0755	0.0973
#56	7	4.406	0.618	0.606	0.121	0.0741	0.0955
#57	8	4.286	0.606	0.569	0.368	0.2162	0.2790
Hub		3.978					
				Total A^T	=	0.7756	1.000

Figure 97. Chute Static Pressure Probe Instrumentation and Associated Base Area Distribution.

Data that describe the dependence of the ratio of the measured average base pressure to the ambient pressure ($\bar{P}_s/P_{amb}$) upon the suppressor pressure ratio are presented in Figure 98. An examination of this figure indicates that:

a. The base pressure of an unshielded chute is not affected significantly by variation in suppressor stream pressure under both static and simulated flight conditions.

b. The base pressure of a 0.97-inch-thick shielded chute is influenced strongly by the presence of the shield flow with the ventilation decreasing rapidly in the range $2.0 < P_r^o < 3.0$.

c. For a given suppressor pressure ratio, the base ventilation decreases with an increase in the shield velocity.

d. The effect of the simulating free-jet on the baseline suppressor base pressure is similar to that of a shield flow in decreasing the base ventilation.

e. Because of the presence of the shield flow between the free jet and the chute, the free jet has no effect on the measured base pressure of the shielded chute.

The static and simulated flight measured thrust loss coefficients (ΔC_{fg}) as functions of suppressor stream pressure ratio P_r^o are shown in Figure 99. The baseline unshielded nozzle static data indicate a gradual decrease in ΔC_{fg} (in the neighborhood of 1%) with the increase in suppressor pressure ratio. Since the base pressure for the unshielded chute was found not to be affected significantly by P_r^o, this decrease is due to the increase in suppressor thrust with increase in P_r^o (see Figure 98). Also, because of the earlier noted decrease in ventilation resulting from the free jet, the base drag of the baseline suppressor increases in flight. At a typical takeoff condition, ΔC_{fg} of the baseline suppressor is 2.2%.

For the shielded configurations, the static thrust loss data of Figure 99 indicate a greater thrust loss due to the earlier observed decreased ventilation with shield flow. For the partially shielded configurations, the increase in ΔC_{fg} noted with flight is contributed by the unshielded half of the suppressor, as the base pressure on the shielded half is unaffected by the free jet.

To show the dependence of the 180° shielded suppressor thrust loss coefficient due to base drag on shield-to-outer stream velocity ratio, the data of Figure 99 are replotted in Figure 100. This figure indicates that ΔC_{fg} increases significantly with increases in shield velocity. At a simulated flight typical takeoff condition, ΔC_{fg} increases from 2.2% for the unshielded suppressor to about 4%, 5.3%, and 7.2% for the 180° shielded configuration at $V_s^{r,o}$ = 0.48, 0.64, and 0.83, respectively.

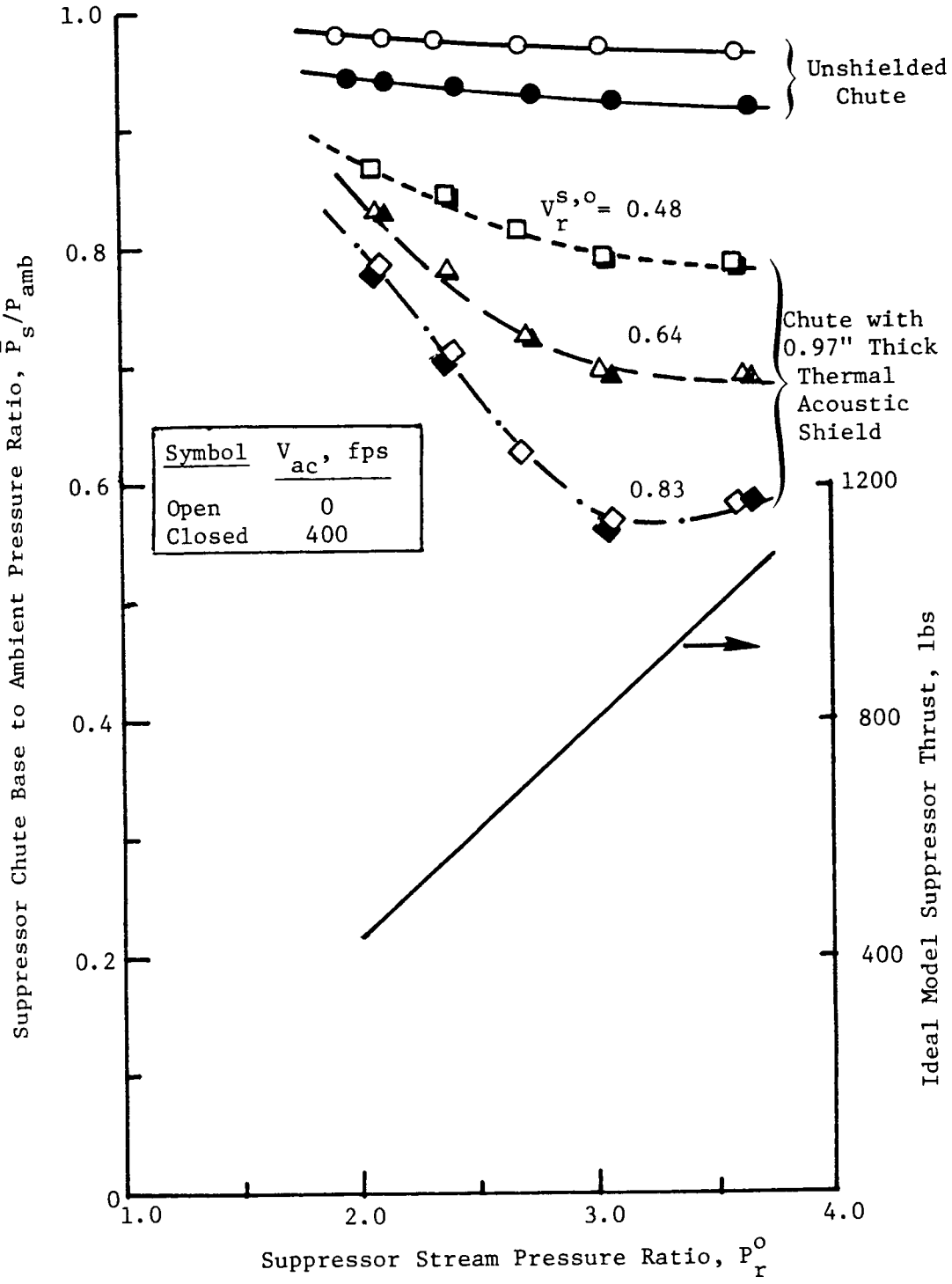

Figure 98. Effect of Shield and Free-Jet Streams on the Suppressor Base Pressure.

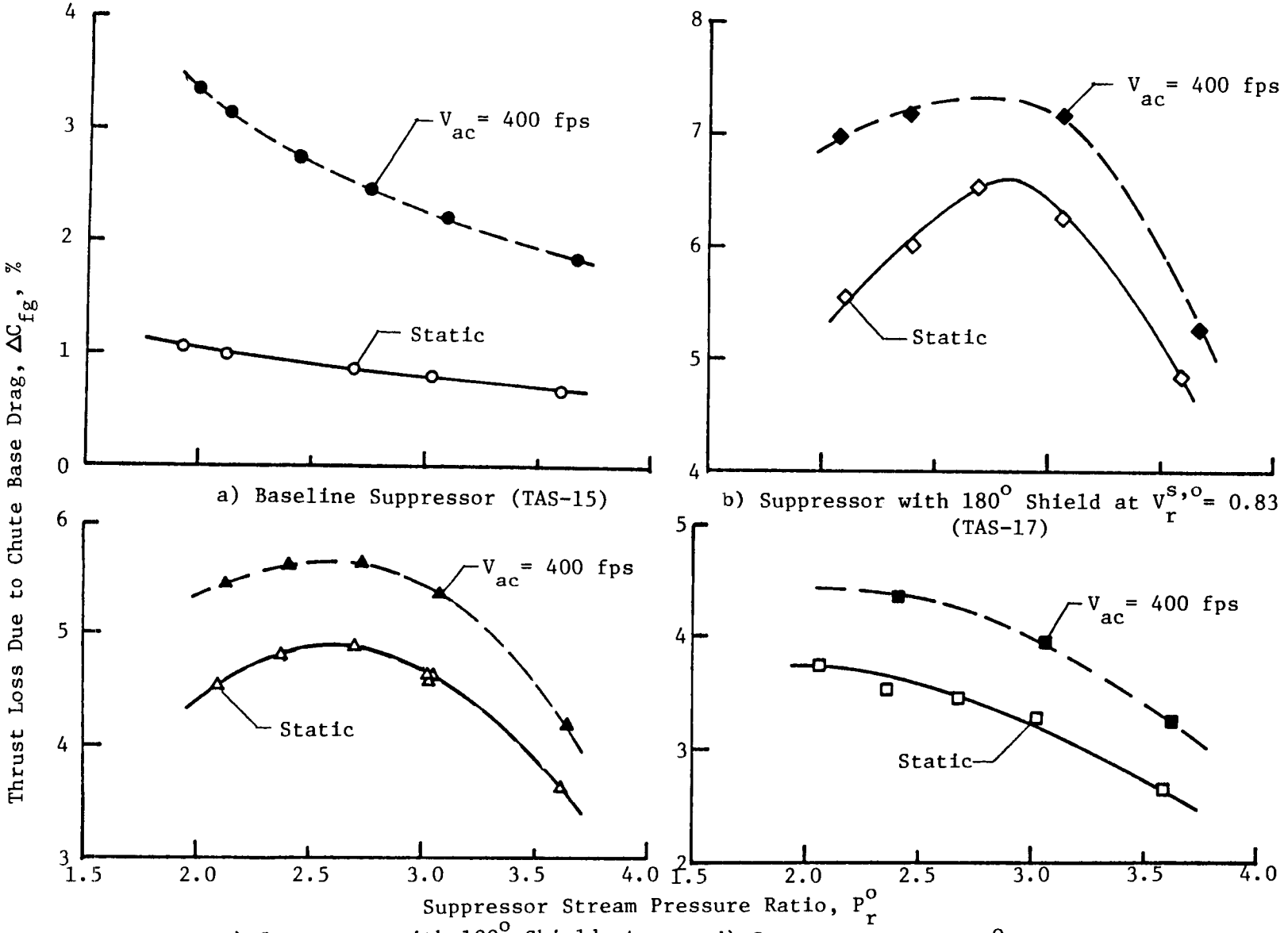

Figure 99. Thrust Loss Coefficient of 20-Shallow-Chute Suppressor Without and With 180° Thermal Acoustic Shield.

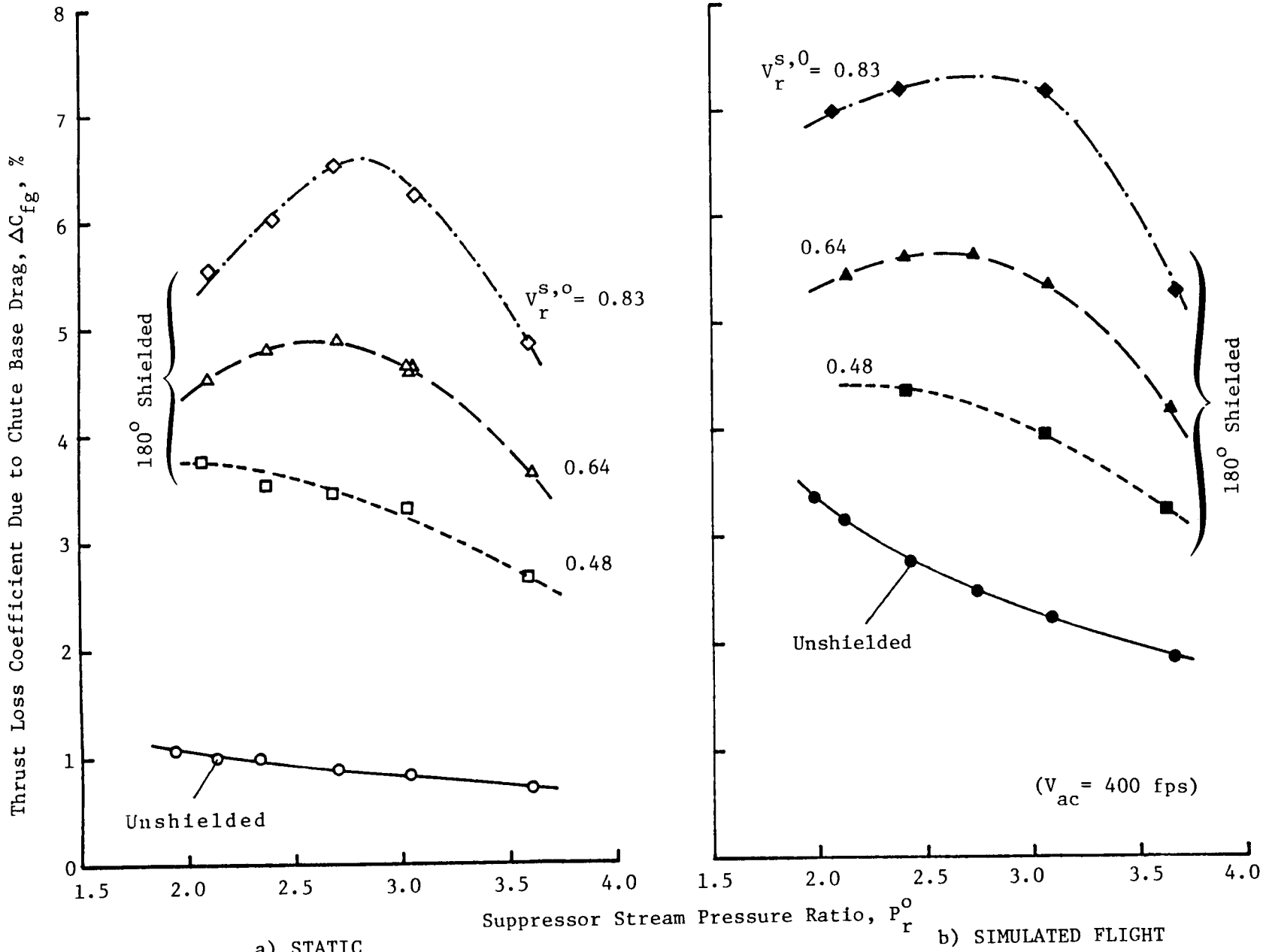

Figure 100. Comparison of Static and Simulated Flight Thrust Loss Coefficient Due to Chute Base Drag for Unshielded and 180° Shielded 20-Shallow-Chute Suppressor.

5.0 AEROACOUSTIC PREDICTIONS FOR UNSUPPRESSED COANNULAR PLUG NOZZLE WITH THERMAL ACOUSTIC SHIELDS

5.1 BACKGROUND

In addition to the measured acoustic and diagnostic data that were presented earlier in Section 4.0, the acoustic and flow field distributions for the unsuppressed coannular plug nozzle, with full and partial thermal acoustic shields, have been predicted during this study. The modified Mani*Gliebe*-Balsa (M*G*B) model (Reference 32) was used.

The M*G*B model is a unified aerodynamic and acoustic prediction method for assessing the noise characteristics of arbitrarily-shaped nozzles. The technique uses an extension of Reichardt's method to predict the jet plume velocity, temperature, and turbulence intensity distribution. The turbulent fluctuations produced in the mixing regions of the jet are assumed to be the primary source of noise generation, as in the classical theories of jet noise. The alteration of the generated noise by the jet plume itself as it propagates through the jet to the far-field observer (sound/flow interaction or fluid shielding) is modeled using the high-frequency shielding theory based on Lilley's equation.

These basic modeling elements (flow field prediction, turbulent mixing noise generation, and sound/flow interaction) have been linked together in a discrete volume-element formulation. The jet plume is divided into elemental volumes, each roughly the size of a representative turbulence correlation volume appropriate to that particular location in the plume. Each volume element is assigned its own characteristic frequency, spectrum, and acoustic intensity. The sound/flow interaction effects for each element are evaluated from the flow environment of the element. The individual volume elements are assumed to be uncorrelated to each other, so that the total contribution to the far-field is the sum of the individual volume element contributions.

As noted earlier, the M*G*B model predicts the flow field and turbulent mixing noise generation for arbitrary nozzle shapes and azimuthally averages the flow field and noise source characteristics to predict the far-field noise distribution. During the single-flow study of this program (Reference 12), the measured acoustic and flow field data of an annular plug nozzle with a partial shield indicated, as expected, azimuthally asymmetric characteristics. Hence, the acoustic modeling of Reference 32 was modified appropriately in Reference 12 to reflect the asymmetric acoustics and flow field of the partial thermal acoustic shielded configurations. The predictions were compared in Reference 12 to the measured acoustic data. The chosen predicted and measured data comparisons indicated good spectral agreement in the front quadrant and similar trends in the aft quadrant. During this investigation, the modified M*G*B model in Reference 12 was used to predict the acoustic and flow field characteristics of an unsuppressed coannular plug nozzle with partial and full thermal acoustic shields. Selected data-theory comparisons of the acoustic

and flow field (mean and turbulent velocity distributions) characteristics are presented in this section. Since the laser velocimeter data were obtained for the unsuppressed coannular plug nozzle with partial shield (see Sections 3.2 and 4.1.5), the flow-field data-theory comparisons are limited to the case of the partially shielded configurations.

5.2 DATA-THEORY COMPARISONS OF FLOW-FIELD AND SUPPRESSION CHARACTERISTICS

Figure 101 specifies the nodal geometry for the baseline unsuppressed coannular plug nozzle (TAS-10), unsuppressed coannular plug nozzle with 180° shield of 0.97-inch thickness (TAS-11), and unsuppressed coannular plug nozzle with 360° shield of 0.47-inch thickness (TAS-14) that were used in performing the predictions. One node is enough to prescribe an axisymmetric flow, whereas a large number of nodes are needed to prescribe the asymmetric flow of the 180° shield configuration (TAS-11). The prescription of nodes for the 180° shield jet is such that a closed surface is represented by the distribution of the nodes.

The following comparisons of data and theory are presented and discussed in this subsection:

a. Change in sound pressure level (ΔSPL) at three angles to the inlet axis due to the partial and full shields on the unsuppressed coannular plug nozzle at tyical takeoff cycle conditions.

b. Change in sound pressure level (ΔSPL) at a typical aft-quadrant observer angle (where the influence of the thermal acoustic shield is maximum), for typical approach and cutback cycle conditions.

c. Axial distribution of mean and turbulent velocities on the shield and unshielded side of the unsuppressed coannular plug nozzle with 180° shield for typical takeoff cycle conditions.

Figure 102 compares the measured and predicted ΔSPL spectra between the unshielded and partially shielded (that is, $\Delta SPL = (SPL)_{TAS-10} - (SPL)_{TAS-11}$) unsuppressed coannular plug nozzle for a typical takeoff cycle for the static condition and at θ_i = 130°, 90°, and 60°. The observer is located right under the partial shield, at the community location (see Figure 101b). A positive value for ΔSPL represents noise suppression by the shield and a negative value for ΔSPL represents amplification of the noise by the shield. All the comparisons in this section are performed using the scale model data measured at a radial distance of 40 feet (12.3 m). The frequencies in this study ranged from 400 Hz to 80 kHz.

Both the measured and predicted ΔSPL at θ_i = 130° (see Figure 102a) indicate that suppression by shield increases as frequency increases. The predicted ΔSPL's are higher than the measured ΔSPL's, indicating that the theoretical model is overestimating the shielding offered by the partial shield.

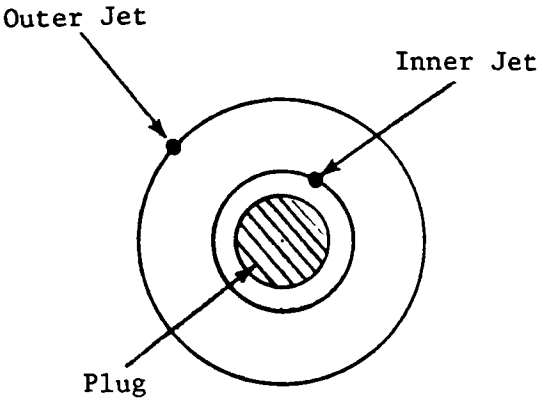

a. Unsuppressed Coannular Plug Nozzle (TAS-10)

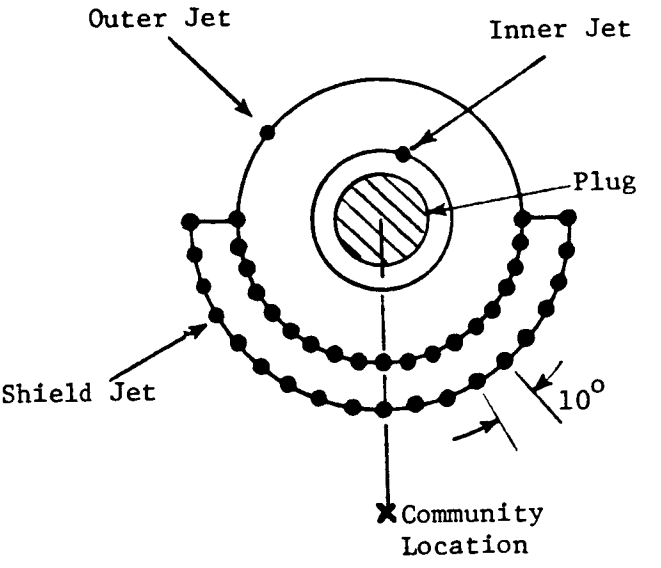

b. Unsuppressed Coannular Plug Nozzle with Partial (180°) Thermal Acoustic Shield (TAS-11)

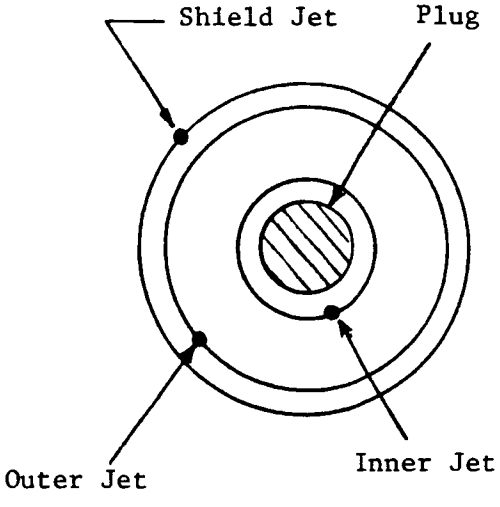

c. Unsuppressed Coannular Plug Nozzle with Full (360°) Thermal Acoustic Shield (TAS-14)

Figure 101. Nodal Geometry for Configurations TAS-10, TAS-11, and TAS-14 for M*G*B Predictions.

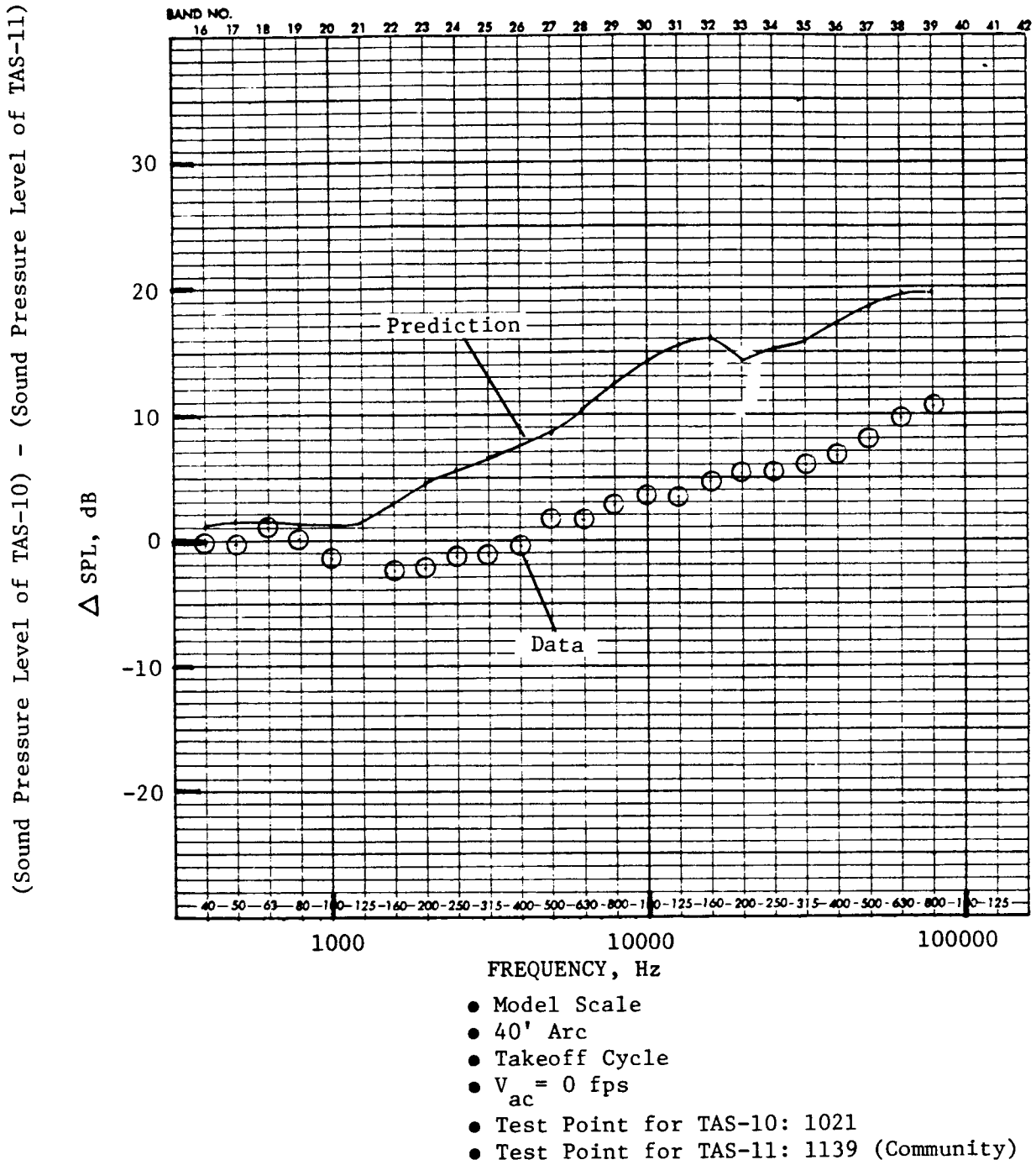

a) At Angle to Inlet Axis $\theta_i = 130^o$

Figure 102. Comparison of the Measured and Predicted ΔSPL Between the Unshielded (TAS-10) and Shielded (TAS-11) Configurations for the Unsuppressed Coannular Plug Nozzle (Static).

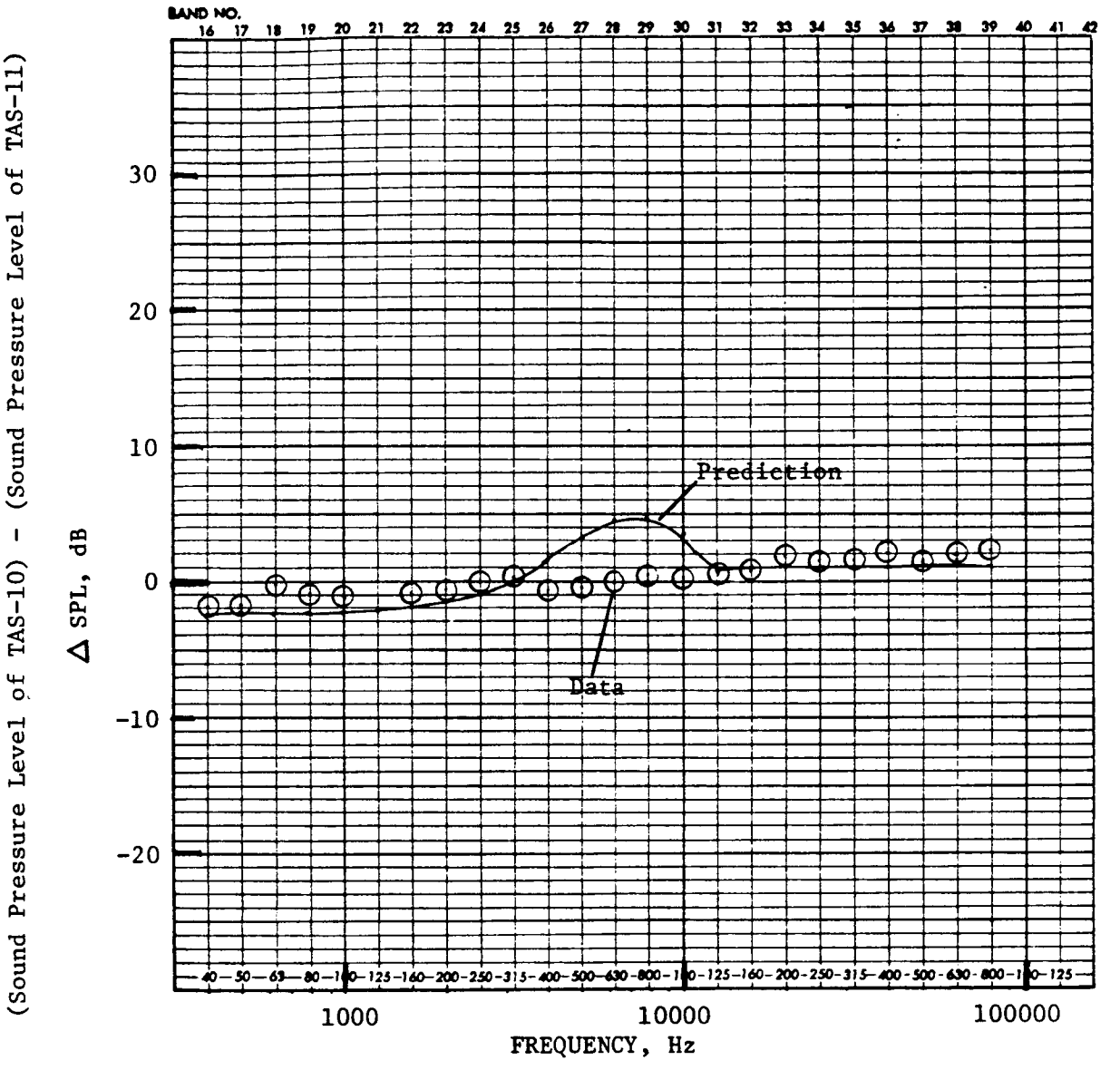

- Model Scale
- 40' Arc
- Takeoff Cycle
- V_{ac} = 0 fps
- Test Point for TAS-10: 1021
- Test Point for TAS-11: 1139 (Community)

b) At Angle to Inlet Axis $\theta_i = 90^o$

Figure 102. Comparison of the Measured and Predicted ΔSPL Between the Unshielded (TAS-10) and Shielded (TAS-11) Configurations for the Unsuppressed Coannular Plug Nozzle (Static). (Continued)

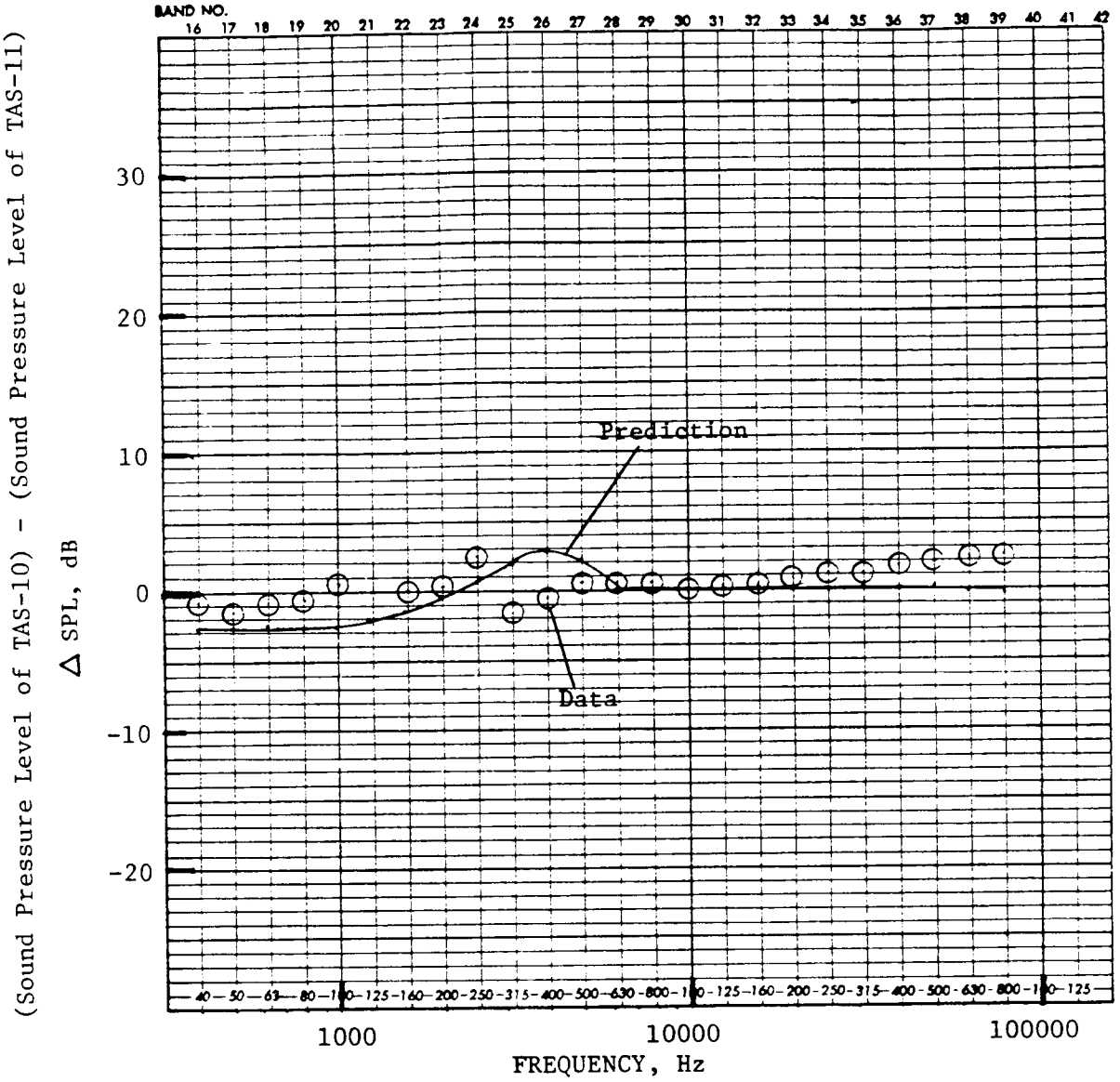

- Model Scale
- 40' Arc
- Takeoff Cycle
- V_{ac} = 0 fps
- Test Point for TAS-10: 1021
- Test Point for TAS-11: 1139 (Community)

c) At Angle to Inlet Axis $\theta_i = 60^{\circ}$

Figure 102. Comparison of the Measured and Predicted ΔSPL Between the Unshielded (TAS-10) and Shielded (TAS-11) Configurations for the Unsuppressed Coannular Plug Nozzle (Static). (Concluded)

A similar observation was made in Reference 12 with the data of annular flow nozzles with partial thermal acoustic shield. This is probably because local jet velocity and static temperature along the line of sight of the observer (which vary azimuthally for the partial shield case) are used in calculating the fluid shielding effect. This approach neglects the scattering of the sound by the turbulent eddies along the line of sight. If one were to use a ray tube of a certain finite thickness with the dominant direction along the line of sight instead of using a line of sight approach in the calculation of the fluid shielding, the scattering effect would be included in some fashion. However, this is beyond the scope of the present study.

The agreement between measured and predicted ΔSPL at $\theta_i = 90°$ is quite reasonable at low and high frequencies (see Figure 102b). At $\theta_i = 90°$, eddy convective amplification and fluid shrouding effects are very small. The discrepancy between the scale model data and predictions in the frequency range of 4 kHz to 10 kHz is attributed to the overprediction of shock cell noise. For a better agreement between the measured and predicted ΔSPL in this region, the shock cell noise computation scheme in the M*G*B model, which currently employs one downstream shock-cell structure, will have to be changed to account for the two-shock-cell structures (on the plug and downstream of the plug) that were identified with coannular plug nozzles (Reference 24).

Figure 102c shows the measured and predicted ΔSPL variables at front quadrant angle of $\theta_i = 60°$. As observed with data at $\theta_i = 90°$, the agreement between the measured and predicted ΔSPL is acceptable at all frequencies except in the region that is dominated by the shock cell noise.

The low frequency data at all three of the observer angles show amplification by the partial shield. However, low frequency amplification by the shield is predicted only at $\theta_i = 60°$ and 90°. In order to determine a reason for this amplification, the measured and predicted axial variations of the mean and turbulent velocities on the shield side and the opposite shield side of TAS-11 are compared in Figures 103 and 104. The velocity measurements made on the opposite shield side of TAS-11 can be assumed to be representative of the velocity measurements for the baseline unsuppressed coannular plug nozzle without any shield (TAS-10), since the edge effects due to the partial shield are not felt at the opposite-to-community location (see Reference 12 for a prediction of the azimuthal variation in the velocity field of an annular plug nozzle with partial shield). Both the data and predictions of the mean velocity (Figure 103) indicate higher levels of mean velocity on the shield side than on the unshield side. Also, both the data and predictions show a sudden dip in the mean velocity near the location of the plug tip. In addition, the data indicate that the azimuthal asymmetry becomes negligible for $X/D_{eq} \geq 8$. However, the predictions indicate a slower decay of the asymmetry, resulting in a higher mean velocity on the shield side due to the reduction in shear stress and, hence, a reduction in the velocity gradient by the shield. The low frequency noise of a jet is created by the large scale eddies situated far downstream of the nozzle exit plane. Since the downstream mean velocity on the shield side is higher than that on the opposite shield side (which resembles the case of nozzle without shield), the low frequency noise of the shielded

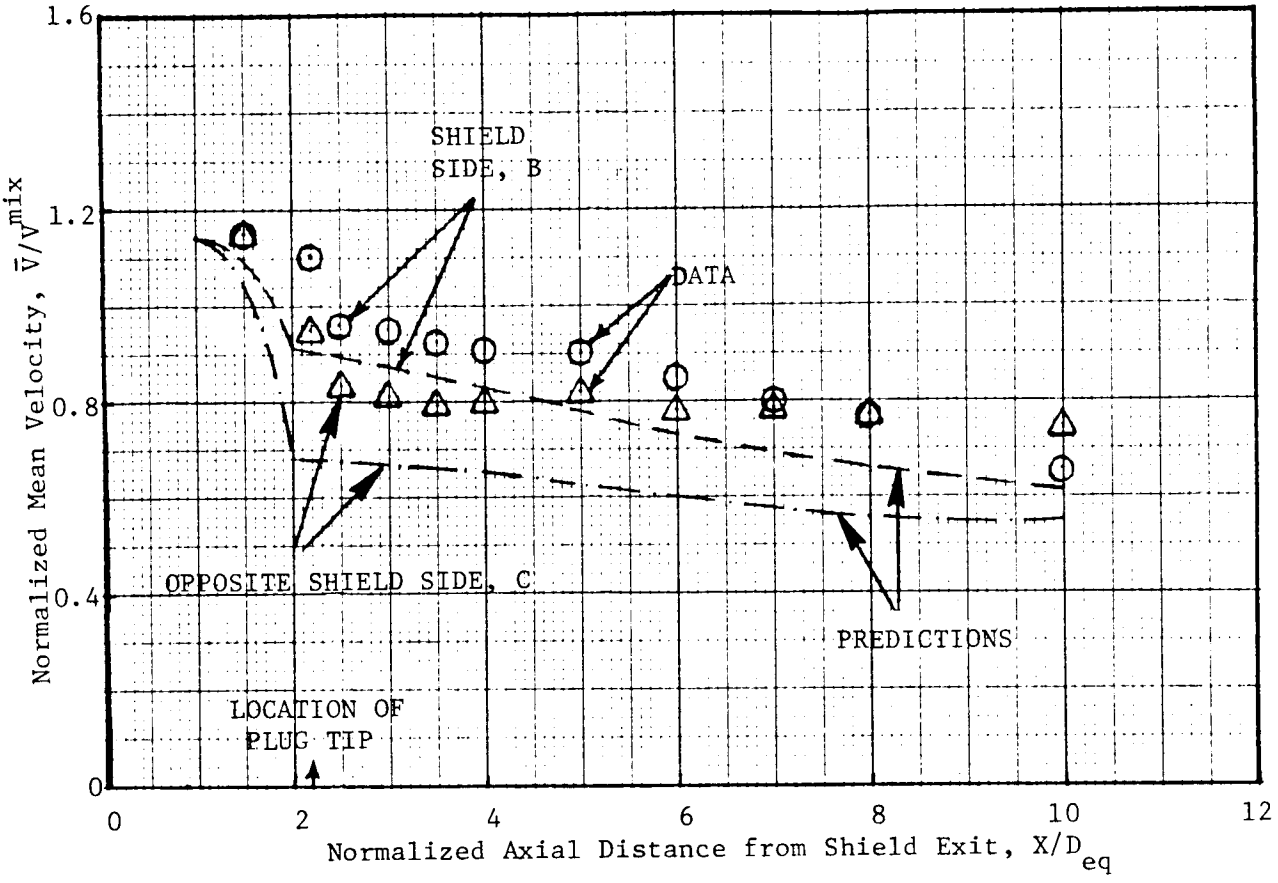

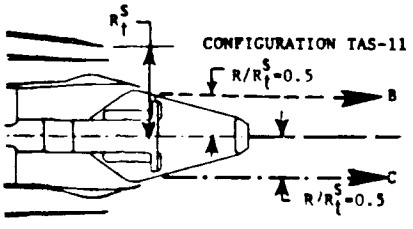

V_{ac} = 0 ft/s

LV PLUME 1: TEST POINT 1139

STREAM	P_T	T_T(°R)	V, fps
INNER	2.28	905	1512
OUTER	3.01	1632	2314
SHIELD	1.49	1617	1447
MIXED	2.36	1533	2011

Figure 103. Comparison of the Predicted and Measured Axial Variation of the Mean Velocity on Shield and Opposite Shield Side for Unsuppressed Coannular Plug Nozzle with Partial Shield.

configuration is expected to be higher than that of the configuration without the shield. Figure 104 shows the axial variation of the measured and predicted turbulent velocities on the shield side and opposite shield side for the unsuppressed coannular plug nozzle with partial shield (TAS-11). For $X/D_{eq} \leq 4$, both the predictions and the data indicate that the turbulent velocities on the shield side are lower than those on the opposite shield side. The measured and predicted values of the turbulent velocities for $X/D_{eq} \approx 2$ to 3 disagree because there is a separated flow downstream of the truncated plug that is not accounted for in the model of the prediction scheme. However, in general, both the predic tions and data indicate that the turbulent velocities on the shield side are higher and lower compared to those on the opposite shield side for $X/D_{eq} > 4$ and $X/D_{eq} \leq 4$, respectively. The lower values of the turbulent velocities on the shield side near the nozzle exit plane are essentially due to the reduced shearing stresses on the shield side. For large values of X/D_{eq}, the shield side flow is found to be more turbulent.

The above presented aerodynamic picture of the flow field of the unsuppressed coannular plug nozzle with partial shield (TAS-11) offers an explanation for the observed amplification of low frequency noise by the shield. The data at all three observer angles (θ_i = 60°, 90°, and 130°) indicated low frequency noise amplification by the shield. The earlier predictions indicated such amplification only at θ_i = 60° and 90°, see Figure 102. Low frequency noise amplification at θ_i = 130° in the predicted data was absent because it was overcome by the excess fluid shielding in the model.

Acoustic data-theory comparisons under simulated flight conditions corresponding to the static takeoff results of Figure 102 are presented in Figure 105. As before, comparisons of the measured and predicted ΔSPL spectra are provided at θ_i = 130°, 90°, and 60° for the simulated flight case. As noted with the static data at θ_i = 130° (Figure 102), the predicted and measured noise suppression due to the shield generally increases with frequency. At this location, both the data and predictions indicate amplification of the low frequency noise by the shield. The agreement between the measured and predicted ΔSPL at θ_i = 90° and 60°, see Figures 105b and 105c respectively, is quite reasonable at low and high frequencies. Disagreements are due to the inadequate modeling of the shock cell noise.

The comparison of the predicted and measured axial variation of the mean and turbulent velocities on the shield and opposite shield sides of the unsuppressed coannular plug nozzle with partial shield, for the simulated flight case and at a tyical takeoff cycle is shown in Figures 106 and 107, respectively. As in the static case (see Figure 103), the mean velocities on the shield side are measured and predicted to be higher than the corresponding mean velocities on the opposite shield side. This is due to a reduction in the velocity gradient in the radial direction on the shield side compared to the side opposite the shield. The turbulent velocity on the shield side is predicted to be lower than that on the opposite shield side for $X/D_{eq} < 5$ and higher than that on the opposite shield side for $X/D_{eq} > 5$. The measured turbulent velocities on the shield side are lower and higher than those on opposite shield side for $X/D_{eq} < 7$ and $X/D_{eq} > 7$, respectively. These trends

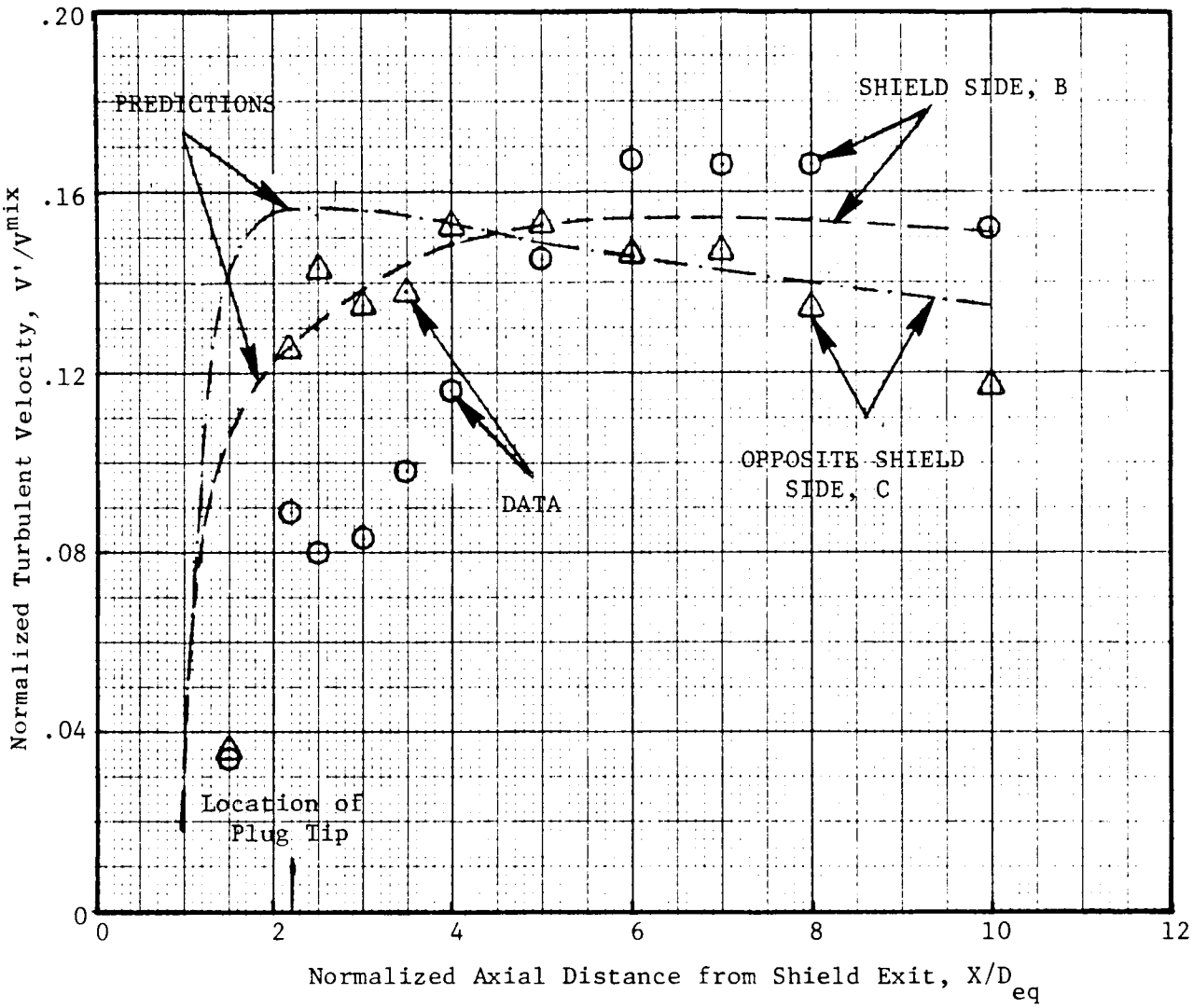

LV PLUME 1: TEST POINT 1139

STREAM	P_r	T_T(°R)	V, fps
INNER	2.28	905	1512
OUTER	3.01	1632	2314
SHIELD	1.49	1617	1447 -
MIXED	2.36	1533	2011 .

V_{ac} = 0 ft/s

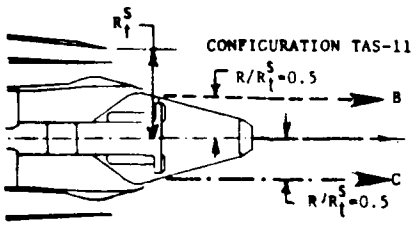

Figure 104. Comparison of the Predicted and Measured Axial Variation of the Turbulent Velocity on Shield and Opposite Shield Side for Unsuppressed Coannular Plug Nozzle with Partial Shield.

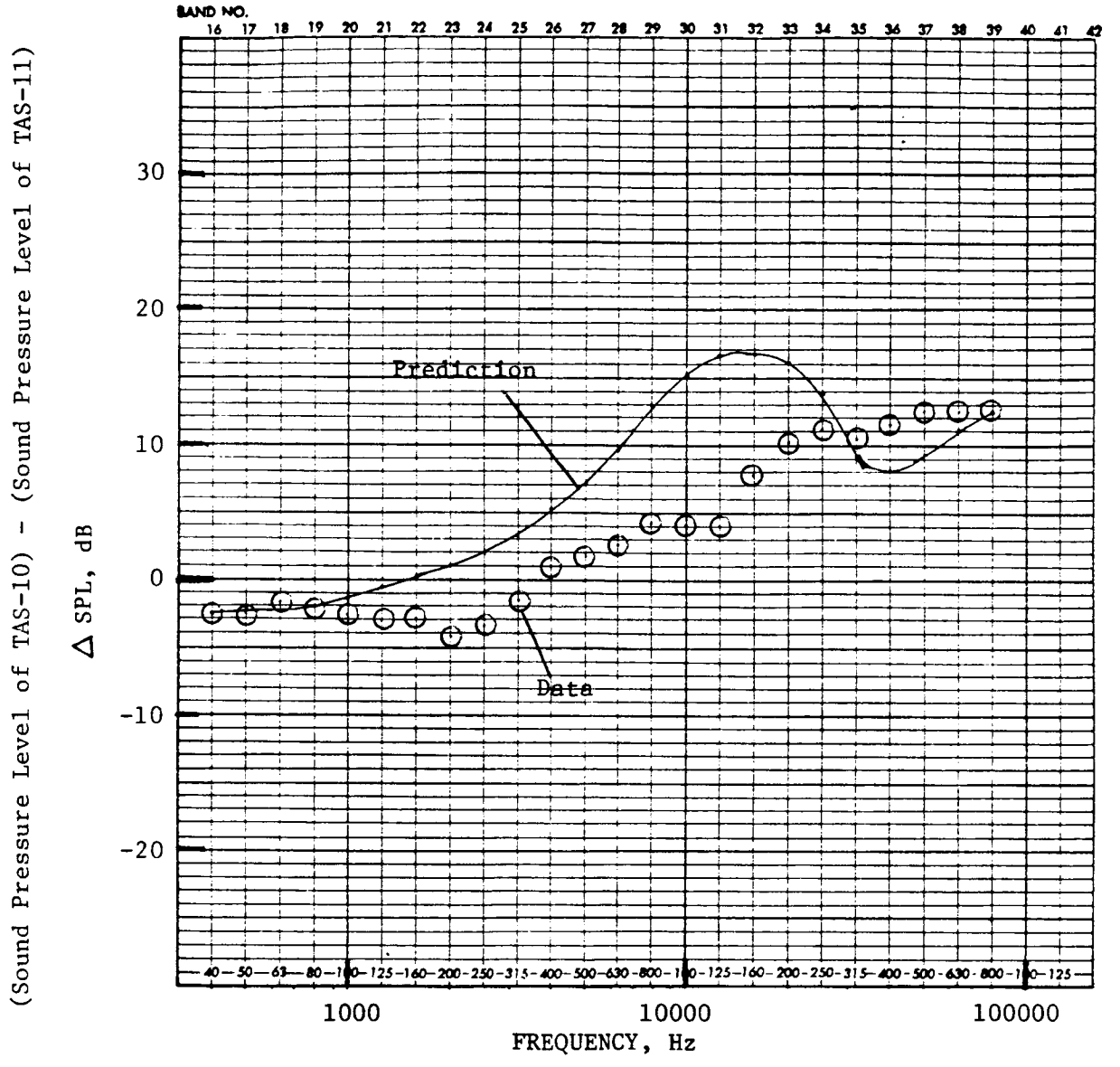

- Model Scale
- 40' Arc
- Takeoff Cycle
- V_{ac} = 400 fps
- Test Point for TAS-10: 1022
- Test Point for TAS-11: 1140 (Community)

a) At Angle to Inlet Axis $\theta_i = 130^o$

Figure 105. Comparison of the Measured and Predicted ΔSPL Between the Unshielded (TAS-10) and Shielded (TAS-11) Configurations for the Unsuppressed Coannular Plug Nozzle (Simulated Flight).

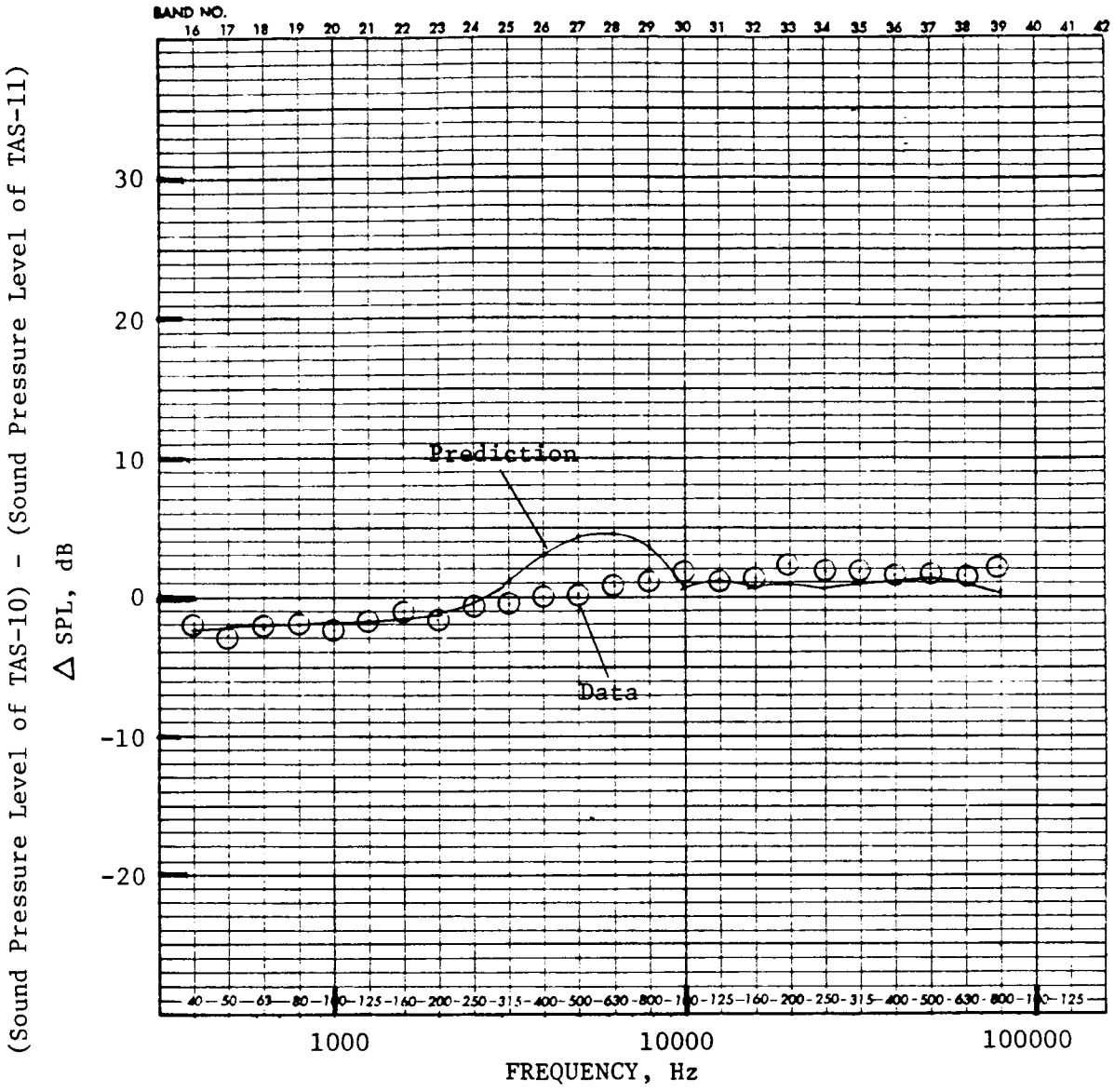

- Model Scale
- 40' Arc
- Takeoff Cycle
- V_{ac} = 400 fps
- Test Point for TAS-10: 1022
- Test Point for TAS-11: 1140 (Community)

b) At Angle to Inlet Axis $\theta_i = 90^\circ$

Figure 105. Comparison of the Measured and Predicted ΔSPL Between the Unshielded (TAS-10) and Shielded (TAS-11) Configurations for the Unsuppressed Coannular Plug Nozzle (Simulated Flight). (Continued)

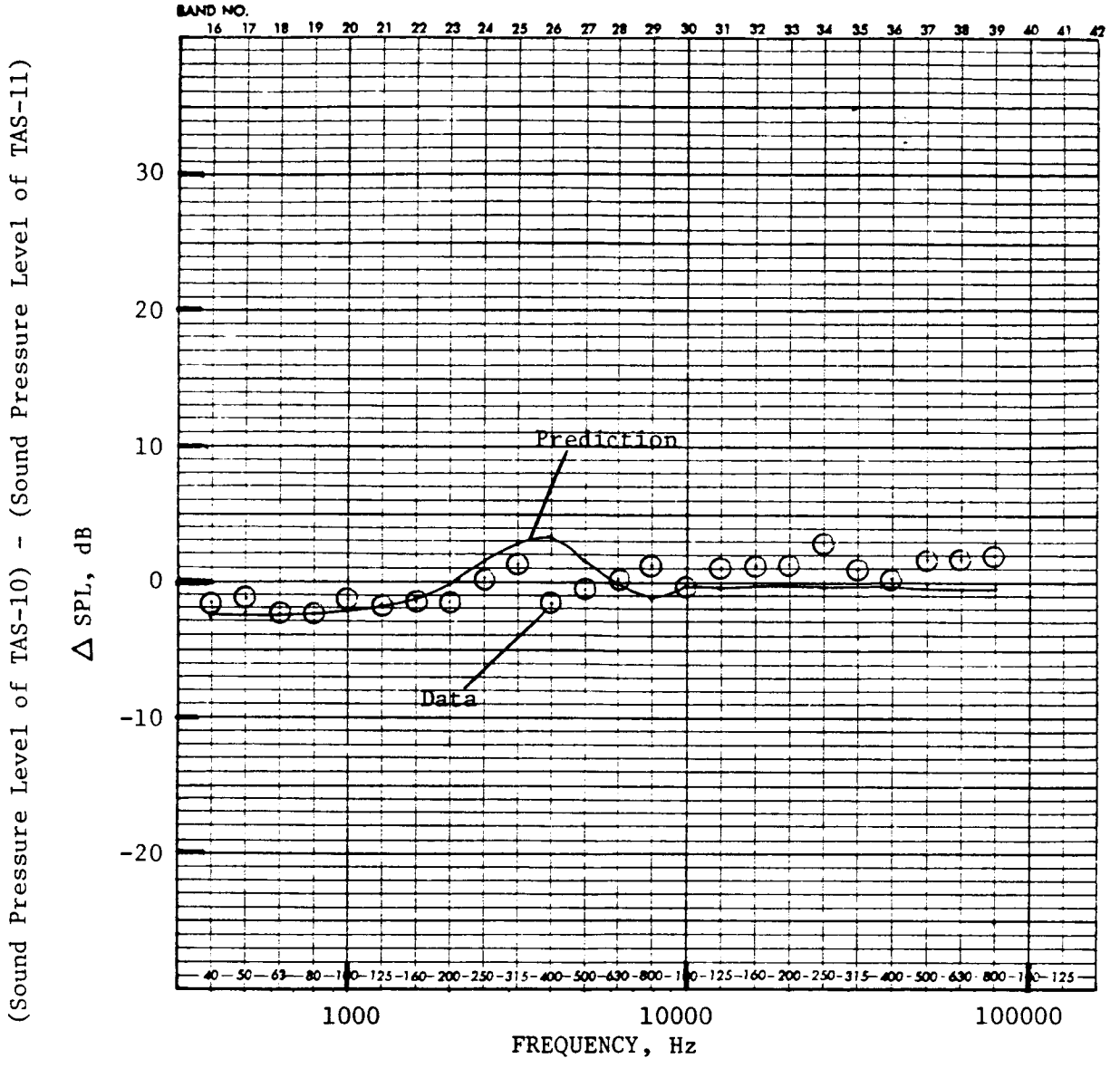

- Model Scale
- 40' Arc
- Takeoff Cycle
- V_{ac} = 400 fps
- Test Point for TAS-10: 1022
- Test Point for TAS-11: 1140 (Community)

c) At Angle to Inlet Axis $\theta_i = 60^\circ$

Figure 105. Comparison of the Measured and Predicted ΔSPL Between the Unshielded (TAS-10) and Shielded (TAS-11) Configurations for the Unsuppressed Coannular Plug Nozzle (Simulated Flight). (Concluded)

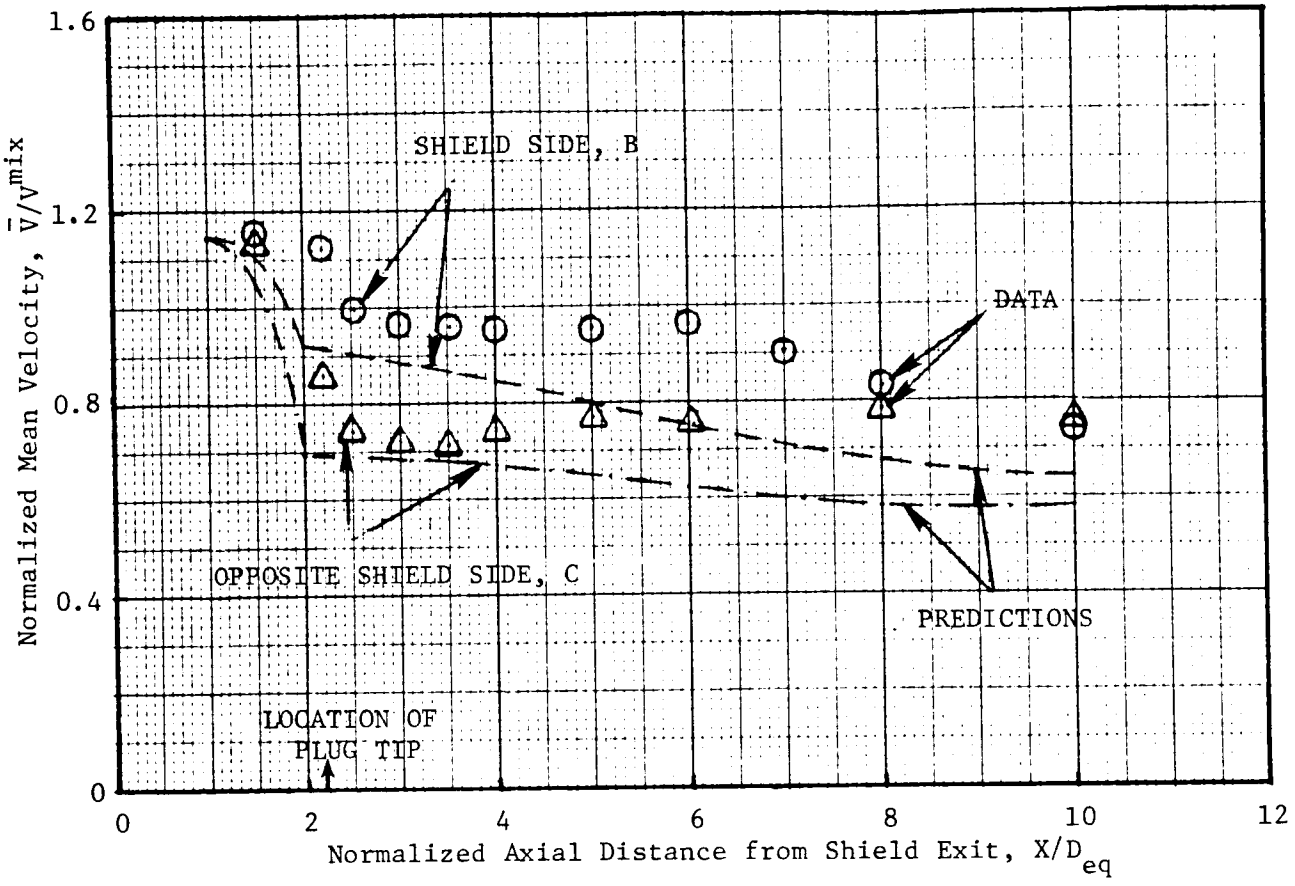

LV PLUME 2: TEST POINT 1140

STREAM	P_r	$T_T(^\circ R)$	V, fps
INNER	2.28	943	1540
OUTER	3.02	1642	2325
SHIELD	1.51	1607	1473
MIXED	2.37	1545	2025

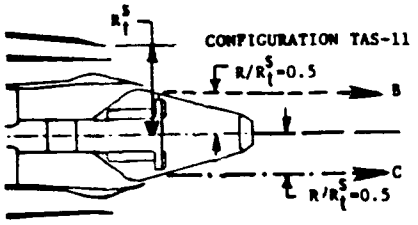

V_{ac} = 400 ft/s

Figure 106. Comparison of the Predicted and Measured Axial Variation of the Mean Velocity on Shield and Opposite Shield Side for Unsuppressed Coannular Plug Nozzle with Partial Shield.

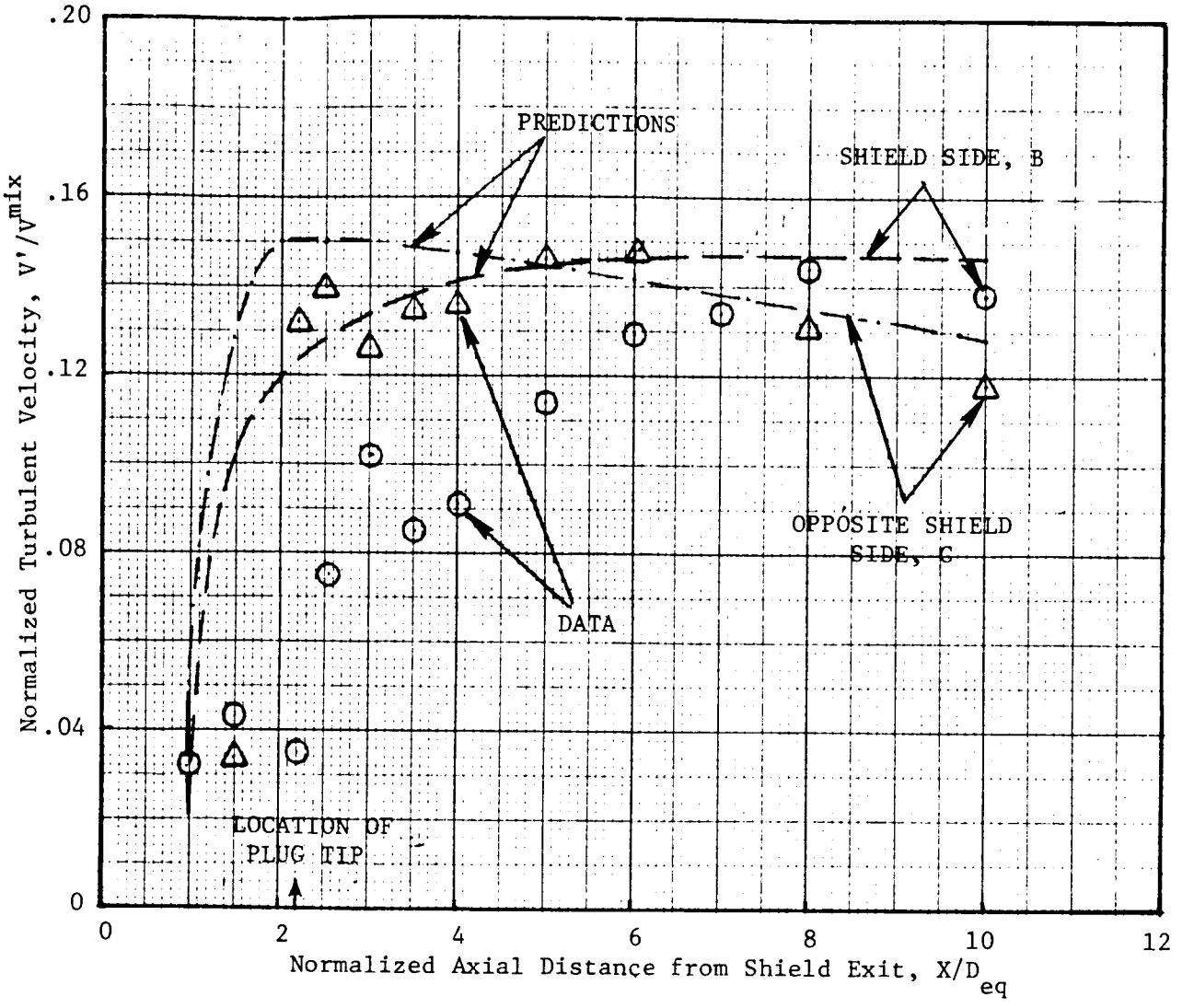

LV PLUME 2: TEST POINT 1140

STREAM	P_r	T_T(°R)	V, fps
INNER	2.28	943	1540
OUTER	3.02	1642	2325
SHIELD	1.51	1607	1473
MIXED	2.37	1545	2025

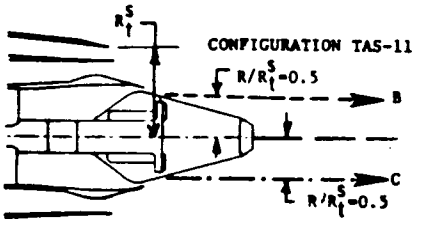

V_{ac} = 400 ft/s

Figure 107. Comparison of the Predicted and Measured Axial Variation of the Turbulent Velocity on Shield and Opposite Shield Side for Unsuppressed Coannular Plug Nozzle with Partial Shield.

are similar to those displayed for the static case (see Figures 103 and 104). Thus, the aerodynamic effect of the shield on the plume development for the simulated flight case is also an elongation of the plume by the shield due to reduced velocity gradient. Hence, the aerodynamic effect noted above is also a reason for the amplification of the low frequency noise by the shield under simulated flight conditions.

The effect of the simulated flight on the mean and turbulent velocities relative to the static is analyzed by comparing the data presented in Figures 106 and 107 to those presented in 103 and 104. Both the predictions and the data of the flow field for the simulated flight case indicate that the mean velocities on the shield side tend to be higher for the simulated flight case than those of the static case. The measured increase in the mean velocity on the shield side due to the simulated flight is more than the predicted increase. A higher level of mean velocity due to the simulated flight is anticipated because the moving free-jet air around the nozzle flow reduces the shearing velocity gradient, unlike the static case in which the ambient air is stationary. The predictions on the shield and opposite shield sides and the data on the shield side confirm this rationale. However, the data on the opposite shield side indicate that the mean velocity decreases because of the free jet. A plausible explanation for this different behavior is found by referring to the radial profiles of the mean velocity presented in Figure 56. The radial traverse data indicate that the velocity profiles are steep in the neighborhood of $R/R_t^S = 0.5$ for $2 \leq X/D_{eq} \leq 5$. Hence, a slight inaccuracy in positioning the laser beams for the axial traverse on the opposite shield side during either the static or simulated flight test could cause the observed inconsistency.

The turbulence velocity measurements and predictions for the simulated flight case are shown in Figure 107. The free jet that simulates the flight streamlines the jet flow and lowers the levels of turbulent velocity for the simulated flight case, as compared to the static case. Comparing Figures 107 and 104 indicates that:

a. The measured peak turbulent velocities on the shield side for the simulated flight and static cases are ≈14.5% and ≈16.8% of V^{mix}, respectively, and

b. The turbulent velocities for the flight case on the shield side tend to be lower than the corresponding static case at all axial locations.

The corresponding predictions indicate that predicted peak turbulent velocity on the shield side for the simulated flight and static cases are, respectively, 14.7% and 15.4% of V^{mix} and the turbulent velocities on the shield and opposite shield side at all axial locations tend to be lower for the simulated flight case than for the static case. The measured turbulent velocity on the opposite shield side does not show any noticeable effect of the simulated flight.

The next set of data-theory comparisons presented in this section deals with the ΔSPL by the full (360°) shield on the unsuppressed coannular plug

nozzle (TAS-14) at a typical takeoff cycle for the static condition. The typical aft-quadrant data presented in Figure 108 indicate an acceptable agreement between the measured and predicted ΔSPL by the shield. The measured data also show a negligible high frequency noise reduction by the shield at the takeoff cycle condition, whereas the predictions showed a modest high frequency noise reduction (4 dB at 80 kHz 1/3 octave band). Both the data and the predictions indicate low frequency noise amplification by the shield. As in the case of the partial shield on the coannular plug nozzle, the agreement between the measured and predicted ΔSPL at θ_i = 90° and 60° is good at low and high frequencies (see Figures 108b and 108c).

Since the acoustic benefit of the shield is mainly in the aft quadrant for the unsuppressed coannular plug nozzle, this section is concluded with data-theory comparisons in the aft quadrant only for typical approach and cutback conditions.

Figures 109 and 110 show comparisons of static ΔSPL by the full shield on the unsuppressed coannular plug nozzle at θ_i = 130° for approach and cutback conditions, respectively. The figures show that the predicted trends agree with the data. It should be noted that suppression levels predicted and measured at the approach and cutback cycle conditions are higher than those indicated earlier at the takeoff cycle. In addition, both the predictions and data indicate that the peak level of suppression due to the full shield at approach and cutback cycles is about the same. However, the high frequency noise reduction potential of the shield is less at high outer and inner jet velocities. A similar observation was made in Reference 12 in the context of the single flow primary nozzles with the thermal acoustic shield. Thus, the M*G*B prediction model has been shown to predict correct trends of spectral suppression characteristics of the shield on an unsuppressed coannular plug nozzle at various cycle conditions.

The principal conclusions of this study are:

- The overall trends in the flow field characteristics of an unsuppressed coannular plug nozzle with partial shield that were predicted by the modified M*G*B model are in reasonable agreement with the corresponding trends in the LV measured data.

- Both the predicted and measured flow field characteristics confirm that the principal reason for the observed amplification of the low frequency noise is the elongation of the jet plume by the shield.

- The predicted suppression of high frequency noise by the shield in the aft quadrant is higher than the measurements; but both the data and predictions show similar trends in the suppression spectra.

- Both the predictions and measurements of the noise suppression by the shield in the aft quadrant indicate that the shield yields appreciable noise reductions at low and middle engine power settings (approach and cutback, respectively) and that its potential to reduce noise at the high power setting (takeoff) decreases.

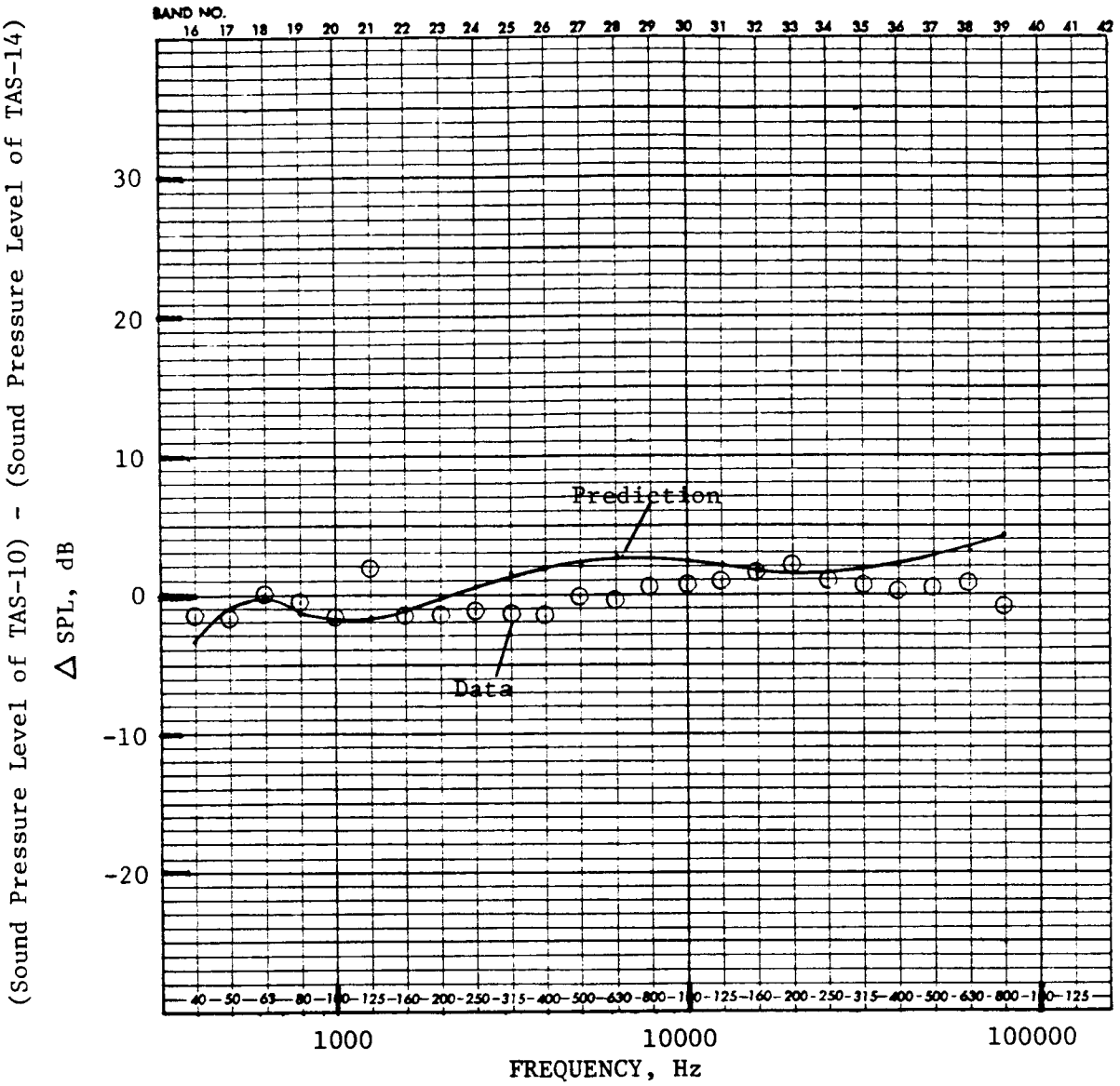

- Model Scale
- 40' Arc
- Takeoff Cycle
- V_{ac} = 0 fps
- Test Point for TAS-10: 1021
- Test Point for TAS-14: 1409 (360° Shield)

a) At Angle to Inlet Axis $\theta_i = 130^\circ$

Figure 108. Comparison of the Measured and Predicted ΔSPL Between the Unshielded (TAS-10) and Shielded (TAS-14) Configurations for the Unsuppressed Coannular Plug Nozzle for a Typical Takeoff Cycle.

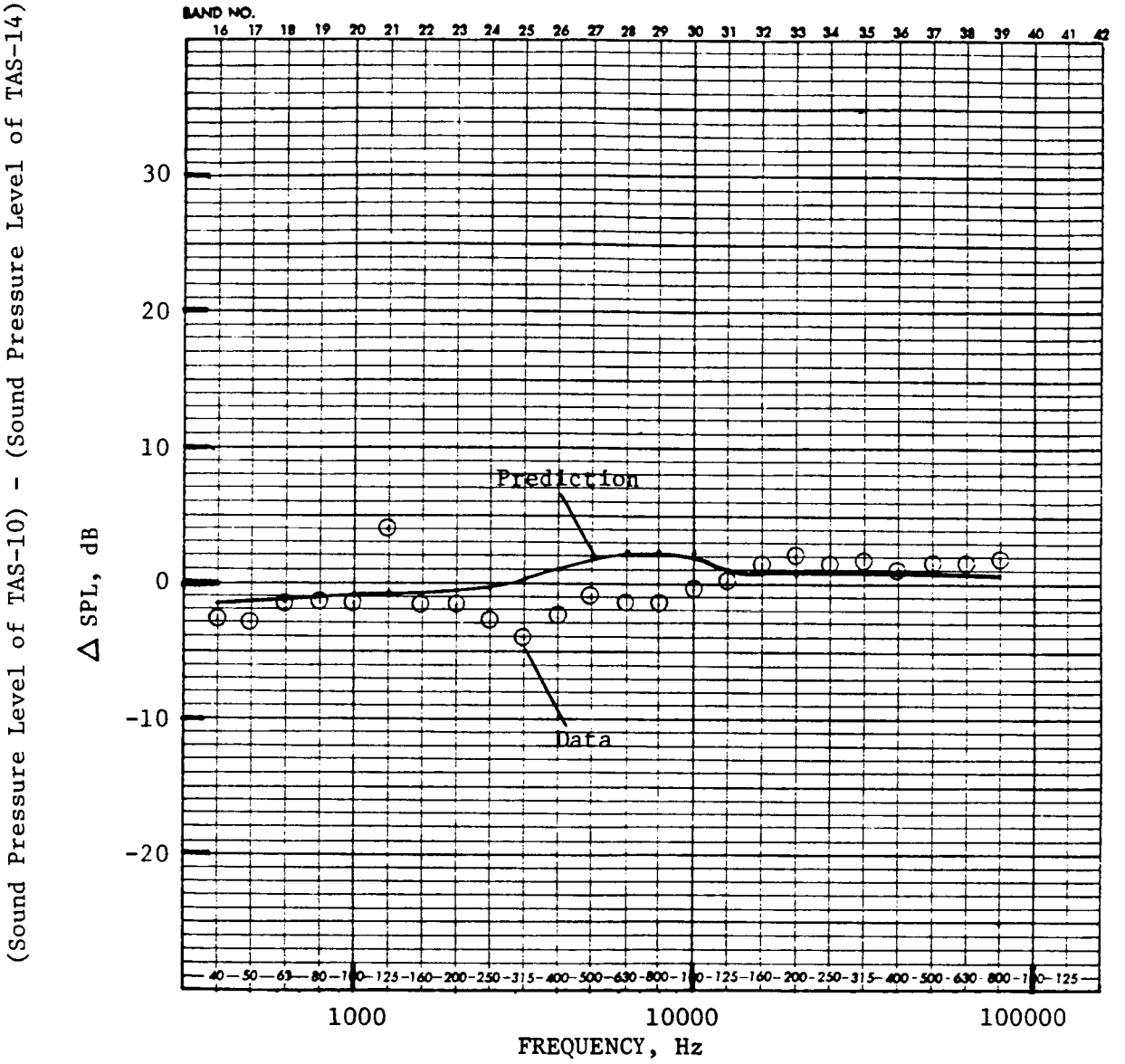

- Model Scale
- 40' Arc
- Takeoff Cycle
- V_{ac} = 0 fps
- Test Poinr for TAS-10: 1021
- Test Point for TAS-14: 1409 (360° Shield)

b) At Angle to Inlet Axis θ_i = 90°

Figure 108. Comparison of the Measured and Predicted ΔSPL Between the Unshielded (TAS-10) and Shielded (TAS-14) Configurations for the Unsuppressed Coannular Plug Nozzle for a Typical Takeoff Cycle. (Continued)

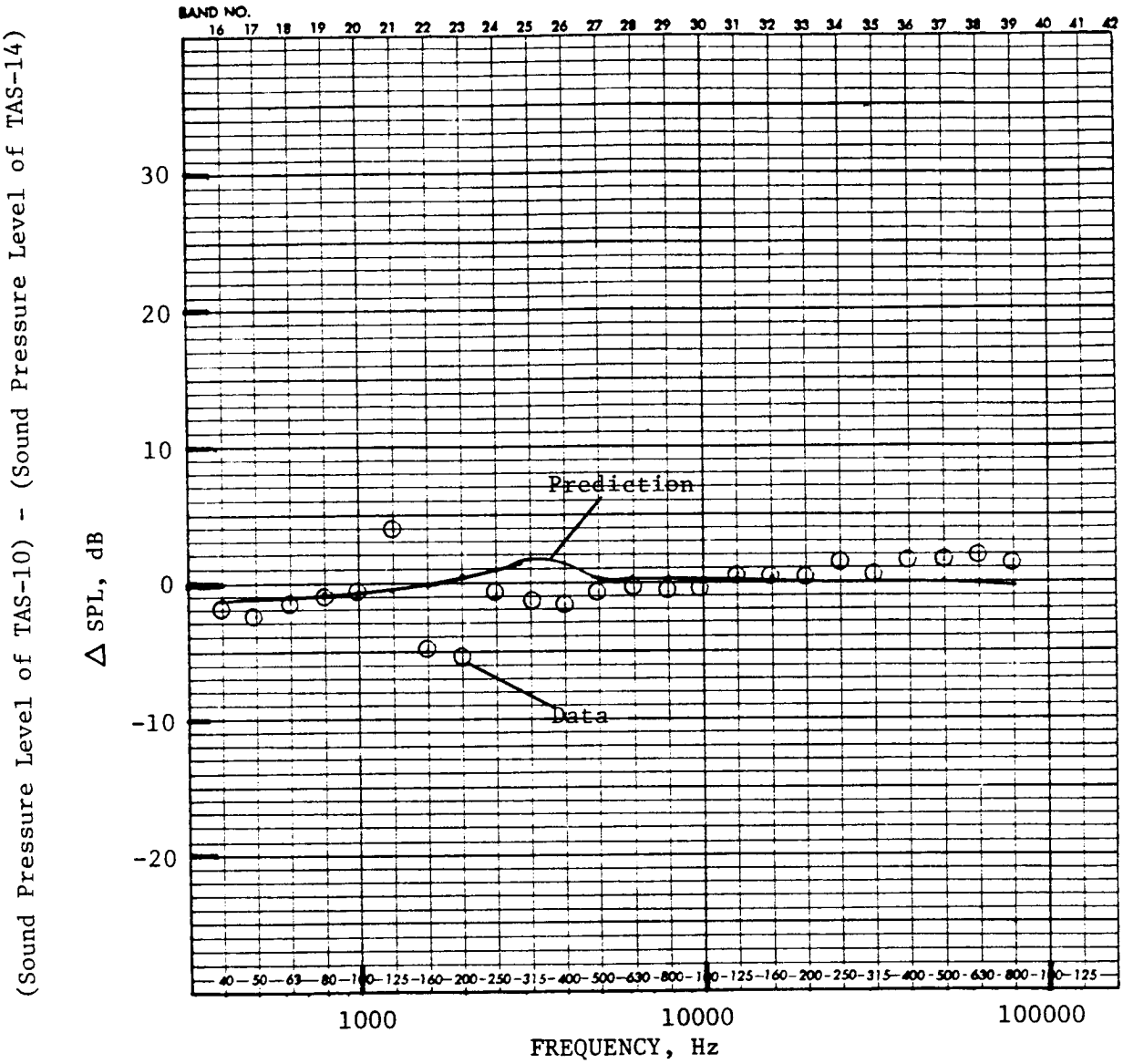

- Model Scale
- 40' Arc
- Takeoff Cycle
- V_{ac} = 0 fps
- Test Point for TAS-10: 1021
- Test Point for TAS-14: 1409 (360° Shield)

c) At Angle to Inlet Axis θ_i = 60°

Figure 108. Comparison of the Measured and Predicted ΔSPL Between the Unshielded (TAS-10) and Shielded (TAS-14) Configurations for the Unsuppressed Coannular Plug Nozzle for a Typical Takeoff Cycle. (Concluded)

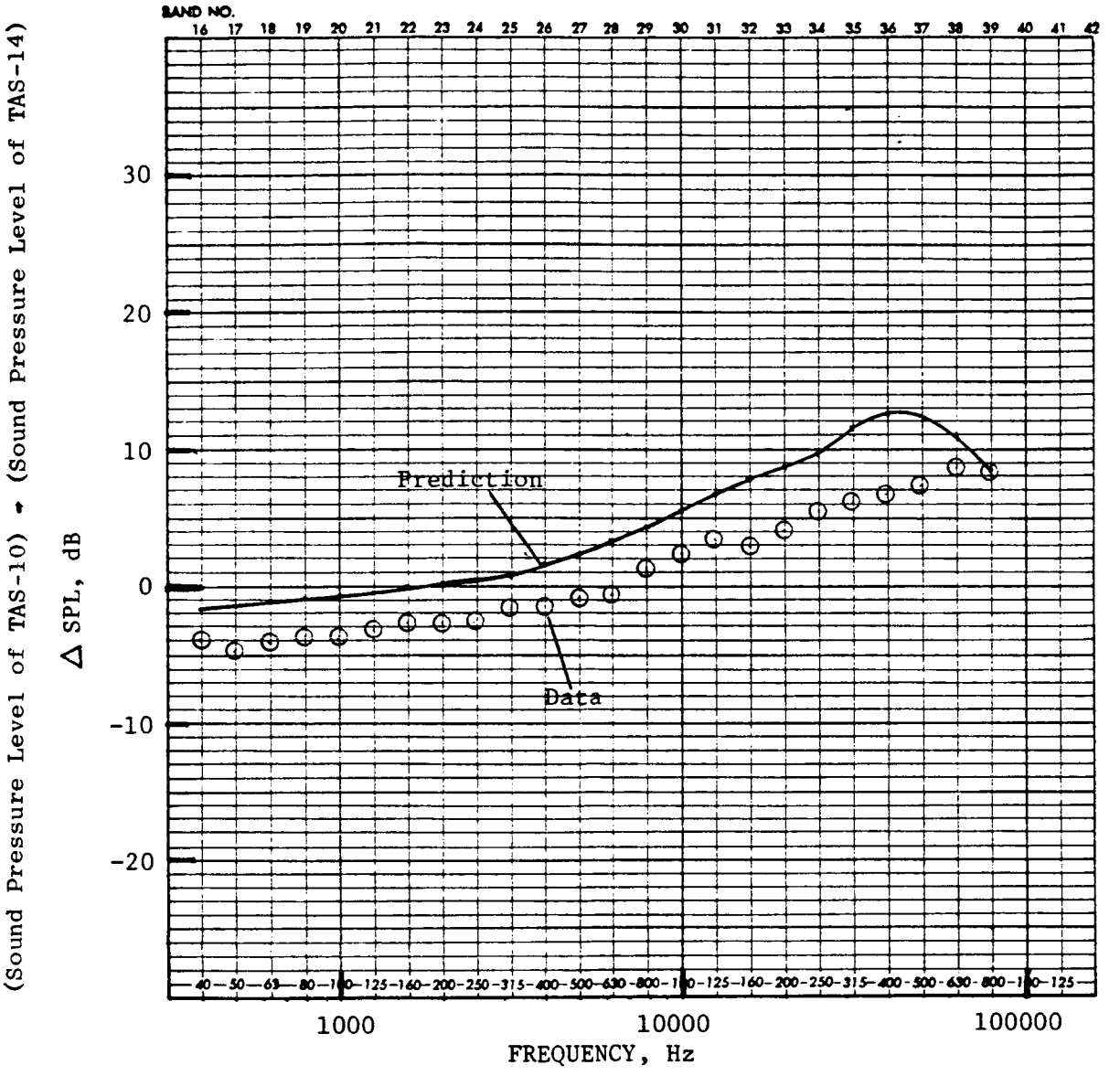

- Model Scale
- 40' Arc
- Approach Cycle
- V_{ac} = 0 fps
- Test Point for TAS-10: 1003
- Test Point for TAS-14: 1403 (360° Shield)
- Angle to Inlet Axis= 130°

Figure 109. Comparison of the Measured and Predicted ΔSPL Between the Unshielded (TAS-10) and Shielded (TAS-14) Configurations for the Unsuppressed Coannular Plug Nozzle for a Typical Approach Cycle.

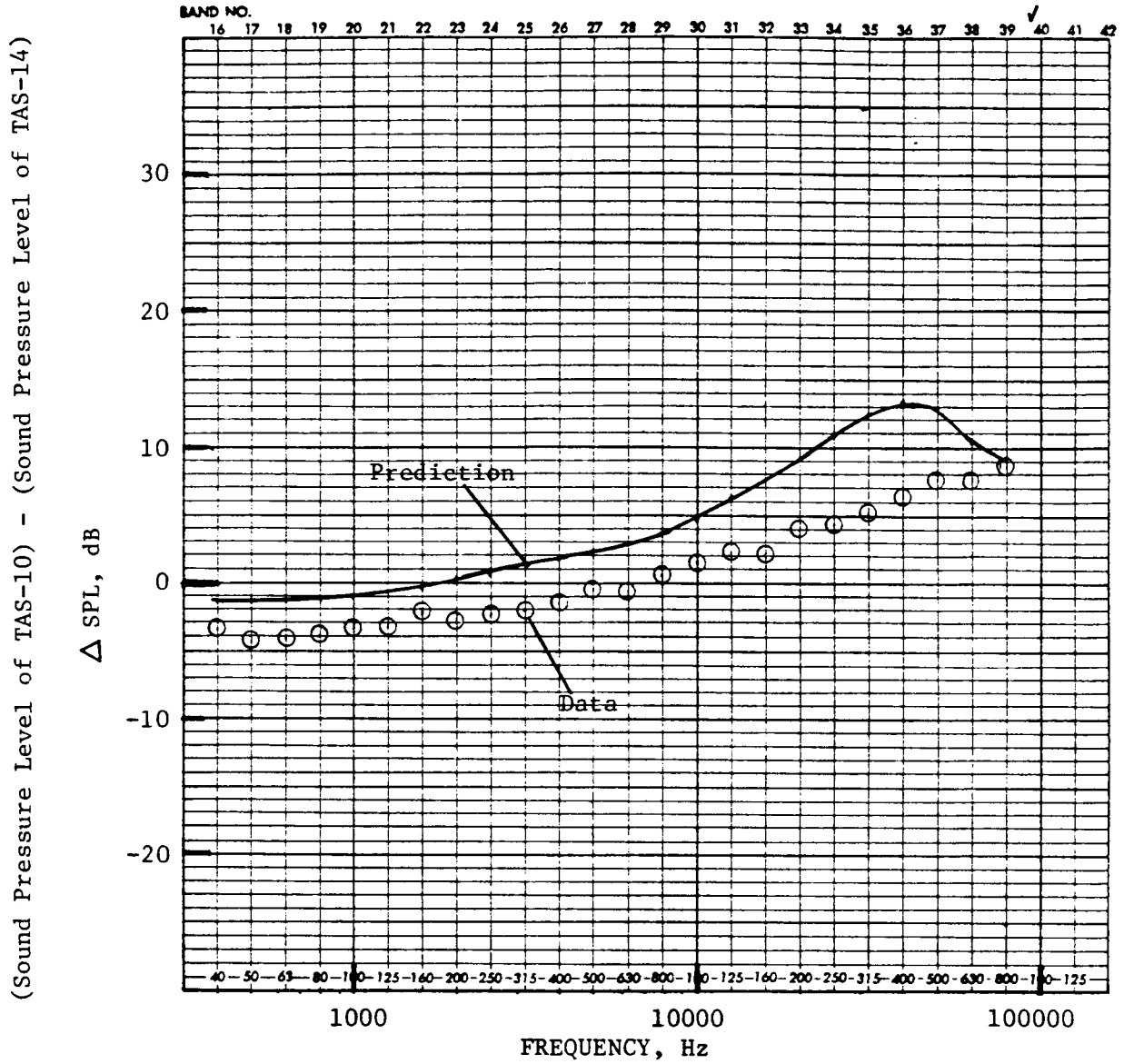

- Model Scale
- 40' Arc
- Cutback Cycle
- V_{ac} = 0 fps
- Test Point for TAS-10: 1005
- Test Point for TAS-14: 1405
- Angle to Inlet Axis= 130^{o}

Figure 110. Comparison of the Measured and Predicted ΔSPL Between the Unshielded (TAS-10) and Shielded (TAS-14) Configurations for the Unsuppressed Coannular Plug Nozzle for a Typical Cutback Cycle.

6.0 CONCLUSIONS

During this investigation, nine scale-model nozzles were tested in the Anechoic Free-Jet Facility to evaluate the effectiveness of thermal acoustic shields on coannular configurations under both static and simulated flight conditions. These tests were conducted at nozzle temperatures and pressure ratios typical of operating conditions of a variable cycle engine and applicable for an advanced supersonic transport. The tested nozzles included baseline (unshielded), 180° shielded and 360° shielded dual-flow coannular plug configurations. The baseline configurations include a high radius ratio unsuppressed coannular plug nozzle and a coannular plug nozzle with a 20-chute outer stream suppressor. The required shielding jets were bled from the heated stream that supplied the flow to the outer nozzle and passed through sets of choke plates to get selected shield-to-outer stream velocity ratios ($V_r^{s,o}$).

A total of 136 acoustic test points, with inverted velocity profiles on the coannular configurations, were conducted. In order to investigate the effect of $V_r^{s,o}$ on the acoustics of partial shielded configurations, tests were conducted at three selected values of $V_r^{s,o}$ (equal to 0.48, 0.64 and 0.83 at a typical takeoff). During each of the acoustic test points with the baseline and 180° shielded suppressed coannular plug nozzles, static pressure data in the chute base region were obtained to assess the influence of the shield stream on the suppressor base drag. Also, aerodynamic measurements with a laser velocimeter were made for four selected plumes.

The significant results from the analyses of measured data are as follows:

- The presence of the partial shield resulted in different mixing characteristics on the shield side relative to the unshield side, which in turn produced significant asymmetry in the measured mean and turbulent velocities. While the distinct presence of the shield was identified in the region of the plug only, the asymmetry in the velocity data were noted to extend up to a length of $X/D_{eq} \sim 10$ from the shield exit.

- At an axial location downstream of the plug but less than $X/D_{eq} \sim 10$, the peak mean velocity on the partial shield side was higher than that on the unshield side, due to the reduced mixing with ambient air on the shield side. The slower mean velocity decay rate then stretched the jet on the shield side. This effect was pronounced with shielded suppressed configurations.

- The 180° shield in community orientation around the suppressed coannular configuration indicated the acoustic benefit at all observer angles during simulated takeoff. While the effect of shield-to-outer stream velocity ratio was very small in the front quadrant and up to $\theta_i = 120°$, significant acoustic benefit beyond $\theta_i = 120°$ was obtained with shield-to-outer stream velocity ratio of 0.64. For example, at

reduction of 3.8 dB in the front quadrant and of 7.1 dB at the peak noise angle of θ_i = 120° was obtained with the shield at $V_{r_{s,o}}$ = 0.64. While the reduction in the aft quadrant by the shielding effect was noted only at very high frequencies, significant noise suppressions at middle and high frequencies were achieved at all angles because of the change in flow field characteristics and source alterations by the shield flow. As a result of the stretching of the jet on the shield side, an increase in the low frequency jet noise was noted with the shielded suppressor configurations relative to the baseline suppressor nozzle.

- With the 180° shield in sideline orientation around the unsuppressed coannular nozzle, the effect of the different shield-to-outer stream velocity ratios was observed to be small.

- The presence of the partial thermal acoustic shield around unsuppressed and suppressed coannular plug nozzles caused an asymmetric acoustic field. Relative to the sideline orientation, the community arrangement of the shield for a given set of flow conditions resulted in a 1.5 to 2 dB reduction in the aft quadrant PNL data.

- For identical shield flow rates, a thick partial shield in community orientation with the suppressor configuration yielded, for $\theta_i \geq 130°$, lower sound pressure levels at all frequencies than did a thin full shield.

- The introduction of a full shield around the suppressed coannular nozzle reduced power level at high frequencies due to shielding of the acoustic sources near the nozzle exit. However, because of the reduced mixing rate, power levels increased at low and middle frequencies.

- A full shield around the unsuppressed coannular plug nozzle yielded the expected power level reductions at high frequencies. However, there was no significant reduction in the overall power level, as no changes were noted in the dominant low and middle frequency power spectra.

- The base drag of the baseline suppressed configuration was not affected significantly by variation in suppressor stream pressure. However, due to a reduction in chute base ventilation, the base drag increased in the presence of free-jet and increased shield flow velocity.

Predictions of the acoustic suppressions and the general flow field characteristics were made using the modified M*G*B model for the full and partial shielded unsuppressed coannular plug nozzle. While the high frequency noise suppression predicted in the aft quadrant was greater than measured, the trends in these two suppression spectra were similar. Also, the trends in the predicted flow field characteristics agreed with the measured data.

7.0 NOMENCLATURE

A	Area
a_{amb}	Ambient speed of sound
AST	Advanced Supersonic Transport
D	Diameter
f	Frequency
F	Thrust
F_D	Base drag
F_{ref}	Reference thrust, 22,820 N (5,130 lb)
h	Flowpath annulus height
k_i	Number of velocity samples in a class interval
L	Shock-cell spacing
ℓ	Shield to outer nozzle exit axial distance
LBM	Mixed shock strength parameter, defined as 10 log $\sqrt{M^2-1}$
LV	Laser Velocimeter
LVM	Mixed jet velocity parameter, defined as 10 log (V^{mix}/a_{amb})
M	Mach number
M_c	Convection Mach Number, U_c/a_{amb}
N	Total number of data samples for a histogram
NF	Normalization Factor, defined in Section 3.1
OAPWL	Overall Sound Power Level, dB re 10^{-12} Watts
P	Pressure
PNL	Perceived Noise Level, dB
PNLN	Normalized Perceived Noise Level, dB, defined in Section 3.1

P_r	Pressure ratio = P_T/P_{amb}
PWL	Sound Power Level, dB re 10^{-12} Watts
R	Radial distance
RH	Relative Humidity, %
R_h	Hub radius
R_t	Tip radius
R_r	Radius ratio, R_h/R_t
SPL	Sound Pressure Level, dB
T	Temperature
t	Time
TAS	Thermal Acoustic Shield
U_c	Convection velocity of eddy
V'	Turbulent velocity
V	Velocity
$\bar{V}$	Mean velocity
VCE	Variable Cycle Engine
W	Weight flow rate
X	Axial distance

Greek Symbols

β	Shock strength parameter, defined as $\sqrt{M^2-1}$
γ	Ratio of specific heats
Δ	Sound Pressure Level difference, dB
θ_h	Hub flowpath angle at throat, degrees
θ_t	Tip flowpath angle at throat, degrees

θ_{th}	Exit plane discharge angle, degrees
θ_{chute}	Angle subtended by each chute, degrees
θ_{flow}	Angle subtended by each flow element, degrees
θ_i	Angle of observer relative to inlet axis, degrees
ρ	Density
ω	Density exponent

Superscripts

chute	Parameter pertaining to a chute
eff	Effective condition for dual stream nozzles
i	Inner stream
mix	Mass averaged mixed stream
o	Outer stream
s	Shield stream
T	Total

Subscripts

ac	Aircraft
amb	Ambient
avg	Average
eq	Equivalent circular convergent (conic) nozzle
flight	In-flight value
i	Inlet
i,k	Index
p	Peak
r	Ratio
s	Static (thermodynamic)
static	Static (without simulated flight)
T	Total (stagnation)

8.0 REFERENCES

1. Vdoviak, J.W., Knott, P.R., and Ebacker, J.J., "Aerodynamic/Acoustic Performance of YJ101/Double Bypass VCE with Coannular Plug Nozzle," NASA CR-159869, January 1981.

2. Fitzsimmons, R.D., McKinnon, R.A., Johnson, E.S., and Brooks, J.R., "Flight and Wind Tunnel Test Results of a Mechanical Jet Noise Suppressor Nozzle," AIAA Paper 80-0165, January 1980.

3. Atwars, J., et al., "Development of Acoustically Lined Ejector Technology for Multitube Jet Noise Suppressor Nozzles by Model and Engine Tests," NASA CR-2382, April 1974.

4. Stringas, E.J., Clapper, W.S., Brausch, J.F., et al., "High Velocity Jet Noise Source Location and Reduction, Task 3 - Experimental Investigation of Suppression Principles, Volume II - Parametric Testing and Source Measurements," General Electric Company Contractor Final Report, FAA-RD-76-79, III-II, December 1978.

5. Janardan, B.A., Majjigi, R.K., Brausch, J.F., and Knott, P.R., "Free-Jet Investigation of Mechanically Suppressed, High-Radius-Ratio Coannular Plug Model Nozzles," Final Report Draft for Contract NAS3-21608, October 1981.

6. Wolf, J.P., "Preliminary Design of an AST Jet Engine Exhaust System Incorporating a Thermal Acoustic Shield Suppressor," General Electric Company, TM-80-46, August 1980.

7. Cowan, S.J. and Crouch, R.W., "Transmission of Sound Through a Two-Dimensional Shielding Jet," AIAA Paper 73-1002, October 1973.

8. Ahuja, K.K. and Dosanjh, D.S., "Heated Fluid Shroud as an Acoustic Shield for Noise Reduction - An Experimental Study," AIAA Paper 77-1286, October 1977.

9. Goodykoontz, J., "Effect of a Semi-Annular Thermal Acoustic Shield on Jet Exhaust Noise," NASA TM 81615, November 1980.

10. Pickup, N., Mangiarotty, R.A., and O'Keefe, J.V., "Tests of a Thermal Acoustic Shield with a Supersonic Jet," AIAA Paper 81-2021, October 1981.

11. Vijayaraghavan, A. and Parthasarathy, S.P., "Noise Shielding by a Hot Subsonic Jet," AIAA Paper 81-2018, October 1981.

12. Majjigi, R.K., Brausch, J.F., Janardan, B.A., Knott, P.R., Balsa, T.F., and Pickup, N., "Free Jet Feasibility Study of Thermal Acoustic Shield Concept for AST/VCE Application - Single Stream Nozzles," NASA CR-3758, July 1984.

13. Majjigi, R.K., "A Unique Spectral Acoustic Prediction Method for Jet and Shock Cell Noise of Mechanical Suppressor Nozzles," General Electric Company, R81AEG363, May 1981.

14. Majjigi, R.K., Janardan, B.A., Brausch, J.F., Hoerst, D.J., Price, A.O. and Knott, P.R., "Free Jet Feasibility Study of a Thermal Acoustic Shield Concept for AST/VCE Application - Single Flow," General Electric Company, Comprehensive Data Report, R82AEB493, October 1982.

15. Vogt, P.G., Bhutiani, P.K., and Knott, P.R., "Free-Jet Acoustic Investigation of High Radius Ratio Coannular Plug Nozzles," General Electric Company, Comprehensive Data Report, Vol. I, 81AEG212, January 1981.

16. Clapper, W.S., et al., "High Velocity Jet Noise Source Location and Reduction; Task IV - Development/Evaluation of Techniques for In-Flight Investigation," R77AEG189, Report No. FAA-RD-76-79, IV, Final Report, U.S. Department of Transportation, February 1977.

17. Shields, F.D. and Bass, H.E., "Atmospheric Absorption of High Frequency Noise and Application to Fractional Octave Bands," NASA CR-2760, June 1977.

18. Knott, P.R., et al., "Supersonic Jet Exhaust Noise Investigation," AFAPL-TR-74-25, June 1974.

19. Knott, P.R., "Supersonic Jet Exhaust Investigation - Volume I Summary Report," AFAPL-TR-76-78, July 1976.

20. Brausch, J.F., "Model Hardware Design Report for a Thermal Acoustic Shield Concept for AST/VCE Application - Dual Stream Nozzle Designs," General Electric Company, R84AEB389, April 1984.

21. Knott, P.R., Janardan, B.A., Majjigi, R.K., Bhutani, P.K., and Vogt, P., "Free Jet Acoustic Investigation of High-Radius-Ratio Coannular Plug Nozzles," Contract NAS3-20619, Report R83AEB574, January, 1984.

22. Janardan, B.A., Majjigi, R.K., Brausch, J.F. and Knott, P.R., "Free Jet Investigation of Mechanically Suppressed, High-Radius-Ratio Coannular Plug Model Nozzles," NASA CR-3596, May 1984.

23. Yamamoto, K., Brausch, J.F., Balsa, T.F., Janardan, B.A., and Knott, P.R., "Experimental Investigation of Shock-Cell Noise Reduction for Single Stream Nozzles in Simulated Flight," General Electric Company, R82AEB492, December 1983.

24. Janardan, B.A., Yamamoto, K., Majjigi, R.K., and Brausch, J.F., "Experimental Investigation of Shock-Cell Noise Reduction for Dual-Stream Nozzles in Simulated Flight," General Electric Company, R83AEB358, March 1984.

25. Brausch, J.F., Whittaker, R.W., and Knott, P.R., "Acoustic and Aerodynamic Nozzle Performance Design Considerations for the NASA AST/VCE Core Drive (CDFS) Acoustic Nozzle Program," General Electric Company, TM 80-216, March 1980.

26. Janardan, B.A., et al., "Free-Jet Investigation of Mechanically Suppressed, High-Radius-Ratio Coannular Plug Model Nozzles," Comprehensive Data Report Volume II - Laser Velocimeter and Base Pressure Data and Facility Description, General Electric Company, R81AEG484, May 1981.

27. Janardan, B.A., Brausch, J.F., and Price, A.O., "Free-Jet Feasibility Study of a Thermal Acoustic Shield Concept for AST/VCE Application - Dual Flow Nozzles," General Electric Company Comprehensive Data Report, 1984.

28. Knott, P.R., et al., "Acoustic Tests of Duct Burning Turbofan Jet Noise Simulation," NASA CR-2966, July 1978.

29. Knott, P.R., Blozy, J.T., and Staid, P.S., "Acoustic and Aerodynamic Performance Investigation of Invested Velocity Profile Coannular Plug Nozzles," NASA CR-3149, June 1979.

30. Dosanjh, D.S., Bhutiani, P.K., and Ahuja, K.K., "Supersonic Jet-Noise Reduction by Coaxial Cold/Heated Jet Flows," Final Report Under Grant No. DoT-05-20094, Syracuse University, March 1977.

31. Harper-Bourne, M., and Fisher, M., "The Noise From Shock Waves in Supersonic Jets," Proceedings of the AGARD Conference on Noise Mechanisms, Brussels, Belgium, AGARD CP131, 1973.

32. Mani, R., Gliebe, P.R., Balsa, T.F., Stringas, E.J., et al., "High Velocity Jet Noise Source Location and Reduction, Task II - Theoretical Developments and Basic Experiments." General Electric Company Contractor Final Report, FAA-RD-76-79, II, 1976.

1. Report No.	2. Government Accession No.	3. Recipient's Catalog No.
NASA CR-3867		

4. Title and Subtitle	5. Report Date
Free Jet Feasibility Study of a Thermal Acoustic Shield Concept for AST/VCE Application - Dual Stream Nozzles	March 1985
	6. Performing Organization Code
7. Author(s)	8. Performing Organization Report No.
B. A. Janardan, J. F. Brausch, and R. K. Majjigi	R84AEB577
	10. Work Unit No.
9. Performing Organization Name and Address	11. Contract or Grant No.
General Electric Company Aircraft Engine Business Group Cincinnati, Ohio 45215	NAS 3-22137
	13. Type of Report and Period Covered
12. Sponsoring Agency Name and Address	Contractor Report
National Aeronautics and Space Administration Washington, D.C. 20546	14. Sponsoring Agency Code
	505-40-74 (E-2392)

15. Supplementary Notes

Final report. Project Manager, Jack H. Goodykoontz, Fluid Mechanics and Instrumentation Division, NASA Lewis Research Center, Cleveland, Ohio 44135.

16. Abstract

The influences of selected geometric and aerodynamic flow variables of an unsuppressed coannular plug nozzle and a coannular plug nozzle with a 20-chute outer stream suppressor were experimentally determined. A total of 136 static and simulated flight acoustic test points were conducted with 9 scale-model nozzles. Also, aerodynamic measurements of four selected plumes were made with a laser velocimeter. The presence of the 180° shield produced different mixing characteristics on the shield side compared to the unshield side because of the reduced mixing with ambient air on the shielded side. This resulted in a stretching of the jet, yielding a higher peak mean velocity up to a length of 10 equivalent diameters from the nozzle exit. The 180° shield in community orientation around the suppressed coannular plug nozzle yielded acoustic benefit at all observer angles for a simulated takeoff. While the effect of shield-to-outer stream velocity ratio was small at angles up to 120°, beyond this angle significant acoustic benefit was realized with a shield-to-outer stream velocity ratio of 0.64. While the reduction in the aft quadrant by shielding was noted only at very high frequencies, significant noise suppressions at middle and high frequencies were achieved at all angles because of changes in the flow fields and source alterations produced by the shield flow. However, as a result of stretching of the jet on the shield side, low frequency jet noise was greater than for the unshielded configuration.

17. Key Words (Suggested by Author(s))	18. Distribution Statement
Jet noise; Thermal acoustic shield; Variable cycle engine; Coannular nozzle; Suppressor nozzle	[redacted]

19. Security Classif. (of this report)	20. Security Classif. (of this page)	21. No. of pages	22. Price
Unclassified	Unclassified	201	

NASA-Langley, 1985